Rhythmic Sensory Stimulation and the Role of Phase Synchronization in Fear Conditioning

Dissertation
zur Erlangung des Doktorgrades der Naturwissenschaften (Dr. rer. nat.)
des Fachbereichs Humanwissenschaften
der Universität Osnabrück

vorgelegt von
Elena Plog, M.Sc. Psychologie

geboren in
Quakenbrück, Deutschland

Osnabrück, 2022

Gutachter/Innen:

1. Prof. Dr. Ursula Stockhorst, Universität Osnabrück

2. Prof. Dr. Thomas Gruber, Universität Osnabrück

Erklärung über die Eigenständigkeit der erbrachten wissenschaftlichen Leistungen

Ich erkläre hiermit, dass ich die vorliegende Arbeit ohne unzulässige Hilfe Dritter und ohne Benutzung anderer als der angegebenen Hilfsmittel angefertigt habe. Die aus anderen Quellen direkt oder indirekt übernommenen Daten und Konzepte sind unter Angabe der Quelle gekennzeichnet. Bei der Auswahl und Auswertung folgenden Materials haben mir die nachstehend aufgeführten Personen in der jeweils beschriebenen Weise entgeltlich/unentgeltlich geholfen:

Angabe der **Author Contributions** (in der Reihenfolge der Autorenschaft)

Study 1. Antov, M.I., **Plog, E.**, Bierwirth, P., Keil, A., & Stockhorst, U. (2020). Visuocortical tuning to a threat-related feature persists after extinction and consolidation of conditioned fear. *Sci Rep* 10, 3926. https://doi.org/10.1038/s41598-020-60597-z

Martin I. Antov: Conceptualization, Methodology, Investigation, Formal analysis, Visualization, Writing – original draft, Writing – review & editing, Project administration. **Elena Plog:** Visualization, Investigation, Writing – review & editing. *Philipp Bierwirth*: Writing – review & editing. *Andreas Keil*: Conceptualization, Methodology, Formal analysis, Writing – review & editing, Supervision. *Ursula Stockhorst*: Conceptualization, Writing – review & editing, Project administration, Supervision.

Study 2. **Plog, E.*,** Antov, M. I.*, Bierwirth, P., Keil, A., & Stockhorst, U. (2022). Phase-synchronized stimulus presentation augments contingency knowledge and affective evaluation in a fear-conditioning task. *ENeuro, 9*(1). https://doi.org/10.1523/ENEURO.0538-20.2021

Elena Plog: Designed research, Performed research, Analyzed data, Wrote the paper. *Martin I. Antov:* Designed research, Performed research, Analyzed data, Wrote the paper. *Philipp Bierwirth:* Analyzed data. *Andreas Keil*: Contributed unpublished reagents/analytic tools, Wrote the paper. *Ursula Stockhorst*: Designed research, Wrote the paper. *Shared first-authorship

Study 3. **Plog, E.,** Antov, M.I., Bierwirth, P., & Stockhorst, U. (under review). Effects of phase synchronization and frequency specificity in the encoding of conditioned fear – a web-based fear conditioning study

Elena Plog: Conceptualization, Data Curation, Formal Analysis, Investigation, Methodology, Project Administration, Software, Validation, Visualization, Writing – Original Draft Preparation, Writing – Review & Editing. *Martin I. Antov:* Conceptualization, Methodology, Software, Writing – Review & Editing. *Philipp Bierwirth:* Conceptualization, Visualization, Writing – Review & Editing. *Ursula Stockhorst:* Conceptualization, Methodology, Supervision, Writing – Review & Editing.

Ausgewählte Teilkomponenten der Online-Umsetzung von Studie 3 wurden mit Unterstützung des *Consultancy Service* von Psychopy® (Nottingham, United Kingdom) entgeltlich programmiert.

Weitere Personen waren an der inhaltlichen materiellen Erstellung der vorliegenden Arbeit nicht beteiligt. Insbesondere habe ich hierfür nicht die entgeltliche Hilfe von Vermittlungs- bzw. Beratungsdiensten (Promotionsberater oder andere Personen) in Anspruch genommen. Niemand hat von mir unmittelbar oder mittelbar geldwerte Leistungen für Arbeiten erhalten, die im Zusammenhang mit dem Inhalt der vorgelegten Dissertation stehen. Die Arbeit wurde bisher weder im In- noch im Ausland in gleicher oder ähnlicher Form einer anderen Prüfungsbehörde vorgelegt.

Osnabrück, 24.05.2022

....
(Ort, Datum)   (Unterschrift)

Table of contents

List of Abbreviations

BLA	basolateral amygdala
CeA	central amygdala
CR	conditioned response
CS	conditioned stimulus
CS+	CS paired the unconditioned stimulus
CS-	CS never paired with the unconditioned stimulus
dACC	dorsal anterior cingulate cortex
dmPFC	dorsomedial prefrontal cortex
EEG	electroencephalography
fMRI	functional magnetic resonance imaging
ITC	intercalated cells
LTD	long-term depression
LTP	long-term potentiation
mPFC	medial prefrontal cortex
NMDA	*N*-methyl-D-aspartate
PET	positron emission tomography
PTSD	post-traumatic stress disorder
SAM	self-assessment manikin
SSRs	steady-state responses
ssVEPs	steady-state visually evoked potentials
TBS	theta-burst stimulation
TMS	transcranial magnetic stimulation
US	unconditioned stimulus
vmPFC	ventromedial prefrontal cortex

General Abstract

Understanding the complexity of memory processing in the brain is a major element of research in biopsychology and neuroscience. Advantages of animal studies comprise various ways to directly manipulate neural activity in memory-processing brain areas with high temporal and spatial precision. In contrast, human studies are often correlational in nature via assessing brain oscillations occurring during different stages of memory processing. Causal experimental approaches addressing the relevant associations are still sparse. As one promising line of research for causal inference in humans, external rhythmic stimulation via technical device or frequency-modulated sensory stimuli is suitable. It can be used to directly modulate brain oscillations and therefore opens the possibility of assessing the causal role of brain rhythms.

In the present thesis this rhythmic sensory stimulation is used in fear conditioning which is a valid model for aversive learning and memory. It aims at 1) investigating *visuocortical tunings* towards a threat-predictive stimulus and, importantly, addressing its persistence over different phases of fear conditioning and 2) for the first time testing the *causal* role of phase-synchronization in different low frequency bands for the association of an initially neutral visual stimulus with an auditory threat cue in both a laboratory and in a web-based fear conditioning paradigm.

In line with these aims, the three empirical studies were designed to use either unimodal or multimodal rhythmic stimulation to modulate oscillatory activity in a generalization fear conditioning paradigm, covering the learning phases habituation, fear acquisition, and extinction on day 1 (Studies 1 to 3), and delayed recall on day 2 (Studies 1, 2). In Study 1, we examined the visuocortical engagement in fear conditioning with a special focus on its persistence across an extinction and delayed recall phase. To account for the very early sensory processing, we assessed steady-state visual responses (as an indicator of visuocortical engagement) that were evoked via rhythmic visual stimulation in an alpha rhythm. We found visuocortical tuning to the threat-predictive stimulus as a result of fear acquisition, while extinction learning prompted rapid changes in orientation tuning: Here, conditioned visuocortical engagement and skin conductance responses to the fear-associated stimulus were strongly reduced. Importantly, delayed recall revealed a brief but precise return-of-tuning to the threat-stimulus in the visual cortex accompanied by a brief, more generalized return-of-fear in skin conductance. In sum, early visual processing shows response patterns that are consistent with memory consolidation and spontaneous recovery. In Study 2, we extended our rhythmic stimulation paradigm from being unimodal to multimodal. This served to

manipulate phase-synchronization between an initially neutral visual stimulus and an auditory threat cue in a memory-relevant theta frequency, and thus to address the associative nature of fear conditioning. We compared the effects of a synchronous (in-phase) condition with an asynchronous (out-of-phase) condition on fear acquisition, extinction learning, and delayed recall. Phase synchronization improved contingency knowledge and facilitated discrimination in terms of rated valence and arousal. However, synchronization did not modify conditioned responding in skin conductance responses and steady-state visually evoked potentials during acquisition, although both measures demonstrated the greatest response to the threat-predictive stimulus. Together, these data support a causal role of theta-phase synchronization in affective evaluation and contingency knowledge during fear acquisition. In Study 3 we extended the modulation of phase-synchronization from a theta to a slower delta rhythm and moreover, transferred our procedure into a web-based fear conditioning paradigm (due to the COVID-19 pandemic). In accordance with Study 2, phase-synchronization augmented the discrimination of generalization stimuli in contingency knowledge. However, it did not affect valence and arousal ratings. Interestingly, the effect of synchronization occurred independent of frequency, i.e., occurred after both theta and delta rhythm. Moreover, and as a prerequisite of Study 3, we proved the ability to successfully conduct complex generalization fear conditioning in an online setting. Together, our data of phase synchronization studies supports a causal role of phase synchronization in the declarative knowledge of contingency for low frequencies rather than in the specific theta frequency.

In sum, the current thesis provides the promising approach of using rhythmic sensory stimulation to modulate very early sensory processing as well as to directly manipulate the precise timing of to-be-associated stimuli in an aversive fear conditioning paradigm. Both methods emphasize the importance of oscillatory brain activity by offering non-invasive ways of direct modulations in order to modify selected stages of the fear learning and memory (e.g., fear acquisition, extinction, and delayed recall).

1 Introduction

1.1 Overview

The ability to memorize and retrieve information is crucial to gain skills and knowledge, to represent lifetime experiences, for motor skills that help us to walk, jump, ride a bike, and adaptively adjust behavior when confronted with threats. The diversity of memories is depicted in a complexity of neuronal circuits that are involved during the encoding, consolidation, storage, and recall. One model to categorize long-term memory is the division into two major systems: explicit, or declarative memory and implicit or non-declarative memory (Sherry & Schacter, 1987). Briefly, explicit (or declarative) memories comprise episodic and semantic information, while implicit (or non-declarative) memory includes procedural information, habituation, and classical (fear) conditioning (Squire, 1998, 2004; Squire & Dede, 2015). Although the differentiation seems to be strict, they often interact instead of existing independent of each other (Squire, 2004).

From basic science as well as due to memory-related disorders like Alzheimer's disease or post-traumatic stress disorders (PTSD) and phobias, there is great interest in a neurobiological understanding of memory processing and its malfunctioning. The formation of memory depends on increased efficiency of information transfer via long-term potentiation (LTP) that ultimately leads to cellular reorganizations and strengthened synaptic connections (Fries, 2005; Lynch, 2004). LTP was most extensively examined in the hippocampal formation, a structure that is especially known for its involvement in encoding, consolidation, and retrieval of declarative memory (Bliss et al., 2018). In a first study, high-frequency tetanic stimulations within the hippocampus of rabbits led to sustained strengthening of the synaptic transmission (Bliss & Lomo). In accordance with Hebb's rule postulating that "cells that fire together wire together" (R. Morris, 1999), this strengthening requires the simultaneous activation of the pre-synapse and a depolarization of the post-synapse (section 1.2).

Besides the established role of LTP in the hippocampus, it was also found in other structures like the amygdala, sensory cortices and the prefrontal cortex (Lynch, 2004), and different types of memory. Importantly, *fear conditioning* is based on *associations* between an initially neutral stimulus and an innate or unconditioned aversive stimulus (section 1.3). It is well-established that the convergence of both stimuli, that often stem from different sensory systems (e.g., a neutral visual and aversive nociceptive stimulus) happens in the lateral nucleus of the amygdala. Here, the

temporal proximity of activating a weak synapse of the initially neutral input and the strong synapse of the innate aversive input lead to synaptic strengthening of the weak synapse via associative LTP (Blair et al., 2001; Orsini & Maren, 2012). As a result, the neutral stimulus receives a threat-predictive value and, hence, elicits fear responses itself. The *main neural circuitry of fear conditioning* comprises the amygdala, the hippocampus, as well as two subdivisions of the medial prefrontal cortex (mPFC, section 1.3.1). In addition, research also revealed fear-conditioning *induced changes in early cortical processing*: Sensory cortices not only receive and process the afferent sensory input stemming from the associated stimuli, but are also affected by structural and functional changes as a consequence of fear conditioning (Bhattarai et al., 2020; Leon et al., 2017; McGann, 2015; Miskovic & Keil, 2012; Rhodes et al., 2018; Thomas et al., 2020; Weinberger et al., 1993). Increased neural processing as early as in primary sensory cortices is assumed to facilitate detection of threat-predictive stimuli (Padmala & Pessoa, 2008). Addressing these plasticity-related changes and its persistence in the visual cortex, Study 1 of the current thesis used sensory repetitive rhythmic stimulation that elicits so-called steady-state visually evoked potentials (ssVEPs) as a special form of electroencephalography (EEG) measures, providing a high signal-to-noise ratio (section 1.3.2).

Fear conditioning is also a great translational model that can be used in humans and animals likewise (LeDoux, 2000). On a neurobiological perspective, however, translational work is challenging: invasive techniques, like stimulation and measuring of LTP within tissue slices of rodents, or more advanced methods like opto- or chemogenetics that allow direct manipulations on a molecular basis cannot be used in human studies (so far at least). One way to still assess changes of stimulus-driven brain activity in animals and humans is the examination of neural *oscillations.* Oscillations are rhythmic fluctuations of neuronal activity that define the degree of excitability at a certain point in time (oscillatory phase; Fell & Axmacher, 2011; Headley & Paré, 2017). When neuronal assemblies within or between brain structures synchronize their oscillatory phase, the orchestrated activity enhances communication and supports synaptic plasticity by increasing the likelihood of generating action potentials. Oscillations occur in different frequency bands that are related to cognition (Jensen et al., 2019). It is assumed that slower rhythms in the *delta or theta range* are specifically suited for communication between distinct brain regions and optimized synaptic plasticity, while faster oscillations (e.g., in the gamma range) coordinate local neuronal activity (Arnulfo et al., 2020). Importantly, synchronized activity of neuronal assemblies is strong

enough to be recordable on the scalp via EEG and therefore provide a non-invasive tool for studying changes in the brain's activity in humans.

Concerning memory processing, oscillations in the theta range[1] - although not exclusively - seem to provide optimal time windows for neural communication and synaptic plasticity (Headley & Paré, 2017). Rodent research as well as human EEG studies revealed increased theta power and synchronization between memory-relevant brain structures during declarative memory task, as well as during various stages of classical fear conditioning (declarative memory: e.g., Fell et al., 2001; Weiss & Rappelsberger, 2000; Place et al., 2016; fear conditioning: e.g., Stujenske et al., 2014; Lesting et al., 2011). Since findings in humans mainly rely on theta oscillations as an indicator of memory, they do not allow causal interpretation. However, a growing number of studies uses rhythmic sensory stimulation to directly 'force' cortical brain activity to synchronize with an external stimulation frequency (so called *entrainment;* Herrmann et al., 2016). Besides the advantages of entraining cortical rhythms with a high signal-to-noise ratio, this approach can be used as "poor men's optogenetic" (Hanslmayr et al., 2019): it opens the possibility to manipulate brain activity and measure its effects on behavioral or physiological outcomes. Interestingly, frequency-modulated sensory stimulation was shown to not only affect cortical areas, like the visual or auditory cortex, but even reached deeper structures like the medial temoral lobe (Becher et al., 2015; Hanslmayr et al., 2019). Hence, rhythmic sensory stimulation might allow the investigation of higher-order processing. Since theta oscillations and its synchronization between memory-related brain regions were already found as an *indicator* for memory encoding and recall (Fell et al., 2001; Summerfield & Mangels, 2005; Weiss & Rappelsberger, 2000), Clouter et al. (2017) used synchronized theta stimulation to provide direct evidence for its *causal* role in the formation of *multimodal associations*: Theta-modulated video-tone pairings (compared with other frequency bands) that were synchronously presented resulted in a better recall of the associations, while asynchronous presentation did not improve memory. Therefore, the study proved for the first time that theta-phase synchronization is causally involved in the encoding of declarative multimodal associations.

Although theta phase synchronization within the fear circuitry was also validated as an indicator of fear expression (Karalis et al., 2016; Lesting et al., 2013; Seidenbecher et al., 2003; Taub et al.,

---

[1]typically ranging from 4-8 Hz in humans and 4-12 Hz in rodents

2018; Zheng et al., 2019; for reviews see Bocchio et al., 2017; Çalışkan & Stork, 2018), its causal role in forming the association between initially neutral and innate aversive stimuli is unknown. To close this gap, Study 2 and Study 3 of the current thesis address the question if *phase synchronization* in a memory-related *theta frequency range* (Study 2) is also directly involved in the acquisition of *fear* memories and has persistent effects throughout extinction and delayed recall, as assessed in fear conditioning paradigms. In addition, the frequency-specificity was tested by comparing theta-phase synchronization with the synchronization in a delta frequency range (Study 2), in one of the first web-based fear conditioning studies. In accordance with Study 1, where we used *visual* repetitive stimulation only, Study 2 and 3 added a frequency-modulated aversive *auditory* stimulus that varied in phase, in relation to the visual stimuli.

In sum, the current thesis aimed at measuring and manipulating brain activity by repetitive rhythmic stimulation in one or two sensory modalities that are involved in fear conditioning. Specifically, we 1) probed the visuocortical engagement during fear acquisition and extinction and its persistence over time during delayed recall and 2) investigated the causal role of theta-specific phase synchronization for the acquisition of multisensory fear memories and their putative persistence after extinction (Study 2-3) and in delayed recall (Study 2).

1.2   The role of neural oscillations for declarative memory

Depending on the content and the way it is recalled, memory is typically divided into an explicit and implicit system. While explicit memories describe information we can consciously recall, like a recollection of specific events from the past, or facts we have acquired, our memory also stores information that are implicitly encoded and recalled more automatically (Squire & Dede, 2015). Despite this apparent distinction of both memory systems they often interact and share common neurobiological mechanisms. As one of these mechanisms, neuronal oscillations are addressed in detail in the following (Headley & Paré, 2017).

Since various brain structures are involved in memory processing, precise communication between and within those structures is necessary for efficient information transfer. Oscillations are assumed to coordinate activity of neuronal assemblies by rhythmically modulating the degree of excitability from an excitatory (peak) to an inhibitory (trough) state (Fell & Axmacher, 2011). Typically, *neural oscillations* are categorized by frequency ranges from low to high (delta, theta, alpha, beta, and gamma). The oscillatory peaks are associated with increased probability of sending as well as

receiving information (Fries, 2005). Therefore, neuronal assemblies that synchronize their oscillatory phase provide optimal windows for communication ('communication through coherence'; Fries, 2005). In a similar vein, synchronized oscillations increase the likelihood of inducing synaptic plasticity – a mechanism that is key for memory processing. It is based on the idea that a large number of neurons, firing in phase-synchrony, i.e., reach the maximum of excitability at the same time when arriving at the post-synapse, are easily successful in eliciting strong depolarization. This can result in cellular reorganizations on the longer run (also known as spike timing-dependent plasticity; Jutras & Buffalo, 2010).

Animal and human studies revealed increased phase synchronization as an *indicator* for declarative memory during and after successful encoding. For example, oscillatory phase coherence in the theta-frequency was found between the hippocampus and the prefrontal cortex in rats that acquired new rules predicting a reward in a hippocampus-dependent Y-maze task (Benchenane et al., 2010). Support for this findings comes from intracranial EEG recordings in humans that showed increased theta synchronization between the same structures during encoding of contextually unexpected (compared with expected) images and, more importantly, for those images that were later remembered (Gruber et al., 2018; for similar results see: Fell et al., 2001; Summerfield & Mangels, 2005; Weiss & Rappelsberger, 2000).

On the cellular level, simultaneous (i.e., *synchronized*) *activity of pre- and postsynaptic* neurons is necessary for the induction for LTP or long-term depression (LTD), two important mechanisms of synaptic plasticity. First evidence of the induction of LTP came from the rabbit hippocampus (Bliss & Lomo, 1973). Tetanic stimulation of the perforant path (forming the synapse between the entorhinal cortex and the dentate gyrus) resulted in synaptic potentiation that persisted over time. Since then, numerous works confirmed and extended this early finding and established the major characteristics of LTP: input-specificity, cooperativity, associativity, and persistence. Of specific interest, LTP requires both a sufficient stimulation intensity at the pre-synaptic neuron, and a simultaneous depolarization at the post-synaptic neuron, a phenomenon that is based on the properties of glutamatergic N-methyl-D-aspartate (NMDA) receptors (Bliss et al., 2018). Only when simultaneously activated, magnesium that blocks the ion channel of NMDA receptors is released and leads to a rapid influx of calcium ions, initiating a cascade of reactions that is, inter alia, responsible for the synaptic strengthening and the persistence of LTP (Alford et al., 1993; Bliss et al., 2018; Herron et al., 1986). Interestingly, pharmacologically evoking theta oscillations

within the hippocampus *in-vitro* and evoking stimulation bursts at the peak vs the trough of a given theta oscillatory phase resulted in the induction of LTP or LTD, respectively (Huerta & Lisman, 1995). Therefore, stimulations in a theta rhythm seems to be specifically suitable for the induction of long-lasting synaptic changes (via LTP), and therefore provides a mechanism that serves memory processing.

Given that precisely timed activity of presynaptic and postsynaptic neurons is a prerequisite for the induction of LTP and thereby for memory processing, neuronal oscillations constitute a putative neurophysiological mechanism facilitating LTP and memory by synchronizing presynaptic activity with postsynaptic excitation (Fell & Axmacher, 2011). However, most of the evidence regarding the role of phase-synchronized oscillations for memory processing is mere correlative. But, importantly, recent research focuses on the *causal* role of phase synchronization for declarative memory by manipulating neuronal activity using a special form of entrainment via two distinct sources (Hanslmayr et al., 2019).

Entrainment per se can be achieved by repetitive rhythmic stimulation either with non-invasive electric or magnetic devices (e.g., transmagnetic stimulation, TMS), invasive electrical devices, or simple sensory stimulation (Hanslmayr et al., 2019; Herrmann et al., 2016). By stimulating the brain rhythmically, it responds with oscillations at the given frequency (so called steady-state responses, SSRs). Therefore, entrainment directly modulates neuronal activity, allowing causal interpretations of effects that result from this modulation. Of importance, entraining sensory areas via sensory stimulation seems to not only affect the corresponding cortices, but was instead even shown to reach deeper brain structures like the temporal lobe: For instance, in epileptic patients with temporal depth electrodes, auditory stimulation successfully modulated EEG power and phase synchronization in temporal brain regions (Becher et al., 2015).

First evidence for the *causal role of phase synchronization* across cortical sites for cognitive performance in humans came from Polanía et al. (2012). During a delayed discrimination recognition task reflecting working memory and sensori-motor decision making, they applied transcranial alternating current stimulation to elicit theta (6 Hz) oscillations in frontal and parietal regions either synchronously (0° phase shift) or asynchronously (180° phase shift). Synchronized theta resulted in attenuated reaction times (indicating better performance) compared with asynchronized or sham stimulation. Therefore, the study was the first in providing *direct* evidence

for the advantage of inter-regionally coordinated oscillations (via phase synchronization) in (working) memory.

Assuming that the formation of memories often involves the binding of multisensory features of a single item or event that are processed in distinct brain regions, coordinated inter-regional neuronal activity is needed that might be provided by oscillatory synchronization. Indeed, an elegant experiment in humans (Clouter et al., 2017) used repetitive rhythmic stimulation of visual and auditory stimuli to examine the causal role of phase synchronization for binding multisensory associations in a declarative memory task: During encoding, *video-tone pairs* were presented rhythmically at a 4 Hz theta frequency in one of two conditions: either in-phase (i.e., 0° phase lag between video and tone) or out-of-phase (i.e., with 90°, 180°, or 270° phase lags between video and tone). Subsequent memory retrieval (forced choice task) revealed a better memory for video-tone pairs that had been presented synchronously compared to those that were present in phase-lag. Intriguingly, the memory-improving effects of phase-synchronized input were restricted to the theta frequency but did not occur in delta (1.7 Hz), alpha (10.5 Hz), and in a non-flickering condition. Moreover, a replication in the same group extended the findings on a trial-by-trial basis and revealed that the degree of phase synchronization during encoding predicted subsequent memory improvement (Wang et al., 2018).

In sum, theta-phase synchronization seems to be a relevant mechanism for the communication between memory-relevant brain areas as well as the induction of synaptic plasticity as a basis of memory processing. In addition, the recent study of Clouter et al. (2017) provides an interesting and promising approach, to non-invasively modulate the frequency and phase of oscillatory activity in humans. This should be extended to other forms than declarative memories.

1.3 Fear conditioning

Classical fear conditioning – typically considered as a form of implicit memory – is used to study the formation, maintenance, recall, and extinction of emotional associative memories. The standard protocol comprises fear acquisition, consolidation, and fear recall as well as extinction acquisition, extinction consolidation, and extinction recall that are described below.

During fear acquisition, an initially neutral stimulus is repeatedly paired with an aversive unconditioned stimulus (US). When a successful association is formed between both stimuli, the

neutral stimulus that is now termed conditioned stimulus (CS), becomes predictive to the threat and hence, elicits a conditioned fear response (CR) itself. Fear responses in rodent laboratory studies are typically measured by freezing behavior (a defensive reaction that is characterized by suppressed movements during threat encounters; Anagnostaras et al., 2010; Bolles, 1970) or avoidance (Bolles, 1970). In humans, conditioned responses are often assessed via physiological responses (e.g., heart rate increase or skin-conductance), subjective ratings (e.g., valence and arousal ratings), changes in brain activity (e.g., increased EEG power in sensory regions), or the knowledge of the CS-US contingency (Lonsdorf et al., 2017). Besides single-cue paradigms or simple differential conditioning paradigms (with *one* CS+ and *one* CS-), human fear conditioning uses complex differential paradigms, including multiple CSs: here, one or multiple CS+ are paired with the US, while multiple CS- serve as safety stimuli (Lonsdorf et al., 2017). Depending on the similarity and the number of CS+ and CS-, differential conditioning can be used to assess the generalization of fear.

When the CS loses it predictive character for the US, the CR (as an indicator of the CS-US association) should decline gradually. To achieve a reduction of the CR, the CS is repeatedly presented without US during extinction acquisition. Importantly, extinction does not erase the existing CS-US fear association, but forms a second CS-noUS memory trace that can inhibit the fear response (Bouton & Moody, 2004; Milad & Quirk, 2012). The existence of two concurrent associations becomes apparent in *return-of-fear phenomena*: Despite a successful extinction, the recovery of fear responses towards the CS was observed after the mere passage of time (spontaneous recovery), a single presentation of the US (reinstatement), and presentation of the CS in a context that differs from the extinction acquisition context (renewal) (Bouton et al., 2021; Bouton & Moody, 2004).

Since fear conditioning is a well-established paradigm for the development, maintenance, and treatment of anxiety- and trauma-related disorders like phobias and PTSD, there is a great interest in understanding the underlying neurophysiological mechanisms. Therefore, the following sections describes brain structures that are typically included in the main *fear circuitry* (section 1.3.1) and presents some findings of the involvement of distributed fear networks, specifically the sensory cortices (section 1.3.2).

1.3.1 Neuronal correlates of fear conditioning: The main fear circuitry

Three major structures are of specific importance in fear conditioning: the amygdala including several subdivisions, parts of the mPFC, as well as the hippocampus. The amygdala is important for the acquisition, storage, and expression of fear (Duvarci & Pare, 2014). It is typically divided in the basolateral amygdala (BLA) including the lateral amygdala (LA) and basal amygdala, the central amygdala (CeA), and intercalated cell masses (ITC). The amygdala receives input from sensory regions, and connects with brain stem areas that are involved in the generation of fear responses (LeDoux & Pine, 2016). In detail, sensory information of mostly multimodal CS and US converges on the same population of neurons in the lateral amygdala (Barot et al., 2008; Romanski et al., 1993) via thalamic and cortical pathways (Orsini & Maren, 2012). While the activation of a strong US synapse causes depolarization of the post-synapse, the initially weak CS synapse does not. However, due to the temporal proximity of CS and US activation, the convergence in the LA meets the requirements of LTP (i.e., activation of a pre-synapse and depolarization of the post-synapse) and therefore the initially weak CS-synapse becomes stronger (Bauer et al., 2002; Humeau et al., 2005; LeDoux, 2000; Maren, 2001; Quirk et al., 1995). The necessity of temporal proximity was confirmed by an optogenetic study in rats that stimulated LA neurons as an US substitute (Johansen et al., 2010). Interestingly, only the pairing of activation by auditory CS presentations and the optogenetic activation of LA neurons (US) resulted in acquisition of fear conditioned responses (i.e., freezing), while the unpaired stimulation did not. Although this study highlights that the encoding of conditioned fear memories is based on Hebbian mechanisms that specifically depend on temporally precise CS and the US convergence, the exact process of *how* the pairing of CS and US lead to LTP of the CS-synapse in the BLA is still unknown (Sun et al., 2020).

After the initial convergence of CS and US, the LA directly and indirectly (e.g., via the basal nucleus of the amygdala) projects to the CeA of the amygdala that is assumed as the main output structure of the fear circuitry (Maren, 2001). The CeA projects to regions like the periaqueductal grey, lateral hypothalamus, or the paraventricular nucleus of the hypothalamus and thus directly initiates physiological, behavioral, and endocrine fear responses (e.g., increased heart rate, freezing, or the release of stress hormones like glucocorticoids; Orsini & Maren, 2012). Accordingly, lesions of the CeA were shown to disrupt fear expression in rhesus monkeys (Kalin et al., 2004) and rats (Hitchcock & Davis, 1991). Of specific importance for extinction, the ITCs

also receive input from the LA and contains inhibitory projections to the CeA. When the ITCs are activated, they prevent the CeA from the initiation of a fear response (Rudy, 2014). Besides the intra-regional connections, the amygdala receives input from two subdivisions of the mPFC with contrasting effects: While the dorsal anterior cingulate cortex (dACC, or prelimibic cortex in rodents) is involved in the expression of fear, the ventromedial prefrontal cortex (vmPFC, or infralimbic cortex in rodents) is assumed to be important in the inhibition of fear responses by activating inhibitory ITCs and thus, plays a specific role for fear extinction (Fullana et al., 2020; Milad & Quirk, 2012; Myers & Davis, 2007). In addition, the hippocampus holds reciprocal connections with the amygdala and is thought to assemble contextual information which can also form an association with the US itself (Maren et al., 2013). Importantly, it is well-established that extinction is highly dependent on context information (and hence, on the hippocampus). This has specific clinical relevance, since exposure therapies that are based on extinction mechanisms often observe fear renewal outside the therapeutic context (Maren et al., 2013; Myers & Davis, 2007).

1.3.2 Fear conditioning in distributed networks: The role of sensory cortices

Besides the typical fear network described above, fear conditioning was also found to induce synaptic changes in distributed networks that include the *sensory cortices* (Herry & Johansen, 2014). The aversive character that the CS receives during the pairing with an aversive US was found to directly affect sensory processing (McGann, 2015). Auditory fear conditioning in rodents (Bakin & Weinberger, 1990; Edeline et al., 1993; Edeline & Weinberger, 1991, 1993; Galván & Weinberger, 2002; Weinberger et al., 1993; for a review see Weinberger, 2015; Weinberger & Bakin, 1998) revealed a frequency-specific modulation of the tonotopic neuronal response in the primary auditory cortex that was characterized by increased activity towards the CS frequency after it was paired with a US. Comparable effects were found in human positron emission tomopraphy (PET) studies (Molchan et al., 1994; J. S. Morris et al., 1998) and a human functional magnetic resonance imaging (fMRI) study that revealed conditioning-related changes of neuronal activity in the primary visual cortex for visual CS that were paired with the US (compared with unpaired CS-US presentations; Knight et al. 1999).

In addition, human EEG studies (generally known for their temporal precision) found increased activity to visual CS+ within a few hundred milliseconds (Dolan et al., 2006; Montoya et al., 1996; Steinberg et al., 2013; Wong et al., 1997). For example, enhanced responses were found as early as 65-90 ms (i.e., retinotopic C1 event-related potential component) after perceptually simple

grating stimuli were paired with the US (Stolarova et al., 2006). The finding suggested that the earliest processing stage is involved in extracting simple features of threat-predictive cues, probably to enable fast and efficient discriminations (Miskovic & Keil, 2012). Further evidence for better discrimination following fear conditioning was given by McTeague et al. (2015): They used a fear generalization paradigm, with 7 Gabor gratings that slightly (by always 10 degrees) differed in orientation. To assess visuocortical activity, they measured ssVEPs: ssVEPs are specific brain responses that are usually generated in the extended visual cortex with strong contributions of the primary visual cortex (Di Russo et al., 2007). They are generated by presenting rhythmic repetitive (or flickering) stimuli, typically at frequencies around 8-10 Hz (Norcia et al., 2015). Interestingly, the cortical activity (i.e., the ssVEPs) tends to adopt the frequency of the external rhythm, hence it provides a very good signal-to-noise ratio that enables the detection of even small amplitude differences (Keil et al., 2003). McTeague et al. (2015) obtained evidence for conditioning-induced discrimination improvements (i.e., discrimination of CS+ and the most similar CS- gratings), indicating that neurons in the visual cortex sharpened their orientation when subjects acquired aversive contingencies via fear conditioning and prioritize the processing of aversive cues. In contrast, the visual association cortex (i.e., the parietal cortex) showed a generalization pattern across the CS gratings during acquisition. Interestingly – and indicating its sensitivity to conditioning principles – this generalization pattern was reduced or even reversed during extinction acquisition. However, the authors did not assess the cortical responses after consolidation in a delayed recall, to test for potential return-of-fear phenomena. In a first fMRI study, extinction-resistant cortical enhancement was revealed in humans (Apergis-Schoute et al., 2014). Using a 2-day auditory conditioning paradigm, the study demonstrated higher blood-oxygen-level-dependent-imaging signals in the auditory association cortex on day 2, while behavioral measures did not show any signs of returned fear during the re-extinction, suggesting that the sensory cortex might remain cautious to act fast in case the threat predictive stimulus returns.

In order to examine potential extinction-resistant cortical activity for *visual* fear conditioning, Study 1 of the current thesis used the generalization design of McTeague et al. (2015) with an additional day 2: Assessing visuocortical engagement in a 24-hour delayed recall allows to account for extinction resistant tunings that might be related to perceptual or attentional biases that are related to affective- and anxiety-related disorders, and thus also of high clinical relevance.

1.3.3 The role of theta oscillations and synchronization in fear conditioning

The previously described involvement of various brain regions in the acquisition, extinction, and recall of established fear and extinction memories requires a communication mechanism that enables an efficient information. *Theta oscillations* were repeatedly shown to provide optimized windows for communication and synaptic plasticity by coordinating neuronal activity within and between distant brain regions (extensively reviewed in: Fell & Axmacher, 2011; Headley & Paré, 2017) covering those that are involved in the main fear circuitry (i.e., amygdala, mPFC, hippocampus). Thus, theta oscillations were examined as an *indicator* in fear acquisition (Taub et al., 2018), consolidation (e.g., Popa et al., 2010), retrieval, and extinction (e.g., Karalis et al., 2016; Lesting et al., 2011).

[A] Rodent studies

Most findings in rodents focused on the involvement of theta oscillations and, more importantly, theta phase synchronization during the *retrieval* of fear memories. Therefore, in the following I will first present studies that indicate the involvement of theta phase synchronization in the *retrieval of fear*, before I move on to single findings addressing the role of theta synchronization in fear consolidation and fear acquisition.

Retrieval of fear: In a first study, Seidenbecher et al. (2003) used a differential fear conditioning paradigm in mice and recorded field potentials in the LA as well as in the hippocampal CA1. During retrieval of fear they found increased theta power in both regions and cross-correlation analysis revealed increasing theta-phase synchronization towards the CS+ in fear-conditioned mice. In contrast, no synchronization occurred in mice that received unpaired CS-US presentations. The results suggested a potential role of theta-phase synchronization in the retrieval of conditioned fear, presumably by improving communication between the involved structures of the fear network. Further studies confirmed the involvement of theta-phase synchronization between the hippocampus and amygdala and found similar oscillatory activity between the dorsomedial mPFC (dmPFC) and the BLA during fear retrieval that was associated with freezing behavior (Karalis et al., 2016; Lesting et al., 2011; Lesting et al., 2013; Likhtik et al., 2014). Interestingly, Likhtik et al. (2014) found that only those mice that properly discriminated between a threat-predicting CS+ and the safety CS- showed CS-type specific increases in theta synchronization between the BLA and mPFC, while theta synchronization in mice that generalized across the CS did not differ between

CS+ and CS-. Therefore, increased communication via theta synchronization between mPFC and BLA was suggested to be involved in evaluative processes of threat and safety.

In addition to the correlative evidence, some of the described animal studies also addressed the *causal role* of theta synchronization: For instance, microstimulation in the hippocampal CA1 and LA was used to entrain both regions in theta frequency either in-phase (0° lag between theta peak in the CA1 and the theta peak in LA) or out-of-phase (180° lag; Lesting et al. 2011). Only phase-synchronized theta stimulation resulted in prolonged freezing towards the CS+ during extinction learning (indicating extinction resistance), and additionally impaired extinction recall. Accordingly, decreased synchronization (either correlatively measured or induced via out-of-phase stimulation) within the BLA-hippocampus-mPFC network was related to reduced freezing during extinction (Lesting et al., 2011). In addition, Karalis et al. (2016) first demonstrated theta synchronized oscillations (4 Hz) in the dmPFC-BLA pathway as an indicator for freezing. In a second step, they manipulated dmPFC oscillations optogenetically. Their results indicated that dmPFC 4-Hz oscillations synchronize the BLA activity and drive the fear response.

Consolidation of fear memories: Besides the suggested involvement of theta phase synchronization in the retrieval of fear, theta coherence was also observed in the amygdala and mPFC during paradoxical sleep in rats after fear conditioning procedure, indicating a potential role of phase synchronization in the consolidation of fear memories (Popa et al., 2010).

Acquisition of fear memories: Additionally, there is first evidence for increased synchronization during the initial formation of fear (i.e., fear acquisition): monkeys that were trained in an aversive tone-odor association task showed increased theta power as well as synchronization between the dACC and the amygdala, suggesting that the fear circuitry not only uses theta synchronization to communicate already conditioned fear or safety signals but also to initially form the aversive association (Taub et al., 2018).

[B] Human studies

Retrieval of fear memories: While the reported studies so far are based on animal work, human EEG-studies also provide convincing results regarding the role of theta oscillations in fear conditioning. In accordance with the findings in animals, fear retrieval was repeatedly related to enhanced theta power at fronto-central electrodes source-localized in the dACC (Bierwirth et al., 2021; Mueller et al., 2014; Sperl et al., 2019). Importantly, the results also suggested that theta

power enhances the communication between the main structures of the fear network as indicated by a positive correlation between fronto-central theta power (measured via EEG) and amygdala activity (measured via fMRI; Sperl et al., 2019). Moreover, a recent study utilized intracranial electrocorticogram recording in epileptic patients to assess theta oscillations in the fear network during fear acquisition (Chen et al., 2021), and revealed increased theta power as well as synchronization between the mPFC and the amygdala. In sum, theta-phase synchronization in humans is also assumed as an important mechanism for the communication between the relevant structures within the fear circuitry.

Although the sum of both animal and human studies provides convincing evidence that theta synchronization plays an important role during different phases of fear conditioning, most of these studies concentrate on the retrieval of fear and used oscillations as an *indicator* of fear expression.

However, so far there is no evidence that theta-phase synchronization is *causally involved in fear acquisition* and thus probably also in the subsequent stages of the fear process. Synchronization in the theta range might be an appropriate mechanism for the formation of the CS-US association for several reasons: first, associations in most fear conditioning paradigms comprise CS and US of different modalities that are processed in distinct sensory cortices and probably required to communicate in some way. Second, sensory information of both CS and US converge onto the same neural population in the LA (Romanski et al., 1993), where the temporal proximity of the activation of the strong US synapse and the weak CS synapse result in strengthening of the CS synapse via associative LTP. Here, theta-phase synchronization might coordinate the peak timing of both stimuli and hence, improve the likelihood for the induction of LTP. Third, Clouter et al. (2017) and Wang et al. (2018) already revealed convincing evidence that theta phase synchronization plays a *causal* role for the successful formation of multisensory associations in a declarative video-tone memory task by entraining phase synchronized vs. asynchronized theta oscillations via repetitive rhythmic stimulation. Study 2 of the current thesis therefore asked whether synchronized sensory input optimizes the formation of the multimodal CS-US association in aversive learning in a laboratory fear conditioning paradigm. To further guarantee that potential effects of phase synchronization are specific to the memory-related theta oscillations, we investigated the effects of theta-phase synchronization compared with synchronization modulations in a delta frequency in Study 3. Due to the ongoing COVID pandemic, we needed to conduct that study in an online setting and established one of the first web-based fear conditioning

approaches. We therefore also aimed at providing evidence for the possibility of using fear conditioning paradigms outside of the laboratory setting.

In sum, based on 1) evidence regarding the extended network of fear processing like the involvement of sensory cortices that is often neglected but might have important clinical implications and 2) missing evidence for the neurobiological mechanisms that are involved in the formation of the initial CS-US association, Study 1 probed the visuocortical engagement during fear acquisition and extinction and, importantly, its persistence over time, while Study 2 and 3 investigated the causal role of theta-specific phase synchronization (compared with a delta frequency) for the acquisition of multisensory fear memories and their putative persistence after extinction (Study 2-3) and in delayed recall (Study 2).

2 Objectives

The current thesis aimed at examining 1) the persistence of visuocortical tunings towards conditioned threat-predicting stimuli, i.e., how sharpened visual processing is affected by fear extinction learning, and how fear and extinction memory are recalled after a 24h consolidation phase. and 2) the causal role of theta-phase synchronization as a mechanism for the formation of the CS-US association during fear acquisition. For each question we used sensory repetitive rhythmical stimulation that is known to entrain neural activity (Herrmann et al., 2016). In Study 1, we chose sensory rhythmic stimulation to assess ssVEP as dependent measure for the visuocortical engagement during fear conditioning, because it is known for its great signal-to noise ratio and was previously linked to emotional memory (Keil et al., 2003). In Study 2 and 3 we took advantage of the possibility to directly modulate (i.e., entrain) neuronal activity with rhythmic presentations of two sensory stimuli. We examined the causal role of phase synchronization in theta (Study 2 and Study 3) vs. delta frequency (Study 3) for the acquisition of fear in a lab-based as well as a web-based paradigm. Besides ssVEPs that were measured for the visuocortical engagement via EEG, the lab-based Studies 1 and 2 recorded skin conductance responses as a valid indictor of physiological arousal. In addition, all studies included subjective ratings of valence and arousal and the declarative knowledge of CS-US contingency via US-expectancy ratings.

2.1 Study 1: Examining visuocortical engagement in fear conditioning using rhythmic visual stimuli

Detecting cues that predict threat is crucial to quickly prepare our bodies and brains for a potential fight or flight reaction. Fear conditioning was repeatedly shown to affect early sensory processing in the way that activation was prioritized for threat-predictive stimuli. As demonstrated by McTeague et al. (2015), a generalization fear conditioning paradigm with simple grating stimuli as CS even resulted in lower-tier visuocortical tunings towards one CS+ (out of 8 gratings including 6 CS- and 1 control stimulus) that was paired with the aversive US. It became apparent in larger ssVEP power towards the CS+ and lateral inhibition towards the most similar CS- gratings at occipital electrodes (i.e., primary visual cortex), suggesting an improvement in discrimination.

Interestingly, McTeague et al. (2015) found a reduction of that tuning during extinction learning or – for more parietal regions (association cortex) – even inverted generalization patterns. However, they did not account for fear and extinction recall (e.g. after 24 hours).

Besides some rodent work that found persistent changes in the auditory cortex for up to 8 weeks (e.g., Weinberger et al., 1993), only one human study addressed the question of persisting sensory tunings in an fMRI auditory fear conditioning study: Apergis-Schoute et al. (2014) revealed extinction resistant changes in the auditory association cortex, even though the physiological responses (skin conductance) as well as the amygdala activity subsided. It suggests that sensory processing remains alarmed in case a previously threat-predicting cue returns.

Consequently, to examine potential extinction-resistance, or in other words, return of tuning, Study 1 (Antov, Plog, Bierwirth, Keil, & Stockhorst, 2020) assessed ssVEPs that are specifically generated in the lower-tier retinotopic cortex. Further measures were skin conductance responses and subjective ratings assessing valence, arousal and declarative US-expectancy. The use of simple grating stimuli with slightly different orientations takes advantage of the orientation specificity of the primary visual cortex (Hubel & Wiesel, 1974) and allows the investigation of orientation-specific changes (tuning) towards the CS+. In accordance with the findings of McTeague et al. (2015), for fear acquisition we expected visuocortical tunings with increased ssVEP power towards the CS+ and reduced power towards the most similar CS- gratings, therefore resembling a lateral inhibition pattern. In addition, peripheral and subjective fear measures (i.e., skin conductance responses, subjective valence and arousal ratings, and US-expectancy ratings) were expected to gradually decrease with decreasing similarity to the CS+, resembling a generalization pattern. Importantly, for the first time, we tested the persistence of early visuocortical tunings, conducting a delayed recall after a consolidation period of 24 hours. Visuocortical prioritization of previously threat-predictive stimuli that sustains after successful extinction might have implications for the understanding of the neurobiology of return-of-fear phenomena that are of clinical importance for affective and anxiety disorders. For example, persistently biased perception might direct the attention to aversively-connoted stimuli or play a role for visually-driven flashbacks that are typical for PTSD.

2.2 Study 2[2]: Examining the causal role of theta-phase synchronization (vs. phase asynchronization) during encoding a fear association in laboratory fear conditioning

In Study 1 (Antov et al., 2020), ssVEPs, elicited by repetitive rhythmic stimulation, were measured as dependent variable for the visuocortical engagement in fear conditioning using a rhythmically modulated visual CS and a static auditory US. In Study 2 (Plog, Antov, Bierwirth, Keil, & Stockhorst, 2022) we switched the focus to stimulation in *two* sensory systems, in a theta-rhythm: here, visual and acoustical stimuli were sinusoidal modulated in order to examine if theta-phase synchronization plays a causal role for the acquisition and encoding of fear. First evidence for the successful application of the "poor men's optogenetic" (Hanslmayr et al., 2019), comes from a declarative video-tone association memory: 4-Hz luminance-modulated videos and 4-Hz amplitude-modulated audios were used to manipulate the exact phase synchronization, i.e., either in-phase (0° lag peak-to-peak) or out-of-phase (90°, 180°, or 270° phase shift; Clouter et al., 2017). They revealed that phase-synchronized video-tone presentations (vs. asynchronous presentation) only in the theta frequency (compared with delta and alpha) resulted in improved memory recall.

Given that fear conditioning typically includes multimodal CS and US that converge onto the same neuron populations in the LA (Romanski et al., 1993), we addressed the question if theta-phase synchronization improves the formation of the CS-US association during fear acquisition and is evident in responding in the subsequent learning phases (extinction learning, and delayed recall). Using a generalization paradigm similar to that of Study 1, we expected that phase-synchronous CS-US presentation (compared with phase-asynchronous presentation) provides optimized conditions for afferent signals to reach further brain structures within the fear circuitry, especially the LA (LeDoux, 2000). More specifically, we investigated memory-improving effects of theta-phase synchronization by assessing different response systems in human fear conditioning covering physiological arousal (skin-conductance responses), visuocortical engagement (via ssVEPs), the subjective evaluation of valence and arousal (affective ratings), and the declarative knowledge of CS-US contingency (US-expectancy ratings).

2.3 Study 3[2]: Examining the causal role of phase synchronization and theta-phase specificity in a web-based fear conditioning paradigm

The results of Study 2 demonstrated memory-improving effects in affective evaluation and declarative knowledge of CS-US contingency with better discrimination between CS+ and similar CS- gratings after phase-synchronized (vs. asynchronized) CS-US presentation in a 4-Hz theta frequency. However, since phase-synchronization was modulated only in theta without comparing it to an additional frequency band (e.g., delta, alpha, or beta) in Study 2, it did not account for frequency specificity. In Study 3 (Plog, Antov, Bierwirth, & Stockhorst, under review), we therefore addressed this question by using in-phase vs. out-of-phase synchronization modulation not only in theta, but in an additional delta frequency (1.7 Hz corresponding to the declarative-memory study of Clouter et al., 2017). Moreover, due to the COVID-19 pandemic, Study 3 was not conducted in the laboratory but instead we developed one of the first web-based fear conditioning procedures, using the almost exact paradigm of Study 2. Due to the web-based approach, we only assessed subjective valence and arousal ratings as well as the declarative knowledge of CS-US contingency but could not measure physiological arousal (skin conductance response) or visuocortical engagement via EEG. Based on the findings of Study 2, we expected that phase asynchronization (compared with synchronization) in the theta-band results in higher US-expectancy ratings towards all CS, as manifested in a broad generalization. In contrast, delta phase synchronization should result in a comparably broad generalization pattern after both, in-phase and out-of-phase CS-US presentation. Additionally, theta-phase synchronization was expected to improve discriminative fear learning between the CS+ and most similar CS- gratings in valence, arousal, and US-expectancies: For theta, we expect a narrow generalization (i.e., better discrimination) after in-phase presentation compared with a broad generalization in the out-of-phase group (i.e., attenuated discrimination). Frequency-modulation in a delta frequency should manifest in a broad generalization pattern, independent of the synchronization condition.

3   General methods

The following section addresses the similarities and differences in the fear conditioning procedure of Study 1-3, the visual stimuli that were used as CS, as well as the auditory stimulus that served as US (**Figure 1**).

3.1   Overall fear conditioning procedure

In all studies (Study 1-3), we used a generalization fear conditioning paradigm, including one CS+ and multiple CS- that were symmetrically distributed around the CS+ with decreasing similarity (**Figure 1A**). The fear conditioning procedure in Study 1 and Study 2 were conducted in the laboratory on 2 consecutive days: Day 1 included habituation, fear acquisition, and extinction; after 24 hours, i.e., on day 2, a delayed recall took place. Study 3 which was conducted in an online-setting, was restricted to day 1, i.e., it included habituation, fear acquisition, and extinction, but no delayed recall (**Figure 1B**).

In contrast to McTeague et al. (2015), who presented each CS 8 times per learning phase, we doubled the number in Study 1, using 16 presentations for each of 8 CS (including 1 CS+, 6 similar CS- and 1 control stimulus), leading to a total of 128 CS presentations in each learning phase (i.e., habituation, acquisition, extinction and the 24-hour delayed recall). The adjustment was made, since we did not use an instructed CS-US contingency protocol[3]. Within acquisition only, the CS+ was paired with the aversive auditory US at a reinforcement rate of 100 %. Since in Study 1, we observed habituation effects in the second half of the trials, in Study 2 and 3 we reduced the number of CS and US presentation: here, each of only 5 CS (including 1 CS+ and 4 CS-) were presented 12 times per learning phase, resulting in a total of 60 trials. Importantly, 12 presentations enabled to have the same number of each phase shift in the out-of-phase group. Again, the CS+ was paired with the aversive auditory US during acquisition only (**Figure 1B**).

---

[3]McTeague et al. (2015) specifically instructed the participants about the exact CS that will be followed by the US prior to fear acquisition. In Study 1 of the current thesis, we only informed the participants that an aversive US will follow one of the CS, without specifying the exact CS.

Figure 1. Experimental design: stimuli, procedure, and the operationalization of the rhythmic sensory stimulation. **A**, Gabor gratings used as CS. The 45° grating served as CS+ (paired with the US during acquisition) in Study 1-3. In Study 1, the other 6 (15° to 75°) plus the control -45° served as CS- (never paired with the US) in Study 2 and 3, CS- gratings comprised the four orientations 25°, 35°, 55°, and 65°. **B** depicts the fear-conditioning procedure for each Study 1-3. Study 1 comprised the learning phases habituation, fear acquisition, and extinction (day 1) and delayed recall (day 2). Each of the 8 CS gratings was presented 16 times in each learning phase. The US was only presented during fear acquisition (16 times co-terminating with the CS+). Study 2 covered the same learning phases as Study 1, however, this time, each of the 5 CS was presented only 12 times per learning phase. In addition, at the end of day 2, the unimodal audio task comprised 75 presentations of the 4 Hz modulated white noise (4 s each) at a non-aversive volume (maximum = 70.4 dB[A]). Study 3 was conducted in one day, including the learning phases habituation, acquisition, and extinction. In accordance with Study 2, each CS was presented 12 times. Prior to the conditioning procedure, participants conducted the audio-amplitude setting. Before habituation as well as after habituation, after acquisition, and after extinction, the compliance control task (CCT) took place. Vertical lines above the timeline in each study procedure indicate the rating time points. **C**, Operationalization of the rhythmic sensory stimulation. In Study 1, the visual CS were frequency-modulated at 14.167 or 15 Hz. Here, only the 15 Hz condition is shown. Black bars show the phase-reversed ("on", "off") modulation of the visual CS, the static auditory US is depicted in grey. In Study 2 and 3, each CS was luminance modulated in either 4 Hz (Study 2 and Study 3) or 1.7 Hz (Study 3). Similarly, the US was amplitude modulated at 4 Hz (Study 2 and Study 3) or 1.7 Hz (Study 3). In Study 2, the audio was presented with a maximum of 96.4 dB(A), in Study 3, the volume depended on the individual audio-amplitude titration. The left column (Study 2 and Study 3) shows phase shifts for the theta band: in-phase, i.e., 0° (beige) shift at the top and out-of-phase, i.e., 90° (light green), 180° (brown), 270° (dark green) shift at the bottom. The right column depicts the same phase-shifts for delta (Study 3).

In all studies, the participants rated each CS and the US for its subjective valence and arousal after habituation, acquisition, extinction, and in Study 1 and 2, before and after 24-hours delayed recall, using the 9-point Self-Assessment Manikins (SAM) scale (Bradley & Lang, 1994). Moreover, US-expectancy ratings were conducted together with the SAM ratings, starting after acquisition (**Figure 1B**). In the laboratory studies (Study 1 and Study 2), we additionally assessed ssVEPs via EEG for the visuocortical engagement and skin conductance responses as a well-established measure of physiological arousal (Boucsein et al., 2012). Electrocardiography and blood pressure were recorded as control parameters only.

3.2 Presentation of visual CS and auditory US

The CS in Study 1-3 were high-contrast, black-and-white Gabor gratings (sinusoidal gratings, filtered with a Gauss function) with a low spatial frequency. The 8 CS in Study 1 or 5 CS in Study 2 and 3, respectively, only differed in orientation relative to vertical 0°: Study 1 comprised grating orientations from 15° to 75° with steps of 10° between each grating (i.e., 15°, 25°, 35°, 45°, 55°, 65°, 75°) plus one -45° oriented grating that served as control stimulus. In Study 2 and 3, we removed the control stimulus as well as the 15° and 75° oriented grating for reasons of time efficiency, resulting in 5 CS (i.e., 25°, 35°, 45°, 55°, 65°). During acquisition, only the 45° orientation served as CS+ and was therefore paired with the aversive US in all studies (**Figure 1A**).

Importantly, each of the Studies 1-3 applied repetitive rhythmic stimulation that was differently modulated in each study in accordance with the particular aim.

Study 1 specifically focused on inducing ssVEPs via rhythmic sensory stimulation of the CS to assess the visuocortical tuning towards the CS+. Therefore, each CS gratings was presented reversing its phase at either 14.167 Hz and 15 Hz that resulted in a flickering "on-off" sensation of each grating (**Figure 1C top panel**). In Study 2 and 3, we used rhythmic sensory stimulation to entrain neural activity in a memory-related 4 Hz frequency (theta; Study 2 and 3) and an additional delta frequency (1.7 Hz; Study 3) as control. Instead of using phase-reversed presentations like in Study 1, the CS were luminance-modulated by multiplying the signal with a 4 Hz sine wave or 1.7 Hz sine wave (0-100 % luminance). We changed the modulation method to achieve gradual increases and decreases of luminance that allow the precise adjustment of phase shifts between the CS and the US (**Figure 1C bottom panel**).

In Study 1, we were not interested in precisely adjusted phase lags between the CS and US presentation. Therefore, the auditory US was a static 98 dB(A) 1-s white noise that co-terminating with each CS+ (**Figure 1C top panel**). In contrast, Study 2 and Study 3 used a 2-s amplitude-modulated auditory US (white noise) by multiplying the audio signal with a sine wave at 4 Hz (theta; Study 2 and 3) or 1.7 Hz (delta; Study 3). To achieve the correct modulation of CS-US phase-synchronization either in-phase or out-of-phase, the US onset was shifted in relation to the phase of CS+. For phase-synchronized CS-US presentation in both 4 Hz and 1.7 Hz, the US followed the CS+ with a phase shift of 0°. In contrast, in phase-asynchronized conditions, the US followed the CS+ with a phase lag of 90°, 180°, and 270° (**Figure 1C bottom panel**).

4   Studies

Paper status at the time of submitting the dissertation (May 24, 2022)

Study 1:

Antov, M. I., Plog, E., Bierwirth, P., Keil, A., & Stockhorst, U. (2020). Visuocortical tuning to a threat-related feature persists after extinction and consolidation of conditioned fear. *Scientific Reports, 10*. https://doi.org/s41598-020-60597-z

Study 2:

Plog, E., Antov, M. I., Bierwirth, P., Keil, A., & Stockhorst, U. (2022). Phase-Synchronized stimulus presentation augments contingency knowledge and affective evaluation in a fear-conditioning task. *ENeuro, 9*(1). https://doi.org/10.1523/ENEURO.0538-20.2021

Study 3:

Plog, E., Antov, M. I., Bierwirth, P., & Stockhorst, U. (under review). Effects of phase synchronization and frequency specificity in the encoding of conditioned fear – a web-based fear conditioning study

Paper status at the time of publishing the dissertation in the repository

Study 1:

Antov, M. I., Plog, E., Bierwirth, P., Keil, A., & Stockhorst, U. (2020). Visuocortical tuning to a threat-related feature persists after extinction and consolidation of conditioned fear. *Scientific Reports, 10*. https://doi.org/s41598-020-60597-z

Study 2:

Plog, E., Antov, M. I., Bierwirth, P., Keil, A., & Stockhorst, U. (2022). Phase-Synchronized stimulus presentation augments contingency knowledge and affective evaluation in a fear-conditioning task. *ENeuro, 9*(1). https://doi.org/10.1523/ENEURO.0538-20.2021

Study 3:

Plog, E., Antov, M. I., Bierwirth, P., & Stockhorst, U. (2023). Effects of phase synchronization and frequency specificity in the encoding of conditioned fear – a web-based fear conditioning study. PLOS ONE 18(3): e0281644. https://doi.org/10.1371/journal.pone.0281644

The printed version of the dissertation is available at Osnabrück University Library, Germany.

4.1 Visuocortical tuning to a threat-related feature persists after extinction and consolidation of conditioned fear

Abstract

Neurons in the visual cortex sharpen their orientation tuning as humans learn aversive contingencies. A stimulus orientation (CS+) that reliably predicts an aversive noise (unconditioned stimulus: US) is selectively enhanced in lower-tier visual cortex, while similar unpaired orientations (CS−) are inhibited. Here, we examine in male volunteers how sharpened visual processing is affected by fear extinction learning (where no US is presented), and how fear and extinction memory undergo consolidation one day after the original learning episode. Using ssVEPs from EEG in a fear generalization task, we found that extinction learning prompted rapid changes in orientation tuning: Both conditioned visuocortical and skin conductance responses to the CS+ were strongly reduced. Next-day re-testing (delayed recall) revealed a brief but precise return-of-tuning to the CS+ in visual cortex accompanied by a brief, more generalized return-of-fear in skin conductance. Explorative analyses also showed persistent tuning to the threat cue in higher visual areas, 24 h after successful extinction, outlasting peripheral responding. Together, experience-based changes in the sensitivity of visual neurons show response patterns consistent with memory consolidation and spontaneous recovery, the hallmarks of long-term neural plasticity.

The full text and online supplementary material of Study 1 can be found at:

https://www.nature.com/articles/s41598-020-60597-z

OPEN

Visuocortical tuning to a threat-related feature persists after extinction and consolidation of conditioned fear

Martin I. Antov [1*], Elena Plog[1], Philipp Bierwirth[1], Andreas Keil[2] & Ursula Stockhorst[1]

Neurons in the visual cortex sharpen their orientation tuning as humans learn aversive contingencies. A stimulus orientation (CS+) that reliably predicts an aversive noise (unconditioned stimulus: US) is selectively enhanced in lower-tier visual cortex, while similar unpaired orientations (CS−) are inhibited. Here, we examine in male volunteers how sharpened visual processing is affected by fear extinction learning (where no US is presented), and how fear and extinction memory undergo consolidation one day after the original learning episode. Using steady-state visually evoked potentials from electroencephalography in a fear generalization task, we found that extinction learning prompted rapid changes in orientation tuning: Both conditioned visuocortical and skin conductance responses to the CS+ were strongly reduced. Next-day re-testing (delayed recall) revealed a brief but precise return-of-tuning to the CS+ in visual cortex accompanied by a brief, more generalized return-of-fear in skin conductance. Explorative analyses also showed persistent tuning to the threat cue in higher visual areas, 24 h after successful extinction, outlasting peripheral responding. Together, experience-based changes in the sensitivity of visual neurons show response patterns consistent with memory consolidation and spontaneous recovery, the hallmarks of long-term neural plasticity.

Classical fear conditioning is a fundamental process of learning and memory in humans and other animals[1]. It enables them to predict threats from cues in the environment and to disregard cues that are no longer predictive. Fear conditioning is also a widely used model in basic neuroscience, psychiatry and neurology. During acquisition in the laboratory, a neutral stimulus predicting an aversive unconditioned stimulus (US) becomes conditioned (CS) and capable of eliciting a defensive response when presented alone. In extinction learning, the CS is repeatedly presented without the US and conditioned responses decline[1–3]. The neural circuitry of fear acquisition and extinction is well established in rodent and primate models and includes the "fear network" of the amygdala, hippocampus, and prefrontal cortex. However, both fear acquisition and extinction induce plastic changes in a wider brain network, including the brain's sensory systems[4–6]. This is well documented in the primary and extended auditory cortex for rodents[7–13] and in few neuroimaging studies in humans[14–17]. By contrast, much less is known about the role of the visual cortex in associative memory and fear conditioning[5]. In general, visual neurons show experience-dependent plasticity, outside the critical periods of development[5,18]. Furthermore, human visuocortical responses to the CS+ predicting a threat are amplified during *fear acquisition*[19–23], resulting in a prioritized processing of threat-predictive cues. Simultaneously, responses to non-predictive CS− (safety cues) are inhibited[24,25]. This visual processing bias is linked to improved perceptual discrimination[26]. Importantly however, it is not clear if the changes in visual processing measured during the learning process are temporary or if they are part of a long-term memory trace.

Limited evidence suggests that cortical processing is responsive to quick changes in the predictive value of cues but also stable enough to support long-term memory. In *extinction learning*, presenting the visual CS alone can reverse associative changes in the visual[25,27] and for auditory CS in the primary auditory cortices[5,7]. Yet, in the auditory association cortex, animal[28–30] and human[31] studies have converged to demonstrate fear-conditioned changes that persisted despite extinction learning. *Extinction* includes learning a new CS-no US association[32,33],

[1]Institute of Psychology, Experimental Psychology II and Biological Psychology, University of Osnabrück, D-49074, Osnabrück, Germany. [2]Department of Psychology and Center for the Study of Emotion and Attention, University of Florida, Gainesville, Florida, 32611, USA. *email: mantov@uni-osnabrueck.de

leaving the original CS-US memory trace mostly intact. At later recall, the competition between the CS-US and the CS-noUS memory traces decides if and how much conditioned responding is shown[32]. Extinguished responses are vulnerable to return-of-fear phenomena, including spontaneous recovery, where conditioned responses return with the mere passage of time[1,33,34]. Yet, the role of the visual cortex in long-term reduction (i.e., good extinction recall) vs. persistence of conditioned responding (i.e., spontaneous recovery) after extinction learning is not clear, hampering our understanding of the neurophysiological mechanisms mediating return-of-fear. Elucidating its role has strong implications regarding the aetiology of affective and anxiety disorders e.g., for understanding persistent attention biases to anxiety-related cues, or visually-driven flashbacks in the face of fear-related stimuli.

In the present study, we tested the alternative hypotheses that visuocortical responses will show extinction recall or spontaneous recovery after a consolidation period. Orientation selectivity is a fundamental organizational property of neurons in the lower-tier, especially the primary visual cortex (V1)[35,36]. Based on previous work[25], we used steady-state visually evoked potentials (ssVEP) as a direct measure of sustained large-scale neural population activity, generated in lower-tier retinotopic cortex[37], to investigate trial-by-trial changes in cortical orientation selectivity. In a generalization paradigm[25], we used seven gratings, differing only in orientation (increasing linearly in 10° steps), as CS. Only one (45°, CS+) was paired with an aversive noise US during acquisition. Due to lateral inhibition of orientation columns in the visual cortex[38], and based on previous findings[25], we expected fear acquisition to amplify cortical responses to the CS+ but reduce them for the most similar CS−, resulting in a 'Mexican hat' tuning pattern. To allow for consolidation, we used a 2-day procedure (Fig. 1A) with acquisition and immediate extinction learning on day 1 and a 24-h delayed-recall test on day 2. To validate the extent to which learning took place, we assessed conditioned skin conductance responses (SCR, an indicator of sympathetic nervous system activity), subjective ratings of CS valence and arousal (evaluative learning), and collected US expectancy ratings (contingency knowledge). For those responses, we expected to see a gradual decrease in responding with decreasing similarity to the CS+, i.e. stimulus generalization[25,39,40] instead of lateral inhibition.

Results

Increased visual cortex responding and selective amplification of the threat-predictive stimulus during fear acquisition.
To examine if learned changes in the orientation tuning of visual cortex neurons represent a long-term CS-US memory trace, we recorded 64-channel electroencephalography (EEG) from 19 male volunteers in a 2-day fear conditioning task (Fig. 1A). On day 1, participants first underwent habituation. High-contrast gratings with 8 different orientations (15°, 25°, 35°, 45°, 55°, 65°, 75°, and control −45°, Fig. 1A) were presented 16 times each in a pseudorandom order. For acquisition, the grating CS were presented again 16 times, the 45° grating (the CS+) co-terminating with a 1-s aversive 98 dB (A) white-noise burst (the US). Extinction learning consisted of 16 presentations of each CS, without the US. After 24 h, delayed recall on day 2 was identical to the extinction phase. We delivered the grating CS in a phase-reversing stream, where the presentation alternated between the phase and counter phase version of a grating at a rate of 14.167 or 15 Hz (7.09 & 7.5 Hz for a full cycle). This evoked a robust phase-reversal ssVEPs at the second harmonic of the full cycle frequency, i.e., at 14.167 and 15 Hz, respectively, with a peak over the occipital pole (Fig. 1B).

We explored how occipital cortex activity is shaped by fear acquisition and extinction across the two experimental days. For this, we first pooled occipital activity from current source density (CSD) spectral power at the driving frequency for three a priori defined sensors around the occipital pole (Oz, O1, and O2, Fig. 1B), where we expected the hypothesized learning effects[25]. Occipital activity was subjected to repeated-measures ANOVA (learning phase [4] × CS orientation [8]) and planned contrasts, designed to test the competing hypotheses of *lateral inhibition* (modelled as a 'Mexican hat' function) vs. fear *generalization* (modelled as a quadratic function, Fig. 2C shows the weights). We used a Bayesian information criterion (BIC)[41] to formally compare the models and report the difference (ΔBIC), where values >2, suggest *positive*, >6 *strong*, >10 suggest *very strong* evidence to prefer the hypothesized model over the alternative[42,43].

We found a significant effect of learning phase ($F_{(1.7,30.2)} = 4.756$, $p = 0.021$, part. $\eta^2 = 0.209$, $N = 19$), due to higher occipital ssVEP power during acquisition (Fig. 2A). The effect was not confined to the CS+ (CS orientation × Learning phase interaction: $F < 1$; CS orientation: $F_{(3.0,54.0)} = 2.300$, $p = 0.088$, part. $\eta^2 = 0.113$; contrasts for acquisition, both $F < 1$).

We repeated the analysis after a habituation correction (Fig. 2B), normalizing each subject's occipital power for each CS through division by the corresponding orientation's mean habituation power – yielding a relative ssVEP change index. Planned contrasts on the habituation corrected data showed a significant 'Mexican hat' fit ($F_{(1,18)} = 4.806$, $p = 0.042$, $r^2_{contrast} = 0.202$) during acquisition (Fig. 2B), but not in extinction or day 2 delayed recall (both $F < 1$). The competing generalization model did not show a significant fit to data from acquisition ($F_{(1,18)} = 0.66$, $\Delta BIC_{(G-L)} = 3.6$, favouring lateral inhibition), extinction or day 2 delayed recall (both $F < 1$). Figure 2C shows the topographical distribution of the lateral inhibition (top row) vs. generalization (bottom row) model fits across the posterior part of the sensors (back view) for habituation-corrected data averaged across all trials of the learning phases acquisition, extinction, and day 2 delayed recall. In sum: besides a general increase in occipital cortex responding during acquisition, correcting for habituation revealed a selective enhancement of occipital ssVEP power for the threat-predictive CS+. Supplementary Figs. S1 and S2 show single subject data.

Single trial analysis reveals fast extinction on day 1 and a brief return-of-tuning in the occipital cortex.
Learning is typically a time-dynamic process and the quality of its outcome changes as a function of the number of training trials. Therefore, we utilized the excellent signal-to-nose ratio of steady-state visually evoked potentials (ssVEPs) to capture trial-by-trial changes in the orientation sensitivity of visual cortex mass neural activity. After converting the ssVEP to current source density (CSD) estimates of cortical surface power at the driving
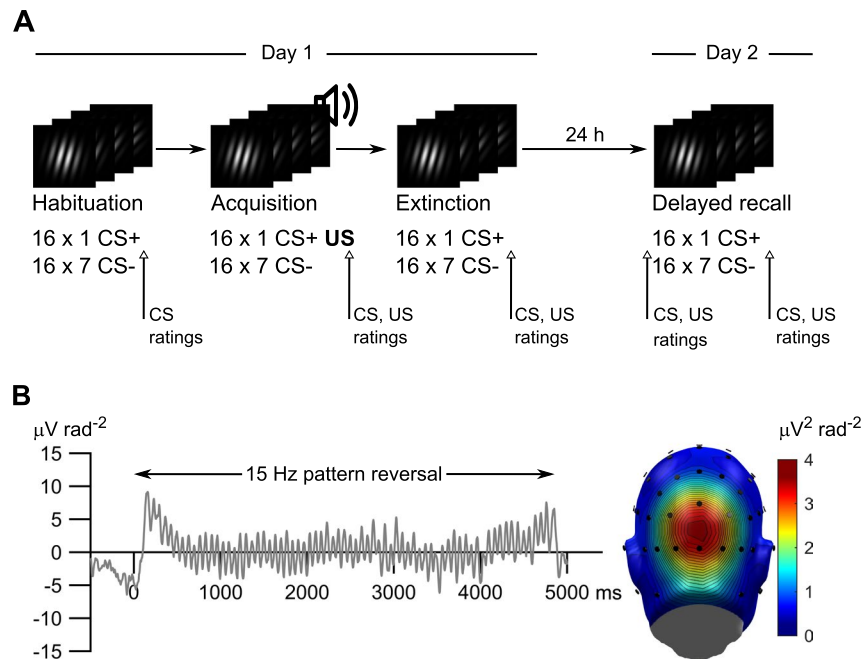
29

Figure 1. Experimental procedure and steady-state evoked potential (ssVEP) time domain and topographical distribution. (**A**) Overview of the procedure and example stimuli used during the 4 phases of the experiment: Habituation, acquisition, extinction, and a 24-h delayed recall. During each learning phase participants ($N = 19$) passively viewed high-contrast grating stimuli with eight different orientations (16 trials for each orientation and learning phase). To evoke a steady-state brain response with a known frequency, each grating reversed phase 71 times per trial at a rate of 15 ($N = 9$) or 14.167 Hz ($N = 10$). This produces the visual impression of the grating jumping slightly from left to right at a steady pace. Only during the acquisition phase one of the gratings (the CS+) was paired with a 1-s, 98 dB (**A**) aversive white noise burst (unconditioned stimulus = US). (**B**) Evoked steady state visuocortical response. *Left:* Representative time domain signal from the middle occipital sensor (Oz) for the 15 Hz phase reversal of one grating orientation (45°), averaged over 16 habituation trials and $N = 9$ participants. *Right:* Scalp distribution of the frequency domain average of the 15 Hz ssVEP power for the same stimulus and participants.

frequency, we pooled the trial-by-trial power averaged for the 3 a priori defined sensors nearest to the occipital pole (Oz, O1, O2, Fig. 3A). For each orientation, single-trial power was normalized by dividing by the habituation mean for the same orientation (all 16 trials). The critical F-values for the competing lateral inhibition ('Mexican hat') vs. generalization (quadratic) models were obtained by calculating permutation distributions on data shuffled across orientations within each participant (4000 permutations), yielding a critical F-value of 5.282. The associated $\Delta \text{BIC}_{(G-L)}$ (generalization – lateral inhibition), are shown by the yellow line in (Fig. 3A).

As previously reported[25], a tuning to the 45° grating signalling the aversive loud noise burst (CS+) emerged quickly. After only two trials during the acquisition phase (Fig. 3A), the third, fourth, and fifth trial showed a significant 'Mexican hat' fit. However, our data also showed that the tuning to the CS+ fluctuated over trials: After the initial tuning, there was a brief reduction. The CS+ tuning then re-emerged again stronger at the end of acquisition (trials 13 and 14). This fluctuation of tuning over trials might explain the lack of statistical significance when subjecting ssVEP averaged over all trials of the learning phase to an ANOVA. During extinction learning trials (day 1), the tuning disappeared almost instantly and overall activity was reduced (Fig. 3A). On day 2, there was a diffuse increase in activity during the initial 3 trials of delayed recall that did not result in a significant generalization or lateral inhibition fit. Interestingly, a tuning to the CS+ re-emerged after 24 hours during delayed recall, most pronounced during trials 8, 9, and 10. Here, activity to the CS+ was enhanced while activity to the 2 most similar CS− was strongly suppressed (Fig. 3A). This resembles a memory consolidation effect and return-of-tuning, despite extinction on day 1 at the level of mass sensory cortical activity. Supplementary Fig. S5 shows the data as conventional line plots with error bars.

Trial-by-trial changes in skin conductance responses show a similar temporal dynamic as occipital cortex responses. In order to describe the temporal dynamics of the sympathetic conditioned responding, we also conducted a single-trial analysis for skin conductance responses. Similar to single-trial ssVEP analysis, we first corrected for habituation level by subtracting the average over 16 habituation trials from each response within a participant and orientation. The result is plotted in Fig. 3B. Again, we fitted F-contrasts representing the lateral inhibition ('Mexican hat') and generalization (quadratic) response patterns. The critical F-value (obtained by calculating permutation distributions with 4000 permutations) was 6.396. For acquisition, a quickly emerging and prominent generalization pattern (Fig. 3B) was the best fit for the data.
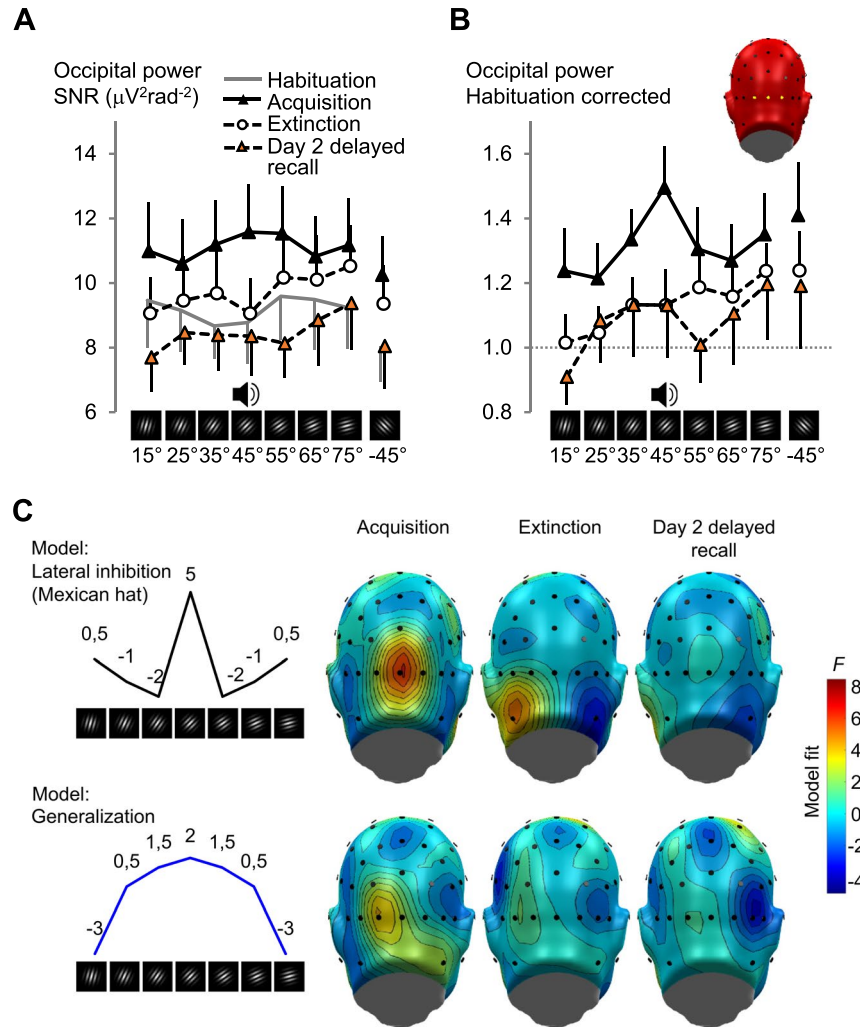
Figure 2. Occipital cortical responses during the different phases of conditioning. (**A**) Changes in the grand average ($N = 19$) of visual electrocortical activity for each learning phase (habituation, acquisition, extinction, and day 2 delayed recall) and for each CS orientation. Regional means of the ssVEP spectral power current source density (CSD, Laplacian space), averaged across 3 occipital midline sensor locations (O1, Oz, O2), were used to estimate the occipital cortex surface potential. Values are signal-to-noise ratios (SNR), i.e., the power at the driving frequency was divided by the average power for the five frequency bins below and four frequency bins above the driving frequency (as the noise estimate). Supplementary Fig. S1 shows single subject data. (**B**) The same data after habituation correction for acquisition, extinction, and day 2 delayed recall. The insert shows a view of the back of the electrode array used, the sensor locations used for averaging are highlighted. Error bars show 1 standard error of the mean (*SEM*). Supplementary Fig. S2 shows single subject data. (**C**) Cortical regions responsive to fear conditioning: Topographical distributions (back views of the scalp) showing results (*F*-values with $N = 19$) of planned contrasts testing for lateral inhibition (top, black line, 'Mexican hat' contrast) versus fear generalization (bottom, blue line, quadratic contrast) of habituation-corrected electrocortical responses across orientations, averaged over all acquisition, extinction, and day 2 delayed recall trials. *F*-values exceeding ± 4.41 indicate a reliable model fit. Fits matching the opposite pattern (i.e., inverted 'Mexican hat' or quadratic) are shown in blue. The numbers above the line-graphs on the left are the weights used for planned contrasts.

As with the lateral inhibition pattern in single-trial ssVEP, the SCR-generalization pattern fluctuated over trials. There was strong generalization for acquisition trials 2–6, followed by a reduction for trials 8–10, and a re-emergence of generalized responses towards the last trials of fear acquisition. Generalization subsided within the first four trials of extinction. During day 2 delayed recall, the single-trial SCR showed a diffuse return-of-fear confined to the first two trials and with a maximum for the 55° CS, followed by the 45° CS+. This pattern did not reach significance in either of the two contrasts (both centred on the 45° CS+).

Lateral temporo-occipital cortex shows persistent tuning to the CS+ 24 h after extinction.
Cortical responses after extinction learning and a consolidation period were not examined until now. Therefore, in an explorative analysis we looked for regions showing prolonged tuning to the CS+ on day 2 over all sensor locations. An examination of the topographical distribution (habituation-corrected data, averaged across all trials
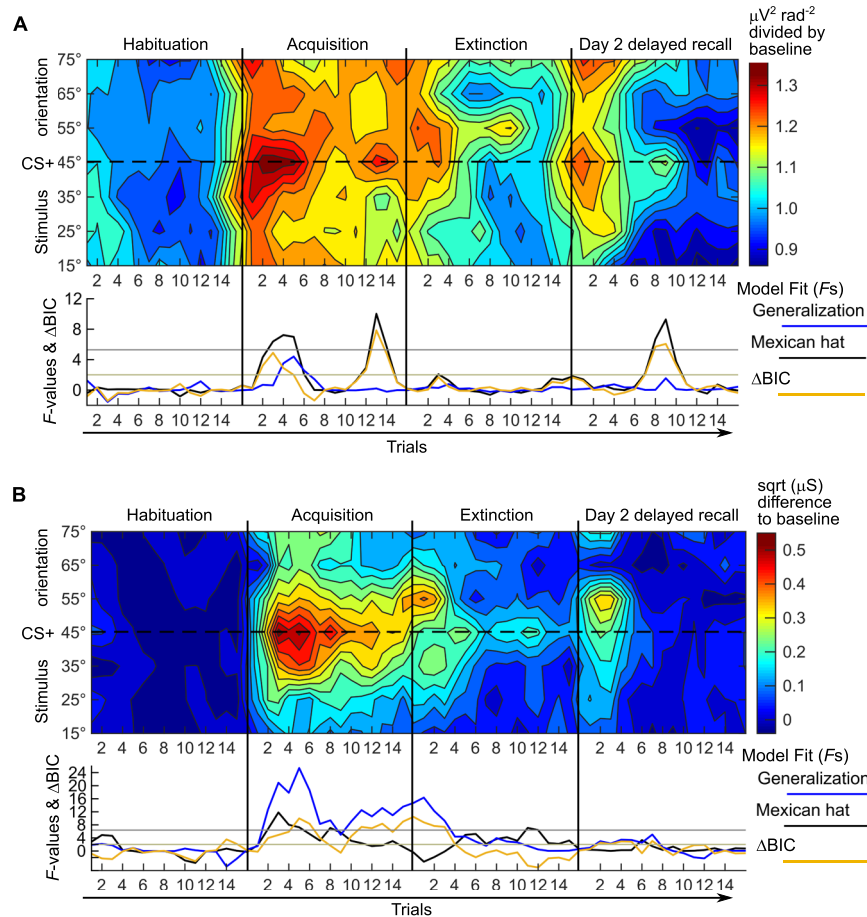
Figure 3. Trial-by-trial development of occipital orientation tuning and sympathetic skin conductance responses (SCR) during conditioning over two days. (**A**) Single-trial cortical responses, pooled across 3 occipital midline sensor locations (O1, Oz, O2). *Top panel:* color-coded single-trial amplitude of the occipital visual electrocortical response during habituation, acquisition, extinction, and day 2 delayed recall. The dynamic of learning and recall in the visual cortex is shown for the 8 CS orientations (shown on the y-axis) with the CS+ (45 degree orientation) in the middle. *Bottom:* model fits (*F*-values from planned contrasts) for the competing hypotheses of fear generalization (blue line) and lateral inhibition (black line, 'Mexican hat'), calculated for each trial. The yellow line shows the $\Delta BIC_{(G-L)} = BIC(\text{Generalization}) - BIC(\text{Lateral inhibition})$, values > 2 favour lateral inhibition, values < -2 favour generalization. Note: Contour plots show no error estimates, see Supplementary Fig. S5 for an alternative depiction. (**B**) Single-trial SCR. *Top:* As in (**A**) but for average color-coded single-trial amplitude of the SCRs. *Bottom:* model fits (planned contrasts) for fear generalization (blue line) and lateral inhibition (black line). The yellow line shows the $\Delta BIC_{(L-G)}$, as we expected generalization for SCR, here values > 2 favour generalization, values < -2 favour lateral inhibition. In both panels: where the data fit an inverted quadratic or 'Mexican hat' contrast, the *F*-values were given a negative sign to denote the inverted fit.

per learning phase) revealed a bilateral region showing a 'Mexican-hat' fit for acquisition, extinction, and (more lateralized to the left) also during delayed recall on day 2 (data not shown). Inspection of single-trial data however, showed a similar but more posterior location including sensors TP7 and TP9 on the left, and to a smaller amount also for the corresponding sensors on the right (TP8, TP10). Figure 4A shows a scalp topography of this effect for trials 5–12 of the delayed recall on day 2, where the fit was most pronounced. Supplementary Figs. S3 and S4 show this for all trials and every learning phase. Therefore, we repeated the single-trial analysis for this bilateral temporo-occipital region pooled from the explorative 4-sensor cluster (TP8, TP10, TP7, and TP9). The critical *F*-value for this 4-sensor cluster (again determined through permutation testing with 4000 iterations) was $F = 4.70$. The results (Fig. 4B) show that for this cluster there was a prolonged and more persistent tuning to the CS+, following a 'Mexican hat' pattern and lasting throughout 11 of the 16 trials of day 2, despite the lack of significant tuning during extinction learning on day 1 (Fig. 4B). Supplementary Fig. S5 shows the data as conventional line plots with error bars.

Sympathetic arousal and subjective responses to the CS validate successful learning and show fear generalization. Finally, to further validate our task with more typical measures of human fear learning, we analysed participant's averaged skin conductance responses (SCR), subjective ratings of CS valence, CS
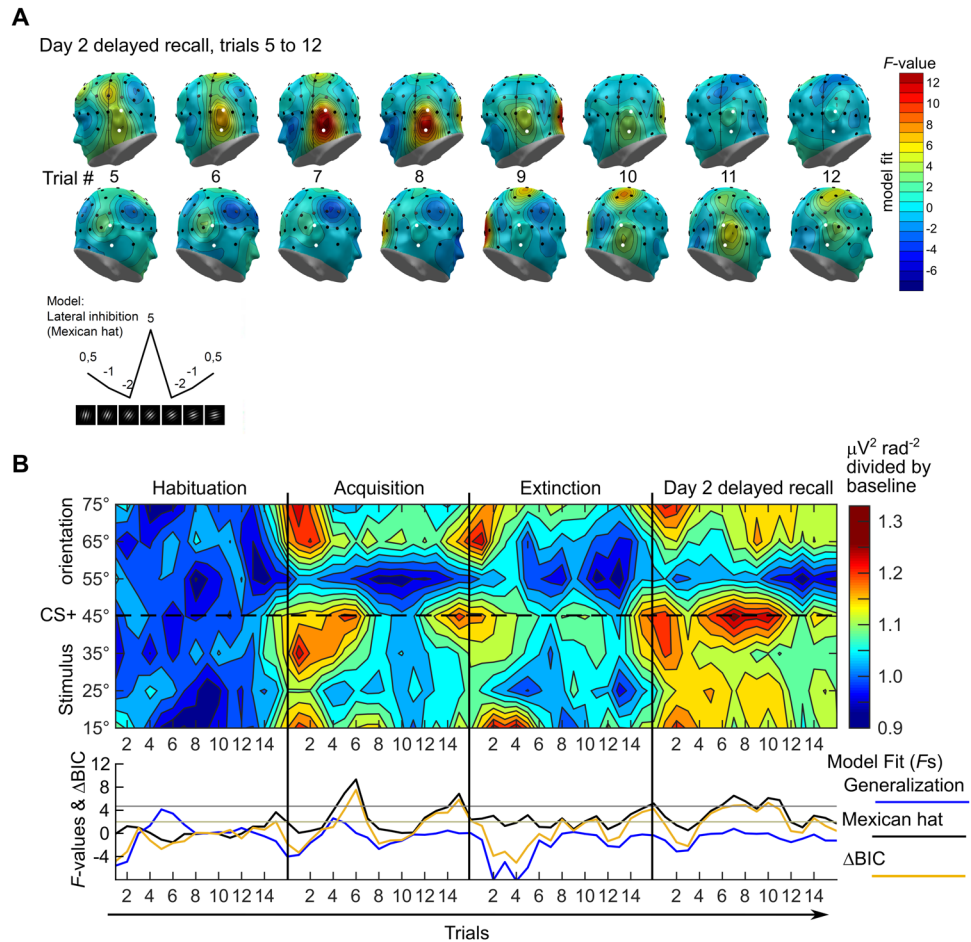
Figure 4. Conditioned tuning over lateral temporo-occipital cortex in single-trial data. (**A**) Topographical distributions (left and right views of the scalp) showing results (*F*-values) of contrasts testing for lateral inhibition ('Mexican hat') for habituation-corrected electrocortical responses across orientations, for trials 5–12 of day 2 delayed recall. The 4 sensors selected for analyses are highlighted white. Fits matching the opposite pattern (i.e., inverted 'Mexican hat') are shown in blue. (**B**) Trial-by-trial development of orientation tuning during conditioning. Top: color-coded single-trial amplitude of the exploratory 4-sensor cluster from the bilateral temporo-occipital region (TP8, TP10, TP7, and TP9), shown for the 7 CS orientations (on the y-axis) with the CS+ (45° orientation) in the middle. *Bottom:* model fits (planned contrasts, *F*-values) for generalization (blue line) and lateral inhibition (black line, 'Mexican hat'), calculated for each trial. The yellow line shows the $\Delta BIC_{(G-L)} = BIC(Generalization) - BIC(Lateral inhibition)$, values >2 favour lateral inhibition, values <−2 favour generalization. Where the data fit an inverted quadratic or 'Mexican hat' function, the *F*-values were given a negative sign to denote the inverted fit. Note: Contour plots show no error estimates, see Supplementary Fig. S5 for an alternative depiction. For completeness, Supplementary Fig. S9 shows 16-trial averages of these 4 sensors, as in Fig. 2A,B.

arousal, and US expectancy. As expected, SCR, as an indicator of sympathetic arousal, showed successful learning. While the CS orientation had no effect on SCR during habituation ($F < 1$), there was a significant impact of CS orientation during acquisition (Fig. 5A, $F_{(2.7,49)} = 7.966$, $p = 0.0003$, part. $\eta^2 = 0.307$; CS orientation × Learning phase interaction: $F_{(3.3,60)} = 8.396$, $p = 0.00006$, part. $\eta^2 = 0.318$). During the acquisition phase, SCR followed the expected conditioned generalization gradient, favouring the CS+ and the two most similar CS−. Indeed, SCR during acquisition were best modelled by a quadratic function with the highest responses to the CS+ (Table 1 summarizes the results from the planned contrasts, and model comparisons for generalization and lateral inhibition for SCR and subjective ratings).

Extinction learning markedly reduced SCR-responding (Fig. 5B, Learning phase [last 4 acquisition trials vs. last 4 extinction trials]: $F_{(1,18)} = 8.246$, $p = 0.010$, part. $\eta^2 = 0.314$), due to a drop in responding to the CS+ and perceptually similar CS− (CS orientation × Learning phase: $F_{(7,126)} = 2.644$, $p = 0.014$, part. $\eta^2 = 0.128$). During the last 4 extinction trials there was no effect of CS orientation ($F_{(7,126)} < 1.11$, Fig. 5B) or evidence of generalization around the CS+ (Table 1). Despite the successful reduction with extinction learning on day 1, the conditioned effect of CS orientation returned after 24 h of consolidation during the first 4 trials on day 2 (last 4 extinction trials vs. first trials on day 2: Fig. 5C, CS orientation × Learning phase: $F_{(7,126)} = 2.680$, $p = 0.013$, part.
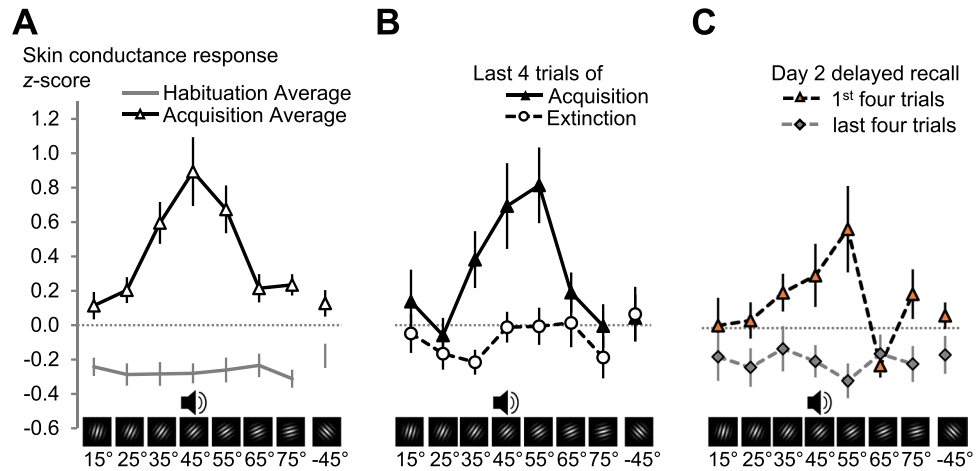
Figure 5. Skin conductance responses during the different phases of fear conditioning. (**A**) Mean ($N = 19$) skin conductance responses averaged over all 16 trials of habituation and acquisition on day 1. (**B**) Shows the means for the last four trials of acquisition and extinction on day 1, respectively. (**C**) The first and last four trials of the delayed recall phase on day 2. In all plots the data are averaged over individual z-scores, standardized on the mean and *SD* of all CS responses of a subject in the experiment. Error bars show ± 1 *SEM*. Supplementary Fig. S6 shows single subject SCR data.

$\eta^2 = 0.130$, CS orientation main effect for the first 4 trials on day 2: $F_{(3,53.3)} = 3.259$, $p = 0.029$, part. $\eta^2 = 0.153$). However, the largest responses during the first 4 trials on day 2 were for the 55° grating, not for the 45° CS+ and the quadratic fit failed to reach significance (Table 1).

For *subjective responses to the CS*, we first compared the arousal and valence ratings collected after habituation, acquisition, and extinction learning on day 1. When rated after habituation, all CS where evaluated as relatively calm (CS main effect: $F < 1$, Fig. 6A). This changed after acquisition (CS × Time point: $F_{(4,71.1)} = 4.080$, $p = 0.005$, part. $\eta^2 = 0.185$). Now the CS+ (45°) and its two nearest neighbours were rated as more arousing (CS effect: $F_{(2.9,52.8)} = 4.361$, $p = 0.009$, part. $\eta^2 = 0.195$), following a generalization gradient (Table 1). After extinction, the arousal ascribed to the stimuli was reduced (Time point: $F_{(1,18)} = 7.655$, $p = 0.013$, part. $\eta^2 = 0.298$) but an enhancement for the CS+ and its neighbours remained (CS: $F_{(2.3,42.1)} = 3.906$, $p = 0.022$, part. $\eta^2 = 0.178$), best modelled by generalization (Table 1). This indicates a reduction, but not a complete extinction of generalized subjective arousal. On day 2 (Fig. 6B), arousal ratings collected before delayed recall were comparable to those measured after extinction on day 1 (Time point and CS × Time point, both $F < 1$, CS: $F_{(2.5,45.8)} = 3.471$, $p = 0.030$, part. $\eta^2 = 0.162$, Table 1). Even after day-2 extinction trials, there was a remaining CS effect (Fig. 6B, $F_{(3.4,60.4)} = 3.192$, $p = 0.025$, part. $\eta^2 = 0.151$), again modelled better by generalization around the CS+.

For valence ratings we found similar results (data not shown). Again, compared to habituation, the rating of the CS+ and its nearest neighbours became more negative after acquisition (CS × Time point: $F_{(2.9,51.7)} = 4.119$, $p = 0.012$, part. $\eta^2 = 0.186$), and this was not abolished after extinction learning on day 1 (CS × Time point: $F < 1$, CS effect: $F_{(2,35.3)} = 3.165$, $p = 0.055$, part. $\eta^2 = 0.150$). In contrast to arousal ratings, conditioned changes in valence were not significant on day 2, neither before nor after the 16 extinction trials on day 2 (CS effects: $F_{(2,35.8)} = 1.705$, $p = 0.196$, part. $\eta^2 = 0.087$, and $F_{(2.6,46)} = 1.682$, $p = 0.190$, part. $\eta^2 = 0.085$, respectively).

We also asked participants to rate for each CS, to what extent they expected it to be followed by the loud noise US (−5 being 100% certain that *no* US would follow, 0 being uncertain, +5 being 100% certain that *this CS would be followed* by a US). We refrained from a US expectancy rating after habituation because it could introduce anticipation effects during acquisition. After acquisition participants were able to identify the CS+ (Fig. 6C, CS effect: $F_{(3.7,59)} = 6.859$, $p = 0.0002$, part. $\eta^2 = 0.300$). Consistent with generalization (Table 1), the US expectancy was highest for the CS+, with the neighbouring two gratings rated as close to uncertain and the more dissimilar gratings rated as relatively safe (Fig. 6C). After extinction, the US expectancy was reduced, especially for the CS+ (CS × Time point: $F_{(4,64)} = 2.651$, $p = 0.041$, part. $\eta^2 = 0.142$), with remaining bias towards the CS+ (CS: $F_{(2.7,47.9)} = 3.583$, $p = 0.024$, part. $\eta^2 = 0.166$), modelled by generalization (Table 1). On day 2 (Fig. 6D), before delayed recall the US expectancy was only descriptively higher (vs. end of day 1, CS × Time point: $F_{(4.4,79.4)} = 1.320$, $p = 0.268$, part. $\eta^2 = 0.068$, CS: $F_{(2.7,47.7)} = 5.590$, $p = 0.003$, part. $\eta^2 = 0.237$). The generalization pattern was attenuated, but not abolished at the end of day 2 (main effect CS: $F_{(3.1,56.3)} = 3.659$, $p = 0.016$, part. $\eta^2 = 0.169$, Table 1).

Discussion

Prior work[25] has established that pairing a specific orientation with an aversive outcome changes orientation selectivity of neuronal populations in the human visual cortex, accompanying the learning of behavioural relevance. We examined if this acquired change in orientation selectivity persists after extinction learning and a subsequent consolidation interval. As expected, conditioning prompted defensive mobilization at the level of autonomic arousal, biased CS evaluation, and produced explicit contingency knowledge, reflected in increased SCR, subjective ratings of arousal, aversion, and US expectancy. In these four measures responding decreased gradually with increasing angular distance from the CS+, showing a pronounced generalization that decreased
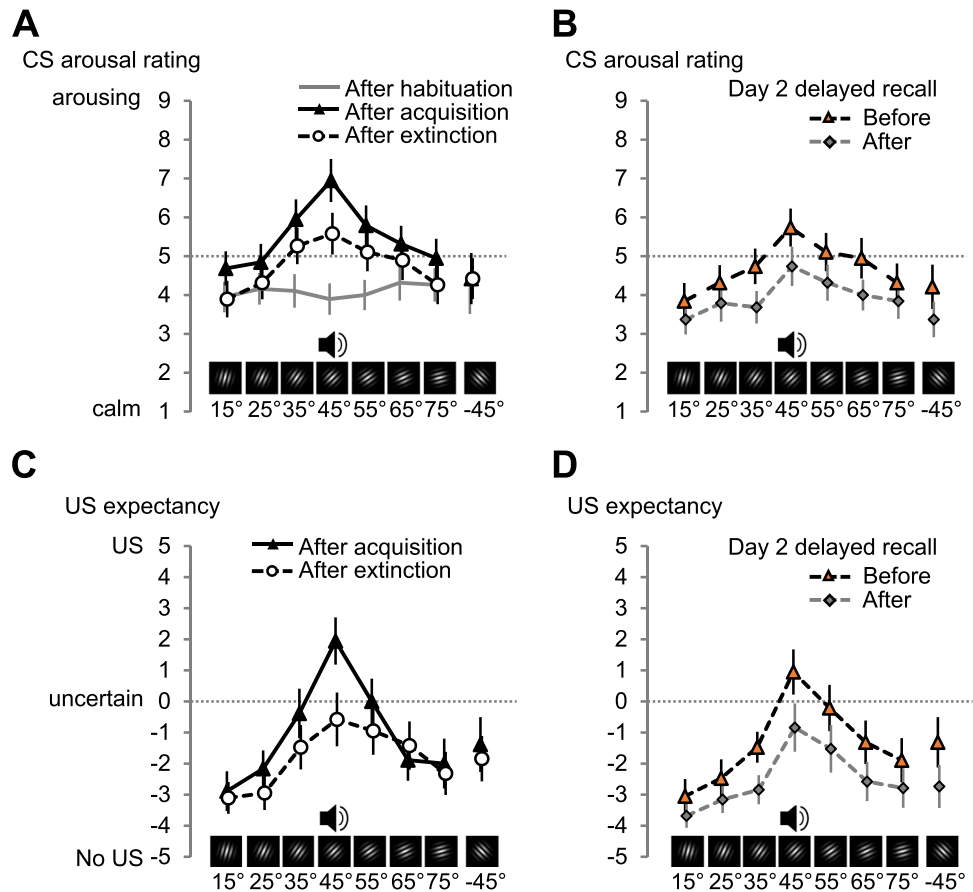
Figure 6. Subjective self-report changes in CS arousal and US expectancy during the different phases of fear conditioning. Mean ($N = 19$) arousal rating for each CS orientation as rated (**A**) after habituation, acquisition, and extinction on day 1 and (**B**) before and after delayed recall on day 2. US expectancy mean ($N = 18$) as rated (**C**) after habituation, acquisition, and extinction on day 1 and (**D**) before and after delayed recall on day 2. Error bars show ±1 *SEM*. Supplementary Figs. S7 and S8 show single subject data for arousal and US expectancy ratings.

but did not disappear with extinction learning. In contrast, visual cortex responding during acquisition was selectively amplified for the CS+ while the most proximal, but not distal, orientations were suppressed, thus following a 'Mexican-hat' function[25]. Such tuning has also been observed in studies of adaptation and feature-based selective attention, where it is often reflected in behavioural and neural population variables[25,36]. It is not known if the origin of emerging lateral inhibitory patterns varies with the task, or if it represents a mechanism common to learning, adaptation, and instructed attention. Future research is needed to examine the differences and similarities between visuocortical prioritization mechanisms under different behavioural constraints. The present study contributes to this emerging literature by providing information regarding the longer-term sequelae of adaptive changes in population tuning: The tuning to the CS+ quickly subsided with immediate extinction on day 1. Despite this, and without further pairing of the CS+ with the US, a strong tuning to the CS+ reappeared briefly on day 2. The trial-by-trial timing of occipital tuning over the course of the two experimental days resembled the temporal progression of conditioned peripheral arousal responses, indexed by SCR. Rather than lateral inhibition, single-trial SCR displayed generalization, with a fast extinction on day 1 and brief return of responding on day 2. Explorative single-trial analyses revealed a temporo-occipital area where cortical tuning to the CS+ on day 2 was present throughout the majority of unreinforced day 2 trials. Our results show that biased visual cortex processing can persist after extinction training and 24 h of consolidation, while remaining flexible enough to reflect short-term changes in the predictive relevance of stimuli. The latter is supported by the rapid reduction in cortical responses during extinction learning in our data. Recent single-trial MEG data show changes in the retinotopic visual cortex within only a few trials of reinforced or unreinforced CS[44].

Unlike previous studies[25], we found that occipital responding to all CS orientations increased during fear acquisition compared to habituation (Figs. 2A and 3A). This was in addition to responses following a 'Mexican hat' pattern, tuned to the CS+, as reported previously[25]. Together, this could indicate two different mechanisms coexisting during acquisition: one increasing overall cortical gain, the second tuning sensitized responding in accordance with the behavioural relevance of stimuli to enable discriminability. In behavioural terms, these mechanisms may be related to enhanced vigilance and sensory discrimination, respectively. Broader increases in cortical gain may reflect overall arousal associated with noradrenergic signalling[45].

SCR ($N = 19$)	Generalization (quadratic)			Lateral inhibition ('Mexican hat')			
	$F_{(1,19)}$	p	$r^2_{contrast}$	$F_{(1,19)}$	p	$r^2_{contrast}$	$\Delta BIC_{(L-G)}$
Habituation (16 trials)	0.01	0.910	0.001	−0.08	0.776	0.004	−0.1
Acquisition (16 trials)	27.81	0.0001	0.594	7.37	0.014	0.280	10.9
Acquisition last 4 trials	11.61	0.003	0.379	1.12	0.304	0.056	8.0
Extinction last 4 trials	0.34	0.567	0.018	0.60	0.449	0.031	−0.3
Day 2 first 4 trials	2.37	0.141	0.111	0.10	0.757	0.005	2.1
Arousal ratings ($N = 19$)							
Habituation	−0.10	0.753	0.073	−0.47	0.500	0.156	−0.4
Acquisition	20.19	0.0003	0.718	9.12	0.007	0.569	6.3
Extinction	23.85	0.0001	0.746	1.59	0.223	0.278	13.9
Day 2 (before)	16.81	0.001	0.685	4.55	0.047	0.440	8.0
Day 2 (after)	9.44	0.007	0.576	6.30	0.022	0.499	2.2
US expectancy ($N = 18$)							
Acquisition	28.32	0.0001	0.782	13.08	0.002	0.649	7.2
Extinction	18.34	0.001	0.710	2.10	0.165	0.323	10.7
Day 2 (before)	26.04	0.0001	0.769	11.59	0.003	0.626	7.2
Day 2 (after)	12.95	0.002	0.647	7.98	0.012	0.554	3.1

Table 1. Results of planned contrasts for generalization and lateral inhibition and model comparison for SCR, subjective CS arousal ratings, and US expectancy ratings. *Note.* $\Delta BIC_{(L-G)}$ is the difference of the estimated Bayesian information criteria for the two competing models. We expected to see generalization for SCR, CS arousal ratings, and US expectancy ratings. Therefore, here $\Delta BIC_{(L-G)} = BIC_{(Lateral\ inhibition)} - BIC_{(Generalization)}$, where $\Delta BIC > 2$, suggests positive, $\Delta BIC > 6$ suggests strong, and $\Delta BIC > 10$ suggest very strong evidence to prefer the generalization model over lateral inhibition. US expectancy has $N = 18$ due to missing ratings from one participant, the associated F-values have 1 and 18 degrees of freedom.

Importantly, we also show a return of cortical orientation tuning on day 2, despite its abolishment in day-1 immediate extinction. This supports two interpretations: (1) Changes in cortical responding acquired during fear conditioning seem to be subject to consolidation processes over the 24-h retention period – a hallmark of plasticity and a clue for the formation of a long-term memory; and (2) The learned changes in cortical orientation tuning follow the rules of associative, rather than perceptual learning. Return of extinguished cortical tuning to the CS+ is consistent with spontaneous recovery, a known phenomenon in conditioning[1,34]. This cannot be explained by processes of perceptual learning, in which the mere exposure to the stimuli would result in plasticity. The explorative finding of persistent tuning to the CS+ in bilateral temporo-occipital cortical areas, despite day 1 extinction and additional extinction on day 2, is of special interest. It may signify a process resembling systems consolidation: cortical processing on day 2 may recruit a different set of visual neurons after the 24-h consolidation period. Indeed, findings from auditory conditioning suggest that older memories may rely more on the higher auditory cortex than newly acquired ones[46,47].

The return of visual cortical tuning observed in the present study may contribute to our understanding of the role of the visual cortex in fear extinction and more generally adds to an ongoing debate about the nature of fear extinction. Return-of-fear phenomena are reliably shown at the behavioural level. Therefore, most contemporary accounts consider extinction as comprising learning a new inhibitory CS-noUS association[2,48,49]. However, at the level of changes in neural circuitry, findings support both – new learning and unlearning, depending on the neural system investigated[50–52]. Studies in mice show that fear acquisition with an auditory CS induces dendritic spine formation in the auditory cortex[53,54]. Yet, these newly formed spines were eliminated with extinction learning (2 days with 5 CS-alone trials per day)[53], supporting the idea that the fear memory trace can be erased with extinction in the primary auditory cortex. Until now this has not been studied for fear-conditioned changes in the visual cortex. Our results show that the visual cortex is able to accomplish fast adaptation to changes in contingency (as seen in immediate extinction), while still exhibiting a long-term bias towards a stimulus that has a history of being dangerous (as evident in the return of cortical tuning on day 2).

Cortical areas showing prolonged or extinction-resistant responding to a fear conditioned stimulus may hold clinical relevance. They could be related to return-of-fear phenomena contributing to relapse after therapy in psychiatric disorders[55], especially for visually-driven flashbacks. For example, increased detection of combat-related words in a rapid visual stream is related to increased visual cortex responding in combat-exposed soldiers with posttraumatic stress disorder compared to combat-exposed soldiers without PTSD[56]. In our data, visuocortical re-tuning, lasting several trials beyond the peripheral arousal responses on day 2, illustrates that visual cortical activity follows a different time course than typically used conditioning measures. Despite behavioural evidence for the safety of the CS+, acquired through extinction learning, such persistent changes may serve to prepare for a fast re-learning if the contingency changes again in the future. In auditory fear conditioning, similar prolonged and apparently extinction-resistant changes were found in the human higher-order auditory association cortex[31], while activation of the primary auditory cortex during extinction learning predicted extinction success[57].

A possible limitation of our findings is that the single extinction session we applied might not be sufficiently extensive to produce a stable reversal of plastic changes. A recent rodent study found that a single extinction session leads to new learning while multiple extinction sessions lead to erasure of the original fear memory in lateral

amygdala neurons[58]. We also employed immediate extinction (i.e., temporally very close to fear acquisition), and some findings suggest that this is associated with more return-of-fear compared to extinction on a different day[59]. Future studies may address these alternative explanations. We also used 'booster trials' at the beginning of acquisition (5 of the first 8 trials were reinforced CS+ trials), therefore effects like repetition priming and other trial-order effects cannot be ruled out in our acquisition data. However, a very similar tuning pattern during acquisition has been observed in other work in the absence of booster trials[25], and effects of trial-order during acquisition cannot account for the returning of tuning after 24 hours – the main finding of the present study. Finally, further studies should replicate and also extend the finding by using other (but the 45°) grating orientations as the CS+.

Our results cannot address the question what information is represented in visual cortex as learning progresses. Our method also does not allow us to pinpoint if any neuronal plasticity happens in the visual cortex itself. Changes in cortical processing measured with our EEG method may also be the result of re-entrant projections from upstream cortical areas exerting a top-down biasing signal on the visual cortex[60]. Nevertheless, animal studies have shown that visual neurons are able to encode different learning-specific information: For example, neurons in the rat V1 encoded the timing of a delayed reward[61]. A recent study[62] identified two distinct populations of neurons in the mouse lateral visual association cortex (LVAC) during an appetitive food-reward learning task. One subset was sensitive to the orientation of a grating, irrespective of the outcome (palatable food, bitter liquid, no outcome). A second subset of neurons was sensitive to the predicted outcome (e.g. food) and motivational strength (i.e., satiety reduced tuning to a food predictive cue) and flexibly shifted their tuning curves with contingency reversal. Neurons with similar properties (coding predicted outcome, sensitive to motivation changes) were also found in the mouse V1[62]. Finally, these visual neurons were also sensitive to trial-by-trial reward history, i.e. responses to a food cue in a given trial would change depending on how many times this cue was rewarded in the preceding trials[62]. The latter corresponds well with human MEG findings[44].

In summary, our findings demonstrate that the lower tier visual cortex responding not only shows flexible and fast adaption in response to changing contingencies associated with visual stimuli. Persistence of biased cortical processing after extinction and a consolidation interval is consistent with the notion that sensory systems participate in the distributed network encoding long-term fear memory[4,5,63]. More mechanistic animal studies are needed to investigate this hypothesis. Future studies may also aim to pinpoint the exact features of behaviourally relevant information represented in visual cortex activity: for example, arousal, prediction error signal, reinforcement timing, motivational strength, and reward history. As fear acquisition and fear extinction are both relevant models for psychiatric disorders related to trauma and stress, it will be important to establish the extent to which cortical processing bias towards danger signals is affected by additional experimental stress induction in humans.

Materials and Methods

Participants.   Volunteers from the University of Osnabrück were screened for exclusion and inclusion criteria. Data from $N = 19$ male students between 18 and 29 years ($M = 23.6$, $SEM = 0.68$), with a BMI between 19.15 and 31.56 kg/m^2 ($M = 24.10$, $SEM = 0.43$) comprised the final sample. Fear extinction and delayed recall are prone to sex differences linked to the female sex hormone 17-beta-estradiol[64,65]. Here, the sex-hormone question was not relevant. We therefore examined only men to avoid potentially confounding sex differences and fluctuations of sex-hormones in women. Participants were excluded in case of acute or chronic physical and psychiatric disorders (e.g., migraine, epilepsy, cardiovascular diseases, and phobias); also hearing impairments or tinnitus, left-handedness, uncorrected vision impairment, alcohol consumption of more than 40 g ethanol/day, drug abuse, smoking more than 5 cigarettes a day or any current medication. All participants were screened for posttraumatic stress disorder (PTSD) using a German version of the Posttraumatic Stress Diagnostic Scale[66] and excluded if they met DSM-IV criteria for PTSD. From the 39 screened students, 9 did not meet the inclusion criteria, 4 additional did not appear for testing, and thus 26 subjects were assigned to the experiment. From those, 5 discontinued the ongoing experiment due to the aversive nature of the task, and one participant had to be excluded from analysis due to experimenter error. Finally, one participant was excluded from analysis because he failed to show an ssVEP signal over occipital areas even in a grand average over all trials (after visual inspection, and circular T-square statistic). The sample size was determined based on previous electroencephalography/magnetoencephalography fear conditioning studies[21,25,44,67] with samples ranging from $N = 15$ to 21. We also considered sample sizes common in perceptual[26], pharmacological[68], and functional brain imaging studies[69] of human fear conditioning and return- of-fear phenomena ($N = 16$ to $N = 20$, per group). The study protocol with all procedures and methods was approved by the ethics committee of the University of Osnabrück and was conducted in accordance with the Declaration of Helsinki guidelines. All procedures were carried out with the adequate understanding and written informed consent of the participants.

Experimental design, fear conditioning stimuli and procedure.   We used a differential fear conditioning protocol comprising four learning phases: habituation, acquisition and immediate extinction learning on day 1, and a 24 h-delayed recall on day 2. To examine if learned changes in the orientation tuning of visual cortex neurons represent a long-term CS-US memory trace, we recorded 64-channel EEG from our participants in this 2-day fear conditioning task (Fig. 1A). The stimuli, the basic learning task, and parts of the EEG analysis strategy follow earlier published work[25].

The CS were high-contrast (maximum Michelson-Contrast: 96%) Gabor patches (sinusoidal gratings, filtered with a Gaussian envelope) with spatial frequency of 0.98 cycles/degree. They were presented centrally on a dark-grey background (100% black setting of the monitor) via a 19" cathode ray tube (CRT) monitor (visual angle 5.7°, vertically and horizontally). Participants viewed the CS while sitting in a comfortable chair in the electromagnetically shielded and sound attenuated experimental chamber, which was lit only by the CS presentation on the monitor during the conditioning phases. The CS had 8 different orientations with angles of 15°, 25°, 35°, 45°, 55°, 65°, 75°, and −45° relative to vertical (see Fig. 2). Using a differential conditioning paradigm, the 45° Gabor

served as CS+ during acquisition, while the other six gratings became CS− stimuli. The −45° orientation was used as an additional condition with very high perceptual dissimilarity to the CS+. The US was a 98 dB (A) white noise, binaurally presented for 1000 ms via two speakers left and right behind the participant.

To evoke ssVEPs (Fig. 1B), each Gabor grating with a given orientation (i.e., each CS) was presented reversing its phase at either 14.167 Hz (10 participants) or 15 Hz (9 participants). We deliberately tested two distinct stimulation frequencies to increase external validity. Each CS presentation (trial) consisted of 71 phase reversals, yielding a CS trial-duration of 5012 ms at 14.167 Hz and 4734 ms at 15 Hz. During the acquisition phase, we extended each trial-duration for 14 additional phase reversals (corresponding to the duration of the 1 s US-presentation). EEG data recorded during US-presentation was excluded from subsequent analyses to avoid contamination of the ssVEP signal by the sound presentation. All gratings were created and all stimuli were presented in Psychophysics Toolbox (RRID:SCR_002881)[70,71] running on MATLAB (RRID: SCR_001622).

In every learning phase each of the 8 CS orientations was presented 16 times (=16 trials of each CS - 128 trials in total per phase). The US was only presented during the acquisition phase. Here, US-presentation started 5012 ms (for 14.167 Hz) or 4734 ms (for 15 Hz) after the onset of every 45° Gabor grating (CS+, 100% reinforcement rate). In acquisition, 5 of the first 8 trials were always reinforced trials where the 45° CS+ co-terminated with the US. The remaining acquisition trials and all trials in habituation, extinction learning, and delayed recall were presented in a pseudorandom order in one of two predefined sequences, counterbalanced across participants (Supplementary Table S1 shows the exact sequences). As in previous studies[25] these booster trials where introduced to assure learning of this rather difficult task, where one CS+ has to be identified among seven very similar CS−. The presentation order was restricted by the rule that no more than two consecutive presentations of the same CS orientation should occur within one conditioning phase. The inter-trial interval (ITI, offset to onset) was a black screen and ranged randomly between 4500 ms to 6500 ms, drawn from a uniform distribution. A white fixation cross was presented in the centre of the screen for the last 1500 ms of each ITI.

EEG recording and pre-processing.

We recorded EEG continuously from 64 active electrodes (Ag/AgCl, actiCAP, Brain Products) filled with electrolyte gel (Super-Visc 10%NaCl, EasyCap) with two 32-channel BrainAmp DC amplifiers (resolution 0.1µV, Brain Products) at a sampling rate of 1000 Hz with a high-pass filter at 0.08 Hz. Efforts were made to keep all impedances below 5 kΩ (manufacturer's recommendation <25 kΩ). FCz was the recoding reference, AFz was ground. To control for vertical and horizontal eye-movement we recorded EOG with electrodes (Ø 4 mm, Ag/AgCl) placed close to the lateral canthus of each eye to record horizontal movements, as well as infra- and supra-orbital in line with the pupil of the right eye to capture vertical movements. To control for muscular blink activity we also recorded EMG of the orbicularis oculi muscle. EMG-electrodes (Ø 5 mm, Ag/AgCl) were placed over the left orbicularis oculi muscle underneath the eye lid, according to current guidelines[72]. A ground for EOG and EMG channels was placed on the forehead.

Pre-processing was accomplished off-line using BrainVision Analyzer 2 software. We used infinite impulse response (IIR), zero phase-shift, Butterworth filters to band-pass the non-segmented data with a high-pass filter with a cut-off frequency (3 dB point) of 0.5 Hz (roll-off: 48 dB/octave) and a low-pass at 40 Hz (3 dB point, 12 dB/octave). We also applied a 50 Hz notch filter (symmetrical, 5 Hz bandwidth, order 16). The data were then re-referenced to an average reference and the recording reference channel was reused as FCz, yielding 65 EEG channels. We then segmented the data from −600 to 5100 ms relative to the onset of each CS. The segments were down-sampled to 250 Hz and subjected to an ocular correction independent component analysis (ICA, as implemented in BrainVision Analyzer 2). After visual inspection of the resulting factors and factor topographies, factors related to horizontal and vertical eye movements, blinks, as well as strong cardiac or muscular artefacts were removed from the reconstructed data. Pre-processed EEG data were exported to MATLAB (RRID: SCR_001622). Trials with remaining artefacts were rejected based on visual inspection of butterfly-plots of each trial. For both experiment days, this left an average of 15.8 trials per condition (range: 13–16) for analysis. There were no significant differences between learning phases or conditions (all $F < 3.34$, all $p > 0.070$). Finally, we performed a scalp current source density (CSD) transform to the data[25,73]. The procedure diminishes volume conduction effects and delivers reference-free data. The CSD values (serving as estimates of cortical surface potentials) are represented on a sphere that approximates a cortical surface and thus serve as a mapping technique. In the present implementation[73], the CSD is projected back onto the original electrode space to facilitate topographical mapping. All analyses were performed on CSD-transformed data, and CSD data are shown throughout the figures.

ssVEP spectral analysis.

The CSD values at each sensor were transformed into the frequency domain using a Fourier Transform of the average over 16 trials for each learning phase (habituation, acquisition, extinction learning, and day 2 delayed recall) and for each CS condition. For the 14.167 Hz stimulation, we used data from 988 to 5012 ms post stimulus onset (1006 sample points). For the 15 Hz stimulation, data from 972 to 4772 ms post stimulus onset was analysed (950 sample points). These time-series data were windowed with a cosine-square window (20 point rise/fall) and subjected to a discrete Fourier transform (MATLAB) with a frequency resolution of 0.2485 Hz at 14.167 Hz driving frequency and 0.2632 Hz at the 15 Hz driving frequency. Fourier coefficients were normalized by the length of the segment. The absolute value of the Fourier coefficients was extracted at the respective driving frequency. These power values were then converted to signal-to-noise ratios using the average power for the five frequency bins below and four frequency bins above the driving frequency. *Habituation corrected values:* To correct for interindividual variance in response strength and pre-experimental orientation bias, we converted occipital ssVEP power to a habituation ratio. For this purpose, we divided each subject's mean occipital power for each CS orientation during acquisition, extinction, and day 2 recall trials by his respective mean power for the same orientation during habituation. This yielded an individual learning phase/habituation ratio for each specific CS. Here, values larger than 1 indicate an enhancement of responding to the specific CS relative to habituation (e.g., 1.5 would correspond to a 50% increase in ssVEP power relative to habituation).

ssVEP single-trial analysis. We obtained estimates of single-trial ssVEP amplitude at the respective driving frequency (i.e., 14.167 & 15 Hz) by calculating a moving-window average for each trial and participant[74,75]. We used data starting 992 (for 14.167 Hz stimulation) and 972 ms (for 15 Hz) after stimulus onset to avoid contamination by the initial event-related brain potential (ERP). Each data segment was first baseline-corrected by subtracting the mean of a −600 to 0 ms pre-stimulus baseline period from each channel. A window with the length of four cycles of the respective driving frequency (14.167 and 15 Hz) was shifted across each detrended data segment in steps of one cycle (70.59 and 66.67 ms, for 14.167 and 15 Hz ssVEP, respectively), and the contents of the window were averaged with each step, resulting in averages containing four cycles of the respective ssVEP. A total of 53 averages were obtained for each trial and condition from each subject of the 14.167 Hz stimulation group ($N = 10$ subjects) and 52 averages for the 15 Hz group ($N = 9$), with the last window starting at 4492 ms for 14.167 Hz and at 4442 ms for 15 Hz. These 4-cycle averages of CSD values were transformed into the frequency domain using discrete Fourier transform (DFT). The Fourier coefficients were normalized by the length of the segment, and the power at the driving frequency was extracted. The data were then corrected for habituation by dividing each single-trial estimate by the mean over the 16 habituation trials within each participant, each CS, and each sensor. Finally, the data were smoothed with a 4-trial moving average.

Skin conductance responses and EKG. Skin conductance was recorded with a 0.5 V constant voltage coupler at a sampling rate of 1000 Hz from two Ag/AgCl electrodes (Ø 10 mm), filled with 0.05 M NaCl paste (TD-246) and fixed on the thenar and hypothenar of the left hand. Skin conductance responses (SCR) to the CS were scored offline. A SCR was scored as the maximum onset-to-peak difference in conductance, with an onset occurring 1 to 4 s and a minimum amplitude of 0.02 µS. If more than one SCR met the criteria in a given trial their amplitudes were summed up. Responses not meeting these criteria were scored as zero. Scoring was blind to experimental conditions. SCRs were square-root transformed to normalize the distribution. Individual responses to each CS trial were transformed to standard z-scores within each participant using the mean and standard deviation computed over all CS responses from this participant.

For single-trial analysis of SCR data, we wanted to stay as comparable as possible to the single-trial analysis of ssVEP power. We took the square-root transformed responses from all CS trials. Within each subject we then subtracted the habituation average (16 trials) from each CS response. A division by the habituation average (as with ssVEP) was not possible, as some participants had a SCR habituation average of zero. Before statistical analysis, this habituation corrected SCR single-trial data were then smoothed within each participant with a 4-trial moving average.

Bipolar electrocardiogram (EKG) was recorded with the active electrodes (8 mm, Ag/AgCl) were placed on the left shinbone and under the right clavicle; ground was placed on the right shinbone. EKG data are not reported here.

Ratings of CS valence and arousal, and US expectancy. The valence and arousal ratings were collected repeatedly (before and after each learning block, paper-pencil, to relieve participants' eyes) for each Gabor grating, using the Self-Assessment Manikin[76], a 9-point graphically presented and verbally anchored scale. Starting after acquisition, participants were also asked to rate to what extent they expected an US to occur with each particular CS (US expectancy rating). Ratings ranged from −5 (certainly no US), over 0 (uncertain) to 5 (certainly a US).

Procedure. The main study consisted of two consecutive experiment days, starting either at 10:00 am, 2:00 pm, or 5:30 pm. Upon arrival at the lab on day 1, EEG and other physiology sensors (SCR, EOG, EMG, ECG, and blood pressure cuff) were attached and participants were seated in a dimly lit, sound-attenuated and electrically shielded experimental chamber. Day 1 included habituation, acquisition, and extinction learning as described above in "*Experimental design, fear conditioning stimuli and procedure*". Prior to habituation participants were informed that they will see a series of flickering gratings at the centre of the monitor. They were also reminded to remain as still as possible and comfortably fixate the centre of the screen during the whole computer task. Prior to acquisition, participants were informed that a loud noise will be presented in combination with one of the gratings. However, they were not instructed as to which specific grating was going to predict the noise. In extinction learning (day 1) and delayed recall (day 2) the participants were not informed that no US would be presented. They were merely asked to remember the task instructions they were given earlier. The learning phases were interspaced with short rest periods (1 min), ratings of CS (after acquisition also US) valence and arousal as well as US expectancy. We also recorded resting-EEG, tonic SCR and ECG, and conducted a blood pressure measurement between learning phases. Here, participants were instructed to avoid any movement (except blinking) and to fixate the centre of the screen for 1.5 minutes.

Statistical analysis. For all analyses, except single-trial analyses, we used (8 × 4) repeated measures ANOVA with the factors CS orientation (15, 25, 35, 45, 55, 65, 75 and −45 degrees) and a factor corresponding to the learning phase (habituation, acquisition, extinction, and day 2). These were followed up by ANOVAs for each learning phase (or rating time point) separately. To test the hypotheses of generalization vs. lateral inhibition, we then subjected the respective values to signed *F*-contrast tests. We used the weights reported by McTeague et al.[25], where generalization was modelled as a quadratic trend with the weights: −3, 0.5, 1.5, 2, 1.5, 0.5, and −3 across means ordered by orientation (15° to 75°). Lateral inhibition was modelled as a 'Mexican hat' (difference of Gaussians) with the weights: 0.5, −1, −2, 5, −2, −1, and 0.5. Effect sizes reported are the $r^2_{contrast}$ values[77]. The fit of the competing models was compared using a Bayesian information criterion[41]. The BIC for a model *M1* was then approximated as BIC'[43] from the $r_{contrast}$ effect sizes as:

$$\text{BIC'}_{\text{M1}} = n \, \ln(1 - r^2_{\text{contrast M1}}) + k \, \ln(n),$$

where n is the number of subjects, and k = number of model parameters (set as $k = 7$ = number of weights for both models). We report the difference (ΔBIC) = BIC' for model 1 minus BIC' for the model 2 (the hypothesized model). ΔBIC values >6 suggest *strong*, and ΔBIC >12 suggest *very strong* evidence to prefer model 2 over model 1[42].

Depending on the measure under analysis, the learning phase factor was defined differently. For uncorrected signal-to-noise ratios of ssVEP occipital power at the driving frequency, the factor included the 4 learning phases (i.e., habituation, acquisition, extinction learning, and day 2 delayed recall). For habituation-corrected ssVEP power, the factor included only 3 levels (acquisition, extinction learning, and day 2 delayed recall), because the habituation correction rendered values for habituation to be equal 1 in every case. For skin conductance responses, we analysed day 1 data separately averaged over all trials of habituation and acquisition. To demonstrate extinction, we compared the last 4 trials of acquisition with the last four trials of extinction learning. As a return-of-fear was only expected for the early portion of day 2 trials, we compared SCR data from the first four trials on day 2 to the last 4 trials of extinction learning on day 1. For subjective ratings the factor time point reflected the learning phase: for arousal and valence there were 5 rating time points (after habituation, after acquisition, after extinction, as well as before and after day 2 extinction trials); for US expectancy there were only 4 (after acquisition, after extinction, as well as before and after day 2 extinction trials). US expectancy has $N = 18$ due to missing ratings from one participant. In case of violations of the sphericity assumption, a Greenhouse-Geisser correction was applied.

For single-trial analyses of occipital ssVEP power and SCR we computed the F-contrasts for a 'Mexican hat' and a quadratic fit (custom MATLAB code based on[25]) for each trial. We addressed multiple comparisons by calculating permutation F-distributions from data where CS orientations and learning phases were randomly shuffled within participants with a total of 4000 F-tests entering each distribution. The 0.95 quantile of this distribution served as the critical F-value for each dependent variable.

We computed the scalp distribution of the 'Mexican hat' vs. quadratic fits (Figs. 2C and 4A) by applying the same contrast weights to habituation-corrected power estimates of each of the 65 scalp electrodes for the average over acquisition, extinction, and day 2 trials (implemented with custom MATLAB code based on[25] and visualized in the EMEGS software[78]). Significance level for all analyses was set at 0.05 and all tests were two-tailed.

Data availability

The data that support the findings of this study are available on request from the corresponding author (M.I.A.).

Code availability

Custom MATLAB scripts used for analyses are available from the corresponding author (M.I.A.) upon request.

References

1. Pavlov, I. P. *Conditioned reflexes: an investigation of the physiological activity of the cerebral cortex*. (Oxford University Press, 1927).
2. Myers, K. M. & Davis, M. Mechanisms of fear extinction. *Mol. Psychiatry* **12**, 120–150 (2007).
3. Furini, C., Myskiw, J. & Izquierdo, I. The learning of fear extinction. *Neurosci. Biobehav. Rev.* **47**, 670–683 (2014).
4. Herry, C. & Johansen, J. Encoding of fear learning and memory in distributed neuronal circuits. *Nat. Neurosci.* **17**, 1644–1654 (2014).
5. McGann, J. P. Associative learning and sensory neuroplasticity: how does it happen and what is it good for? *Learn. Mem.* **22**, 567–76 (2015).
6. Kass, M. D., Rosenthal, M. C., Pottackal, J. & McGann, J. P. Fear learning enhances neural responses to threat-predictive sensory stimuli. *Science* **342**, 1389–1392 (2013).
7. Weinberger, N. M. New perspectives on the auditory cortex: Learning and memory. in *Handbook of Clinical Neurology* (eds. Celesia, G. G. & Hickok, G.) vol. 129, 117–147 (Elsevier B.V., 2015).
8. Bakin, J. S. & Weinberger, N. M. Classical conditioning induces CS-specific receptive field plasticity in the auditory cortex of the guinea pig. *Brain Res.* **536**, 271–286 (1990).
9. Edeline, J.-M. Beyond traditional approaches to understanding the functional role of neuromodulators in sensory cortices. *Front. Behav. Neurosci.* **6**, 1–14 (2012).
10. Froemke, R. C., Merzenich, M. M. & Schreiner, C. E. A synaptic memory trace for cortical receptive field plasticity. *Nature* **450**, 425–429 (2007).
11. Letzkus, J. J. *et al.* A disinhibitory microcircuit for associative fear learning in the auditory cortex. *Nature* **480**, 331–335 (2011).
12. Boatman, J. A. & Kim, J. J. A thalamo-cortico-amygdala pathway mediates auditory fear conditioning in the intact brain. *Eur. J. Neurosci.* **24**, 894–900 (2006).
13. Wigestrand, M. B., Schiff, H. C., Fyhn, M., LeDoux, J. E. & Sears, R. M. Primary auditory cortex regulates threat memory specificity. *Learn. Mem.* **24**, 55–58 (2017).
14. Morris, J. S., Friston, K. J. & Dolan, R. J. Experience-dependent modulation of tonotopic neural responses in human auditory cortex. *Proc. R. Soc. B Biol. Sci.* **265**, 649–657 (1998).
15. Thiel, C. M., Friston, K. J. & Dolan, R. J. Cholinergic modulation of experience-dependent plasticity in human auditory cortex. *Neuron* **35**, 567–574 (2002).
16. Kluge, C. *et al.* Plasticity of human auditory-evoked fields induced by shock conditioning and contingency reversal. *PNAS Proc. Natl. Acad. Sci. United States Am.* **108**, 12545–50 (2011).
17. Staib, M. & Bach, D. R. Stimulus-invariant auditory cortex threat encoding during fear conditioning with simple and complex sounds. *Neuroimage* **166**, 276–284 (2018).
18. Gavornik, J. P. & Bear, M. F. Higher brain functions served by the lowly rodent primary visual cortex. *Learn. Mem.* **21**, 527–33 (2014).
19. Moratti, S., Keil, A. & Miller, G. A. Fear but not awareness predicts enhanced sensory processing in fear conditioning. *Psychophysiology* **43**, 216–26 (2006).

20. Moratti, S. & Keil, A. Not what you expect: experience but not expectancy predicts conditioned responses in human visual and supplementary cortex. *Cereb. Cortex* **19**, 2803–9 (2009).
21. Song, I. & Keil, A. Differential classical conditioning selectively heightens response gain of neural population activity in human visual cortex. *Psychophysiology* **51**, 1185–1194 (2014).
22. Knight, D. C., Smith, C. N., Stein, E. A. & Helmstetter, F. J. Functional MRI of human Pavlovian fear conditioning: patterns of activation as a function of learning. *Neuroreport* **10**, 3665–3670 (1999).
23. Morris, J. S., Buchel, C. & Dolan, R. J. Parallel neural responses in amygdala subregions and sensory cortex during implicit fear conditioning. *Neuroimage* **13**, 1044–1052 (2001).
24. Moratti, S., Giménez-Fernández, T., Méndez-Bértolo, C. & de Vicente-Pérez, F. Conditioned inhibitory and excitatory gain modulations of visual cortex in fear conditioning: Effects of analysis strategies of magnetocortical responses. *Psychophysiology* **54**, 882–893 (2017).
25. McTeague, L. M., Gruss, L. F. & Keil, A. Aversive learning shapes neuronal orientation tuning in human visual cortex. *Nat. Commun.* **6**, 7823 (2015).
26. Rhodes, L. J., Ruiz, A., Ríos, M., Nguyen, T. & Miskovic, V. Differential aversive learning enhances orientation discrimination. *Cogn. Emot.* **9931**, 1–7 (2017).
27. Miskovic, V. & Keil, A. Perceiving threat in the face of safety: excitation and inhibition of conditioned fear in human visual cortex. *J. Neurosci.* **33**, 72–8 (2013).
28. Weinberger, N. M. Physiological memory in primary auditory cortex: characteristics and mechanisms. *Neurobiol. Learn. Mem.* **70**, 226–251 (1998).
29. Quirk, G. J., Armony, J. L. & LeDoux, J. E. Fear conditioning enhances different temporal components of tone-evoked spike trains in auditory cortex and lateral amygdala. *Neuron* **19**, 613–624 (1997).
30. Armony, J. L., Quirk, G. J. & LeDoux, J. E. Differential effects of amygdala lesions on early and late plastic components of auditory cortex spike trains during fear conditioning. *J. Neurosci.* **18**, 2592–2601 (1998).
31. Apergis-Schoute, A. M., Schiller, D., LeDoux, J. E. & Phelps, E. A. Extinction resistant changes in the human auditory association cortex following threat learning. *Neurobiol. Learn. Mem.* **113**, 109–114 (2014).
32. Quirk, G. J. & Mueller, D. Neural mechanisms of extinction learning and retrieval. *Neuropsychopharmacology* **33**, 56–72 (2008).
33. Bouton, M. E. Context and behavioral processes in extinction. *Learn. Mem.* **11**, 485–494 (2004).
34. Rescorla, R. A. Spontaneous Recovery. *Learn. Mem.* **11**, 501–509 (2004).
35. Hubel, D. H. & Wiesel, T. N. Sequence regularity and geometry of orientation columns in the monkey striate cortex. *J. Comp. Neurol.* **158**, 267–293 (1974).
36. Paik, S.-B. & Ringach, D. L. Link between orientation and retinotopic maps in primary visual cortex. *PNAS Proc. Natl. Acad. Sci. United States Am.* **109**, 7091–6 (2012).
37. Norcia, A. M., Appelbaum, L. G., Ales, J. M., Cottereau, B. R. & Rossion, B. The steady-state visual evoked potential in vision research: a review. *J. Vis.* **15**, 1–46 (2015).
38. Shapley, R., Hawken, M. & Ringach, D. L. Dynamics of orientation selectivity in the primary visual cortex and the importance of cortical inhibition. *Neuron* **38**, 689–699 (2003).
39. Lissek, S. *et al.* Neural substrates of classically conditioned fear-generalization in humans: A parametric fMRI study. *Soc. Cogn. Affect. Neurosci.* **9**, 1134–1142 (2014).
40. Dymond, S., Dunsmoor, J. E., Vervliet, B., Roche, B. & Hermans, D. Fear generalization in humans: systematic review and implications for anxiety disorder research. *Behav. Ther.* **46**, 561–582 (2015).
41. Schwarz, G. Estimating the dimension of a model. *Ann. Stat.* **6**, 461–464 (1978).
42. Wagenmakers, E.-J. A practical solution to the pervasive problems of p values. *Psychon. Bull. Rev.* **14**, 779–804 (2007).
43. Raftery, A. E. Bayesian model selection in social research. In *Sociological Methodology* vol. 25, 111 (1995).
44. Yuan, M., Giménez-Fernández, T., Méndez-Bértolo, C. & Moratti, S. Ultra-fast cortical gain adaptation in the human brain by trial-to-trial changes of associative strength in fear learning. *J. Neurosci.* **38**, 0977–18 (2018).
45. Mather, M., Clewett, D., Sakaki, M. & Harley, C. W. Norepinephrine ignites local hotspots of neuronal excitation: how arousal amplifies selectivity in perception and memory. *Behav. Brain Sci.* **39**, e200 (2016).
46. Cambiaghi, M., Grosso, A., Renna, A. & Sacchetti, B. Differential recruitment of auditory cortices in the consolidation of recent auditory fearful memories. *J. Neurosci.* **36**, 8586–8597 (2016).
47. Cambiaghi, M. *et al.* Higher-order sensory cortex drives basolateral amygdala activity during the recall of remote, but not recently learned fearful memories. *J. Neurosci.* **36**, 1647–1659 (2016).
48. Rescorla, R. A. & Heth, C. D. Reinstatement of fear to an extinguished conditioned stimulus. *J. Exp. Psychol. Anim. Behav. Process.* **1**, 88–96 (1975).
49. Bouton, M. E. & Moody, E. W. Memory processes in classical conditioning. *Neurosci. Biobehav. Rev.* **28**, 663–674 (2004).
50. Clem, R. L. & Schiller, D. New learning and unlearning: strangers or accomplices in threat memory attenuation? *Trends Neurosci.* **39**, 340–351 (2016).
51. Pape, H.-C. & Paré, D. Plastic synaptic networks of the amygdala for the acquisition, expression, and extinction of conditioned fear. *Physiol. Rev.* **90**, 419–463 (2010).
52. Herry, C. *et al.* Neuronal circuits of fear extinction. *Eur. J. Neurosci.* **31**, 599–612 (2010).
53. Lai, C. S. W., Adler, A. & Gan, W.-B. Fear extinction reverses dendritic spine formation induced by fear conditioning in the mouse auditory cortex. *Proc. Natl. Acad. Sci.* **115**, 9306–9311 (2018).
54. Keifer, O. P. Jr. *et al.* Voxel-based morphometry predicts shifts in dendritic spine density and morphology with auditory fear conditioning. *Nat. Commun.* **6**, 7582 (2015).
55. Vervliet, B., Craske, M. G. & Hermans, D. Fear extinction and relapse: state of the art. *Annu. Rev. Clin. Psychol.* **9**, 215–248 (2013).
56. Todd, R. M. *et al.* Soldiers with posttraumatic stress disorder see a world full of threat: magnetoencephalography reveals enhanced tuning to combat-related cues. *Biol. Psychiatry* **78**, 821–829 (2015).
57. Reddan, M. C., Wager, T. D. & Schiller, D. Attenuating neural threat expression with imagination. *Neuron* **100**, 994–1005 (2018).
58. An, B. *et al.* Amount of fear extinction changes its underlying mechanisms. *Elife* **6**, e25224 (2017).
59. Maren, S. Nature and causes of the immediate extinction deficit: A brief review. *Neurobiol. Learn. Mem.* **113**, 19–24 (2014).
60. Pennartz, C. M. A., Dora, S., Muckli, L. & Lorteije, J. A. M. Towards a unified view on pathways and functions of neural recurrent processing. *Trends Neurosci.* **42**, 589–603 (2019).
61. Shuler, M. G. & Bear, M. F. Reward timing in the primary visual cortex. *Science* **311**, 1606–1609 (2006).
62. Ramesh, R. N., Burgess, C. R., Sugden, A. U., Gyetvan, M. & Andermann, M. L. Intermingled ensembles in visual association cortex encode stimulus identity or predicted outcome. *Neuron* **100**, 900–915.e9 (2018).
63. Meissner-Bernard, C., Dembitskaya, Y., Venance, L. & Fleischmann, A. Encoding of odor fear memories in the mouse olfactory cortex. *Curr. Biol.* **29**, 367–380.e4 (2019).
64. Stockhorst, U. & Antov, M. I. Modulation of fear extinction by stress, stress hormones and estradiol: a review. *Front. Behav. Neurosci.* **9**, 359 (2016).
65. Antov, M. I. & Stockhorst, U. Stress exposure prior to fear acquisition interacts with estradiol status to alter recall of fear extinction in humans. *Psychoneuroendocrinology* **49**, 106–118 (2014).
66. Foa, E. B. *Posttraumatic diagnostic scale manual.* (National Computer Systems, 1995).

67. Petro, N. M. *et al.* Multimodal imaging evidence for a frontoparietal modulation of visual cortex during the selective processing of conditioned threat. *J. Cogn. Neurosci.* **29**, 953–967 (2017).
68. Gerlicher, A. M. V., Tüscher, O. & Kalisch, R. Dopamine-dependent prefrontal reactivations explain long-term benefit of fear extinction. *Nat. Commun.* **9** (2018).
69. Meir Drexler, S., Merz, C. J. & Wolf, O. T. Preextinction stress prevents context-related renewal of fear. *Behav. Ther.* **49**, 1008–1019 (2018).
70. Brainard, D. H. & Vision, S. The psychophysics toolbox. *Spat. Vis.* **10**, 433–436 (1997).
71. Kleiner, M. *et al.* What's new in Psychtoolbox-3? *Perception* **36**, ECVP Abstract Supplement (2009).
72. Blumenthal, T. D. *et al.* Committee report: Guidelines for human startle eyeblink electromyographic studies. *Psychophysiology* **42**, 1–15 (2005).
73. Junghöfer, M., Elbert, T., Leiderer, P., Berg, P. & Rockstroh, B. Mapping EEG-potentials on the surface of the brain: A strategy for uncovering cortical sources. *Brain Topogr.* **9**, 203–217 (1997).
74. Keil, A. *et al.* Early modulation of visual perception by emotional arousal: evidence from steady-state visual evoked brain potentials. *Cogn. Affect. Behav. Neurosci.* **3**, 195–206 (2003).
75. Keil, A. *et al.* Electrocortical and electrodermal responses covary as a function of emotional arousal: a single-trial analysis. *Psychophysiology* **45**, 516–523 (2008).
76. Bradley, M. M. & Lang, P. J. Measuring emotion: the Self-Assessment Manikin and the Semantic Differential. *J. Behav. Ther. Exp. Psychiatry* **25**, 49–59 (1994).
77. Rosnow, R. L., Rosenthal, R. & Rubin, D. B. Contrasts and correlations in effect-size estimation. *Psychol. Sci.* **11**, 446–453 (2000).
78. Peyk, P., De Cesarei, A. & Junghöfer, M. Electromagnetic encephalography software: Overview and integration with other EEG/MEG toolboxes. *Comput. Intell. Neurosci.* **2011** (2011).

Acknowledgements

Author contributions

Conceptualization: M.I.A., U.S. and A.K. Methodology: A.K. and M.I.A. Investigation: E.P. and M.I.A. Formal analysis: M.I.A. and A.K. Visualization: M.I.A. and E.P. Writing – original draft: M.I.A. Writing – review & editing: M.I.A., U.S., A.K., E.P. and P.B. Funding acquisition: U.S. (departmental budget) and M.I.A (G.A.-Lienert-Foundation Scholarship), AK (NIMH grant R01 MH112558A). Project administration: M.I.A. and U.S. Supervision: U.S. and A.K.

Competing interests

The authors declare no competing interests.

Additional information

Supplementary information is available for this paper at https://doi.org/10.1038/s41598-020-60597-z.

Correspondence and requests for materials should be addressed to M.I.A.

Reprints and permissions information is available at www.nature.com/reprints.

Publisher's note Springer Nature remains neutral with regard to jurisdictional claims in published maps and institutional affiliations.

Supplementary Figures & Tables.

Title: Visuocortical tuning to a threat-related feature persists after extinction and consolidation of conditioned fear.

Authors: Martin I. Antov, Elena Plog, Philipp Bierwirth, Andreas Keil, and Ursula Stockhorst

Note. To assure the comparability of our figures with previous work using this specific fear conditioning task (McTeague et al. *Nat. Commun.* **6**, 7823 [2015]) we have plotted values as *Mean* ± 1 *SEM* in Figures 2, 4, and 5 of the manuscript. The Supplementary Figures S1, S2, and S6-S8 included here, show the same data with a combination of dot plots (representing individual values of every subject that entered the respective statistical analysis) and boxplots. This should help with transparency and allow the reader to judge the full variance and distribution of the raw data.

February 10, 2020

Supplementary Figures & Tables. SREP-19-40764B. *Visuocortical tuning to a threat-related feature persists after extinction and consolidation of conditioned fear.*

1

43

Suppl. Fig. S1 | Occipital cortical responses during the different phases of conditioning. Changes in visual electrocortical activity for the learning phases **(a)** *habituation*, **(b)** *acquisition*, **(c)** *extinction*, and **(d)** *day 2 delayed recall*, shown for each CS-orientation (on the x-axes). In all sub-plots **(a-d)** the data show ssVEP spectral power current source density (CSD, Laplacian space), averaged across 3 occipital midline sensor locations (O1, Oz, O2). All values are signal to noise-ratios (SNR), i.e., the power at the driving frequency was divided by the average power for the five frequency bins below and four frequency bins above the driving frequency (as the noise estimate). The insert to the right from subplot **(a)** shows a view of the back of the electrode array used, the sensor locations used for averaging are highlighted in yellow. These data are shown in the manuscript in Fig. 2b with $M \pm 1$ *SEM*.

Each **black dot** shows the SNR of a single subject ($N = 19$). For the **boxplots**: the cyan **boxes** are drawn between the 25th and 75th percentile, the **horizontal line** marks the median. The boxplot **whiskers** extend above and below the box to the most extreme data points that are within a distance to the box equal to 1.5 times the interquartile range (Tukey boxplot). The narrowing of the boxes displays **notches** at median $\pm$ 1.58 x interquartile range / ($\sqrt{N}$). **Yellow diamonds** connected with a solid black line show the means ($N = 19$) and the **gray shaded area** around the means shows the 95% confidence interval of the mean.

February 10, 2020

Supplementary Figures & Tables. SREP-19-40764B. *Visuocortical tuning to a threat-related feature persists after extinction and consolidation of conditioned fear.*

2

44

Suppl. Fig. S2 | The same data as in Suppl. Fig. 1 after habituation correction. Each subject's occipital power for each CS-orientation during acquisition, extinction, and day 2 delayed recall was normalized through division by the corresponding orientation's mean power during habituation: **(a)** *acquisition*, **(b)** *extinction*, and **(c)** *day 2 delayed recall.* These data are shown in the manuscript in Fig. 2b with $M \pm 1$ *SEM*.

Each **black dot** shows the SNR of a single subject ($N = 19$). For the **boxplots**: the cyan **boxes** are drawn between the 25th and 75th percentile, the **horizontal line** marks the median. The boxplot **whiskers** extend above and below the box to the most extreme data points that are within a distance to the box equal to 1.5 times the interquartile range (Tukey boxplot). The narrowing of the boxes displays **notches** at median ± 1.58 x interquartile range / ($\sqrt{N}$). **Yellow diamonds** connected with a solid black line show the means ($N = 19$) and the **gray shaded area** around the means shows the 95% confidence interval of the mean.
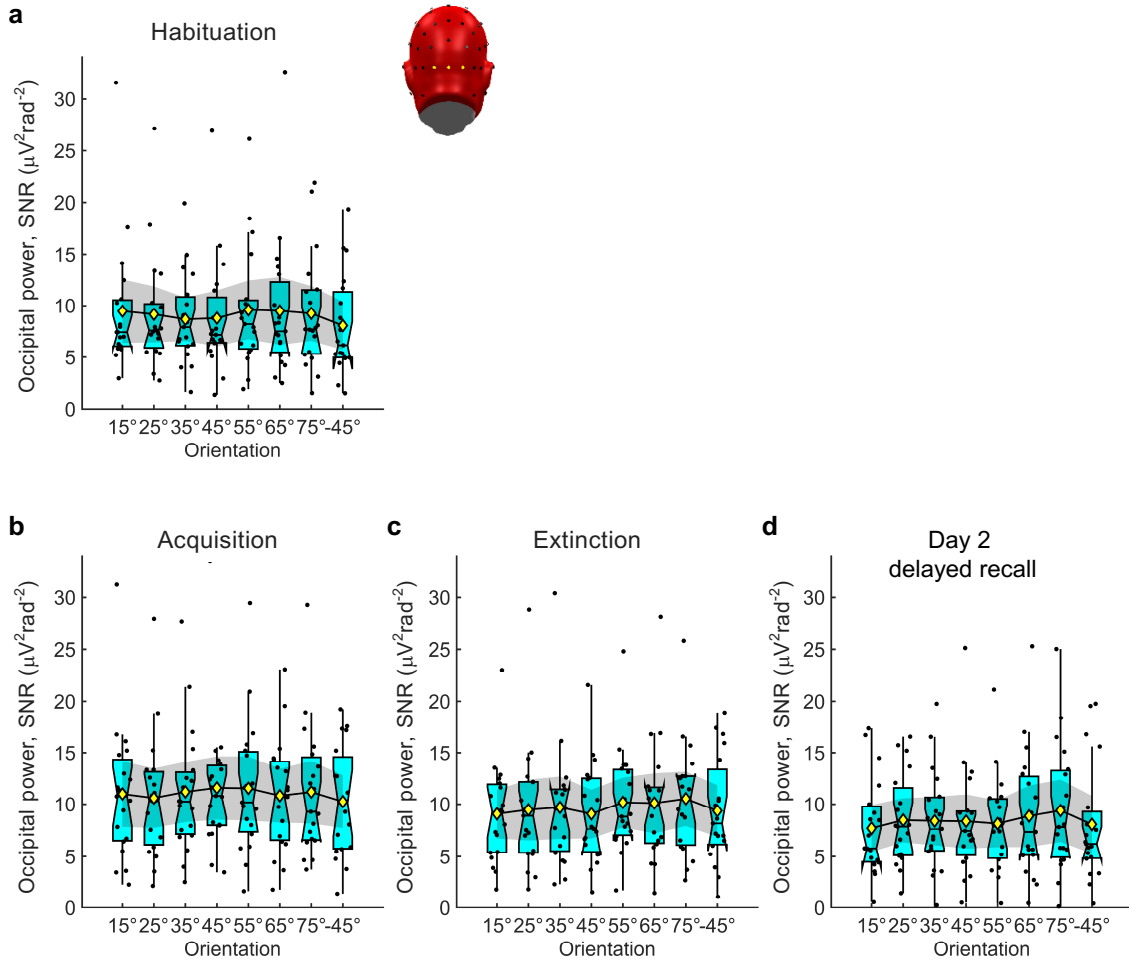
February
10, 2020

Supplementary Figures & Tables. SREP-19-40764B. *Visuocortical tuning to a threat-related feature persists after extinction and consolidation of conditioned fear.*

3

45

Suppl. Fig. S3 | Topographical distributions of 'Mexican hat' statistical fits over single trial data, left view of the scalp. Color maps show *F*-values, black dots the EEG-electrode positions. **(A)** *Habituation*, **(B)** *acquisition*, **(C)** *extinction*, and **(D)** *day 2 delayed recall.* Parts of these (trials 5-12 from day 2) are shown in the manuscript Fig. 4A.

February 10, 2020

Supplementary Figures & Tables. SREP-19-40764B. *Visuocortical tuning to a threat-related feature persists after extinction and consolidation of conditioned fear.*
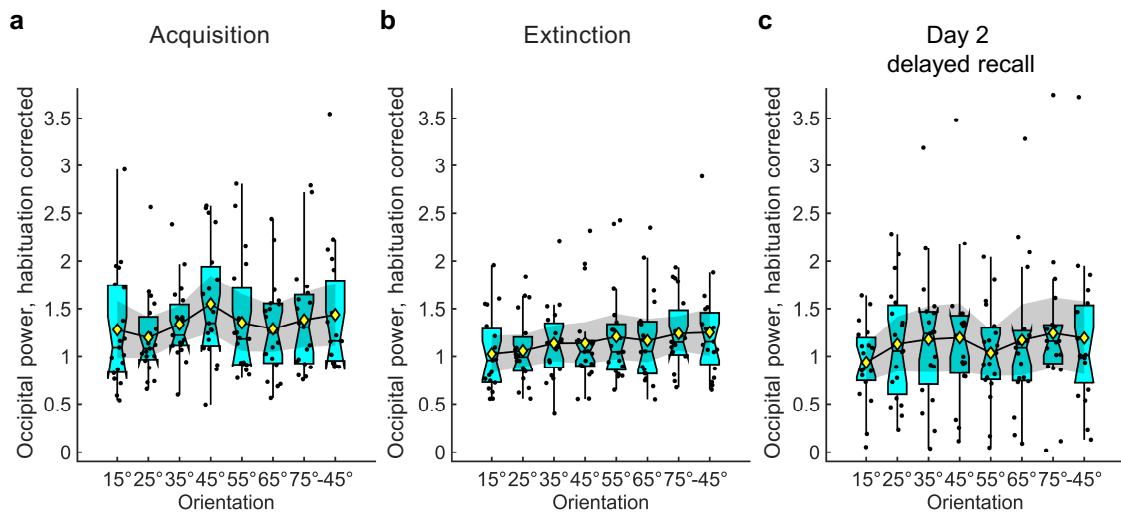
4

46

Suppl. Fig. S4 | Topographical distributions of 'Mexican hat' statistical fits over single trial data, right view of the scalp. Color maps show *F*-values, black dots the EEG-electrode positions. **(A)** *Habituation*, **(B)** *acquisition*, **(C)** *extinction*, and **(D)** *day 2 delayed recall*. Parts of these (trials 5-12 from day 2) are shown in the manuscript Fig. 4A.

February 10, 2020

Supplementary Figures & Tables. SREP-19-40764B. *Visuocortical tuning to a threat-related feature persists after extinction and consolidation of conditioned fear.*

5

47
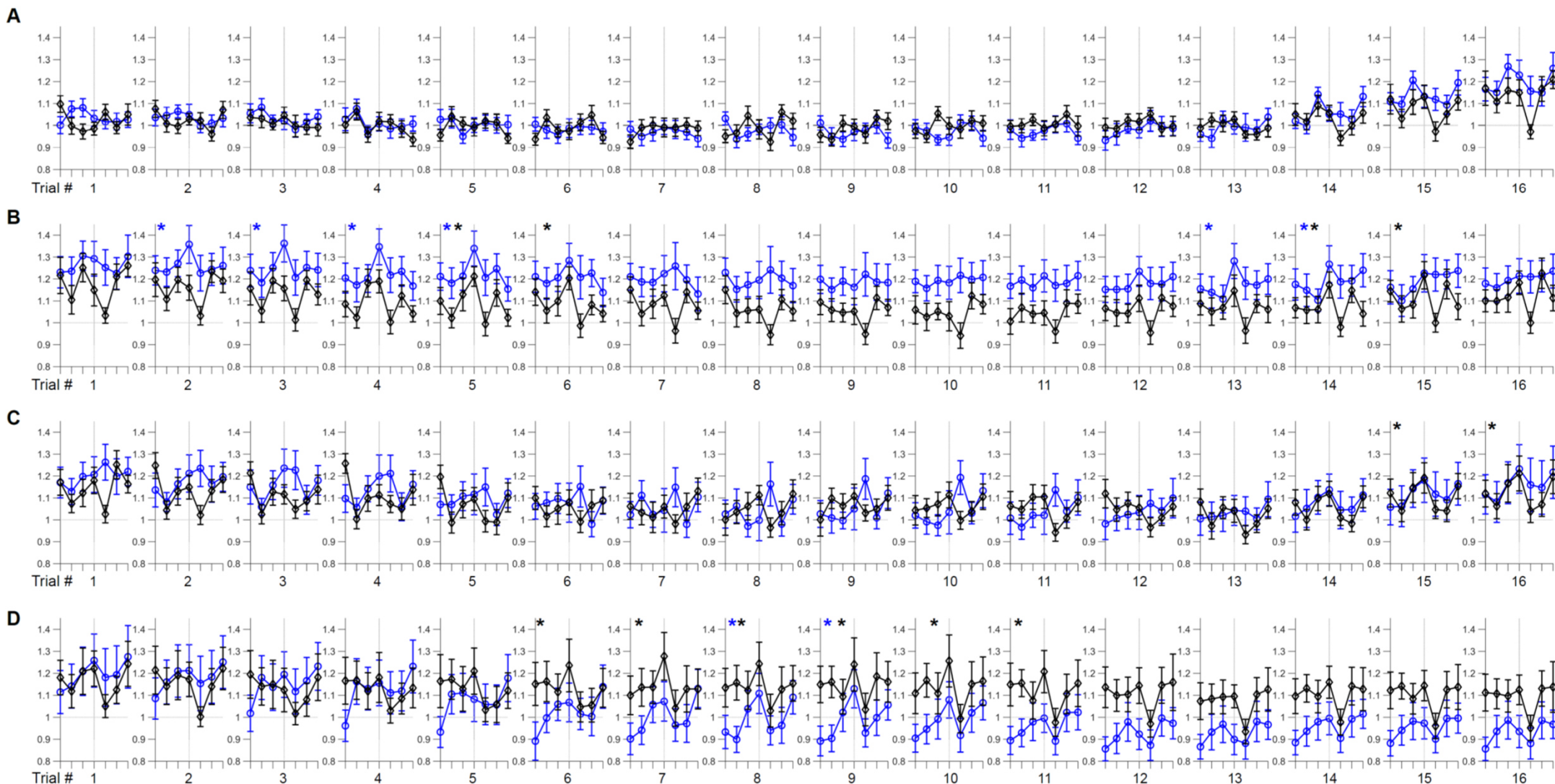
Suppl. Fig. S5 | Alternative depiction of single-trial data for a priori occipital and exploratory bilateral temporo-occipital regions. Changes in visual electrocortical activity for the learning phases **(A)** *habituation*, **(B)** *acquisition*, **(C)** *extinction*, and **(D)** *day 2 delayed recall*. Each subplot shows data from one trial, CS-orientation is on the x-axes (left to right: 15°, 25°, 45°, 55°, 65°, 75°), vertical grey dotted lines mark the CS+ (45°). Data shown are the same as in the contour plots in manuscript Fig. 3A and Fig. 4B, here as line plots with error estimates. In all sub-plots **(A-D)** the ***blue line*** shows data averaged across the 3 a priori occipital midline sensor locations (O1, Oz, O2); the ***black line*** shows data averaged across the 4 sensors of the exploratory bilateral temporo-occipital region (TP8, TP10, TP7, and TP9). As in manuscript Fig. 3A and 4B, all values (y-axes) are changes in single-trial power estimates at the driving frequency, relative to habituation, i.e. power for each data point divided by the average of the 16 habituation single-trial estimates at the respective CS orientation. Asterisks at the upper left of a subplot denote a substantial 'Mexican hat' fit (contrast F-value > 4.25). Error bars show ± 1 *SEM*.

February 10, 2020

Supplementary Figures & Tables. SREP-H840764B. *Visuocortical tuning to a threat-related feature persists after extinction and consolidation of conditioned fear.*

6

Suppl. Fig. S6 | Skin conductance responses during the different phases of fear conditioning. (a) *Habituation average,* **(b)** *acquisition average*, **(c)** *acquisition last 4 trials,* **(d)** *extinction last 4 trials*, **(e)** *first 4 trials*, and **(f)** *last 4 trials* of *delayed recall on day 2*. The data (N = 19) are individual z-scores standardized on the mean and SD of all responses in the experiment. These data are shown in the manuscript in Fig. 5a and b with M ± 1 *SEM*.

Each **black dot** shows the z-score of a single participant (N = 19, averaged over 16 trials for day 1, and over 8 trials for day 2). For the **boxplots**: the cyan **boxes** are drawn between the 25th and 75th percentile, the **horizontal line** marks the median. The boxplot **whiskers** extend above and below the box to the most extreme data points that are within a distance to the box equal to 1.5 times the interquartile range (Tukey boxplot). The narrowing of the boxes displays **notches** at median ± 1.58 x interquartile range / ($\sqrt{N}$). **Yellow diamonds** connected with a solid black line show the means (N = 19) and the **gray shaded area** around the means shows the 95% confidence interval of the mean.
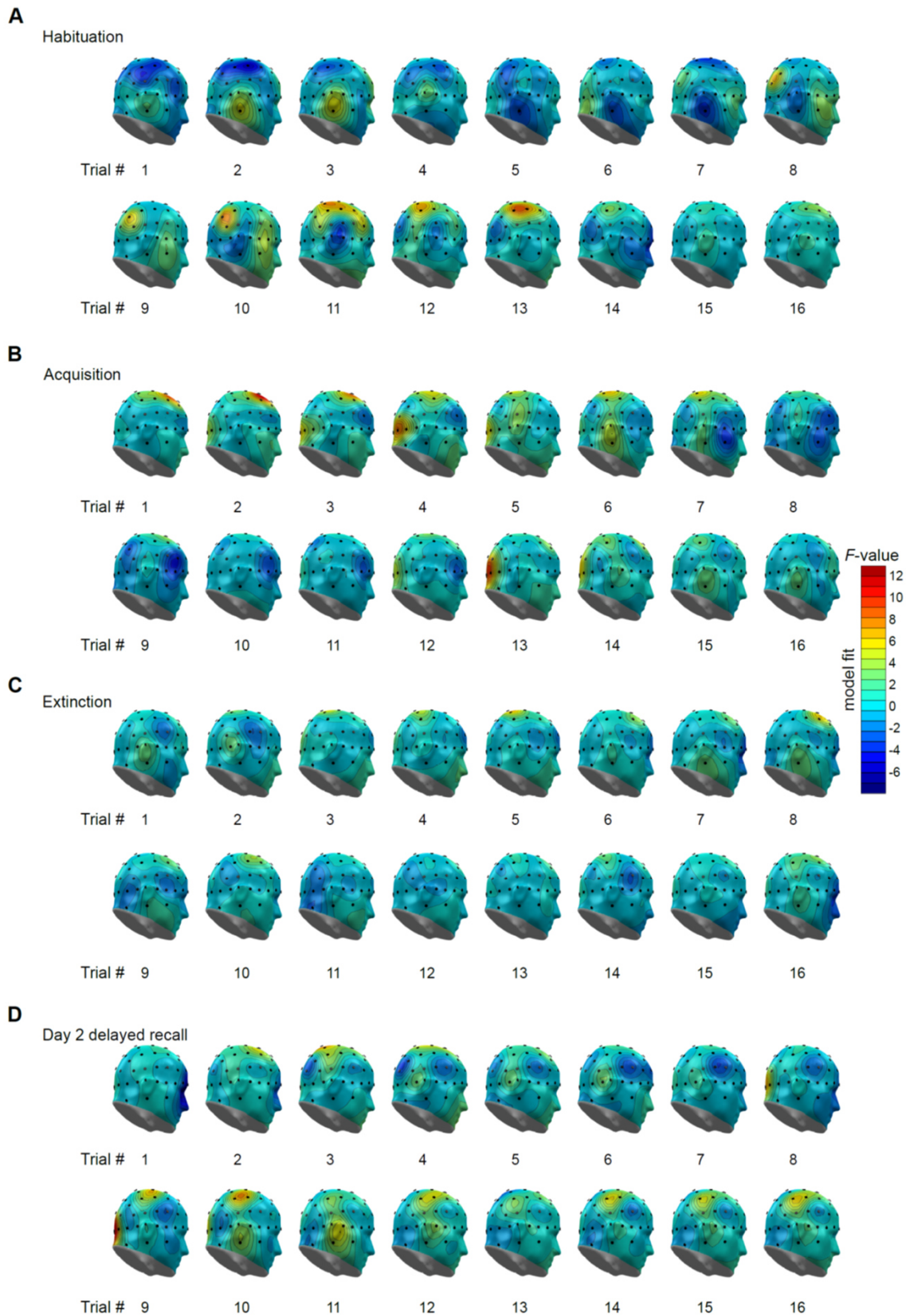
February 10, 2020

Supplementary Figures & Tables. SREP-19-40764B. *Visuocortical tuning to a threat-related feature persists after extinction and consolidation of conditioned fear.*

7

49
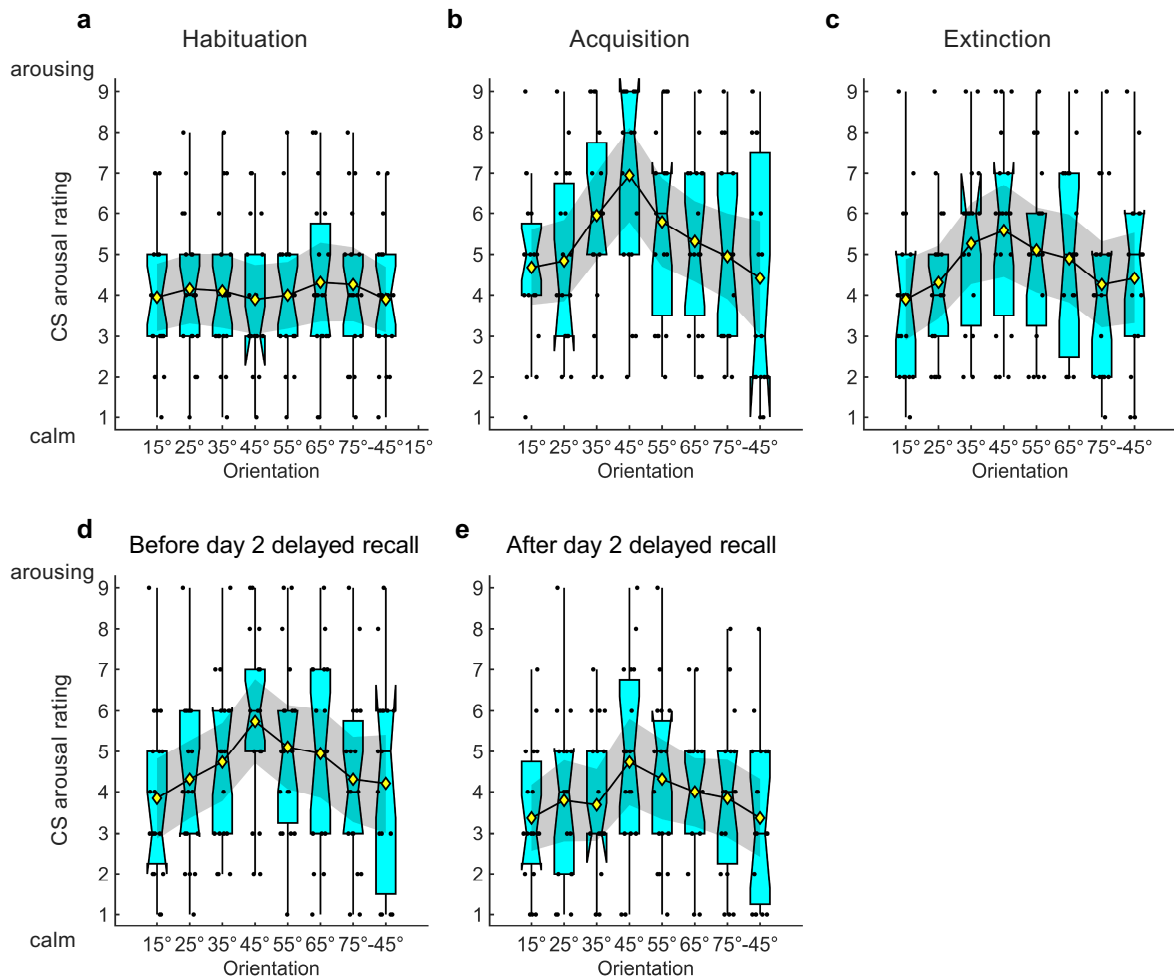
Suppl. Fig. S7 | Subjective self-report changes in CS arousal ratings during the different phases of fear conditioning. Values for each CS-orientation from all *N* = 19 subjects, as rated on day 1 **(a)** *after habituation*, **(b)** *after acquisition*, and **(c)** after extinction, as well as **(d)** *before,* and **(e)** *after delayed recall on day 2*. These data are shown in the manuscript in Fig. 5a and b with *M* ± 1 *SEM*.

Each **black dot** shows the rating of a single participant (*N* = 19). For the **boxplots**: the cyan **boxes** are drawn between the 25th and 75th percentile, the **horizontal line** marks the median. The boxplot **whiskers** extend above and below the box to the most extreme data points that are within a distance to the box equal to 1.5 times the interquartile range (Tukey boxplot). The narrowing of the boxes displays **notches** at median ± 1.58 x interquartile range / ($\sqrt{N}$). **Yellow diamonds** connected with a solid black line show the means (*N = 19*) and the **gray shaded area** around the means shows the 95% confidence interval of the mean.
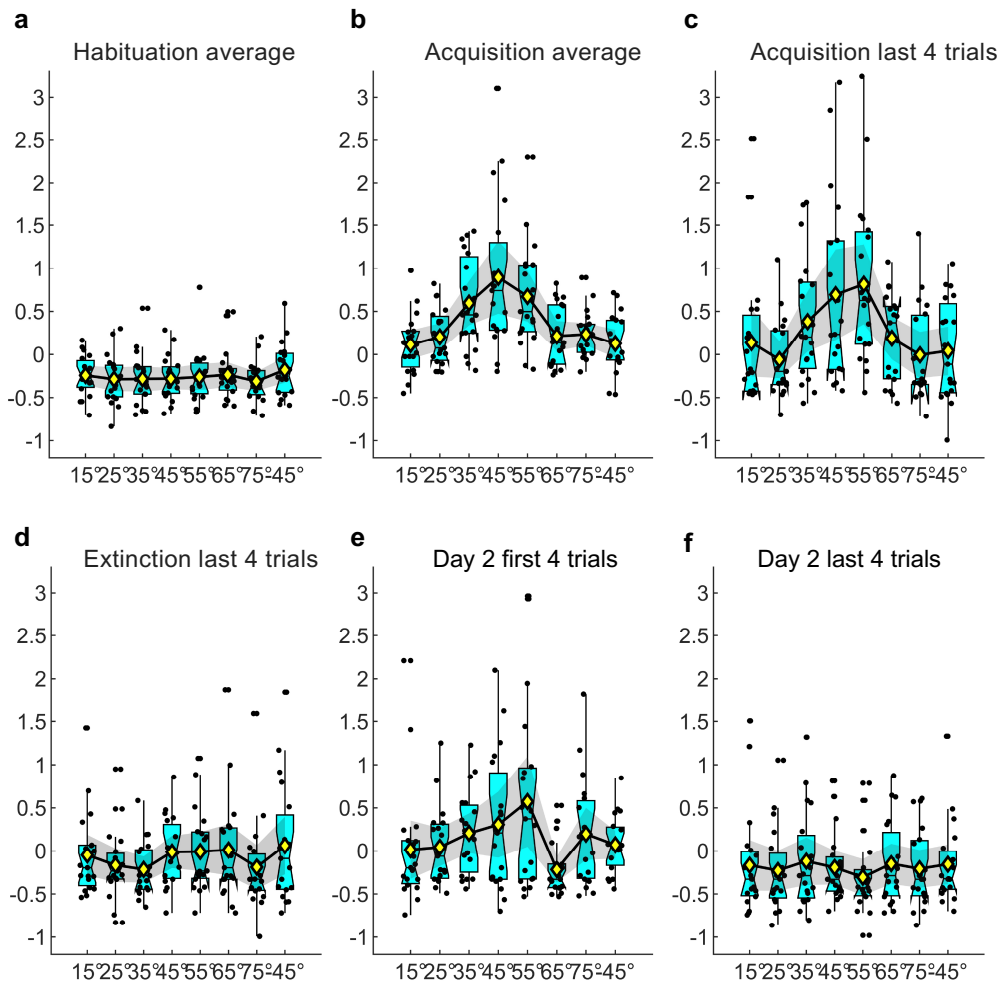
February 10, 2020

Supplementary Figures & Tables. SREP-19-40764B. *Visuocortical tuning to a threat-related feature persists after extinction and consolidation of conditioned fear.*

8

50
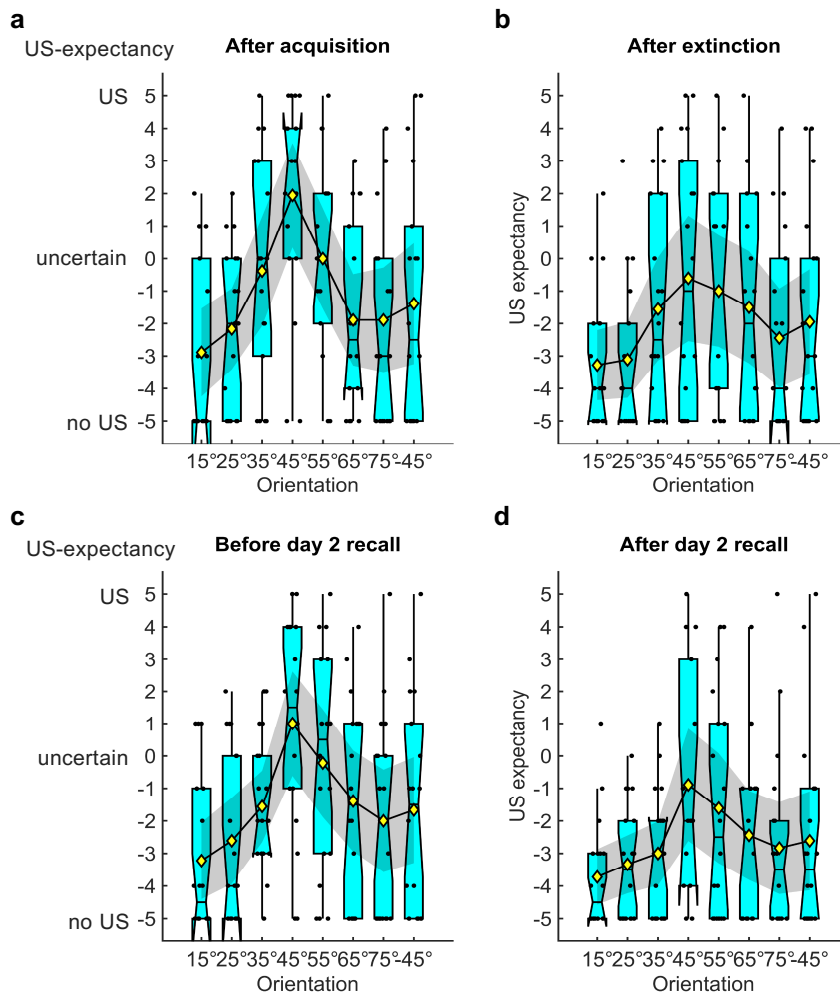
Suppl. Fig. S8 | Subjective self-report changes in US-expectancy ratings during the different phases of fear conditioning. Values for each CS-orientation from *N* = 18 (one participant did not provide US-expectancy ratings), as rated on day 1 **(a)** *after acquisition*, and **(b)** after extinction, as well as **(c)** *before,* and **(d)** *after delayed recall on day 2*. These data are shown in the manuscript in Fig. 5c and d with *M* ± 1 *SEM*.

Each ***black dot*** shows the US-expectancy rating of a single participant (*N* = 18). For the ***boxplots***: the cyan ***boxes*** are drawn between the 25th and 75th percentile, the ***horizontal line*** marks the median. The boxplot ***whiskers*** extend above and below the box to the most extreme data points that are within a distance to the box equal to 1.5 times the interquartile range (Tukey boxplot). The narrowing of the boxes displays ***notches*** at median ± 1.58 x interquartile range / ($\sqrt{N}$). ***Yellow diamonds*** connected with a solid black line show the means (*N = 18*) and the ***gray shaded area*** around the means shows the 95% confidence interval of the mean.

February 10, 2020

Supplementary Figures & Tables. SREP-19-40764B. *Visuocortical tuning to a threat-related feature persists after extinction and consolidation of conditioned fear.*

9

51

a

Lateral temporo-occipital power
SNR ($\mu V^2 rad^{-2}$)

— Habituation
—▲— Acquisition
—○— Extinction
—▲— Day 2 delayed recall

15° 25° 35° 45° 55° 65° 75° -45°

b

Lateral temporo-occipital power
Habituation corrected

15° 25° 35° 45° 55° 65° 75° -45°
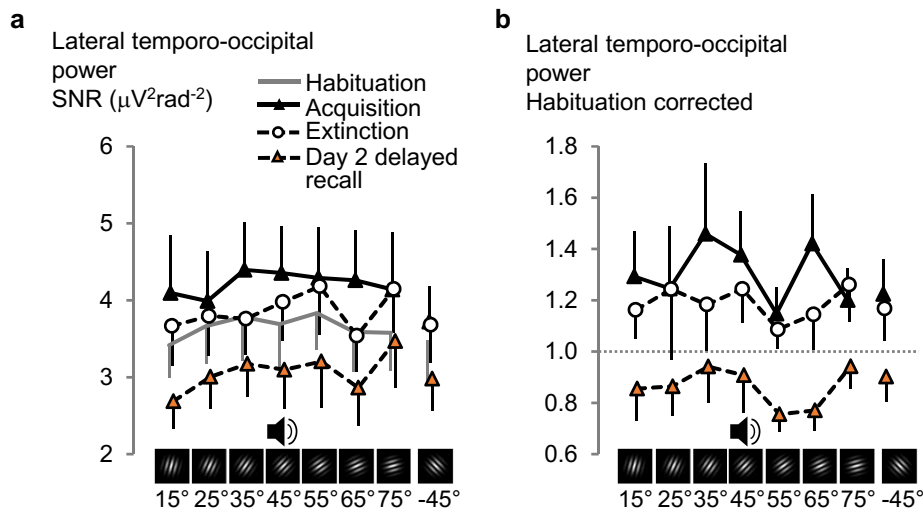
Suppl. Fig. S9 | As in manuscript Fig. 2A, 2B, for completeness: Lateral temporo-occipital cortical responses averaged over 16 trials for each phase of conditioning. (a) Changes in the grand average (*N* = 19) of visual electrocortical activity for each learning phase (habituation, acquisition, extinction, and day 2 delayed recall) and for each CS orientation. Regional means of the ssVEP spectral power current source density (CSD, Laplacian space), averaged across the bilateral temporo-occipital region pooled from the explorative 4-sensor cluster (TP8, TP10, TP7, and TP9). Values are signal-to-noise ratios (SNR), i.e., the power at the driving frequency was divided by the average power for the five frequency bins below and four frequency bins above the driving frequency (as the noise estimate). **(b)** The same data after habituation correction for acquisition, extinction, and day 2 delayed recall.

Suppl. Table 1. Trial order of stimuli during the experiment in sequence 1 and sequence 2

HABITUATION						ACQUISITION						EXTINCTION						DAY 2 DELAYED RECALL					
Sequence 1			Sequence 2			Sequence 1			Sequence 2			Sequence 1			Sequence 2			Sequence 1			Sequence 2		
Trial #	Repeat #	CS orientation	Trial #	Repeat #	CS orientation	Trial #	Repeat #	CS orientation	Trial #	Repeat #	CS orientation	Trial #	Repeat #	CS orientation	Trial #	Repeat #	CS orientation	Trial #	Repeat #	CS orientation	Trial #	Repeat #	CS orientation
1	1	55	1	1	45	1	1	45	1	1	45	1	1	55	1	1	-45	1	1	75	1	1	75
2	1	15	2	1	-45	2	2	45	2	2	45	2	1	35	2	1	25	2	1	15	2	1	55
3	1	-45	3	1	25	3	1	25	3	1	25	3	1	-45	3	1	25	3	1	35	3	2	55
4	1	25	4	2	-45	4	3	45	4	3	45	4	1	25	4	1	55	4	1	45	4	1	25
5	2	15	5	1	35	5	1	65	5	1	65	5	2	35	5	1	35	5	1	75	5	2	75
6	2	55	6	1	65	6	1	-45	6	1	-45	6	1	15	6	1	15	6	2	45	6	3	55
7	1	65	7	1	15	7	4	45	7	4	45	7	1	65	7	2	-45	7	1	25	7	1	-45
8	2	65	8	2	35	8	5	45	8	5	45	8	1	45	8	2	35	8	1	55	8	1	15
9	1	45	9	3	-45	9	1	35	9	2	65	9	2	55	9	2	65	9	2	15	9	1	35
10	1	75	10	3	35	10	1	55	10	1	35	10	1	75	10	1	75	10	3	45	10	2	25
11	3	15	11	2	25	11	2	-45	11	1	55	11	2	45	11	2	75	11	3	15	11	3	25
12	2	75	12	2	45	12	2	25	12	6	45	12	2	75	12	2	55	12	2	35	12	1	45
13	1	35	13	1	55	13	1	15	13	1	15	13	3	55	13	2	15	13	3	35	13	3	75
14	2	25	14	1	75	14	1	75	14	2	15	14	3	-45	14	3	15	14	1	65	14	2	45
15	3	75	15	2	55	15	3	25	15	2	-45	15	3	75	15	2	25	15	2	25	15	4	75
16	2	35	16	2	75	16	2	15	16	2	25	16	3	45	16	3	65	16	2	-45	16	2	35
17	2	45	17	2	65	17	6	45	17	3	65	17	3	-45	17	3	35	17	2	55	17	1	65
18	3	65	18	3	45	18	2	65	18	3	15	18	1	15	18	1	45	18	2	75	18	2	65
19	2	-45	19	2	15	19	3	65	19	4	65	19	4	-45	19	2	45	19	4	35	19	4	55
20	4	65	20	3	65	20	2	75	20	1	75	20	3	35	20	3	-45	20	3	25	20	3	65
21	3	25	21	3	75	21	7	45	21	2	75	21	4	55	21	3	45	21	3	75	21	3	35
22	3	-45	22	3	15	22	2	55	22	2	35	22	3	15	22	3	55	22	2	65	22	2	15
23	3	35	23	4	35	23	3	-45	23	3	-45	23	2	65	23	3	75	23	4	25	23	2	-45
24	3	55	24	4	45	24	3	15	24	4	15	24	2	25	24	4	65	24	4	45	24	3	45
25	4	-45	25	3	55	25	4	25	25	7	45	25	3	25	25	4	-45	25	3	55	25	4	35
26	4	15	26	4	55	26	4	15	26	5	65	26	4	35	26	4	35	26	3	-45	26	3	15
27	4	35	27	4	75	27	3	75	27	3	75	27	4	25	27	4	45	27	4	15	27	3	-45
28	4	55	28	4	65	28	4	65	28	4	-45	28	4	15	28	4	15	28	4	55	28	4	65
29	4	75	29	4	-45	29	3	55	29	5	-45	29	4	45	29	4	75	29	3	65	29	4	45
30	3	45	30	3	25	30	4	-45	30	6	65	30	3	65	30	3	25	30	4	75	30	4	25
31	4	45	31	4	15	31	2	35	31	3	25	31	4	65	31	4	25	31	4	-45	31	4	15
32	4	25	32	4	25	32	4	75	32	3	35	32	4	75	32	4	55	32	4	65	32	4	-45
33	5	-45	33	5	65	33	5	65	33	5	55	33	5	25	33	5	35	33	5	45	33	5	-45
34	5	25	34	6	65	34	5	-45	34	3	55	34	5	45	34	5	45	34	5	25	34	5	65
35	5	55	35	5	55	35	3	35	35	4	75	35	6	45	35	5	55	35	5	35	35	5	45
36	5	45	36	5	35	36	4	55	36	4	55	36	5	75	36	6	55	36	6	25	36	5	75
37	5	15	37	7	65	37	6	65	37	8	45	37	5	55	37	6	35	37	5	55	37	5	55
38	6	55	38	5	-45	38	8	45	38	4	25	38	5	35	38	5	15	38	6	55	38	6	-45
39	6	25	39	8	65	39	5	25	39	5	25	39	5	15	39	7	55	39	6	45	39	6	75
40	7	25	40	5	45	40	4	35	40	4	35	40	5	-45	40	5	-45	40	7	55	40	6	55
41	5	65	41	6	55	41	4	35	41	4	35	41	6	55	41	5	75	41	5	75	41	6	25
42	6	-45	42	5	15	42	5	15	42	6	-45	42	6	35	42	5	25	42	6	35	42	6	25
43	6	45	43	7	55	43	6	35	43	5	35	43	6	-45	43	6	65	43	5	15	43	5	15
44	6	65	44	5	75	44	9	45	44	9	45	44	6	25	44	6	-45	44	8	55	44	5	35
45	7	65	45	9	65	45	5	55	45	5	55	45	6	65	45	6	15	45	7	-45	45	7	25
46	7	-45	46	6	75	46	6	25	46	9	45	46	7	-45	46	7	-45	46	7	45	46	6	65
47	5	75	47	6	25	47	6	-45	47	6	25	47	6	65	47	6	65	47	6	15	47	6	35
48	7	55	48	5	25	48	7	25	48	7	35	48	7	45	48	7	65	48	6	-45	48	7	75
49	5	35	49	6	45	49	7	35	49	7	55	49	7	35	49	6	25	49	6	75	49	7	65
50	6	15	50	7	45	50	8	25	50	8	35	50	6	75	50	8	55	50	7	15	50	7	55
51	6	35	51	8	55	51	6	55	51	6	55	51	7	25	51	7	25	51	7	75	51	6	45
52	8	25	52	6	35	52	10	45	52	6	55	52	8	35	52	7	-45	52	5	65	52	7	35
53	6	-45	53	6	25	53	6	15	53	5	75	53	7	75	53	7	15	53	6	65	53	7	45
54	6	75	54	9	55	54	7	55	54	8	65	54	6	15	54	7	35	54	7	25	54	8	35
55	7	75	55	7	35	55	8	35	55	7	55	55	8	75	55	8	35	55	8	75	55	8	45
56	8	55	56	6	-45	56	7	65	56	7	25	56	8	45	56	6	75	56	8	15	56	8	75
57	8	65	57	7	25	57	5	75	57	8	55	57	8	65	57	6	45	57	8	45	57	6	15
58	7	35	58	7	15	58	9	25	58	9	65	58	8	65	58	7	75	58	7	35	58	8	25
59	7	45	59	7	75	59	10	25	59	7	-45	59	7	55	59	8	15	59	7	65	59	8	65
60	7	15	60	8	45	60	8	55	60	10	45	60	7	15	60	7	45	60	8	65	60	7	-45
61	8	35	61	8	35	61	6	75	61	7	15	61	8	25	61	8	65	61	7	-45	61	7	15
62	9	55	62	7	-45	62	8	65	62	8	25	62	8	-45	62	8	45	62	8	-45	62	8	15
63	8	45	63	8	25	63	9	55	63	9	55	63	8	15	63	8	25	63	8	25	63	8	55
64	9	65	64	8	-45	64	7	15	64	9	25	64	8	55	64	8	75	64	8	35	64	8	-45
65	9	35	65	9	45	65	10	55	65	10	25	65	9	75	65	9	55	65	9	-45	65	9	15
66	8	75	66	8	75	66	9	65	66	8	15	66	9	35	66	9	25	66	9	45	66	9	35
67	9	45	67	9	-45	67	8	15	67	6	75	67	9	-45	67	9	-45	67	9	25	67	10	35
68	9	-45	68	9	25	68	7	-45	68	10	55	68	9	15	68	9	35	68	9	65	68	9	25
69	10	35	69	9	35	69	11	45	69	11	45	69	10	15	69	10	-45	69	9	75	69	9	55
70	10	65	70	10	55	70	9	15	70	8	-45	70	9	55	70	9	45	70	9	35	70	9	-45
71	9	75	71	10	35	71	11	55	71	7	75	71	10	-45	71	10	45	71	10	-45	71	10	55
72	10	55	72	11	35	72	12	55	72	12	55	72	10	75	72	9	15	72	10	-45	72	9	45
73	8	15	73	9	75	73	10	65	73	8	75	73	9	45	73	11	-45	73	10	25	73	9	65
74	11	35	74	10	25	74	7	75	74	11	45	74	9	25	74	9	75	74	10	65	74	11	55
75	11	65	75	10	45	75	11	25	75	9	15	75	10	25	75	10	15	75	11	25	75	10	-45
76	11	55	76	10	-45	76	9	35	76	12	45	76	10	75	76	10	75	76	10	45	76	10	45
77	10	45	77	8	15	77	8	15	77	9	-45	77	11	75	77	10	25	77	11	35	77	10	25
78	11	45	78	9	15	78	9	-45	78	13	35	78	11	-45	78	11	25	78	10	75	78	10	65
79	9	25	79	10	75	79	13	55	79	13	55	79	12	55	79	12	55	79	9	55	79	11	65
80	12	65	80	11	45	80	8	75	80	11	25	80	11	25	80	9	65	80	10	55	80	9	75
81	10	25	81	12	35	81	11	65	81	12	25	81	10	65	81	10	65	81	9	15	81	11	-45
82	9	15	82	10	65	82	10	35	82	10	35	82	12	25	82	10	55	82	12	25	82	11	45
83	10	-45	83	11	65	83	9	75	83	10	15	83	10	45	83	11	75	83	11	65	83	10	75
84	10	75	84	12	45	84	12	25	84	13	25	84	11	45	84	11	65	84	11	75	84	11	35
85	11	25	85	10	15	85	12	45	85	9	75	85	10	55	85	11	15	85	10	15	85	10	15
86	10	15	86	11	25	86	10	-45	86	10	75	86	10	65	86	11	45	86	11	-45	86	12	35
87	12	25	87	11	15	87	14	55	87	10	65	87	10	35	87	11	55	87	11	55	87	11	25
88	12	45	88	11	75	88	13	45	88	11	75	88	12	-45	88	12	65	88	12	75	88	11	15
89	11	75	89	12	75	89	10	75	89	11	35	89	11	55	89	11	35	89	11	45	89	11	75
90	11	-45	90	12	65	90	11	55	90	13	45	90	12	75	90	12	75	90	12	45	90	12	65
91	12	55	91	12	15	91	12	65	91	10	-45	91	11	65	91	12	25	91	11	15	91	12	15
92	11	15	92	11	-45	92	13	25	92	11	15	92	11	35	92	12	55	92	12	35	92	12	55
93	12	15	93	11	55	93	11	75	93	11	-45	93	12	65	93	12	15	93	12	65	93	12	-45
94	12	-45	94	12	25	94	11	15	94	14	55	94	12	45	94	12	35	94	12	15	94	12	75
95	12	35	95	12	-45	95	11	-45	95	12	15	95	12	55	95	12	45	95	12	55	95	12	25
96	12	75	96	12	35	96	10	35	96	11	65	96	12	35	96	12	-45	96	12	-45	96	12	45
97	13	75	97	13	-45	97	11	35	97	15	55	97	13	15	97	13	35	97	13	15	97	13	15
98	13	65	98	13	45	98	12	15	98	12	65	98	13	45	98	13	-45	98	13	-45	98	13	35
99	14	65	99	13	25	99	12	75	99	13	15	99	13	75	99	14	35	99	13	55	99	13	65
100	13	45	100	13	35	100	13	35	100	14	45	100	13	35	100	13	55	100	14	15	100	13	75
101	13	15	101	13	65	101	14	65	101	12	75	101	14	15	101	13	75	101	13	35	101	14	35
102	13	-45	102	13	75	102	14	45	102	14	25	102	14	45	102	13	65	102	13	45	102	14	15
103	13	35	103	13	55	103	12	-45	103	13	65	103	14	35	103	14	75	103	15	15	103	13	45
104	13	25	104	14	65	104	12	35	104	13	75	104	13	65	104	14	55	104	16	15	104	14	75
105	14	25	105	14	45	105	14	25	105	14	15	105	13	55	105	13	45	105	13	75	105	15	75
106	15	65	106	14	35	106	13	-45	106	12	-45	106	14	75	106	15	35	106	14	55	106	13	55
107	14	15	107	14	25	107	15	65	107	15	15	107	15	75	107	14	45	107	14	35	107	14	45
108	13	55	108	13	15	108	13	75	108	13	-45	108	13	-45	108	15	55	108	14	15	108	14	55
109	14	35	109	15	45	109	14	-45	109	12	35	109	13	25	109	13	25	109	14	75	109	16	75
110	15	25	110	15	35	110	14	75	110	14	-45	110	15	35	110	15	75	110	13	65	110	15	25
111	15	15	111	14	-45	111	13	15	111	14	65	111	15	15	111	14	25	111	13	25	111	15	35
112	14	-45	112	14	75	112	14	15	112	15	-45	112	16	35	112	13	15	112	14	65	112	15	55
113	14	45	113	16	35	113	13	35	113	15	25	113	14	55	113	14	65	113	15	75	113	14	25
114	14	75	114	15	65	114	15	-45	114	16	15	114	14	75	114	15	65	114	15	65	114	13	-45
115	15	-45	115	14	55	115	15	25	115	13	35	115	14	-45	115	15	25	115	15	45	115	14	-45
116	14	55	116	15	15	116	15	15	116	15	45	116	14	65	116	16	55	116	16	35	116	15	15
117	15	75	117	15	-45	117	16	25	117	14	35	117	15	65	117	16	75	117	16	65	117	14	65
118	15	45	118	16	45	118	14	35	118	14	75	118	15	45	118	14	-45	118	13	-45	118	15	15
119	16	75	119	16	25	119	15	45	119	15	65	119	15	-45	119	15	-45	119	16	75	119	16	55
120	15	55	120	15	55	120	15	75	120	15	75	120	14	65	120	14	35	120	14	-45	120	15	-45
121	16	45	121	14	15	121	16	-45	121	16	65	121	14	25	121	16	65	121	15	55	121	15	65
122	16	65	122	16	55	122	16	75	122	15	35	122	15	25	122	16	-45	122	15	-45	122	16	65
123	16	15	123	16	-45	123	16	45	123	16	25	123	15	15	123	15	15	123	14	25	123	16	35
124	15	35	124	15	55	124	15	35	124	16	35	124	16	15	124	16	25	124	15	25	124	15	25
125	16	25	125	16	65	125	16	15	125	16	45	125	16	45	125	15	45	125	16	45	125	16	45
126	16	-45	126	15	75	126	16	35	126	16	75	126	16	55	126	16	35	126	16	-45	126	16	45
127	16	35	127	16	15	127	16	55	127	16	-45	127	16	25	127	16	45	127	16	55	127	16	-45
128	16	55	128	16	75	128	16	65	128	16	55	128	16	-45	128	16	15	128	16	25	128	16	25

4.2 Phase-synchronized stimulus presentation augments contingency knowledge and affective evaluation in a fear-conditioning task

Abstract

Memory often combines information from different sensory modalities. Animal studies show that synchronized neuronal activity in the theta band (4–8 Hz) binds multimodal associations. Studies with human participants have likewise established that theta-phase synchronization augments the formation of declarative video–tone pair memories. Another form of associative learning, classical fear conditioning, models nondeclarative, emotional memory with distinct neuronal mechanisms. Typical fear-conditioning tasks pair a conditioned stimulus (CS) in one modality with an aversive unconditioned stimulus (US) in another. The present study examines the effects of CS–US synchronization in the theta band on fear memory formation in humans. In a fear generalization procedure, we paired one of five visual gratings of varying orientation (CS) with an aversive auditory US. We modulated the luminance of the CS and the volume of the US at a rate of 4 Hz. To manipulate the synchrony between visual and auditory input during fear acquisition, one group (N= 20) received synchronous CS–US pairing, whereas the control group (N= 20) received the CS–US pairs out of phase. Phase synchronization improved CS–US contingency knowledge and facilitated CS discrimination in terms of rated valence and arousal, resulting in narrower generalization across the CS gratings compared with the out-of-phase group. In contrast, synchronization did not amplify conditioned responding in physiological arousal (skin conductance) and visuocortical engagement (steady-state visually evoked potentials) during acquisition, although both measures demonstrated tuning toward the CS. Together, these data support a causal role of theta-phase synchronization in affective evaluation and contingency report during fear acquisition.

The full text and online supplementary material of Study 2 can be found at:

https://www.eneuro.org/content/9/1/ENEURO.0538-20.2021

Cognition and Behavior

Phase-Synchronized Stimulus Presentation Augments Contingency Knowledge and Affective Evaluation in a Fear-Conditioning Task

Elena Plog,[1,*] Martin I. Antov,[1,*] Philipp Bierwirth,[1] Andreas Keil,[2] and Ursula Stockhorst[1]

Abstract

Memory often combines information from different sensory modalities. Animal studies show that synchronized neuronal activity in the theta band (4–8 Hz) binds multimodal associations. Studies with human participants have likewise established that theta-phase synchronization augments the formation of declarative video–tone pair memories. Another form of associative learning, classical fear conditioning, models nondeclarative, emotional memory with distinct neuronal mechanisms. Typical fear-conditioning tasks pair a conditioned stimulus (CS) in one modality with an aversive unconditioned stimulus (US) in another. The present study examines the effects of CS–US synchronization in the theta band on fear memory formation in humans. In a fear generalization procedure, we paired one of five visual gratings of varying orientation (CS) with an aversive auditory US. We modulated the luminance of the CS and the volume of the US at a rate of 4 Hz. To manipulate the synchrony between visual and auditory input during fear acquisition, one group ($N = 20$) received synchronous CS–US pairing, whereas the control group ($N = 20$) received the CS–US pairs out of phase. Phase synchronization improved CS–US contingency knowledge and facilitated CS discrimination in terms of rated valence and arousal, resulting in narrower generalization across the CS gratings compared with the out-of-phase group. In contrast, synchronization did not amplify conditioned responding in physiological arousal (skin conductance) and visuocortical engagement (steady-state visually evoked potentials) during acquisition, although both measures demonstrated tuning toward the CS^+. Together, these data support a causal role of theta-phase synchronization in affective evaluation and contingency report during fear acquisition.

Key words: associative memory; fear conditioning; multisensory; oscillations; phase synchronization; theta band

---

Significance Statement

Because of methodological limitations, examining the causal role of oscillatory synchrony in association formation has been challenging so far. Using repetitive, rhythmic sensory stimulation in a memory-related 4 Hz frequency, we examined the role of phase synchronization in fear conditioning. While synchronization improved the contingency knowledge and affective evaluation, physiological arousal and visuocortical activity were unaffected by the phase modulation. Our results represent an initial step toward establishing the causal effects of theta-phase synchronization in associative fear learning, thus improving our understanding of the neurophysiological mechanisms of fear memory encoding.

Introduction

Phase synchronization of brain oscillations has been proposed as a mechanism supporting neuronal communication and plasticity (Fell and Axmacher, 2011). A theoretical perspective holds that the ongoing oscillatory phase reflects the excitability of a neural population and therefore determines a window for successful long-term potentiation (LTP), a cellular process underlying learning and plasticity (Lynch, 2004). Research in rodents has shown that the induction of LTP or long-term depression (LTD) critically depends on oscillatory phases and the stimulation or recording site: while LTP was induced in behaving rats when the hippocampal CA1 was stimulated at the oscillatory peak, LTD resulted from stimulation at the trough (Hyman et al., 2003). Using trace eyeblink conditioning in rabbits and recordings in the hippocampal fissure, CS presentation in the trough induced phase-locked, regular (theta) oscillations that were in turn associated with better learning, whereas CS presentation to the peak impaired regularity and learning (Nokia et al., 2015). Note that the theta phase reverses between the hippocampal fissure and the CA1 region. Since LTP requires precise timing between presynaptic and postsynaptic activation in the millisecond range (Markram et al., 1997), orchestrating activity by phase synchronization of neuronal oscillations is a potential mechanism supporting LTP. Among other oscillatory phenomena, oscillations in the theta range (4–8 Hz in primates, 4–12 Hz in rodents) and their synchronization among memory-related brain sites are linked to memory performance (Headley and Paré, 2017). Rodent research (Benchenane et al., 2010; Place et al., 2016) and human EEG studies (Weiss and Rappelsberger, 2000; Summerfield and Mangels, 2005) found increased theta synchronization among brain regions during different episodic memory tasks, suggesting that theta synchronization facilitates communication (Fell and Axmacher, 2011).

Intriguingly, studies in humans have causally linked theta-phase synchronization to episodic associative memory. Repetitive, rhythmic sensory stimulation eliciting steady-state evoked potentials (Clouter et al., 2017; Wang et al., 2018) enables experimental control over response frequency in a sensory region and corresponding phase synchrony between regions (Thut et al., 2011; Herrmann et al., 2016; Hanslmayr et al., 2019). Synchronizing the oscillatory phase evoked by periodically modulated visual and auditory stimuli facilitated the encoding of an episodic audiovisual memory (Clouter et al., 2017; Wang et al., 2018), suggesting theta-phase synchronization as a mechanism for binding multisensory episodic memories. The synchronized input is assumed to increase temporally-organized neuronal firing, which in turn may result in LTP (Buzsáki, 2002; Fries, 2015).

Although LTP is best understood in the hippocampus, its associative and synapse-specific properties make it a potential mechanism for plasticity in other regions (Maren and Fanselow, 1995; Orsini and Maren, 2012; Bliss et al., 2018). For example, fear conditioning, a paradigm of associative emotional memory, involves associative plasticity within the lateral nucleus of the amygdala (Kim and Cho, 2017), but also in other structures processing the conditioned stimulus (CS) and the unconditioned stimulus (US; Herry and Johansen, 2014). Sensory information of both stimuli (typically, different modalities) converge onto the same neuronal populations in the lateral amygdala (LA; Romanski et al., 1993). Activating weak CS synapses in temporal proximity to strong US synapses initiates a cascade of cellular reorganization, strengthening CS synapses and enabling the CS to elicit fear responses (Blair et al., 2001; Orsini and Maren, 2012). Importantly, theta synchronization among medial prefrontal cortex, amygdala, and hippocampus plays a role during fear conditioning (Seidenbecher et al., 2003; Karalis et al., 2016; Taub et al., 2018; Zheng et al., 2019; for review, see Bocchio et al., 2017; Çalişkan and Stork, 2018). However, its causal role in forming CS–US associations is unknown.

The current study asked whether synchronized sensory input helps the formation of a multisensory CS–US association in aversive learning. Using rhythmic external stimulation (Clouter et al., 2017; Wang et al., 2018), we presented the visual CS and auditory US "in-phase" or "out-of-phase" in a 2-day fear conditioning procedure with generalization (five similar CS). We hypothesized that theta-band (4 Hz) synchronization of two distinct sensory systems promotes the CS–US association. Specifically, it was expected that in-phase presentation facilitates fear acquisition, whereas out-of-phase presentation prompts poor fear conditioning. Synchronizing the multisensory input is expected to orchestrate neuronal activity in the sensory cortices (so-called entrainment). If synchronization in the theta range provides a window for successful LTP, it should optimize conditions for synchronous afferent signals reaching further structures within the fear network, especially the lateral amygdala (Romanski et al., 1993; LeDoux, 2000). To assess different response systems in human fear conditioning, we measured conditioned responses in physiological arousal, affective evaluation of arousal and valence, contingency knowledge of CS and US, and visuocortical engagement.

Materials and Methods

Participants

The final sample comprised 40 healthy, right handed students from the University of Osnabrück (19 - 30 years, $M = 22.2$, $SEM = 0.35$; 20 women). To control for sex

hormone fluctuations, female participants were included only if they used monophasic oral contraceptives (pill) and were examined between the 6th and 20th day of pill intake (i.e., in the pill-on phase). Participants were screened via self-report questionnaire and a structured interview for inclusion and exclusion criteria in a screening session that was always conducted on a different day than the actual main experiment. Students with acute or chronic physical and/or psychiatric disorders (e.g., migraine, epilepsy, cardiovascular diseases, and phobias) were not eligible. Further exclusion criteria encompassed hearing and/or uncorrected vision impairments, tinnitus, acute medication, drug abuse, average alcohol consumption exceeding 20 or 40 g ethanol/d (for women and men, respectively), and smoking more than five cigarettes per day. Volunteers were screened for post-traumatic stress disorder (PTSD) using a translated version of the Posttraumatic Stress Diagnostic Scale (Foa, 1995; Steil and Ehlers, 2000) and excluded if they met the criteria of the DSM-IV (Diagnostic and Statistical Manual of Mental Disorders, fourth edition) for PTSD. From 64 volunteers (34 women), 46 (25 women) were eligible to participate, 3 women did not appear to the appointment, and 3 volunteers (2 women) discontinued the main experiment because of the aversive nature of the conditioning paradigm, leading to our final sample of 40 participants. Within the female and male subsamples, participants were randomly assigned to one of two groups, the in-phase or out-of-phase group, with the same number of men and women in each group (in-phase group, 10 women; out-of-phase group, 10 women).

The study was approved by the ethics committee of the University of Osnabrück and conducted in accordance with the Declaration of Helsinki guidelines. Written informed consent was obtained from all participants after adequate understanding of the explained procedures. Each participant was free to choose between participation credits (four credits) or a corresponding amount of money (32 €) for finishing the screening and day 1 and 2 of our conditioning procedure.

Experimental design and stimuli

We used a 2-day fear conditioning procedure, including habituation, acquisition, immediate extinction on day 1, and a 24 h delayed recall on day 2 (Fig. 1B). Our study comprised a 5×2 mixed factorial design within each learning phase, with five CS orientations of the below characterized Gabor gratings (25°, 35°, 45°, 55°, and 65°) as the within-subject factor and synchronization (in-phase, 0° phase shift; vs out-of-phase, 90°, 180°, and 270° phase shift); as the experimental between-subject factor.

Five high-contrast, black-and-white Gabor gratings (i.e., a sinusoid grating filtered with a Gauss function) with a low spatial frequency served as the visual CS. The five CS differed only in orientation (25°, 35°, 45°, 55°, and 65°, relative to vertical 0°; Fig. 1A). The CSs were presented for 5 s centrally on a dark gray background (100% black setting on the monitor). During the presentation, the experimental chamber was lit only by the CS on the screen. Technical failure forced us to exchange the monitor from a 19 inch (model P911, Acer) to a 17 inch (model CPD-E220E, Sony) cathode ray tube (CRT) after examining the

first 12 participants. We matched stimulus properties as closely as possible with the new monitor. The relevant parameters were comparable: 85 Hz refresh rate, low spatial frequency (0.96 vs 0.81 cycles/°), large central CS presentation (5.70° vs 5.73° visual angle), and high contrast (96% Michelson for both monitors).

As the US, we used a 2 s, broadband white noise (20 Hz to 22 kHz, 44,100 bits/s, 16 bits/sample), presented binaurally at a maximum of 96.5 dB(A) over two loudspeakers positioned 0.7 m left and right behind the participant. For an additional unimodal audio task (at the end of session on day 2), we presented the same white noise for 4 s at a nonaversive sound-pressure level with a maximum of 70.4 dB(A).

The intensity of the visual CS, the aversive auditory US, and the nonaversive auditory noise (unimodal task) was modulated at 4 Hz (see also Clouter et al., 2017). The luminance of the visual CS was sinusoidally modulated in 4 Hz, where luminance changed at each screen refresh, resulting in 21 steps per cycle (0–100% luminance). The amplitude of the auditory signal was sinusoidally modulated (0–100%) in 4 Hz by multiplying the signal vector with a 4 Hz sine wave at the native 44.1 kHz audio sampling rate. Presentation of each 4 Hz modulated stimulus (auditory and visual) always started at 0% intensity, increasing to 100% in the first half cycle.

Conditioning procedure

Our procedure included habituation, acquisition, and immediate extinction on day 1, as well as a 24 h delayed recall on day 2 (Fig. 1B). During habituation, each 5 s, 4 Hz modulated CS was presented 12 times in pseudorandom order. Before acquisition, participants were instructed that only one of the 5 CS orientations will be followed by an aversively loud noise, without specifying which orientation. During the acquisition phase, each 4 Hz modulated CS was again presented 12 times. However, the 45° CS (CS$^+$) was always paired (12 times) with the 2 s, 4 Hz modulated aversive noise US (reinforcement rate, 100%), while the other orientations were not (25°, 35°, 55°, and 65° gratings as CS$^-$; Fig. 1B). Previous work has used this same generalization paradigm, with 45° gratings serving as CS$^+$, while also establishing that there are no systematic preconditioning differences between different grating orientations on the measures used here (McTeague et al., 2015). Previous work has also demonstrated that conditioning is seen across orientations and with counterbalancing (Moratti and Keil, 2005). Together, to facilitate interpretation and comparison with prior work, this led us to adopt a fixed contingency between 45° and the US. Each CS presentation was prolonged for the duration of the US, adding 2 s (i.e., 7 s duration for the CS$^+$ and the CS$^-$ gratings during acquisition). For the 45° CS$^+$, the last 2 s of visual CS overlapped with the auditory US presentation.

Since retinal phototransduction was shown to be slower than auditory transduction (~50 ms for visual stimuli vs 10 ms for auditory stimuli; Lennie, 1981; King and Palmer, 1985), the onset of the auditory US had a 40 ms delay relative to the CS onset (Clouter et al., 2017). The slower transduction of visual stimuli is also in line with recordings
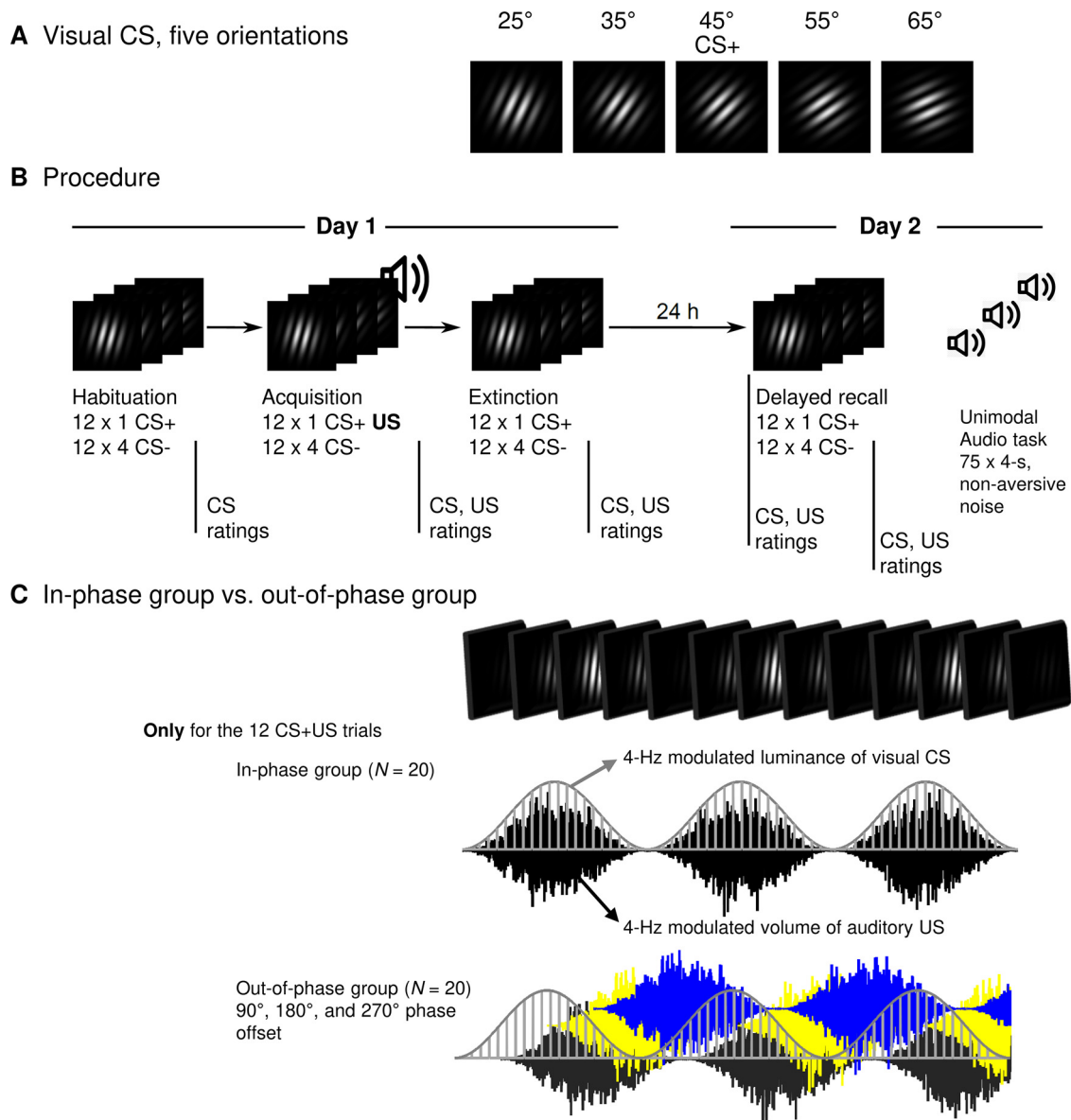
A Visual CS, five orientations

25°   35°   45°   55°   65°
              CS+

B Procedure

Figure 1. Experimental design: stimuli, procedure, and the operationalization of the in-phase group versus the out-of-phase group. **A**, Gabor gratings used as CSs. The 45° grating served as CS$^+$ (paired with the US during acquisition). The other four served as CS$^-$ (never paired with the US). The luminance of each CS was sinusoidally modulated at 4 Hz. The US was a broadband white noise, amplitude modulated at 4 Hz and presented at a maximum of 96.5 dB(A). **B**, Fear-conditioning procedure with the learning phases habituation, fear acquisition, and extinction (day 1) and delayed recall (day 2). Each CS grating was presented 12 times in each learning phase. The US was only presented during fear acquisition (12 times coterminating with the CS$^+$). At the end of day 2, the unimodal audio task comprised 75 presentations of the 4 Hz modulated white noise (4 s each) at a nonaversive volume (maximum = 70.4 dB(A)]. Vertical lines below the timeline indicate the rating time points. Extended Data Figure 1-1 shows the specific trial orders 1 and 2 that were used. **C**, Operationalization of the in-phase group versus the out-of-phase group. Fear conditioning for both groups was identical to the only exception that the in-phase group received the 12 CS$^+$ US pairings during acquisition without a phase shift (0°) and the out-of-phase group received the CS$^+$ US pairings with phase shifts of 90°, 180°, and 270° (four trials each). In **C**, the top row shows a simplified depiction of a CS changing luminance at 4 Hz for 750 ms. The bottom part of **C** shows the first 750 ms of an overlapping CS$^+$ US presentation for the two groups. The light gray curve shows the luminance of the CS$^+$ (each vertical line shows one step following the 85 Hz refresh rate of the monitor). The black (0° phase shift), dark gray (90°), yellow (180°), and blue (270°) graphs show a downsampled representation of the 4 Hz modulated, white noise US.

in the amygdala after visual versus auditory stimulation. The earliest activity occurred between 40 and 80 ms (up to 316 ms, depending on the pathway to the amygdala that differs in length) after visual stimulation (Luo et al.,

2010; Silverstein and Ingvar, 2015 for review, see McFadyen et al., 2017). In contrast, auditory information was recorded as early as 10–40 ms in single units of anesthetized as well as freely moving rats (Romanski et al.,

A Processing example   **B** Stimulation validation
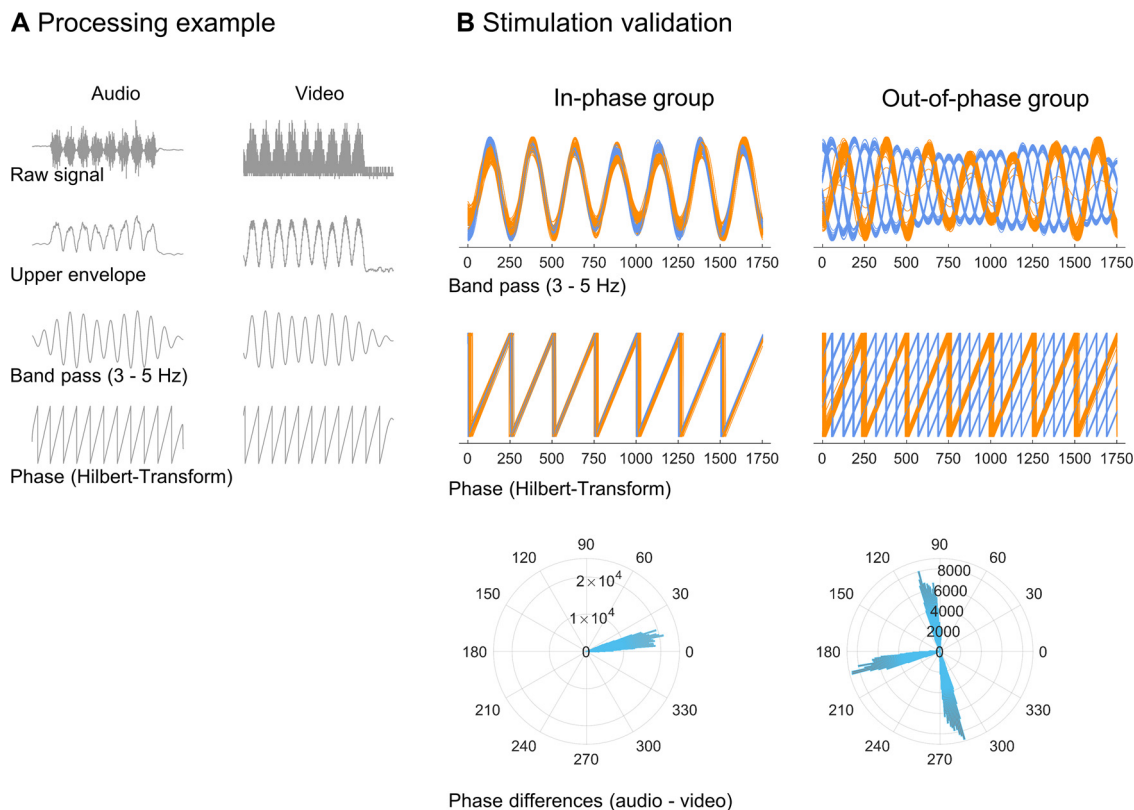
Figure 2. Processing steps and validation of in-phase versus out-of-phase stimulation. **A**, Processing example (one trial of one participant) of our audio (microphone in front of the participant's speakers) and video signal (photodiode attached to the participants' monitor). Data were segmented relative to the onset of a US (i.e., 12 segments per subject). Before analysis, video data were shifted 40 ms forward in time to account for the 40 ms time shift programmed into the stimulus presentation. Data were rectified, bandpass filtered between 3 and 5 Hz, and subjected to a Hilbert transform. Instantaneous phase information at 4 Hz was extracted from the imaginary part of the analytic signal. **B**, Visualization of in-phase (left column) and out-of-phase (right column) CS^+–US stimulation for all CS^+–US trials and all participants (12×20 trials per group). Each thin orange line shows the video signal of one participant and one trial. Each thin blue line shows the audio signal (one participant and trial). In **B**, the top rows show bandpass-filtered data; the middle row shows the extracted phase information; and at the bottom, polar histograms show the clustering of all phase differences per group.

1993; Quirk et al., 1995). This temporal difference in processing from receptors to the afferent neurons in the CNS has to be considered when entraining the brain with multisensory information in a synchronous way. Thus, adjusting for a temporal delay in one modality is necessary to achieve theta synchronization of visual CS and auditory US in the sensory cortices and facilitating synchrony of both inputs on the LA. CS presentation followed one of two random sequences (Extended Data Fig. 1-1), with trial order constrained to not allow more than two consecutive CSs of the same orientation. Additionally, the acquisition phase started with a booster sequence, where five of the first seven trials were CS^+–US pairings.

The following immediate extinction, and the 24 h delayed recall phase comprised only CS presentations (12 times each, no US), as in the habituation phase. The aversive US was not presented at any point except in the 12 CS^+–US pairings in the acquisition phase. However, neither before immediate extinction learning nor before 24 h delayed recall, participants were informed that no US will occur in the following stimulation phase.

Between the end of one CS presentation and the beginning of the next one, a black screen was shown for 3–5 s

(random from a uniform distribution) during learning phases (1.5–3 s during the unimodal audio task), followed by a white fixation cross at the center of the screen for 1.5 s, resulting in an intertrial interval (ITI) between 4.5 and 6.5 s.

In accordance with the study by Clouter et al. (2017), the 12 pairings of the 4 Hz modulated CS^+ and US were realized with either 0° (i.e., 0 ms) phase shift (in-phase group), or 90° (62.5 ms), 180° (125 ms), and 270° (187.5 ms) phase shifts for four USs each (out-of-phase group; Fig. 1C). Accounting for the 40 ms delay between rapid auditory and later visual processing times, input with a phase lag of 0° causes phase-synchronized cortical activity in the visual and auditory cortex (Clouter et al., 2017). This synchronized activity at the primary cortices is expected to increase the synchronized afferent signals reaching the amygdala, where CS–US convergence occurs, hence supporting associative plasticity in the lateral amygdala (Blair et al., 2001; Bocchio et al., 2017). In contrast, phase lags between 90° and 270° (i.e., timing shifts of 62.5–187.5 ms) should result in a suboptimal level of excitability and therefore decrease the likelihood of synaptic changes.

The experiment was conducted in an electromagnetically shielded and sound-attenuated experimental chamber,

where participants were seated in a comfortable chair positioned centrally in front of the monitor. The experiment, including all stimuli, was created in MATLAB (version 2019b; RRID:SCR_001622) using the Psychophysics Toolbox (RRID:SCR_002881; Brainard, 1997; Kleiner et al., 2007).

Sensory stimulation validation

To validate the temporal fidelity of the stimulation, we analyzed data from two sources: a photograph diode (photograph sensor; Brain Products) attached to the participant's monitor; and a microphone (built into a StimTrak, BrainVision) positioned in front of the participant's speakers. Both signals were recorded at 1000 Hz with a recorder (BrainVision). The photograph diode was placed over the upper right corner of the CRT monitor where a smaller version of the Gabor gratings appeared during the same monitor refresh cycle (and far outside of the CS presentation area) in the same sinusoidal luminance modulation as the original CS gratings. Pilot studies using photograph sensors at both the upper corner (small-test Gabor) and the central screen (actual CS grating) showed excellent synchrony of both stimuli. The onset of the central grating was consistently 0.5 refresh cycles after the onset of the miniature grating in the top left corner (i.e., $\sim$5.9 ms). Using an Analyzer (BrainVision), data from the photograph sensor and the microphone were segmented from -320 to 2500 ms relative to the onset of a US (i.e., 12 segments per subject) and visually inspected for artifacts. A subset of segments was excluded, as microphone data were corrupted or missing because of the failure of the StimTrack batteries (in 5 of 40 participants). For visualization, the remaining data were exported to MATLAB and rescaled from $-\pi$ to $+\pi$. Further analysis was computed over 7.02 cycles of microphone and video data (1755 ms), disregarding the last cycle of audio stimulation. Video data from -40 to $+1715$ ms relative to US onset were used. In contrast, microphone data from 0 to 1755 ms entered analysis. This effectively shifts video data 40 ms forward in time to account for the 40 ms time shift programmed into the stimulus presentation. Microphone data were first rectified (square root of the signal squared). Both the photograph sensor and microphone channels were bandpass filtered between 3 and 5 Hz, using the *bandpass* function of the MATLAB Signal Processing Toolbox with an IIR (infinite impulse response) filter (60 dB attenuation at the edge frequencies) and a steepness of 0.95. Instantaneous phase information at 4 Hz for the audio and video signals was extracted from the imaginary part of the analytic signal after a Hilbert transform (Fig. 2A).

This analysis Fig. 2B also demonstrates that there was very little variability in the timing of sensory stimulation within a trial, as well as between trials and between participants of one group.

Dependent variables

Steady-state visually evoked potentials (ssVEPs; via EEG), skin conductance responses (SCRs), and subjective ratings served as dependent outcomes. Further, horizontal and vertical eye movements were recorded by electrooculography (EOG) with a bipolar BrainAmpExG

Amplifier (BrainProducts) to detect and eliminate artifacts in the EEG recordings.

EEG parameters

EEG recording and preprocessing. A 64-channel EEG was recorded on both days with two 32-channel BrainAmp DC amplifiers with a resolution of 0.1 μV (Brain Products). The 64 active electrodes (Ag/AgCl, actiCAP, Brain Products) were filled with electrolyte gel (Super-Visc 10% NaCl, EasyCap) and positioned according to the extended international 10–20 system. Efforts were made to keep impedances <5 kΩ (manufacturer recommendation, <25 kΩ). FCz served as the recording reference, and AFz served as the ground. A sampling rate of 1000 Hz and a high-pass filter at 0.016 Hz were used. In addition to the EEG, EOG was recorded with four Ag/AgCl electrodes (Ø, 4 mm) to control for eye movements. Two electrodes were placed on the lateral canthus of each eye for horizontal movements, and two electrodes were placed infraorbital and supraorbital, in line with pupil of the right eye, for vertical movements. An electrode on the forehead was attached as the ground.

Offline preprocessing was done with Analyzer 2 Software (version 2.1.2.327; BrainVision). Raw data were bandpass filtered between 1 and 100 Hz using Butterworth (zero phase shift) filters with a 3 dB low cutoff at 1 Hz (time constant, 0.1592; order 8) and a 3 dB high cutoff at 100 Hz (order 4). Additional 50 and 100 Hz (bandwidth, 1 Hz; order 4) notch filters were applied to eliminate line noise. Data were segmented from -1250 to 7500 ms relative to a CS onset, and an ocular correction independent component analysis (ICA), as implemented in BrainVision Analyzer, was applied. After visual inspection of the resulting factors and factor topographies, factors related to horizontal and vertical eye movements, blinks, as well as strong cardiac or muscular artifacts were removed from the reconstructed data. ICA-corrected data were rereferenced to an average reference, and the recording reference was reincluded in the data as a 65th channel at position FCz. The segments were cut to an interval between -1000 and 5000 ms relative to CS onset. With this segmentation, the US intervals were excluded from further analyses to avoid contamination of our EEG data. After another visual inspection, we rejected segments with remaining artifacts. On average, 3.93 segments were rejected per participant (0–15 rejected of 240 segments for each participant). Data were downsampled to 512 Hz, in accordance with the findings of Clouter et al. (2017), and were exported to MATLAB (MathWorks; RRID:SCR_00162). To increase spatial specificity, reduce volume conduction effects, and obtain reference-free data, we conducted a scalp current source density (CSD) transform (Junghöfer et al., 1997). The CSD values (as estimates of cortical surface potentials) are represented on a sphere, approximating a cortical surface. For scalp-level analyses and topographical mapping, the CSD was projected back onto the original electrode space. Analyses were performed on CSD-transformed data, and CSD data are shown throughout the figures.

Validation of visual and auditory entrainment (unimodal). To validate the visual cortical entrainment at 4 Hz, we first
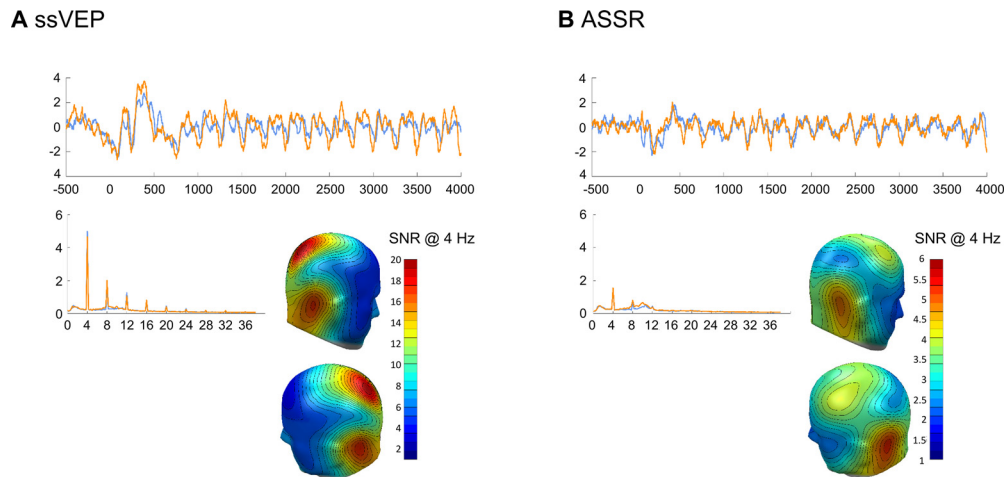
A ssVEP

B ASSR

Figure 3. ssVEP and the auditory steady-state response 4 Hz signal in the time domain and frequency domain, as well as the scalp distribution of the 4 Hz signal. **A**, **B**, The signal-to-noise ratio, averaged over all 40 participants (i.e., regardless of factor group) is presented for the visual (**A**) and auditory (**B**) 4 Hz stimulation. Orange lines show averaged data from participants of the in-phase group, blue lines show data from the out-of-phase group.

averaged CSD-transformed data over all habituation trials at each sensor of a participant in the time domain [disregarding CS orientations (i.e., averaging 5×12 trials per subject)]. Habituation trials were not only strictly unimodal visual stimulation but preceded any pairing of the CS with the aversive US. To avoid early event related potentials entering the frequency domain analysis, Fourier transform was applied on data from 750 to 5000 ms (i.e., containing 17 cycles of 4 Hz) post-CS onset. These data were windowed with a cosine-square window (20 point rise/fall) and subjected to a discrete Fourier transform (MATLAB) with a frequency resolution of 0.24 Hz. We extracted the absolute values of the Fourier coefficients at 4 Hz and transformed the resulting power values to signal-to-noise ratios (SNRs), using the average of five frequency bins <4 Hz and four frequency bins >4 Hz.

To validate auditory entrainment, we used the unimodal audio task at the end of day 2, as it reflected 4 Hz unimodal auditory stimulation, without concurrent visual stimulation. EEG data from the audio-only task were subjected to the same preprocessing pipeline as CS-related data. As for the visual unimodal data described above, CSD data were segmented (here from −1000 to 4100 ms, relative to audio stimulus onset) and averaged per participant and sensor over the 75 audio-only trials. Fourier transform was applied on windowed data (cosine-square, 20 point rise/fall) starting from 500 to 4000 ms after audio onset (i.e., containing 14 cycles of 4 Hz), resulting in a frequency resolution of 0.29 Hz. Like for the visual stimulation, we converted the power at 4 Hz to SNRs, using the average of the five frequency bins below and four above the frequency of interest as noise estimates.

Figure 3 shows the scalp distribution of the 4 Hz SNR averaged over participants ($N = 40$), for the visual (Fig. 3A) 4 Hz stimulation and the auditory 4 Hz stimulation (Fig. 3B). The average topographies are consistent with typical visual and auditory steady-state evoked potential at 4 Hz,

respectively. Specifically, the relatively low driving frequency of 4 Hz has traditionally been shown to prompt larger spread of the ssVEP topography, reflective of longer individual stimulation cycles, which allow spreading across the visual hierarchy (Skrandies, 2007). However, the topographies of the 4 Hz EEG signal showed some variation between subjects. Therefore, for subsequent analyses in the frequency domain, including single-trial analyses of CS-related activity, we selected the six individual sensors for each participant showing the highest SNR at 4 Hz.

ssVEP single-trial analysis. We conducted a single-trial analysis to be able to show the temporal evolution of visual cortical engagement over the course of learning trials. For single-trial analysis, we used data segments between −1000 and 5000 ms, relative to CS onset as 0 (in sample points at 512 Hz sample rate, this is 1–3072 sample points with zero being sample point 512). First, we sampled it up from 512 to 1536 Hz. Upsampling the data ensured an integer number of sampling points per one cycle for the 4 Hz as well as its harmonics (up to 16 Hz). At 1536 Hz, one cycle of the driving frequency (4 Hz) is 384 samples (instead of 128 at 512 Hz). By subtracting the mean of the 1000 ms prestimulus interval, the data were baseline corrected. The power extraction of single trials was based on the analysis window between 750 and 5000 ms (relative to 0 ms = CS onset). Over this analysis window, a moving average procedure was conducted. We obtained averages by shifting a window with a length of four cycles of the frequency of interest (i.e., 4 Hz) across the detrended data segments in steps of one cycle and averaging the contents of the window with each step (12 steps, last four-cycle step starting at 3000 ms after CS onset). We then transformed the single-trial estimates from the time into the frequency domain using discrete Fourier transform (DFT) and extracted the power at the driving frequency as the absolute of the Fourier coefficients, normalized by the length of FFT (here, 1536 sample points).

Interindividual variance in response strength and pre-experimental bias was corrected by calculating a habituation ratio for each CS (via division by habituation mean over all 60 trials of each participant, disregarding the different CS orientations), with values >1 describing an enhancement and <1 describing a decrease of ssVEP power compared with habituation. In addition, single-trial data were smoothed with a moving average along the 12 trials (5 point symmetrical, shrinking at the end points) within each learning phase and CS orientation (5 orientations × four learning phases with 12 trials each). For plots showing the temporal evolution of ssVEP over trials, we pooled data over sensors as the average of the individually defined six maximal SNR sensors for each participant. The individual sensors entering this six-sensor cluster were defined as the six sensors showing the highest SNR at 4 Hz during habituation trials for a participant [see above, Validation of visual and auditory entrainment (unimodal)]. Of note: while single-trial data are interesting and informative, we have no prior evidence allowing us to formulate specific hypotheses about group differences (in phase vs out of phase) in the temporal dynamics of ssVEP. Therefore, these data were averaged over all trials of a learning phase before statistical testing for group effects.

Skin conductance responses and electrocardiography, and blood pressure. In addition to ssVEP power tunings toward specific CS gratings, we used SCRs as a common measure of learning-induced changes in physiological arousal to the CS. As our laboratory is configured for stress-associated questions by default, we also recorded electrocardiography (EKG) and blood pressure (BP) as control parameters only. EKG and BP will not be reported in the Results section. We used a Brainamp ExG amplifier (Brain Products) and a 0.5 V constant voltage coupler to record SCRs with a sampling rate of 1000 Hz and a resolution of 0.0061 μS. We attached two Ø 10 mm (inner diameter) electrodes, filled with 0.05% NaCl paste (TD-246) on the thenar and hypothenar of the left hand (nondominant) of each participant (Boucsein et al., 2012). No additional filters were applied. Data were downsampled to 200 Hz in BrainVision Analyzer 2.1 and exported to MATLAB. Responses with an onset latency between 1 and 4 s and a minimum amplitude of 0.02 μS were automatically scored using Ledalab (Benedek and Kaernbach, 2010). If more than one response met the criteria, single responses were summed up. Responses that did not meet the criteria were scored as zero. After Ledalab scoring, we used an additional visual inspection of heat maps of single trials and corrected 42 values (of 240 trials × 40 participants = 9600 total values) that were overscored or underscored by Ledalab. To further correct for interindividual differences and push distribution toward normal, we calculated z-values using the means and SDs of CS and US responses of all learning phases (habituation, acquisition, immediate extinction, and delayed recall) per participant. In accordance with ssVEPs, single-trial data were smoothed with a moving average along the 12 trials (5 point symmetrical, shrinking at the end points) within each learning phase and CS orientation (5 orientations × 4 learning phases with 12 trials each). The z-standardized SCRs

were then averaged across the 12 trials of each learning phase, and the averages were used in all statistical analyses.

For the recording of EKG, we positioned three Ø 8 mm (inner diameter) electrodes (filled with 5% NaCl EKG paste, GE Medical Systems Information Technologies) under the right collarbone, the left shinbone, and (as ground electrode) on the right shinbone.

Systolic and diastolic BP were measured at discrete measurement points using a semiautomatic electronic sphygmomanometer (bosotron 2, Bosch + Sohn). Therefore, an inflatable cuff was placed around the left upper arm, with the sensor plate positioned over the brachial artery at heart level.

Subjective ratings: valence, arousal, and US expectancy

A paper–pencil version of the 9 point pictorial Self-Assessment Manikin (SAM; Bradley and Lang, 1994) scale was used to evaluate each CS orientation for its valence (from negative to positive) and arousal (from excited to calm). Ratings were conducted after habituation, acquisition, and immediate extinction, as well as before and after 24 h delayed recall. In addition, we asked the participants to rate their expectancy that a US occurs with the depicted grating with answers ranging from −5 (very certain, no), to 0 (uncertain), to 5 (very certain, yes). Except for after habituation, paper−pencil US expectancy ratings were conducted together with our SAM ratings.

Overall procedure

The study covered the following two parts: the screening session, lasting ~1 h, explaining the general procedure of the main session, testing for inclusion and exclusion criteria and obtaining informed consent (for description, see the Participants section); and the main conditioning study. Screening and the main study were scheduled on different days.

Main conditioning study

The main session was conducted on two consecutive days, starting at 10:00 A.M., 2:00 P.M., or 5:30 P.M. The duration of day 1 and day 2 of the main session were 2 and 1 h, respectively. At the beginning of day 1 and day 2, we attached EEG, EKG, EOG, and SCR electrodes, and positioned the inflatable cuff for BP measures. Habituation, acquisition, and immediate extinction took place on day 1, while a 24 h delayed recall took place on day 2. After each learning phase on day 1 (i.e., after habituation, acquisition, and immediate extinction) as well as before and after delayed recall on day 2, resting periods, SAM and US expectancy ratings (except after habituation, where SAMs were conducted without US expectancy ratings, since no US has occurred), and EKG, SCR, as well as BP measures were performed (Fig. 1B).

Before starting the computer task, we read the standardized "general information about the experiment," including a description of the procedure and the stimuli we were about to present. Subjects were instructed to sit comfortably and avoid any movements (except eye blinking) for the entire duration of the computer tasks and the explicitly
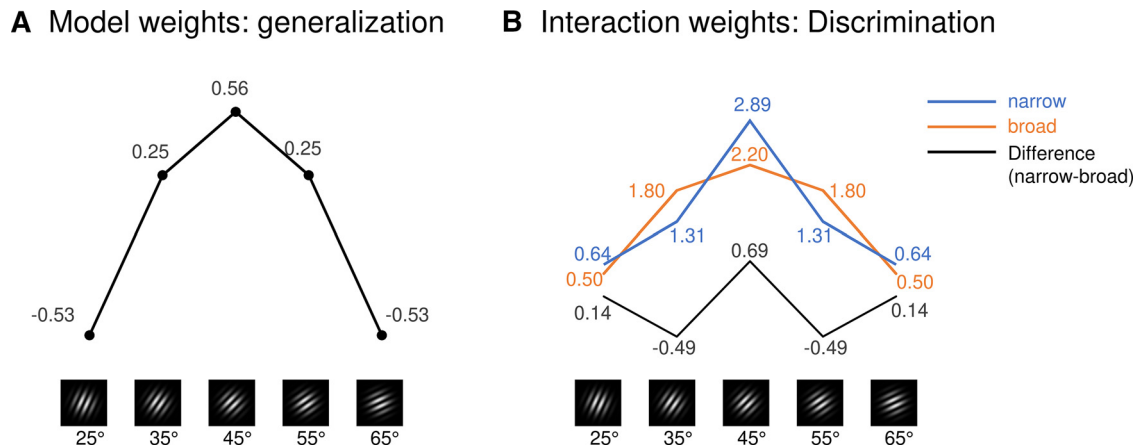
A Model weights: generalization   **B** Interaction weights: Discrimination

Figure 4. Contrast weights. *A*, Generalization weights to test the fit for a generalized fear response toward the CS^+ and neighboring CS^- orientations, independent of the factor group. *B*, Contrast weights (discrimination) to test the group $\times$ orientation interaction. The weights shown for a narrow (blue) and broad (orange) generalization pattern are just examples that if subtracted (narrow – broad) produce the exact discrimination weights we used for the group $\times$ orientation interaction contrast (numbers in black font, 0.142, −0.498, 0.694, −0.498, 0.142), resembling a Mexican Hat (black line). For better readability, contrast weights in the graphs A and B are inserted with 2 decimals.

announced measurement periods. During the resting phases, subjects were encouraged to move carefully to avoid the detachment of electrodes. At the beginning of habituation, subjects were asked to fixate on an upcoming white cross in the center of the screen followed by some black and white "flickering" gratings. Before acquisition, we informed the participants that a loud flickering noise would be presented with only one of the gratings. However, we did not specify which of the five orientations would predict the aversive noise. Before immediate extinction (day 1) and delayed recall (day 2), participants were asked to remember the instructions, without informing them that no aversive noise would be presented.

Statistical analysis

We submitted each of the memory outcome measures (i.e., US expectancy ratings, affective valence and arousal ratings, SCRs, and ssVEPs) to a 5×2 repeated-measures ANOVA, conducted using SPSS software (version 26.0; SPSS). The mixed ANOVA included the within-subject factor orientation (i.e., the five CSs: 25°, 35°, 45°, 55°, and 65°) and the between-subject factor group (i.e., in-phase group, 0° phase offset; vs out-of-phase group, 90°, 180°, and 270° phase offset). To test for the expected form of the orientation effect independent of group, we conducted a custom contrast for generalization, using contrast weights adapted from prior studies (Fig. 4A; generalization weights: −0.529, 0.247, 0.564, 0.247, and −0.529).

As this is the first attempt to compare a synchronized versus nonsynchronized condition with a fear generalization design, we hypothesized that group differences may manifest in one of the following three possible ways: (1) synchronized CS–US presentation may lead to major increases in CS responding not limited to the CS^+ (this would be evident in a main effect group in the ANOVA); (2) synchronized CS–US presentation may dramatically change the pattern of responding over the

five different CSs (this could be evident in an orientation $\times$ group interaction in the ANOVA); and (3) finally, synchronized CS–US presentation may alter the width of the generalization curve. This could optimize learning, resulting in a narrower generalization and thus better discrimination among the five CSs, without changing overall response levels or dramatically changing the response pattern. ANOVA interactions would not be able to detect this. Therefore, we designed a custom contrast for the group $\times$ orientation interaction, using the LMATRIX command for contrast coefficient matrices in SPSS. We obtained the contrast weights by subtracting a broader generalization profile (Fig. 4B, orange line and font) from a narrower generalization profile (Fig. 4B, blue line and font), resulting in a form resembling a "Mexican Hat" (weights: 0.142, −0.489, 0.694, −0.489, and 0.142). We expected group differences to manifest during (or directly after) acquisition. However, to explore the longevity of potential group effects, we repeated our 5×2 ANOVA and the custom Mexican Hat group $\times$ orientation contrast for immediate extinction and delayed recall on day 2.

Results

Phase synchronization causes a better discrimination between CS^+ and neighboring CS^- gratings in the US expectancy ratings

We found an effect of orientation on US expectancies collected immediately after the CS^+ was repeatedly aversively reinforced during acquisition ($F_{(3,109)} = 12.491$, $p = 6.764E\text{-}7$, partial $\eta^2 = 0.247$; Table 1, a). The resulting pattern reflected generalization around the CS^+ (Fig. 5), with the CS^+ and the most similar gratings receiving the highest US expectancy scores (generalization contrast fit: $F_{(1,38)} = 28.360$, $p = 0.000005$, partial $\eta^2 = 0.427$, Table 1, b). In addition, data revealed a main effect of group ($F_{(1,38)} = 7.310$, $p = 0.010$, partial $\eta^2 = 0.161$; Table 1, c), but no group $\times$ orientation interaction (Table 1, d). Here, the out-

Table 1: Summary of statistical analyses

	Data structure	Type of test	Effects	Statistic	p Value	Effect size
US expectancy						
Acquisition						
a	Normal	ANOVA	ME: o	$F_{(3,109)} = 12.491$	6.764E-7	$\eta^2_p = 0.247$
b	Normal	ANOVA	GEN	$F_{(1,38)} = 28.360$	0.000005	$\eta^2_p = 0.427$
c	Normal	ANOVA	ME: g	$F_{(1,38)} = 7.310$	0.010	$\eta^2_p = 0.161$
d	Normal	ANOVA	o × g INT	$F_{(3,109)} = 1.133$	0.338	$\eta^2_p = 0.029$
e	Normal	ANOVA	MEX	$F_{(1,38)} = 4.796$	0.035	$\eta^2_p = 0.112$
Extinction						
f	Normal	ANOVA	ME: g	$F_{(1,38)} = 0.621$	0.436	$\eta^2_p = 0.016$
g	Normal	ANOVA	o × g INT	$F_{(3,113)} = 1.363$	0.258	$\eta^2_p = 0.035$
h	Normal	ANOVA	MEX	$F_{(1,38)} = 6.660$	0.014	$\eta^2_p = 0.149$
Delayed recall (day 2)						
i	Normal	ANOVA	ME: g	$F_{(1,36)} = 0.688$	0.412	$\eta^2_p = 0.019$
j	Normal	ANOVA	o × g INT	$F_{(3,100)} = 1.172$	0.323	$\eta^2_p = 0.032$
k	Normal	ANOVA	MEX	$F_{(1,36)} = 3.090$	0.087	$\eta^2_p = 0.079$
Valence and arousal						
Acquisition						
i	Normal	ANOVA$_{Val}$	ME: o	$F_{(3,96)} = 7.756$	0.000272	$\eta^2_p = 0.170$
m	Normal	ANOVA$_{Aro}$	ME: o	$F_{(3,100)} = 10.928$	0.000008	$\eta^2_p = 0.223$
n	Normal	ANOVA$_{Val}$	GEN	$F_{(1,38)} = 12.352$	0.001	$\eta^2_p = 0.245$
o	Normal	ANOVA$_{Aro}$	GEN	$F_{(1,38)} = 19.587$	0.000078	$\eta^2_p = 0.340$
p	Normal	ANOVA$_{Val}$	ME: g	$F_{(1,38)} = 1.221$	0.276	$\eta^2_p = 0.031$
q	Normal	ANOVA$_{Val}$	o × g INT	$F_{(3,96)} = 1.502$	0.224	$\eta^2_p = 0.038$
r	Normal	ANOVA$_{Aro}$	ME: g	$F_{(1,38)} = 1.248$	0.271	$\eta^2_p = 0.032$
s	Normal	ANOVA$_{Aro}$	o × g INT	$F_{(3,100)} = 1.658$	0.187	$\eta^2_p = 0.042$
t	Normal	ANOVA$_{Val}$	MEX	$F_{(1,38)} = 9.228$	0.004	$\eta^2_p = 0.195$
u	Normal	ANOVA$_{Aro}$	MEX	$F_{(1,38)} = 7.325$	0.010	$\eta^2_p = 0.162$
Extinction						
v	Normal	ANOVA$_{Val}$	ME: g	$F_{(1,38)} = 1.810$	0.186	$\eta^2_p = 0.045$
w	Normal	ANOVA$_{Val}$	o × g INT	$F_{(3,117)} = 0.647$	0.590	$\eta^2_p = 0.017$
x	Normal	ANOVA$_{Aro}$	ME: g	$F_{(1,38)} = 0.355$	0.555	$\eta^2_p = 0.009$
y	Normal	ANOVA$_{Aro}$	o × g INT	$F_{(3,112)} = 0.437$	0.724	$\eta^2_p = 0.011$
Delayed recall (day 2)						
z	Normal	ANOVA$_{Val}$	ME: g	$F_{(1,36)} = 0.074$	0.788	$\eta^2_p = 0.002$
aa	Normal	ANOVA$_{Val}$	o × g INT	$F_{(3,96)} = 0.216$	0.864	$\eta^2_p = 0.006$
bb	Normal	ANOVA$_{Aro}$	ME: g	$F_{(1,36)} = 0.239$	0.628	$\eta^2_p = 0.007$
cc	Normal	ANOVA$_{Aro}$	o × g INT	$F_{(3,100)} = 0.121$	0.938	$\eta^2_p = 0.003$
SCRs						
Acquisition						
dd	Normal	ANOVA	ME: o	$F_{(3,96)} = 14.856$	3.1057E-7	$\eta^2_p = 0.281$
ee	Normal	ANOVA	GEN	$F_{(1,38)} = 31.987$	0.000002	$\eta^2_p = 0.457$
ff	Normal	ANOVA	ME: g	$F_{(1,38)} = 0.931$	0.341	$\eta^2_p = 0.024$
gg	Normal	ANOVA	o × g INT	$F_{(3,96)} = 0.833$	0.461	$\eta^2_p = 0.021$
Extinction						
hh	Normal	ANOVA	ME: g	$F_{(1,38)} = 1.170$	0.286	$\eta^2_p = 0.030$
ii	Normal	ANOVA	o × g INT	$F_{(3,117)} = 0.921$	0.435	$\eta^2_p = 0.024$
Delayed recall (day 2)						
jj	Normal	ANOVA	ME: g	$F_{(1,38)} = 0.002$	0.965	$\eta^2_p = 0.00005$
kk	Normal	ANOVA	o × g INT	$F_{(3,116)} = 1.483$	0.222	$\eta^2_p = 0.038$
ssVEPs						
Acquisition						
ll	Normal	ANOVA	ME: o	$F_{(4,137)} = 5.696$	0.000479	$\eta^2_p = 0.130$
mm	Normal	ANOVA	GEN	$F_{(1,38)} = 8.447$	0.006	$\eta^2_p = 0.182$
nn	Normal	ANOVA	o × g INT	$F_{(4,137)} = 1.042$	0.384	$\eta^2_p = 0.027$
Extinction						
oo	Normal	ANOVA	ME: g	$F_{(1,38)} = 2.957$	0.094	$\eta^2_p = 0.072$
pp	Normal	ANOVA	o × g INT	$F_{(4,147)} = 0.418$	0.790	$\eta^2_p = 0.011$
Delayed recall (day 2)						
qq	Normal	ANOVA	ME: g	$F_{(1,38)} = 5.354$	0.026	$\eta^2_p = 0.123$
rr	Normal	ANOVA	o × g INT	$F_{(3,122)} = 0.556$	0.657	$\eta^2_p = 0.014$

Table shows statistical analyses including p value and effect size for each memory outcome measure, separated by learning phase. For each outcome measure, we calculated repeated-measures ANOVAs with the CS orientation as the within-subject factor and the group (in-phase group vs out-of-phase group) as the between-subject factor. Successful conditioning (i.e., increased response toward the CS$^+$ respective of group) was validated by the main effects of orientations (noted in the column effects as ME: o). To account for the specific symmetric generalization pattern (CS$^+$ in the middle), additional generalization contrast fits were used (noted as GEN). The main effects of group (ME: g) and group × orientation interactions (o × g INT) addressed differences between in-phase and out-of-phase conditioning. Better grating discrimination versus stronger generalization across orientations are described by a Mexican Hat contrast fit for the group × orientation interactions (MEX). ANOVA, Mixed repeated-measures ANOVA; ME, main effect; o, orientation; η^2_p, partial η^2; g, group; MEX, Mexican Hat contrast fit of orientation × group interaction; INT, interaction; GEN, generalization fit; Val, valence; Aro, arousal.
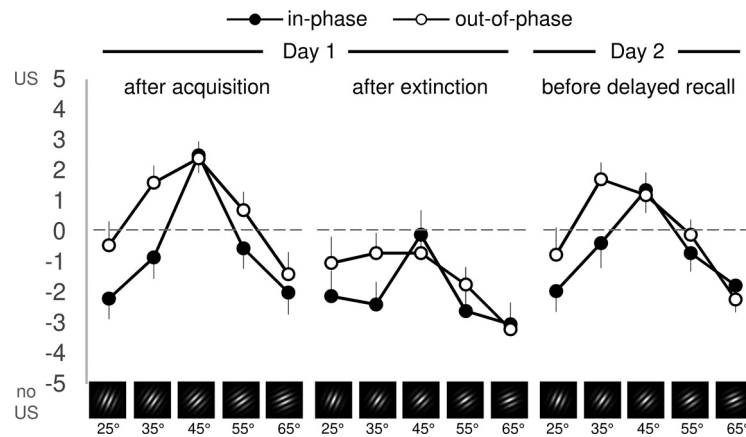
Figure 5. US expectancy ratings separated for each measurement point: after acquisition, after extinction on day 1, and before delayed recall on day 2 in the in-phase and the out-of-phase groups. US expectancy was rated per CS on scale ranging from −5 (very certain, no US after this CS) over 0 (uncertain) to 5 (very certain, a US will follow this CS). Each data point presents the mean US expectancy rating for each CS orientation (averaged over participants per group and measurement point), error bars show 1 SEM. Extended Data Figure 5-1 shows discrimination indices (CS$^+$ minus the weighted average of all CS$^-$) and estimation statistics for US expectancy ratings. For transparency, Extended Data Figure 5-2 shows discrimination indices that result when subtracting the unweighted average of the CS$^-$ from the CS$^+$.

of-phase group showed broader generalization of the US expectancy ratings, while the in-phase group had a narrower generalization pattern with more discrimination between the CS$^+$ and the four CS$^-$ (Fig. 5). This was supported by a significant orientation × group interaction in the form of a Mexican Hat ($F_{(1,38)} = 4.796$, $p = 0.035$, partial $\eta^2 = 0.112$; Table 1, e). As a comprehensive index of CS discrimination (i.e., CS$^+$ vs average of all CS$^-$), we calculated discrimination indices by subtracting the weighted average of CS$^-$ responses from the CS$^+$ responses (Extended Data Fig. 5-1). To account for the fact that the 35° and 55° CS$^-$ orientations only differ from the CS$^+$ by 10° and are thus harder to discriminate, these orientations were multiplied with a weight of 0.33[...] before averaging. The more dissimilar orientations (25°, 65°) differ by 20° from the CS$^+$ and are easier to discriminate. Therefore, these two were weighted with 0.166[...] (i.e., half of the weight of the more similar orientations). Although the CS$^-$ weights account for the perceptual difference, they are not directly derived from a psychophysics curve. Extended Data Figure 5-1 depicts estimation statistics for the discrimination indices within each learning phase by presenting individual values as well as the effect sizes (Hedge's g) as a bootstrap 95% confidence interval (5000 samples; Ho et al., 2019). To increase transparency, Extended Data Figure 5-2 shows the same for a discrimination index computed with the unweighted average of the four CS$^-$ values.

For US expectancy ratings collected after extinction, we found no main effect of group or a group × orientation interaction (Table 1, f, g). However, even after extinction trials, the in-phase group showed a narrower generalization pattern than the out-of-phase group (Fig. 5). Mexican Hat contrast fit for the orientation × group interaction ($F_{(1,38)} = 6.660$, $p = 0.014$, partial $\eta^2 = 0.149$, Table 1, h). On day 2, 24 h later (Fig. 5, Extended Data Fig. 5-1, day 2

before delayed recall) we found no group differences in US expectancy ratings (no main effect group, no orientation × group interaction; Table 1, i, j), and the generalization was no longer significantly narrower in the in-phase group (Mexican Hat orientation × group interaction; Table 1, k).

Synchronization leads to a narrower rating pattern toward the CS$^+$ in valence and arousal ratings after fear acquisition

For both, valence and arousal ratings after acquisition (Fig. 6), we found a prioritization of the CS$^+$ similar to that for US expectancy (main effect orientation: valence: $F_{(3,96)} = 7.756$; $p = 0.000272$; partial $\eta^2 = 0.170$; Table 1, l; arousal: $F_{(3100)} = 10.928$; $p = 0.000008$; partial $\eta^2 = 0.223$; Table 1, m). Again, reflecting the generalization around the CS$^+$ (generalization fit: valence: $F_{(1,38)} = 12.352$; $p = 0.001$; partial $\eta^2 = 0.245$; Table 1, n; arousal: $F_{(1,38)} = 19.587$; $p = 0.000078$; partial $\eta^2 = 0.340$; Table 1, o). Here, mixed ANOVA showed no group main effect or orientation × group interaction for valence (Table 1, p, q) and arousal (Table 1, r, s). However, in both measures the in-phase group showed a narrower generalization than the out-of-phase group (Fig. 6). This was evident in significant orientation × group interactions in the form of a Mexican Hat for valence ($F_{(1,38)} = 9.228$; $p = 0.004$; partial $\eta^2 = 0.195$; Table 1, t) and arousal ($F_{(1,38)} = 7.325$; $p = 0.010$; partial $\eta^2 = 0.162$; Table 1, u). The discrimination indices (CS$^+$ vs averaged CS$^-$) as well as estimation plots, including individual values and effect sizes, are additionally presented in Extended Data Figure 6-1.

After extinction, there were no effects of synchronization in valence (group main effect or orientation × group interaction; Table 1, v, w) or arousal (group main effect or orientation × group interaction; Table 1, x, y). The same was true for valence and arousal ratings on day 2 (group

A Valence ratings
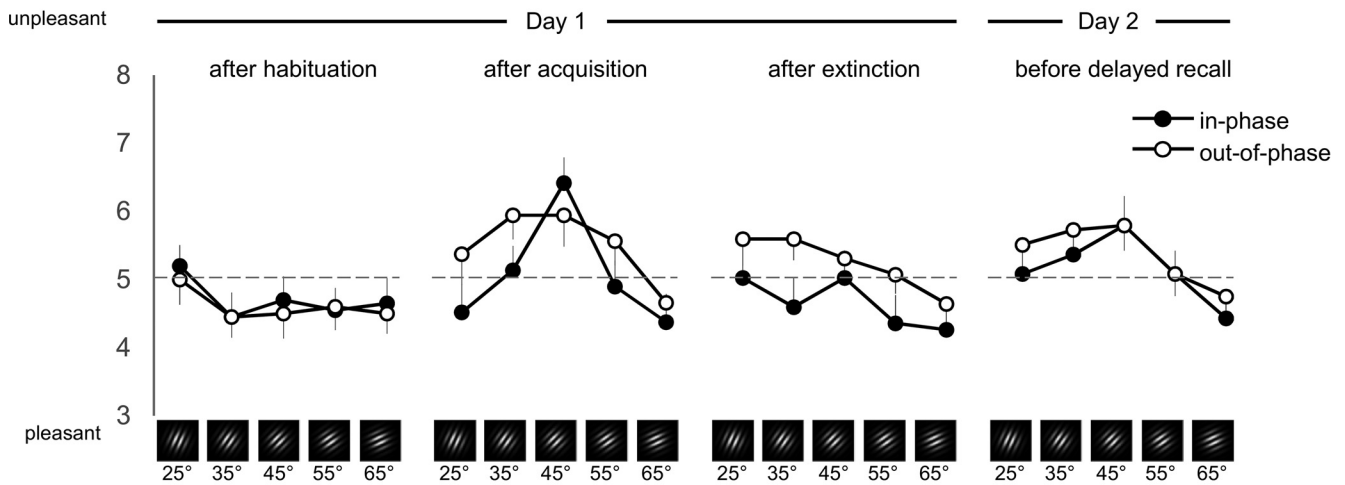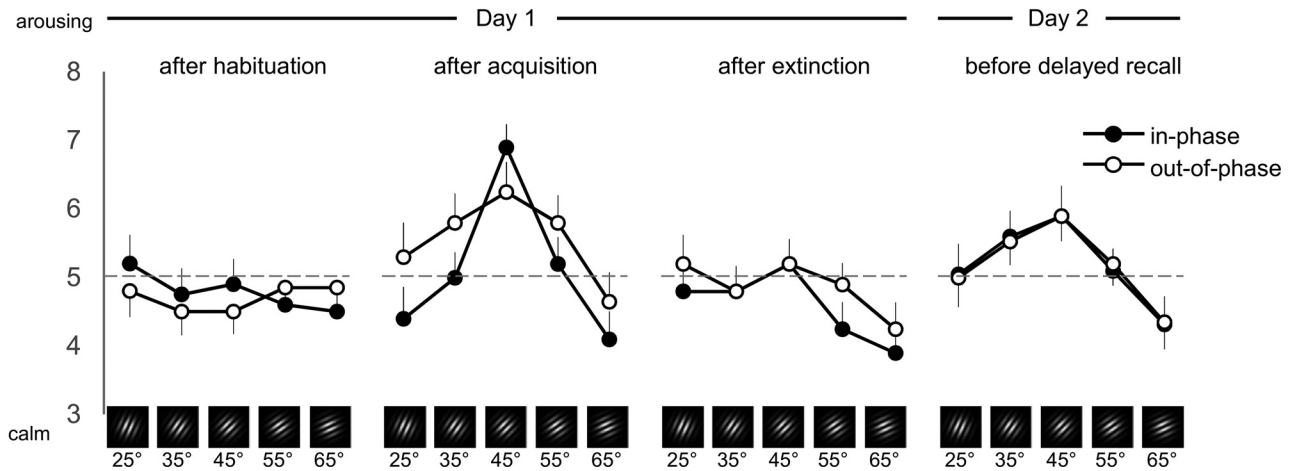
B Arousal ratings

Figure 6. *A*, *B*, Valence ratings (*A*) and arousal ratings (*B*) separated for each measurement point: after habituation, after acquisition, after extinction (day 1), and before delayed recall (day 2). Valence was rated with the Self-Assessment Manikin on a 9-point scale from 1 (unpleasant) to 9 (pleasant). For better comparability with arousal ratings, valence ratings were recoded, changing the scale from 1 (pleasant) to 9 (unpleasant). Arousal was also rated with the Self-Assessment Manikin, here ranging from 1 (calm) to 9 (arousing). Each data point presents valence or arousal ratings, respectively, for each CS orientation (averaged over participants per group and measurement point), error bars show 1 SEM. Note: for better visualization, the *y*-axis is scaled from 3 to 8 instead of showing the full range from 1 to 9. Extended Data Figure 6-1 shows discrimination indices (CS$^+$ minus the weighted average of all CS$^-$) and estimation statistics of valence and arousal data. Extended Data Figure 6-2 additionally shows the discrimination indices that use the unweighted average of all CS$^-$ values for subtraction.

main effect and orientation × group interaction: valence, Table 1, z, aa; arousal, Table 1, bb, cc).

SCRs showed the typical increase toward the reinforced CS$^+$ but were unaffected by the synchronization conditions

Figure 7, *A* and *B*, depicts the SCRs on a trial-by-trial basis to visualize the temporal dynamics of moving-averaged and *z*-transformed SCRs. In addition, *z*-values (i.e., without moving average) SCRs are presented in Extended Data Figure 7-1. However, as single trials are subject to noise, SCRs were analyzed using averaged data (Fig. 7C),

as described in the Materials and Methods section. Pairing the CS$^+$ orientation with the aversive US within acquisition led to the predicted increase of SCR toward the reinforced grating (main effect orientation: $F_{(3,96)} = 14.856$, $p = 3.1057E-7$, partial $\eta^2 = 0.281$; Table 1, dd). The response pattern was described by generalization around the CS$^+$ (generalization fit: $F_{(1,38)} = 31.987$, $p = 0.000002$, partial $\eta^2 = 0.457$; Table 1, ee). However, this was independent of group (main effect group and orientation × group interaction; Table 1, ff, gg, Extended Data Fig. 7-2 for discrimination indices and estimation statistics). Looking at Figure 7 (Extended Data Fig. 7-1), it is unusual that SCRs toward the CS$^+$ seem already increased on the very first trial
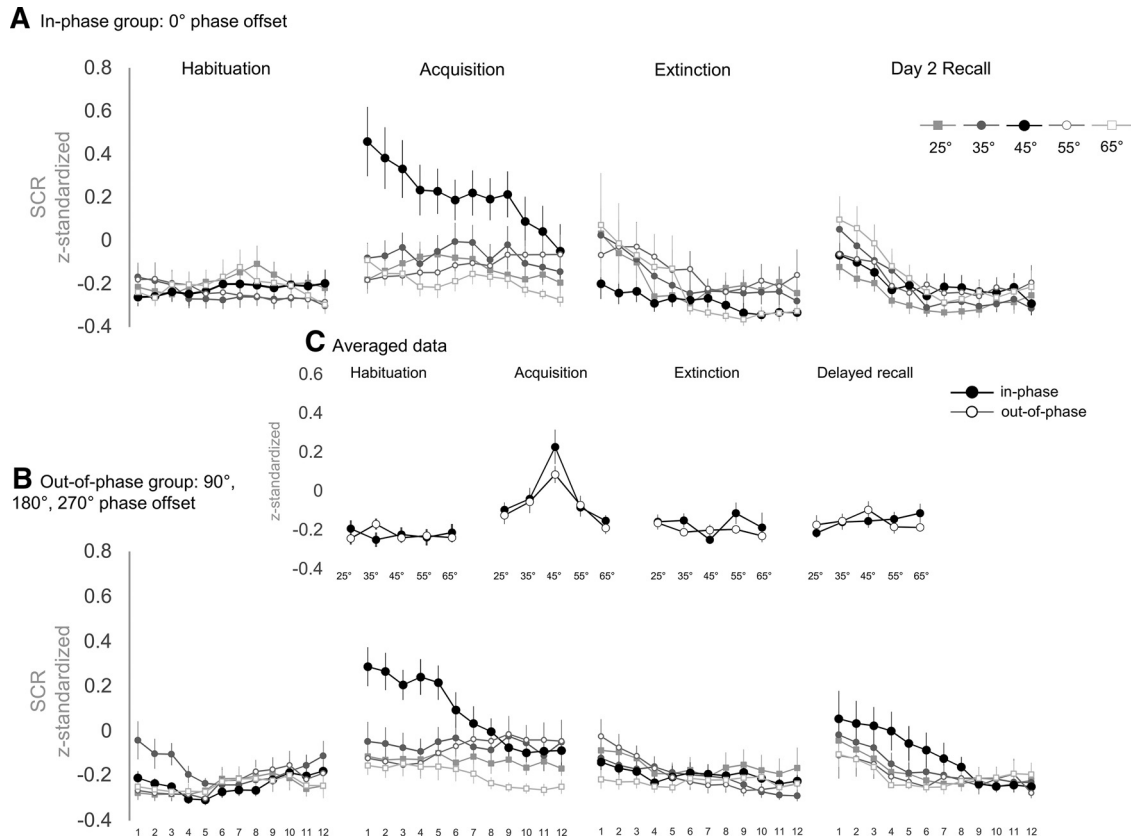
Figure 7. *A–C*, Single-trial (*A*, *B*) and averaged (*C*) skin conductance responses. Single-trial SCRs are separated by the synchronization condition into the in-phase group (0° phase offset; *A*) and the out-of-phase group (90°, 180°, and 270° phase offset; *B*). Single-trial data are *z*-transformed SCRs, averaged over participants per group for each trial and CS orientation. Before averaging, data were smoothed over the 12 trials of a learning phase using a moving average (5 points long, symmetrical, shrinking at the end points). *C* depicts averaged data over 12 trials of habituation, acquisition, extinction, and delayed recall to visualize the response patterns within each learning phase. Here, each data point presents *z*-transformed SCRs of each CS orientation averaged over participants and trials per group. The *z*-transformation was calculated with the means and SDs over CS and US responses of all learning phases (habituation, acquisition, immediate extinction, delayed recall) per participant. Error bars show ±1 SEM. Extended Data Figure 7-1 shows single-trial SCR data without smoothing (i.e., no moving average). Extended Data Figure 7-2 shows discrimination indices (CS⁺ minus the weighted average of all CS⁻) for SCR and estimation statistics. Extended Data Figure 7-3 depicts discrimination indices without weighting the averaged CS⁻ values.

of acquisition, independent of the applied smoothing procedure (Extended Data Fig. 7-1, unsmoothed data). However, explorative analyses of group differences without the first trial did not change the results (i.e., there was still no overall difference between groups and no significant orientation × group interaction).

During extinction, there was no difference between groups (main effect group and orientation × group interaction; Table 1, hh, ii) and also on day 2 synchronization had no effects (main effect group and orientation × group interaction; Table 1, jj, kk).

ssVEP power revealed a tuning toward the visual CS⁺ that was similar in both groups

Figure 8, *A* and *B*, depicts ssVEPs on trial-by-trial basis to visualize temporal dynamics, and Extended Data Figure 8-1 shows ssVEP ratios without a moving average. However, as for the SCRs, ssVEPs were analyzed using averaged data (Fig. 8C), as described in the Materials and Methods section.

ssVEPs during acquisition revealed a conditioned power increase toward the CS⁺ and neighboring gratings (main effect orientation: $F_{(4,137)} = 5.696$, $p = 0.000479$, partial $\eta^2 = 0.130$; Table 1, ll). It was described by a generalization pattern around the CS⁺ (generalization fit: $F_{(1,38)} = 8.447$, $p = 0.006$, partial $\eta^2 = 0.182$; Table 1, mm). However, this prioritization was not affected by group (orientation × group interaction; Table 1, nn). In similarity to SCRs during acquisition, Figure 8, *A* and *B*, indicates an increased ssVEP ratio toward the CS⁺ on the very first trial. However, considering the unsmoothed data in Extended Data Figure 8-1, the power increase here seems to be an artifact of the applied smoothing procedure. As depicted in Figure 8C, synchronization also had no effects on ssVEPs in extinction. Consequently, we found neither a significant main effect of group nor an orientation × group interaction (Table 1, oo, pp). Intriguingly,
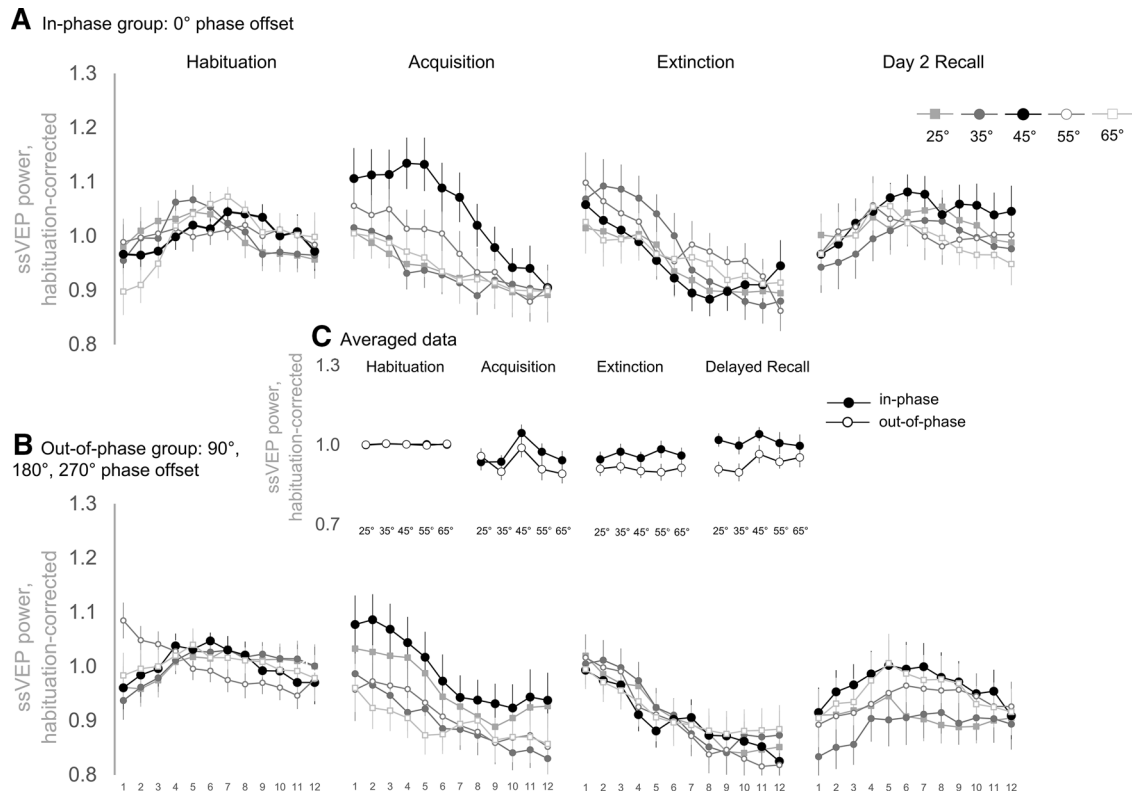
Figure 8. *A–C*, Single-trial (*A*, *B*) and averaged (*C*) power of the 4 Hz ssVEPs for each learning phase (habituation, acquisition, extinction, and delayed recall). Single-trial data are separated by the synchronization condition into the in-phase group (0° phase offset; *A*) and the out-of-phase group (90°, 180°, and 270° phase offset; *B*). The ssVEP power is shown as the SNR at 4 Hz, corrected for habituation-level responding. Correction was performed by dividing individual SNR values by the average SNR from habituation (mean over all 60 trials of each participant, disregarding the different CS orientations). Therefore, values >1 describe an enhancement, and values <1 describe a decrease of ssVEP-SNR at 4 Hz relative to habituation. Single-trial data were smoothed over trials via a moving average along the 12 trials of each learning phase (5 point symmetrical shrinking at the end points). Each data point in *A* and *B* represents habituation corrected SNR for each trial and CS orientation, averaged over participants per group. *C* depicts data averaged over the 12 trials of habituation, acquisition, extinction, and delayed recall to visualize the response patterns within each phase. Error bars show ±1 SEM. Note: habituation data in *C* are nearly "flat" at ~1 because of the habituation correction, as described above and in the Materials and Methods section. Extended Data Figure 8-1 shows single-trial data without the moving-average. Extended Data Figure 8-2 depicts discrimination indices with weighted CS- averages (CS+ minus weighted average of all CS-) and Extended Data Figure 8-3 shows discrimination indices without weighting the averaged CS- responses.

the ssVEP power during delayed recall on day 2 was generally higher in the in-phase group than in the out-of-phase group ($F_{(1,38)}$ = 5.354, p = 0.026, partial η^2 = 0.123, Table 1, qq), although this effect was independent of orientation (orientation × group interaction; Fig. 8C, Table 1, rr). In accordance with ratings and the SCRs, discrimination indices (weighted CS$^+$ minus averaged CS$^-$ gratings) and estimation plots depicting individual values and effects sizes are presented in Extended Data Figure 8-2.

Discussion

The formation of associative memories is an elemental aspect of human behavior, but its underlying neurocomputations are largely unknown. One group of theoretical notions has emphasized the role of phase-synchronized oscillations for binding representations of conditioned cues to behavioral outcomes (Headley and Paré, 2017). Recent research has increasingly used external rhythmic stimulation to test the role of phase relations in specific frequency bands for the formation of working memory (Polanía et al., 2012; Violante et al., 2017) and audiovisual associations (Clouter et al., 2017; Wang et al., 2018). Based on these previous findings, we applied this method for the first time in a fear-conditioning paradigm. Modulating the phase shift of a visual CS and aversive auditory US that was presented in the memory-relevant theta frequency allowed us to causally interpret phase synchronization in fear conditioning. To assess the various response systems that are important in fear learning (Lang et al., 2000), we measured skin conductance responses, indexing the physiological arousal of fear; the ratings of valence and arousal to capture the subjective evaluation of each stimulus; and US expectancy, which assesses the participant's knowledge of the CS–US association. Additionally, ssVEPs provided information about visuocortical engagement and tuning patterns in sensory processing.

The measures we collected in the current study reflect different facets of the associative conditioning process and as such responded differently to the experimental manipulations. In accordance with our hypothesis, synchronized CS–US presentation facilitated the ability to identify the CS$^+$ as the grating that was most likely followed by the aversive US. Remarkably, participants that received synchronized CS–US presentation discriminated the CS$^+$ more precisely from the neighboring CS$^-$ gratings (which only differed in an orientation shift of 10°). Participants in the out-of-phase group, in contrast, generalized across the CS$^+$ or the most similar CS$^-$ gratings. We therefore conclude that the synchronous input of two (multimodal) stimuli stemming from two sensory modalities strengthens the cognitive representation of the CS–US association.

Consistent with the US expectancies, the subjective valence and arousal ratings reflected the effects of phase synchronization. While participants who received in-phase stimulation were more sensitive to changes in the perceived valence and arousal of the CS$^+$, participants in the out-of-phase group reported generalized arousal and unpleasantness across the CS$^+$ and neighboring CS$^-$ gratings. Hence, synchronous input not only sharpens the cognitive representation of CS–US contingency but seems to have a similar influence on the affective evaluation.

Surprisingly, there were no corresponding effects in the SCR or ssVEP data. Considering SCR data, during acquisition both groups showed the strongest response toward the CS$^+$ grating, independent of synchronization. Especially in the single-trial data, however, the in-phase group appears to respond stronger to the CS$^+$, which seems to be more pronounced in the first trials. We therefore exploratively tested the potential group difference by segmenting the trials into trial blocks (three blocks with four trials per block). However, adding this within factor to our statistical analysis did not reveal any significant differences between the groups in different phases of acquisition. One possible explanation of the higher SCRs in the beginning of acquisition might be the booster sequence that was used (i.e., five of the first seven gratings were CS$^+$ gratings). The booster and the applied criterion to not allow more than two consecutive CS of the same orientation might also be the reason for another unusual observation within our SCR results: irrespective of the factor group and independent of the applied smoothing procedure, SCR toward the CS$^+$ was already increased on the very first trial. While we applied the booster sequence for a better comparability with previous findings (McTeague et al., 2015; Antov et al., 2020), future studies should consider a different approach to minimize the similar trial order effect. Nevertheless, there were no differences between the in-phase and out-of-phase group; thus, this observation does not change the following interpretations.

An effect of phase synchronization was also missing in the ssVEP-data. Although we were able to detect a tuning pattern with the greatest power for the reinforced CS$^+$ grating for 4 Hz stimulus presentation as previously described for stimulation in the low beta range (McTeague et al., 2015; Antov et al., 2020), the pattern did not differ between in-phase and out-of-phase group.

A possible explanation for the observed discrepancies in the different variables could be the involvement of different memory types we might have assessed with our measures. Although fear conditioning is a well established and widely used paradigm, it is difficult to strictly distinguish the mechanisms behind each response system. For example, skin conductance responses measure physiological arousal during fear learning (although it is not restricted to fear conditioning) and is often considered as a measure of the unaware fear reaction, especially dependent on the amygdala (Knight et al., 2003, 2006; Christopoulos et al., 2019; but see also Lovibond and Shanks, 2002; Sevenster et al., 2014). US expectancy ratings, on the contrary, are considered to specifically reflect declarative knowledge of the CS–US contingency (Boddez et al., 2013), which is known to include additional brain structures like the hippocampus. Bechara et al. (1995) observed a neural dissociation between implicit and explicit aspects of a fear-conditioning procedure. While patients with bilateral amygdala lesions were unable to elicit SCRs but had an intact memory for the declarative facts, patients with bilateral lesions of the hippocampus showed the exact opposite effects (i.e., they acquired SCRs but failed to recall declarative facts). Speculating that the effects of visual–auditory stimulation is not only restricted to early sensory cortices, but influences deeper brain regions in the course of rhythmic processing, our results might be explainable based on these distinct systems: theta phase synchronization might especially modulate the path involved in forming declarative facts about the CS–US pairing (i.e., US expectancy ratings), probably including the hippocampus, without influencing the emotional conditioning comprising the amygdala. One possible mechanism could be that the phase-synchronous visual CS$^+$ and auditory US simultaneously arrive at neural populations in the hippocampus, increasing the likelihood of long-term potentiation and thereby enhancing synaptic strength (Fell and Axmacher, 2011). Although the EEG method used here does not allow the drawing of conclusions about mechanisms at the synaptic level in subcortical structures, one might also speculate why the heightened CS–US association in the rating data is not reflected in metrics thought to reflect limbic processing (i.e., the SCRs). There are two potential explanations that we highlight in this context. (1) In various species, theta-phase synchronization has predominantly been examined in the context of LTP in the hippocampus (Huerta and Lisman, 1995; Buzsáki, 2002; Hyman et al., 2003; Lega et al., 2012), which is specifically relevant in the formation of declarative memory (Eichenbaum, 1999; Clouter et al., 2017; Wang et al., 2018). Thus, one may speculate that theta-phase synchronization is linked to hippocampus-dependent processes, whereas the exact timing of CS and US may play a lesser role in amygdala-dependent fear learning. However, some studies have found theta-phase synchronization between the amygdala and other important structures of the fear circuit (e.g., hippocampus, ventrolateral PFC, anterior gyrus cinguli) as well as within the subnuclei of the amygdala (Seidenbecher et al., 2003; Karalis et al., 2016; Taub et al., 2018; Zheng et al., 2019; for review, see Bocchio et al., 2017; Çalişkan

and Stork, 2018) during different stages of the fear-conditioning process, supporting the general influence of theta synchronization during fear memory formation. As such, future work may characterize the role of synchronization within and between specific brain regions for the establishing and maintenance of fear memories. (2) More importantly, however, is the question whether synchronized theta rhythms propagate to the amygdala. Sensory information reaches the amygdala via multiple pathways, among which some are faster and subcortical, or "low," routes; and others are slower, or "high," cortical routes (Silverstein and Ingvar, 2015). Since our method of visual and auditory synchronized (vs asynchronized) theta stimulation is delivered globally and is unlikely to target one specific pathway, the timing might not have been suitable to enable locally specific synchronization. Considering that we used a generalization paradigm with similar CS gratings, we may offer the speculation that the challenging discrimination of the CS^+ requires a more demanding processing via the slow, cortical route, while the simple aversive US reaches the amygdala via the fast, subcortical pathway. Thus, the 40 ms we added to the US might have been insufficient to achieve theta synchronization when the CS and US reach the LA. Because of the relatively long CS–US overlap of 2 s, we additionally cannot rule out that our synchronized stimulation reached the amygdala via the thalamic route first, but then also via cortical routes, leading to cancellation of the first CS–US phase synchronization, hence minimizing the suggested effects.

Another interesting consideration in this context is the role of theta synchronization between the amygdala and hippocampus for pattern separation of emotional images. Examining presurgical epilepsy patients, Zheng et al. (2019) found that bidirectional theta synchronization between both structures was associated with the ability to discriminate an encoded image and a new, but similar, "lure" image in a test phase. Considering that most of our results consist of a better discrimination between the aversive CS^+ and the most similar CS^- gratings, synchronized CS–US presentation might be beneficial for the amygdalo–hippocampal communication, associated with enhanced discrimination of emotional content. However, further research with additional outcome measures is needed to pinpoint all underlying neurophysiological processes. For example, future studies may attempt to experimentally untangle declarative and nondeclarative memory processes involved in fear conditioning, including their reactivity to synchronized presentation. Measuring amygdala and hippocampus activity via fMRI or in experimental animals may also help to clarify the influence of synchronized presentation on distinct subprocesses of fear conditioning and their associated neural substrates.

One important consideration when interpreting the current results is the fact that group differences were mostly restricted to the encoding phase of fear (acquisition), although we expected that improved fear learning after synchronous presentation prompts greater extinction resistance. Contrary to expectations, we did not find

extinction-resistant patterns in the in-phase group during immediate extinction or delayed recall. However, using a reinforcement rate of 100% is known to cause rapid extinction (Haselgrove et al., 2004; Dunsmoor et al., 2007), which could make it harder to detect between-group effects. Moreover, because extinction leads to the formation of a new (i.e., CS–no-US) memory trace that inhibits the original fear memory, future research may use a second CS^+ stimulus that is not extinguished, which will aid in assessing the long-lasting effects of theta-phase synchronization on fear memory recall (i.e., the trace that was causally manipulated by theta-synchronized stimulation). Additionally, animal and human work suggests that prolonged stimulus-free periods during encoding are associated with the more effective production of long-term memory (Philips et al., 2013; Jiang et al., 2020). Increasing the ITIs might help to form more robust memory traces that persist over time. Another possible cause for the absence of long-term effects of stimulation phase is that the externally modulated CS–US stimulation only affects short-term or working memory processes but does not have any effects on actual long-term memory. In two comparable studies focusing on declarative memory Clouter et al. (2017) and their follow-up study by Wang et al. (2018) used a distractor task as a time gap between the encoding and recall of the learned video–tone associations, which only lasted for 30 s, likely too short a time to inform the formation of long-term memory.

Although the current study provided evidence of a causal role of theta-phase synchronization in the context of fear conditioning, there are some limitations to consider. First, our sample size was chosen to detect medium to strong effect sizes, which was based on previous studies (Clouter et al., 2017; Wang et al., 2018). Therefore, we cannot rule out the possibility that we could not detect small effect sizes. This is especially interesting for the SCR data, where the responses are descriptively stronger after in-phase CS–US presentation, but the statistics did not show significant differences. Increasing the statistical power via a greater sample size might help to even detect small effect sizes. Second, we cannot conclude that the stimulation effects observed here are specific to the theta band, because we did not test other frequencies. However, both animal model studies that examined theta-phase synchronization in the fear network (Seidenbecher et al., 2003; Taub et al., 2018), as well as entrainment studies that focused on working and declarative memory (Alekseichuk et al., 2016; Clouter et al., 2017; Violante et al., 2017) support the current conclusion that synchronization in the theta-frequency band is specifically important for fear memory formation. Third, we did not explicitly ask whether participants were able to detect the synchronous or asynchronous timing between CS and US, and therefore we cannot rule out that out-of-phase or in-phase stimulation exerted effects based on phenomenological, perceptual differences. Nevertheless, we used the exact time lags used by both Clouter et al. (2017) and Wang et al. (2018), who did not observe any interference with perceptual judgments or decline in performance. In addition, Clouter et al. (2017) conducted a control

experiment with static stimuli, which, on a perceptual basis, represents the best-case scenario for perceptual binding and still found better results after theta-synchronized video–audio presentation. Fourth, although EEG data showed a group-independent tuning toward the CS$^+$ grating, supporting the conditioned effects on sensory processing, the hypothesized sharpening in the in-phase group was not confirmed. What we found is a general increase in ssVEP-power in the in-phase group during day 2, suggesting a stronger engagement of the sensory cortex. However, based on the present data, we cannot establish to what extent this effect was caused by the theta-phase synchronization on day 1 as opposed to arising as an epiphenomenon (e.g., of the cognitive changes induced by the synchronization). Fifth, theta synchronization may not facilitate learning, but desynchronized stimulation may disrupt ongoing oscillatory processes, resulting in less precise (i.e., more generalized) fear responses (Alekseichuk et al., 2017). To clarify this assumption, future work may include a third group in which participants are presented with nonflickering CS and US stimuli.

Finally, an important limitation is that we were not able to show that participants' auditory and visual EEG responses were synchronized or desynchronized as intended. This was because of the limited number of trials and noisy US data. In contrast to previous work with innocuous stimuli, the US in a fear-conditioning experiment has to be highly aversive. Inherently, this means that the duration of the US (the only period in which auditory and visual stimulation overlap) will produce noisy EEG data with many movements, a startle response, and other artifacts. This is why EEG studies of human fear conditioning (regardless of the US used and the number of trials) typically do not analyze any data during the US presentation window. Because the US is aversive, we did not want to expose participants to more noise than absolutely necessary. Thus, based on previous experiments, we limited the duration of a single US to 2000 ms and the number of US trials to 12 per participant. In combination with inherently noisy EEG data during a US presentation precluded us from localizing and analyzing phase differences in the brain response. This should be addressed with a modified design in future studies. Nevertheless, we did verify the precise nature of the bimodal stimulation on a single-trial and single-subject level (Fig. 2). Importantly, earlier work (Clouter et al., 2017; Wang et al., 2018) with 4 Hz audio–video synchronization using larger trial numbers and nonaversive audio stimulation have shown that precise audio–video stimulation results in synchronized responding in the auditory and visual cortex. Future studies may also consider extending the temporal gap between the acquisition phase and the delayed recall, because previous work has indicated that theta-band synchronization between the amygdala and sensory cortices affects the storage of fear information in remote, but not recent, fear retrieval (Sacco and Sacchetti, 2010; Do-Monte et al., 2015).

In conclusion, the current study represents an initial step toward establishing the causal effects of theta-phase synchronization for fear memory formation. Our results replicate the importance of synchronization for acquiring new cognitive representations, measured via US expectancy ratings, and affective evaluation (subjective valence and arousal ratings). By contrast, the present evidence was mixed at the level of sympathetic (skin conductance) and visuocortical (ssVEPs) engagement. Future studies may further explore the differentiation between different response systems in the context of fear conditioning. Leveraging the potential of rhythmic stimulation and synchronization while taking into account the evolution of fear acquisition across the learning phases will ultimately assist in improving our understanding of the mechanisms behind the acquisition of learned fear responses.

References

Alekseichuk I, Turi Z, Amador de Lara G, Antal A, Paulus W (2016) Spatial working memory in humans depends on theta and high gamma synchronization in the prefrontal cortex. Curr Biol 26:1513–1521.

Alekseichuk I, Pabel SC, Antal A, Paulus W (2017) Intrahemispheric theta rhythm desynchronization impairs working memory. Restor Neurol Neurosci 35:147–158.

Antov MI, Plog E, Bierwirth P, Keil A, Stockhorst U (2020) Visuocortical tuning to a threat-related feature persists after extinction and consolidation of conditioned fear. Sci Rep 10:3926.

Bechara A, Tranel D, Damasio H, Adolphs R, Rockland C, Damasio A (1995) Double dissociation of conditioning and declarative knowledge relative to the amygdala and hippocampus in humans. Science 269:1115–1118.

Benchenane K, Peyrache A, Khamassi M, Tierney PL, Gioanni Y, Battaglia FP, Wiener SI (2010) Coherent theta oscillations and reorganization of spike timing in the hippocampal- prefrontal network upon learning. Neuron 66:921–936.

Benedek M, Kaernbach C (2010) A continuous measure of phasic electrodermal activity. J Neurosci Methods 190:80–91.

Blair HT, Schafe GE, Bauer EP, Blair HT, Schafe GE, Bauer EP, Rodrigues SM, Ledoux JE (2001) Synaptic plasticity in the lateral amygdala: a cellular hypothesis of fear conditioning. Learn Mem 8:229–242.

Bliss TVP, Collingridge GL, Morris RGM, Reymann KG (2018) Long-term potentiation in the hippocampus: discovery, mechanisms and function. Neuroforum 24:A103–A120.

Bocchio M, Nabavi S, Capogna M (2017) Synaptic plasticity, engrams, and network oscillations in amygdala circuits for storage and retrieval of emotional memories. Neuron 94:731–743.

Boddez Y, Baeyens F, Luyten L, Vansteenwegen D, Hermans D, Beckers T (2013) Rating data are underrated: validity of US expectancy in human fear conditioning. J Behav Ther Exp Psychiatry 44:201–206.

Boucsein W, Fowles DC, Grimnes S, Ben-Shakhar G, Roth WT, Dawson ME, Filion DL (2012) Publication recommendations for electrodermal measurements. Psychophysiology 49:1017–1034.

Bradley MM, Lang PJ (1994) Measuring emotion: the self-assessment manikin and the semantic differential. J Behav Ther Exp Psychiatry 25:49–59.

Brainard DH (1997) The Psychophysics Toolbox. Spat Vis 10:433–436.

Buzsáki G (2002) Theta oscillations in the hippocampus. Neuron 33:325–340.

Çalişkan G, Stork O (2018) Hippocampal network oscillations as mediators of behavioural metaplasticity: insights from emotional learning. Neurobiol Learn Mem 154:37–53.

Christopoulos GI, Uy MA, Yap WJ (2019) The body and the brain: measuring skin conductance responses to understand the emotional experience. Organ Res Methods 22:394–420.

Clouter A, Shapiro KL, Hanslmayr S (2017) Theta phase synchronization is the glue that binds human associative memory. Curr Biol 27:3143–3148.e6.

Do-Monte FH, Quiñones-Laracuente K, Quirk GJ (2015) A temporal shift in the circuits mediating retrieval of fear memory. Nature 519:460–463.

Dunsmoor JE, Bandettini PA, Knight DC (2007) Impact of continuous versus intermittent CS-UCS pairing on human brain activation during Pavlovian fear conditioning. Behav Neurosci 121:635–642.

Eichenbaum H (1999) The hippocampus and mechanisms of declarative memory. Behav Brain Res 103:123–133.

Fell J, Axmacher N (2011) The role of phase synchronization in memory processes. Nat Rev Neurosci 12:105–118.

Foa EB (1995) Posttraumatic diagnostic scale manual. Minneapolis, MN: National Computer Systems.

Fries P (2015) Communication through coherence. Neuron 88:220–235.

Hanslmayr S, Axmacher N, Inman CS (2019) Modulating human memory via entrainment of brain oscillations. Trends Neurosci 42:485–499.

Haselgrove M, Aydin A, Pearce JM (2004) A partial reinforcement extinction effect despite equal rates of reinforcement during pavlovian conditioning. J Exp Psychol Anim Behav Process 30:240–250.

Headley DB, Paré D (2017) Common oscillatory mechanisms across multiple memory systems. NPJ Sci Learn 2:1.

Herrmann CS, Strüber D, Helfrich RF, Engel AK (2016) EEG oscillations: from correlation to causality. Int J Psychophysiol 103:12–21.

Herry C, Johansen JP (2014) Encoding of fear learning and memory in distributed neuronal circuits. Nat Neurosci 17:1644–1654.

Ho J, Tumkaya T, Aryal S, Choi H, Claridge-Chang A (2019) Moving beyond P values: data analysis with estimation graphics. Nat Methods 16:565–566.

Huerta PT, Lisman JE (1995) Bidirectional synaptic plasticity induced by a single burst during cholinergic theta oscillation in CA1 in vitro. Neuron 15:1053–1063.

Hyman JM, Wyble BP, Goyal V, Rossi CA, Hasselmo ME (2003) Stimulation in hippocampal region CA1 in behaving rats yields long-term potentiation when delivered to the peak of theta and long-term depression when delivered to the trough. J Neurosci 23:11725–11731.

Jiang L, Wang L, Yin Y, Huo M, Liu C, Zhou Q, Yu D, Xu L, Mao R (2020) Spaced training enhances contextual fear memory via activating hippocampal 5-HT2A receptors. Front Mol Neurosci 12:317.

Junghöfer M, Elbert T, Leiderer P, Berg P, Rockstroh B (1997) Mapping EEG-Potentials on the surface of the brain: a strategy for uncovering cortical sources. Brain Topogr 9:203–217.

Karalis N, Dejean C, Chaudun F, Khoder S, Rozeske R, Wurtz H, Bagur S, Benchenane K, Sirota A, Courtin J, Herry C (2016) 4-Hz oscillations synchronize prefrontal-amygdala circuits during fear behavior. Nat Neurosci 19:605–612.

Kim WB, Cho J (2017) Encoding of discriminative fear memory by input-specific LTP in the amygdala. Neuron 95:1129–1146.

King AJ, Palmer AR (1985) Integration of visual and auditory information in bimodal neurones in the guinea-pig superior colliculus. Exp Brain Res 60:492–500.

Kleiner M, Brainard D, Pelli D, Ingling A, Murray R, Broussard C (2007) What's new in Psychtoolbox-3? Paper presented at *ECVP '07, the Thirtieth European Conference on Visual Perception*, Arezzo, Italy, August.

Knight DC, Nguyen HT, Bandettini PA (2003) Expression of conditional fear with and without awareness. Proc Natl Acad Sci U S A 100:15280–15283.

Knight DC, Nguyen HT, Bandettini PA (2006) The role of awareness in delay and trace fear conditioning in humans. Cogn Affect Behav Neurosci 6:157–162.

Lang PJ, Davis M, Ohman A (2000) Fear and anxiety: animal models and human cognitive psychophysiology. J Affect Disord 61:137–159.

LeDoux JE (2000) Emotion circuits in the brain. Annu Rev Neurosci 23:155–184.

Lega BC, Jacobs J, Kahana M (2012) Human hippocampal theta oscillations and the formation of episodic memories. Hippocampus 22:748–761.

Lennie P (1981) The physiological basis of variations in visual latency. Vision Res 21:815–824.

Lovibond PF, Shanks DR (2002) The role of awareness in Pavlovian conditioning: empirical evidence and theoretical implications. J Exp Psychol Anim Behav Process 28:3–26.

Luo Q, Holroyd T, Majestic C, Cheng X, Schechter J, James Blair R (2010) Emotional automaticity is a matter of timing. J Neurosci 30:5825–5829.

Lynch MA (2004) Long-term potentiation and memory. Physiol Rev 84:87–136.

Maren S, Fanselow M (1995) Synaptic plasticity in the basolateral amygdala induced by hippocampal formation stimulation *in vivo*. J Neurosci 15:7548–7564.

Markram H, Lübke J, Frotscher M, Sakmann B (1997) Regulation of synaptic efficacy by coincidence of postsynaptic APs and EPSPs. Science 275:213–215.

McFadyen J, Mermillod M, Mattingley JB, Halász V, Garrido MI (2017) A rapid subcortical amygdala route for faces irrespective of spatial frequency and emotion. J Neurosci 37:3864–3874.

McTeague LM, Gruss LF, Keil A (2015) Aversive learning shapes neuronal orientation tuning in human visual cortex. Nat Commun 6:7823.

Moratti S, Keil A (2005) Cortical activation during Pavlovian fear conditioning depends on heart rate response patterns: an MEG study. Brain Res Cogn Brain Res 25:459–471.

Nokia MS, Waselius T, Mikkonen JE, Wikgren J, Penttonen M (2015) Phase matters: responding to and learning about peripheral stimuli depends on hippocampal θ phase at stimulus onset. Learn Mem 22:307–317.

Orsini CA, Maren S (2012) Neural and cellular mechanisms of fear and extinction memory formation. Neurosci Biobehav Rev 36:1773–1802.

Philips GT, Kopec AM, Carew TJ (2013) Pattern and predictability in memory formation: from molecular mechanisms to clinical relevance. Neurobiol Learn Mem 105:117–124.

Place R, Farovik A, Brockmann M, Eichenbaum H (2016) Bidirectional prefrontal-hippocampal interactions support context-guided memory. Nat Neurosci 19:992–994.

Polanía R, Nitsche MA, Korman C, Batsikadze G, Paulus W (2012) The importance of timing in segregated theta phase-coupling for cognitive performance. Curr Biol 22:1314–1318.

Quirk GJ, Repa JC, LeDoux JE (1995) Fear conditioning enhances short-latency auditory responses of lateral amygdala neurons: parallel recordings in the freely behaving rat. Neuron 15:1029–1039.

Romanski LM, Clugnet MC, Bordi F, LeDoux JE (1993) Somatosensory and auditory convergence in the lateral nucleus of the amygdala. Behav Neurosci 107:444–450.

Sacco T, Sacchetti B (2010) Role of secondary sensory cortices in emotional memory storage and retrieval in rats. Science 329:649–656.

Seidenbecher T, Laxmi TR, Stork O, Pape H (2003) Amygdalar and hippocampal theta rhythm synchronization during fear memory retrieval. Science 301:846–850.

Sevenster D, Beckers T, Kindt M (2014) Fear conditioning of SCR but not the startle reflex requires conscious discrimination of threat and safety. Front Behav Neurosci 8:32.

Silverstein DN, Ingvar M (2015) A multi-pathway hypothesis for human visual fear signaling. Front Syst Neurosci 9:101.

Skrandies W (2007) The effect of stimulation frequency and retinal stimulus location on visual evoked potential topography. Brain Topogr 20:15–20.

Steil R, Ehlers A (2000) Posttraumatische Diagnoseskala (PDS). Jena, Germany: Psychologisches Institut, Universität Jena.

Summerfield C, Mangels JA (2005) Coherent theta-band EEG activity predicts item-context binding during encoding. Neuroimage 24:692–703.

Taub AH, Perets R, Kahana E, Paz R (2018) Oscillations synchronize amygdala-to-prefrontal primate circuits during aversive learning. Neuron 97:291–298.e3.

Thut G, Schyns PG, Gross J (2011) Entrainment of perceptually relevant brain oscillations by non-invasive rhythmic stimulation of the human brain. Front Psychol 2:170.

Violante IR, Li LM, Carmichael DW, Lorenz R, Leech R, Hampshire A, Rothwell JC, Sharp DJ (2017) Externally induced frontoparietal synchronization modulates network dynamics and enhances working memory performance. Elife 6:1–22.

Wang D, Clouter A, Chen Q, Shapiro KL, Hanslmayr S (2018) Single-trial phase entrainment of theta oscillations in sensory regions predicts human associative memory performance. J Neurosci 38:6299–6309.

Weiss S, Rappelsberger P (2000) Long-range EEG synchronization during word encoding correlates with successful memory performance. Brain Res Cogn Brain Res 9:299–312.

Zheng J, Stevenson RF, Mander BA, Mnatsakanyan L, Hsu FPK, Vadera S, Knight RT, Yassa MA, Lin JJ (2019) Multiplexing of theta and alpha rhythms in the amygdala-hippocampal circuit supports pattern separation of emotional information. Neuron 102:887–898.e5.

Extended data.

Title: Phase-synchronized stimulus presentation augments contingency knowledge and affective evaluation in a fear-conditioning task.

Authors: Elena Plog, Martin I. Antov, Philipp Bierwirth, Andreas Keil, and Ursula Stockhorst

Extended Data. *Phase-synchronized stimulus presentation augments contingency knowledge and affective evaluation in a fear-conditioning task.*

Extended data Figure 1-1. Table of trial list 1 and 2 for CS presentation order within each learning phase.

Trial	Habituation		Acquisition		Immediate Extinction		Delayed Recall	
	trial list 1	trial list 2	trial list 1	trial list 2	trial list 1	trial list 2	trial list 1	trial list 2
1	35°	45°	45°	45°	25°	55°	35°	65°
2	65°	35°	45°	45°	35°	45°	65°	55°
3	35°	25°	65°	35°	55°	55°	45°	35°
4	55°	65°	45°	45°	35°	35°	55°	45°
5	45°	25°	55°	45°	45°	65°	25°	55°
6	25°	45°	45°	55°	65°	25°	45°	25°
7	65°	65°	45°	45°	55°	65°	65°	65°
8	55°	45°	55°	65°	25°	45°	45°	25°
9	25°	35°	25°	45°	55°	35°	35°	35°
10	45°	65°	35°	25°	35°	25°	55°	25°
11	55°	25°	45°	55°	65°	35°	65°	65°
12	35°	55°	55°	35°	35°	65°	45°	45°
13	25°	25°	65°	65°	55°	35°	25°	55°
14	45°	45°	25°	35°	25°	25°	65°	45°
15	65°	55°	55°	25°	35°	45°	25°	65°
16	25°	45°	35°	35°	25°	35°	35°	35°
17	45°	25°	25°	55°	55°	45°	55°	55°
18	35°	35°	55°	35°	45°	55°	45°	45°
19	55°	45°	65°	55°	25°	45°	55°	25°
20	65°	65°	25°	65°	65°	35°	35°	35°
21	45°	55°	45°	55°	55°	55°	45°	55°
22	55°	65°	35°	35°	25°	65°	35°	35°
23	25°	55°	55°	55°	55°	35°	65°	65°
24	65°	35°	25°	65°	65°	55°	25°	45°
25	45°	45°	65°	25°	45°	45°	45°	55°
26	25°	65°	35°	45°	35°	55°	25°	45°
27	55°	35°	25°	25°	45°	25°	55°	65°
28	35°	45°	65°	25°	25°	55°	35°	35°
29	65°	65°	55°	65°	55°	65°	25°	65°
30	35°	35°	65°	35°	35°	45°	65°	25°
31	65°	55°	25°	65°	45°	65°	35°	65°
32	35°	45°	35°	25°	65°	45°	55°	35°
33	65°	65°	45°	65°	35°	35°	65°	25°
34	55°	25°	35°	45°	65°	25°	45°	45°
35	25°	55°	25°	35°	45°	35°	35°	65°
36	45°	45°	65°	55°	65°	65°	55°	35°
37	35°	65°	55°	25°	45°	65°	25°	45°
38	55°	25°	25°	45°	35°	55°	65°	25°
39	25°	35°	55°	25°	25°	25°	25°	55°
40	45°	25°	65°	55°	55°	45°	35°	45°
41	55°	65°	55°	25°	25°	25°	45°	55°
42	25°	35°	35°	35°	45°	55°	65°	25°
43	45°	35°	45°	45°	65°	65°	35°	55°
44	35°	55°	35°	25°	35°	25°	55°	35°
45	65°	35°	25°	45°	45°	65°	25°	45°
46	45°	65°	45°	25°	65°	25°	35°	25°
47	35°	25°	65°	55°	35°	35°	45°	35°
48	55°	55°	35°	65°	65°	45°	55°	65°
49	65°	25°	55°	35°	35°	55°	65°	25°
50	25°	45°	45°	65°	55°	45°	25°	55°
51	65°	35°	35°	25°	65°	25°	45°	65°
52	35°	55°	55°	55°	45°	55°	65°	45°
53	65°	35°	35°	65°	55°	65°	35°	65°
54	55°	55°	45°	55°	45°	45°	55°	25°
55	45°	25°	25°	35°	25°	65°	25°	35°
56	25°	45°	65°	65°	65°	55°	55°	55°
57	35°	55°	35°	35°	55°	25°	45°	25°
58	55°	25°	25°	45°	25°	35°	55°	55°
59	45°	65°	65°	65°	45°	25°	65°	35°
60	25°	55°	65°	55°	25°	35°	25°	45°

Figure 1-1. Table of trial lists 1 and 2 for CS presentation order within each learning phase. The table shows the sequential order of CS presentation across the 60 trials of each learning phase. CS were Gabor gratings differing only in orientation (orientation degrees are shown in the second to last columns). The first column (Trial) shows the sequential number (e.g., trial 2 was the second CS seen by a participant in the specified learning phase). Each participant within the in-phase and out-of-phase groups was randomly assigned to receive stimuli according to list 1 or 2. Assignment to list 1 and 2 was balanced across groups.

Extended data Figure 5-1. Weighted discrimination indices for US-expectancy ratings.
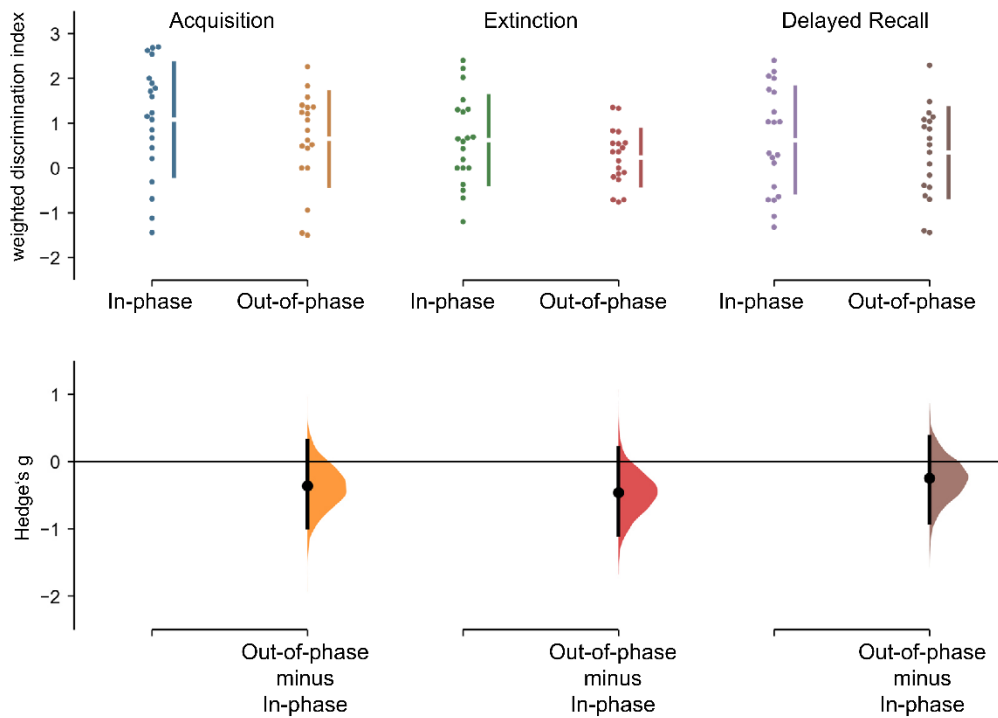
Figure 5-1. Weighted discrimination indices for US expectancy ratings. US expectancy ratings were first *z*-transformed within each participant using the mean and SD of all US expectancy ratings of a participant. With the *z*-transformed data we computed a weighted discrimination index per learning phase as the difference between the rating of the reinforced 45° (CS⁺) grating and the weighted average of the four CS⁻ gratings. Weights for the CS⁻ correspond to the angular difference in orientation between the four CS⁻ orientations (25°, 35°, 55°, 65°) and the CS⁺ orientation (45°). The two more similar CS⁻ orientations (±10° to the CS⁺) were weighted with 0.33[…], while the more dissimilar orientations (±20° to the CS⁺) were weighted with 0.166[…]. Data and effect sizes are shown as a Cumming estimation plot (http://www.estimationstats.com). Top row, Swarm plots show the raw discrimination indices per learning phase (each dot is the discrimination index of one participant). Group statistics are indicated to the right of each swarm as gapped lines (gap = mean, line length = 1 SD). Bottom row, Effect size estimates (Hedges' *g*, black dots) for the three relevant comparisons (in-phase vs out-of-phase for each learning phase) and their 95% confidence interval (CI; vertical error bars). The unpaired Hedge's *g*: for acquisition: –0.364 [95% CI, –0.981, 0.315], *p* = 0.2578; for extinction: –0.463 [95% CI, –1.089, 0.205], *p* = 0.1532; for delayed recall: –0.249 [95% CI, –0.907, 0.370], *p* = 0.4206. The 5000 bootstrap samples were taken for CI estimation; the CI is bias corrected and accelerated. The two-sided *p* values are the likelihoods of observing the effect sizes, if the null hypothesis of zero difference is true. For each permutation *p* value, 5000 reshuffles of the group labels were performed.

Extended data Figure 5-2. Unweighted discrimination indices for US-expectancy ratings.
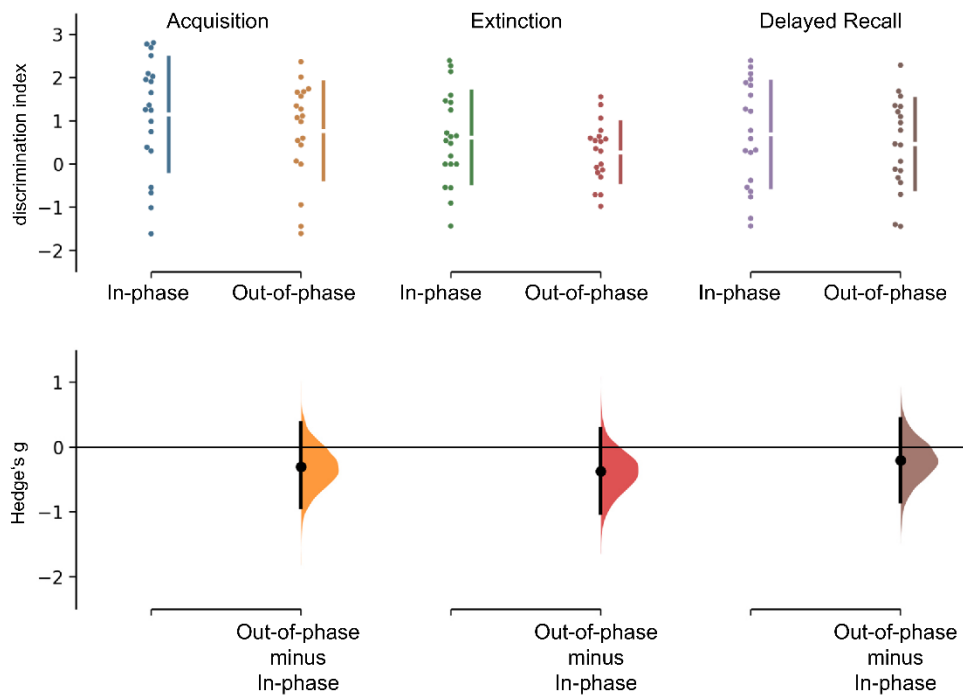
Figure 5-2. Unweighted discrimination indices for US expectancy ratings. US expectancy ratings were *z*-transformed within each participant using the mean and SD of all US expectancy ratings of a participant. The unweighted discrimination index shown is the difference between ratings of the CS^+ and the unweighted average of the four CS^- orientations. Data and effect sizes are shown as a Cumming estimation plot (http://www.estimationstats.com). See the legend of Extended Data Figure 5-1 for a detailed description of a Cumming estimation plot. The unpaired Hedge's *g*: for acquisition:–0.306 [95% CI, –0.928, 0.375], $p = 0.3356$; for extinction: –0.372 [95% CI, –1.021, 0.289], $p = 0.2346$; for delayed recall: –0.198 [95% CI, –0.842, 0.433], $p = 0.5166$. The 5000 bootstrap samples were taken for CI estimation; the CI is bias corrected and accelerated. The two-sided *p* values are the likelihoods of observing the effect sizes, if the null hypothesis of zero difference is true. For each permutation *p* value, 5000 reshuffles of the group labels were performed.

Extended data Figure 6-1. Weighted discrimination indices for valence and arousal ratings.
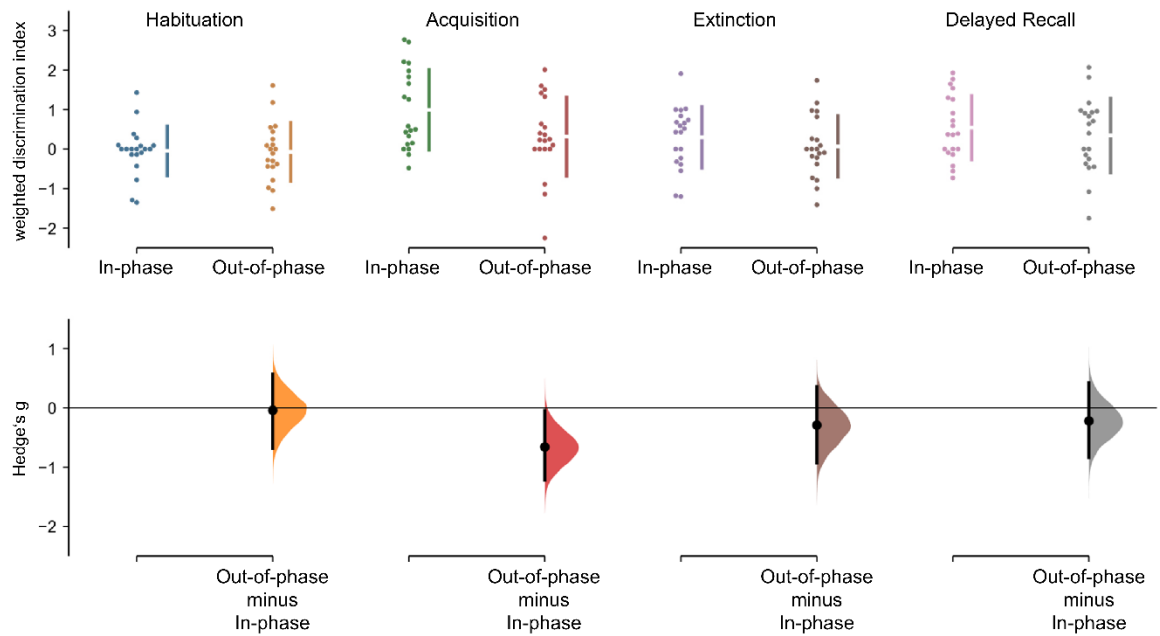
(A) Valence ratings
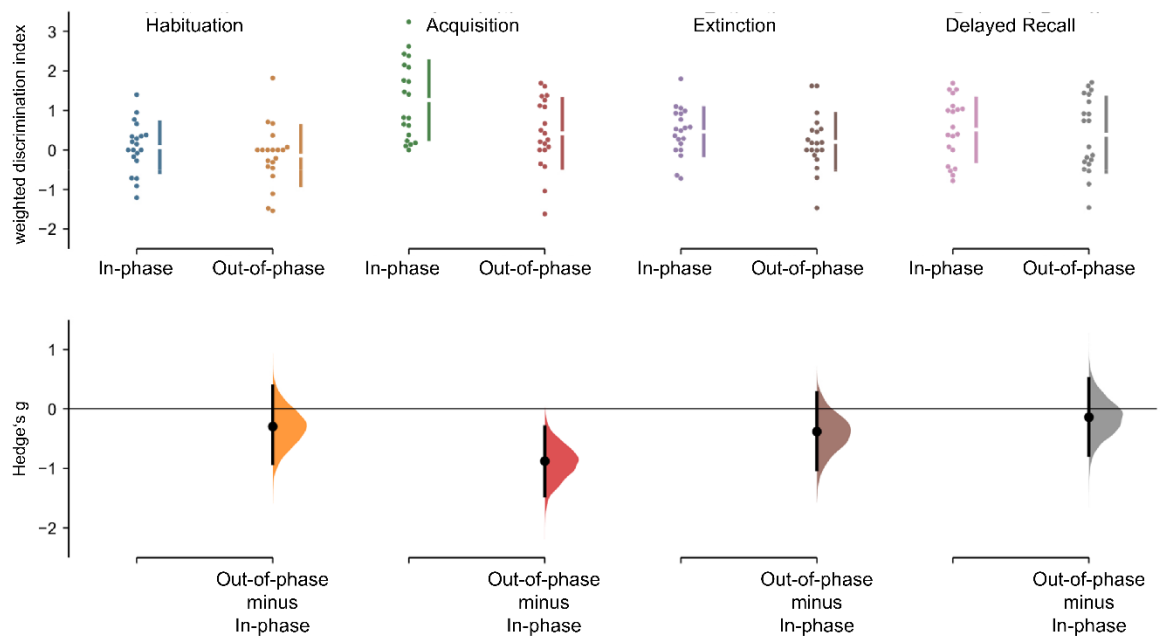
(B) Arousal ratings

Figure 6-1. *A*, *B*, Weighted discrimination indices for valence ratings (*A*) and arousal ratings (*B*). Valence and arousal ratings were first *z*-transformed within each participant using the mean and SD of all ratings of valence and arousal of a participant, respectively. With the *z*-transformed data, we computed a weighted discrimination index per learning phase as the difference between the reinforced $45°$ (CS^+) grating and the weighted average of the four CS^- gratings. Weights for the CS^- correspond to the angular difference in orientation between the four CS^- orientations ($25°$, $35°$, $55°$, $65°$) and the CS^+ orientation ($45°$): the two more similar CS^- orientations ($\pm 10°$ to the CS^+) were weighted with 0.33[…], while the more dissimilar orientations ($\pm 20°$ to the CS^+) were weighted with 0.166. Data and effect sizes are shown as a Cumming estimation plot (http://www.estimationstats.com).

Extended Data. *Phase-synchronized stimulus presentation augments contingency knowledge and affective evaluation in a fear-conditioning task.*

See the legend of Extended Data Figure 5-1 for a detailed description of a Cumming estimation plot. For valence data (**A**), the unpaired Hedge's *g*: for habituation: –0.039 [95.0% CI, –0.680, 0.568], *p* = 0.896; for acquisition: –0.660 [95% CI, –1.219, 0.048], *p* = 0.0372; for extinction: –0.291 [95% CI, –0.925, 0.354], *p* = 0.3522; and delayed recall: –0.218 [95% CI, –0.832, 0.423], *p* = 0.4848. For arousal data (**B**), the unpaired Hedge's *g*: for habituation: –0.296 [95% CI, –0.914, 0.386], *p* = 0.3372; for acquisition: –0.877 [95% CI, –1.459, 0.302], *p* = 0.0074; for extinction: –0.382 [95% CI, –1.020, 0.273], *p* = .2216, and for delayed recall, –0.142 [95% CI, –0.778, 0.510], *p* = 0.6472. The 5000 bootstrap samples were taken for CI estimation; the CI is bias corrected and accelerated. The two-sided *p* values are the likelihoods of observing the effect sizes, if the null hypothesis of zero difference is true. For each permutation *p* value, the 5000 reshuffles of the group labels were performed.

Extended data Figure 6-2. Unweighted discrimination indices for valence and arousal ratings.
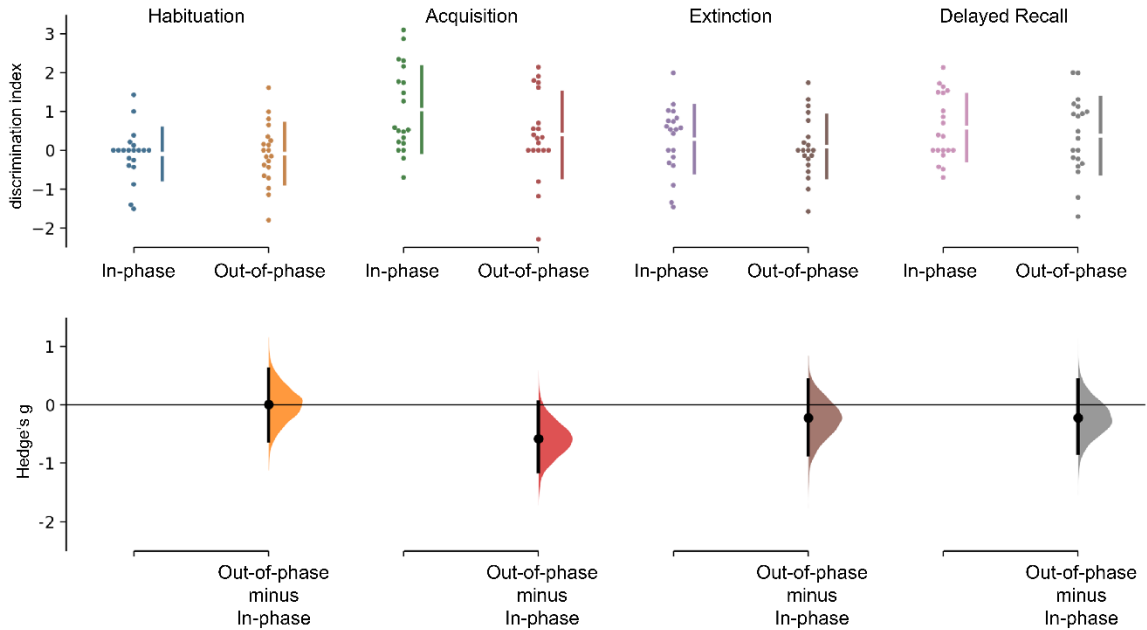
(A) Valence ratings
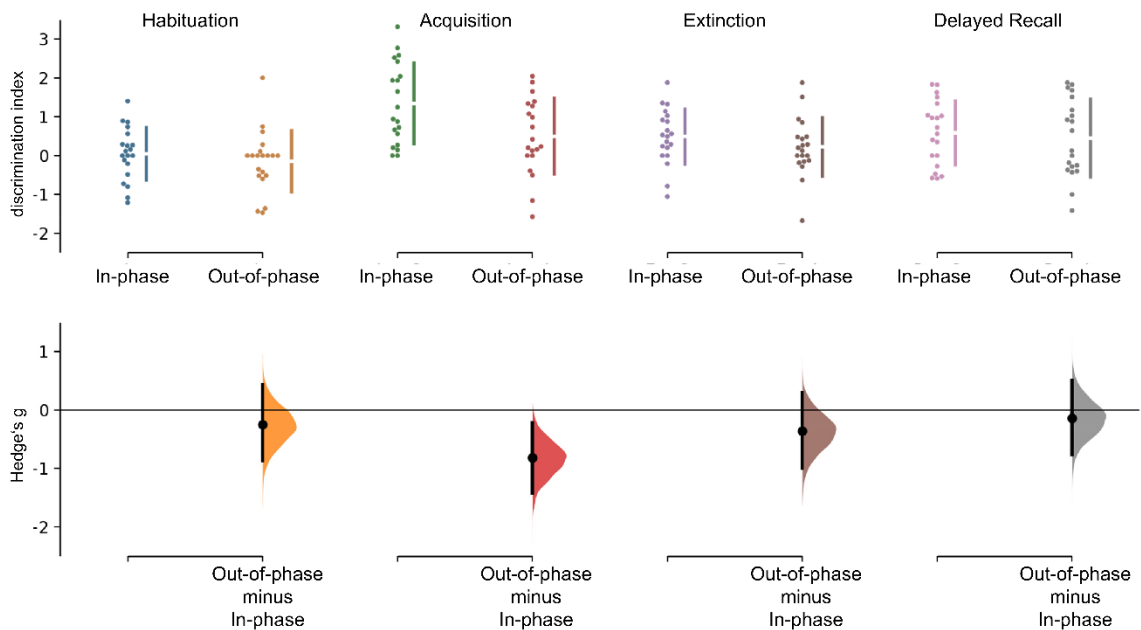
(B) Arousal ratings

Figure 6-2. *A*, *B*, Unweighted discrimination indices for valence (*A*) and arousal (*B*) ratings. Ratings were *z*-transformed within each participant using the mean and SD of all valence and arousal ratings of a participant, respectively. The unweighted discrimination index shown is the difference between ratings of the CS$^+$ orientation and the unweighted average of the four CS$^-$ orientations. Data and effect sizes are shown as a Cumming estimation plot (http://www.estimationstats.com). See the legend of Extended Data Figure 5-1 for a detailed description of a Cumming estimation plot. For valence data (*A*), the unpaired Hedge's *g*: for habituation: 0.011 [95% CI, –0.622, 0.618], *p* = 0.9678; for acquisition, –0.578 [95% CI, –1.153, 0.047], *p* = 0.07; for extinction: –0.220 [95% CI, –0.864, 0.423], *p* = 0.488; for delayed recall: –0.218 [95% CI, –0.826, 0.422], *p* = 0.485. For

arousal data (**B**), the unpaired Hedge's g: for habituation: –0.255 [95% CI, –0.866, 0.439], $p = 0.407$; for acquisition: –0.820 [95% CI, –1.424, –0.225], $p = 0.0128$; for extinction: –0.361 [95% CI, –1.001, 0.295], $p = 0.2466$; for delayed recall: –0.141 [95% CI, –0.774, 0.503], $p = 0.6512$. The 5000 bootstrap samples were taken for CI estimation; the CI is bias corrected and accelerated. The two-sided p values are the likelihoods of observing the effect sizes, if the null hypothesis of zero difference is true. For each permutation p value, 5000 reshuffles of the group labels were performed.

Extended data Figure 7-1. Single-trial data of skin conductance responses (SCRs) without smoothing over trials.

(A) In-phase group: 0° phase offset
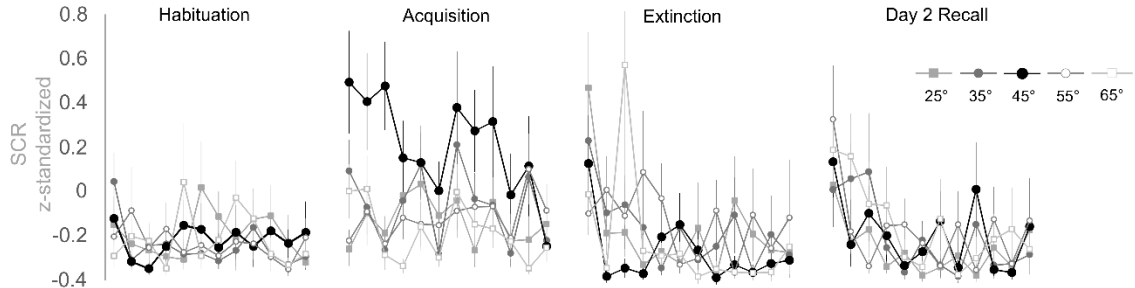
(B) Out-of-phase group: 90°, 180°, 270° phase offset
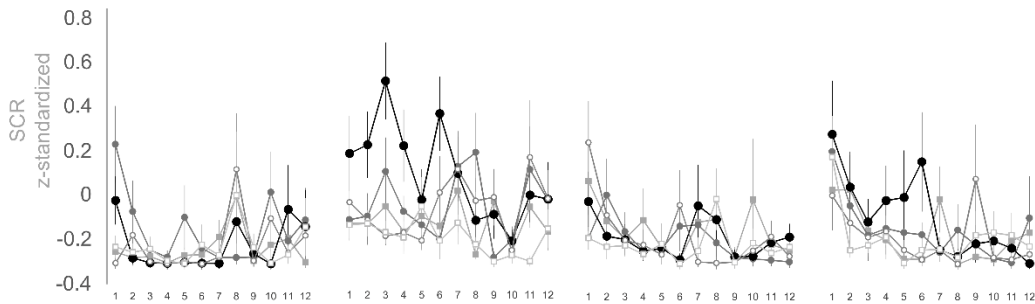
Figure 7-1. Single-trial data of SCRs without smoothing over trials. Same data as in Figure 7, *A* and *B*, plotted without the moving average over trials. SCRs are separated by learning phase (habituation, acquisition, extinction on day 1, and delayed recall on day 2) and by the synchronization condition into the in-phase group (i.e., 0° phase offset; *A*) and the out-of-phase group (i.e., 90°, 180°, and 270° phase offset; *B*). Error bars show ± 1 SEM.

Extended data Figure 7-2. Weighted discrimination indices for averaged skin conductance responses (SCRs).
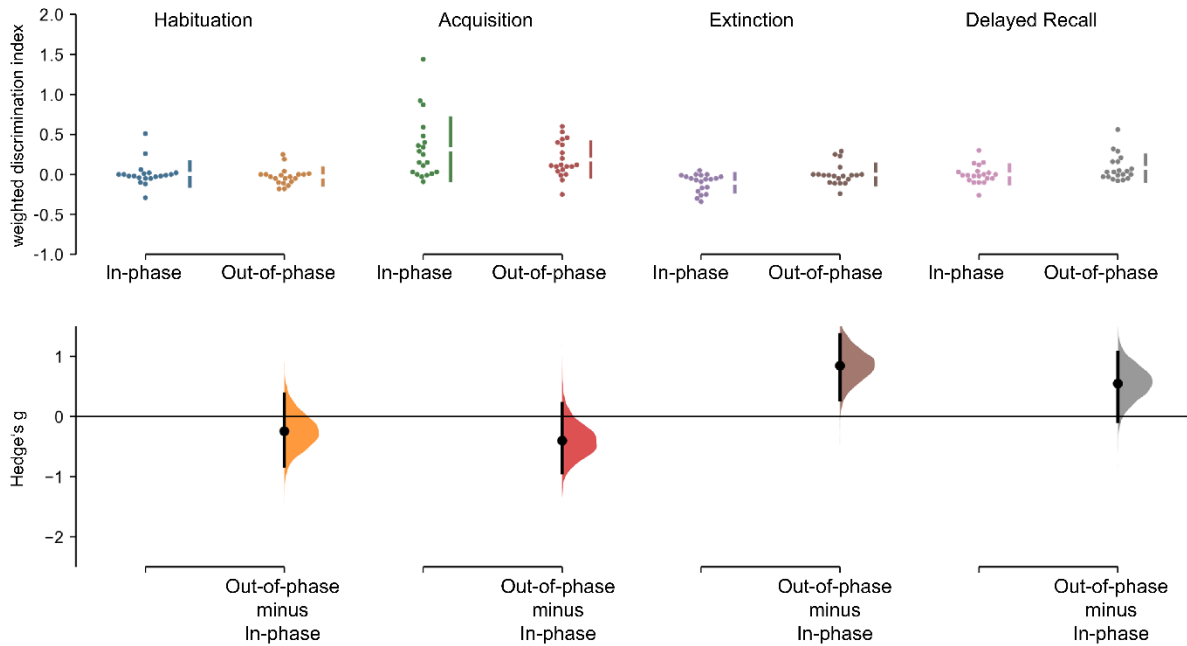
Figure 7-2. Weighted discrimination indices for averaged for averaged SCRs. SCRs were first *z*-transformed within each participant using the means and SDs over CS and US responses of all learning phases (habituation, acquisition, extinction, delayed recall). With the *z*-transformed data, we computed a weighted discrimination index per learning phase as the difference between the reinforced 45° (CS$^+$) grating and the weighted average of the four CS$^-$ gratings. Weights for the CS$^-$ orientations correspond to the angular difference in orientation between the four CS$^-$ orientations (25°, 35°, 55°, 65°) and the CS$^+$ orientation (45°): the two more similar CS$^-$ orientations (±10° to the CS$^+$) were weighted with 0.33[…], while the more dissimilar orientations (±20° to the CS$^+$) were weighted with 0.166[…]. Data and effect sizes are shown as a Cumming estimation plot (http://www.estimationstats.com). See Extended Data Figure 5-1 legend for a detailed plot description. The unpaired Hedge's *g*: for habituation: –0.249 [95% CI, –0.827, 0.371], *p* = 0.451; for acquisition: –0.405 [95% CI, –0.938, 0.211], *p* = 0.2044; for extinction: 0.847 [95% CI, 0.277, 1.361], *p* = 0.0096; for delayed recall: 0.535 [95% CI, –0.091, 1.056], *p* = 0.0916.

Extended data Figure 7-3. Unweighted discrimination indices for averaged skin conductance responses (SCRs).
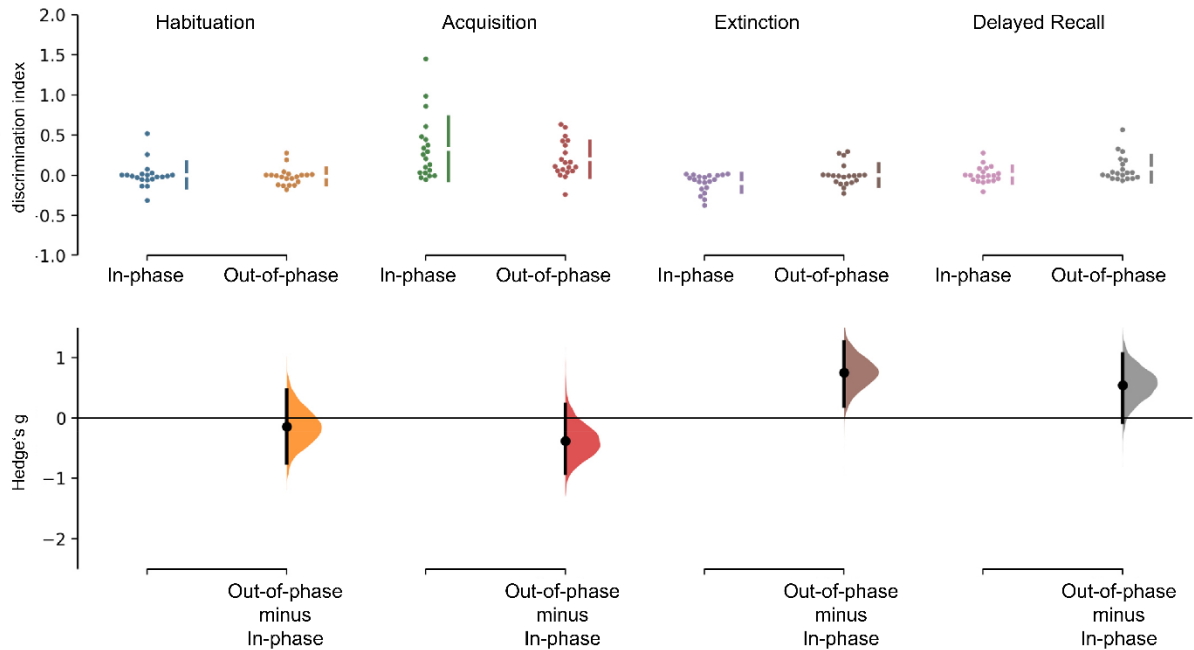
Figure 7-3. Unweighted discrimination indices for averaged SCRs. SCRs were *z*-transformed within each participant using the means and SD over CS and US responses of all learning phases (habituation, acquisition, extinction, delayed recall). The unweighted discrimination index shown is the difference between SCR to the CS$^+$ and the unweighted average of the four CS$^-$ orientations. Data and effect sizes are shown as a Cumming estimation plot (http://www.estimationstats.com). See Extended Data Figure 5-1 legend for a detailed plot description. The unpaired Hedge's *g*: for habituation: –0.146 [95% CI, –0.754, 0.461], *p* = 0.6618; for acquisition: –0.385 [95% CI, –0.920, 0.230], *p* = 0.2296; for extinction: 0.754 [95% CI, 0.197, 1.259], *p* = 0.0212; for delayed recall: 0.549 [95% CI, –0.071, 1.059], *p* = 0.0848. The 5000 bootstrap samples were taken for CI estimation; the CI is bias corrected and accelerated. The two-sided *p* values are the likelihoods of observing the effect sizes if the null hypothesis of zero difference is true. For each permutation *p* value, 5000 reshuffles of the group labels were performed.

Extended data Figure 8-1. Single-trial power of the 4 Hz steady-state visually evoked potentials (ssVEPs) without smoothing over trials.

(A) In-phase group: 0° phase offset

(B) Out-of-phase group: 90°, 180°, 270° phase offset
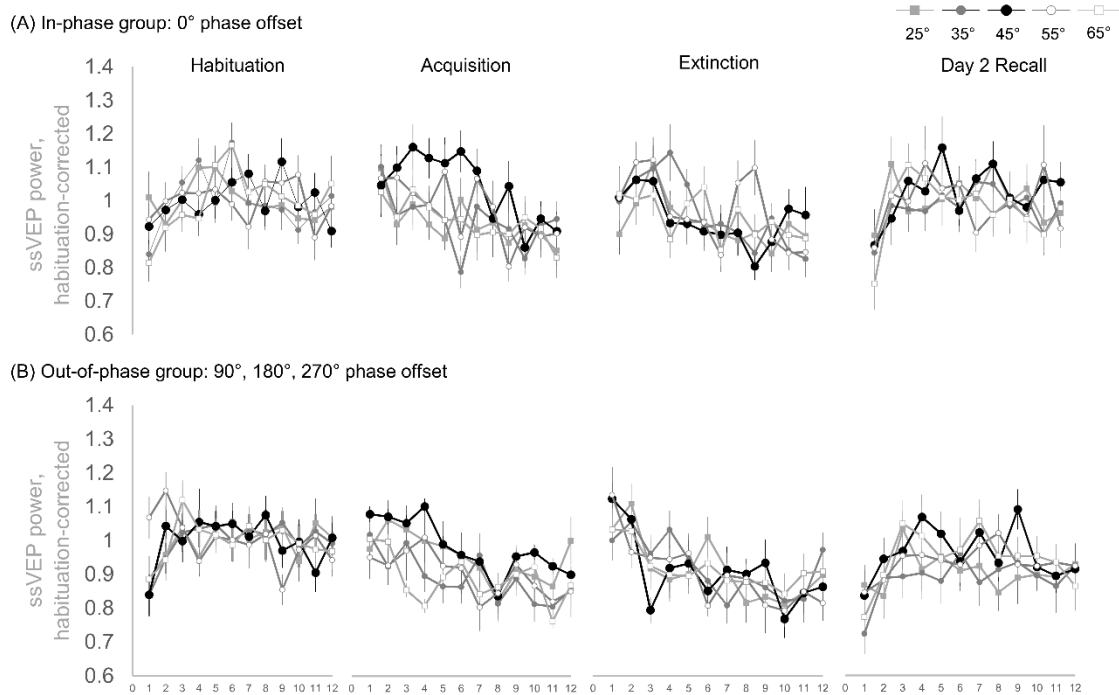
Figure 8-1. Single-trial power of the 4 Hz ssVEPs without smoothing over trials. Same data as in Figure 8, *A* and *B*, plotted without the moving average over trials. Single trials are separated by learning phase (habituation, acquisition, extinction on day 1, and delayed recall on day 2) and by the synchronization condition into the in-phase group (i.e., 0° phase offset; *A*) and the out-of-phase group (i.e., 90°, 180°, 270° phase offset; *B*). Error bars show ±1 SEM.

Extended Data Figure 8-2. Weighted discrimination indices for ssVEPs.
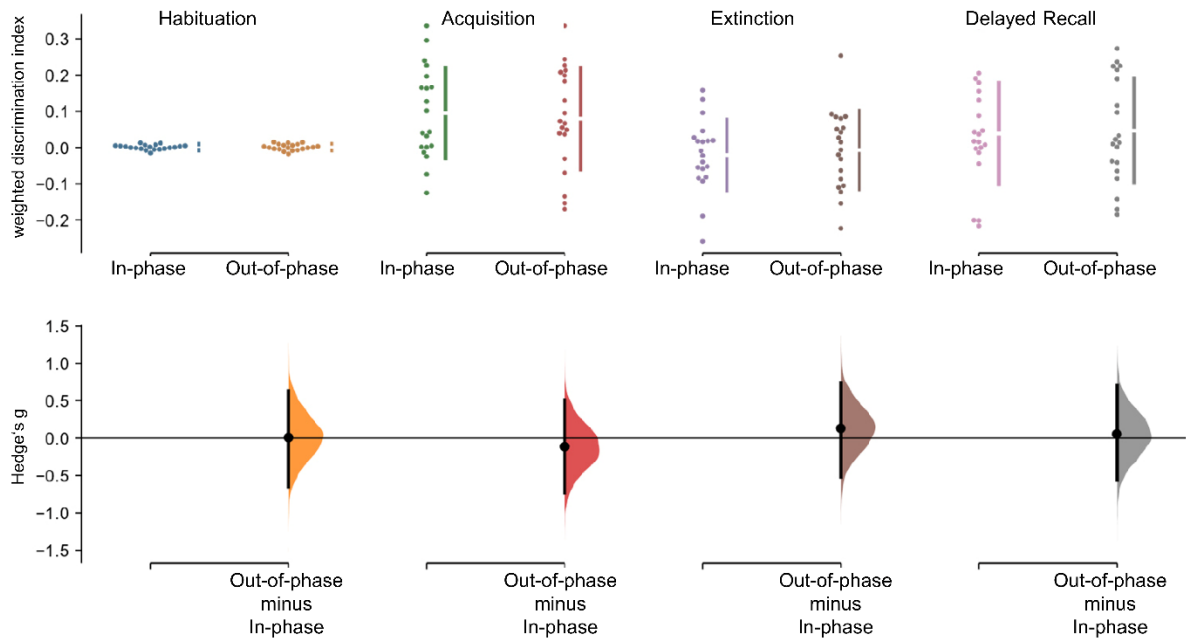
Figure 8-2. Weighted discrimination indices for ssVEPs. Within each learning phase, using the habituation corrected SNR at 4 Hz (Fig. 8C), we computed a weighted discrimination index per learning phase as the difference between the reinforced 45° (CS^+) grating and the weighted average of the four CS^- gratings. Weights for the CS^- correspond to the angular difference in orientation among the four CS^- orientations (25°, 35°, 55°, 65°) and the CS^+ orientation (45°): the two more similar CS^- orientation (±10° to the CS^+) were weighted with 0.33[…], while the more dissimilar orientations (±20° to the CS^+) were weighted with 0.166[…]. Data and effect sizes are shown as a Cumming estimation plot (http://www.estimationstats.com). See Extended Data Figure 5-1 legend for a detailed plot description. The unpaired Hedge's g: for habituation: 0.008 [95% CI, –0.652, 0.633], $p = 0.979$; for acquisition: –0.114 [95% CI, –0.731, 0.511], $p = 0.7084$; for extinction: 0.130 [95% CI, –0.519, 0.741], $p = 0.683$; for delayed recall: 0.054 [95% CI, –0.564, 0.702], $p = 0.08622$. The 5000 bootstrap samples were taken for CI estimation; the CI is bias corrected and accelerated. The two-sided p values are the likelihoods of observing the effect sizes if the null hypothesis of zero difference is true. For each permutation p value, 5000 reshuffles of the group labels were performed.

Extended Data Figure 8-3. Unweighted discrimination indices for ssVEPs.
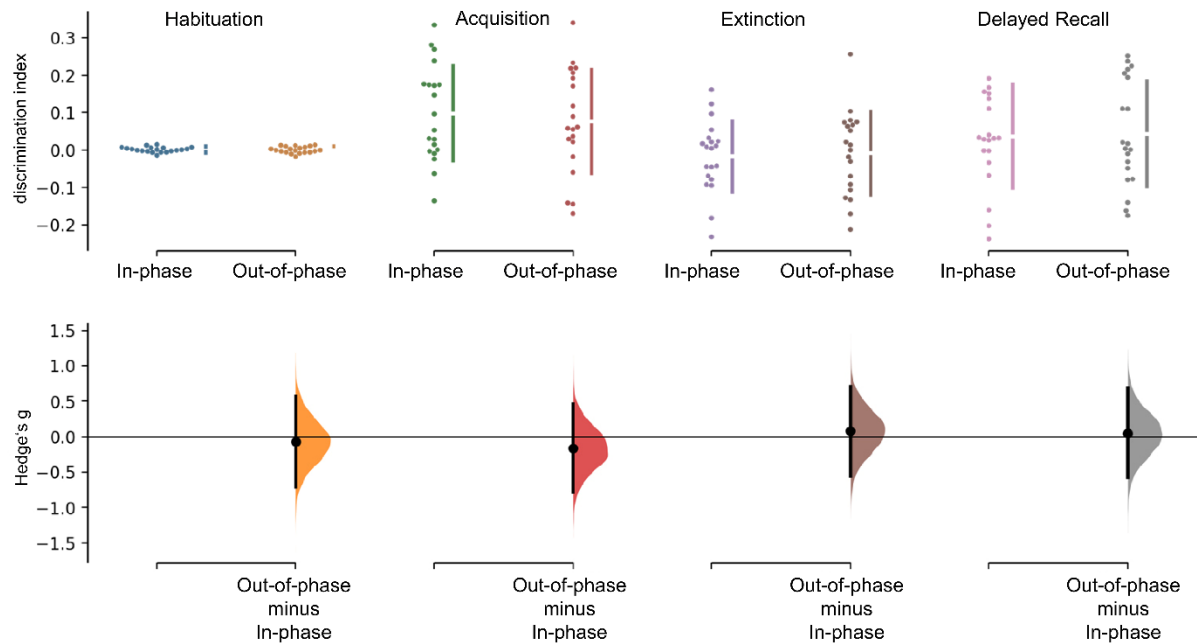
Figure 8-3. Unweighted discrimination indices for ssVEPs. Here, the discrimination index was computed as the difference between the reinforced 45° orientation (CS^+) grating and the unweighted average of the four CS^- orientations. Data and effect sizes are shown as a Cumming estimation plot (http://www.estimationstats.com). See Extended Data Figure 5-1 legend for a detailed plot description. The unpaired Hedge's g: for habituation: –0.074 [95% CI, –0.708, 0.569], $p = 0.8106$; for acquisition: –0.161 [95% CI, –0.774, 0.464], $p = 0.6074$; for extinction: 0.080 [95% CI, –0.561, 0.706], $p = 0.7948$; for delayed recall: 0.044 [95% CI, –0.579, 0.687], $p = 0.891$. The 5000 bootstrap samples were taken for CI estimation; the CI is bias corrected and accelerated. The two-sided p values are the likelihoods of observing the effect sizes, if the null hypothesis of zero difference is true. For each permutation p value, 5000 reshuffles of the group labels were performed.

4.3   Effects of phase synchronization and frequency specificity in the encoding of conditioned fear – a web-based fear conditioning study

Abstract

Oscillatory synchronization in the theta-frequency band was found to play a causal role in binding information of different modalities in declarative memory. Moreover, there is first evidence from a laboratory study that theta-synchronized (vs. asynchronized) multimodal input in a classical fear conditioning paradigm resulted in better discrimination of a threat-associated stimulus when compared to perceptually similar stimuli never associated with the aversive unconditioned stimulus (US). Effects manifested in affective ratings and ratings of contingency knowledge. However, theta-specificity was not addressed so far. Thus, in the present pre-registered web-based fear conditioning study, we compared synchronized (vs. asynchronized) input in a theta-frequency band vs. the same synchronization manipulation in a delta frequency. Based on our previous laboratory design, five visual gratings of different orientations (25°, 35°, 45°, 55°, 65°) served as conditioned stimuli (CS) with only one (CS+) paired with the auditory aversive US. Both CS and US were luminance or amplitude modulated, respectively, in a theta (4 Hz) or delta (1.7 Hz) frequency. In both frequencies, CS-US pairings were presented either in-phase (0° phase lag) or out-of-phase (90°, 180°, 270°), resulting in four independent groups (each group $N = 40$). Phase synchronization augmented the discrimination of CSs in CS-US contingency knowledge but did not affect valence and arousal ratings. Interestingly, this effect occurred independent of frequency. In sum, the current study proves the ability to successfully conduct complex generalization fear conditioning in an online setting. Based on this prerequisite, our data supports a causal role of phase synchronization in the declarative CS-US associations for low frequencies rather than in the specific theta-frequency band.

The full text and online supplementary material of Study 3 can be found at:

https://journals.plos.org/plosone/article?id=10.1371/journal.pone.0281644

Effects of phase synchronization and frequency specificity in the encoding of conditioned fear–a web-based fear conditioning study

Elena Plog 🔘*, **Martin I. Antov** 🔘¤, **Philipp Bierwirth** 🔘, **Ursula Stockhorst**

Experimental Psychology II and Biological Psychology, Institute of Psychology, University of Osnabrück, Osnabrück, Germany

¤ Current address: Developmefigntal Cognitive Psychology, Institute of Psychology, University Regensburg, Regensburg, Germany
* eplog@uni-osnabrueck.de

Abstract

Oscillatory synchronization in the theta-frequency band was found to play a causal role in binding information of different modalities in declarative memory. Moreover, there is first evidence from a laboratory study that theta-synchronized (vs. asynchronized) multimodal input in a classical fear conditioning paradigm resulted in better discrimination of a threat-associated stimulus when compared to perceptually similar stimuli never associated with the aversive unconditioned stimulus (US). Effects manifested in affective ratings and ratings of contingency knowledge. However, theta-specificity was not addressed so far. Thus, in the present pre-registered web-based fear conditioning study, we compared synchronized (vs. asynchronized) input in a theta-frequency band vs. the same synchronization manipulation in a delta frequency. Based on our previous laboratory design, five visual gratings of different orientations (25˚, 35˚, 45˚, 55˚, 65˚) served as conditioned stimuli (CS) with only one (CS +) paired with the auditory aversive US. Both CS and US were luminance or amplitude modulated, respectively, in a theta (4 Hz) or delta (1.7 Hz) frequency. In both frequencies, CS-US pairings were presented either in-phase (0˚ phase lag) or out-of-phase (90˚, 180˚, 270˚), resulting in four independent groups (each group $N = 40$). Phase synchronization augmented the discrimination of CSs in CS-US contingency knowledge but did not affect valence and arousal ratings. Interestingly, this effect occurred independent of frequency. In sum, the current study proves the ability to successfully conduct complex generalization fear conditioning in an online setting. Based on this prerequisite, our data supports a causal role of phase synchronization in the declarative CS-US associations for low frequencies rather than in the specific theta-frequency band.

Introduction

Phase synchronization in the theta band is regarded as an important mechanism for synaptic plasticity and communication between and within brain regions [1, 2]. The assumption is mainly based on work in rodents [e.g., 3, 4] and human EEG-studies [5, 6], showing that theta-phase synchronization increases during encoding and successful retrieval of memory content. Most human studies that examined the role of theta-phase synchronization in memory are correlative in nature with (theta) synchronization as an "epiphenomenal oscillatory signature of memory" [1, p. 1]. Recently, Clouter et al. [7] provided first experimental evidence of a *causal* role of phase synchronization for the formation of episodic associative memory in humans using a simple but elegant non-invasive technique. They applied repetitive rhythmic sensory stimulation in the theta band and concurrently presented visual and auditory stimuli. The theta modulation of stimulus features allows experimental control over phase synchrony of the input. Intriguingly, phase-synchronized compared with asynchronized presentation resulted in an improved memory recall of video-tone pairs [7]. Moreover, this synchronization effect was specific for the theta frequency, whereas it did not occur at an alpha (10.5 Hz) or a delta (1.7 Hz) stimulation frequency. The findings were later replicated and extended [8], making a strong case that phase synchronization in the theta band is causally involved in the formation of multimodal declarative memory traces.

In terms of memory systems, classical fear conditioning is typically considered a separate, non-declarative type of memory with different neural correlates rooted in the brain's defensive system [9–11]. Yet, classical conditioning typically also relies on multimodal associations between a neutral stimulus (conditioned stimulus, CS) in one modality (e.g., a visual stimulus) and an aversive, unconditioned stimulus (US) processed by a different sensory system (e.g., the nociceptive in case of an electric shock, or the auditory in case of an aversive tone). It is well established that during fear conditioning, the sensory information from the CS and US converges in the lateral amygdala [LA, 12–14]. Here, activating the weaker CS synapses and strong US synapses in close temporal proximity is crucial to initiate a strengthening of the weak CS synapse, enabling the CS to elicit a fear response by itself [9, 12]. Common oscillatory mechanisms (including synchronization in the theta band) may be shared across different memory systems of the brain [15]. While various studies in animals and humans show the importance of synchronization in the theta band during different stages of fear acquisition and extinction [16–19], its causal role in forming CS-US associations was unknown. To close this gap and focus on the causal role of theta synchronization in fear conditioning, we extended earlier findings in declarative memory [7, 8], applying repetitive rhythmic sensory stimulation to classical fear conditioning in humans [20]. We investigated the effects of theta-phase synchronized vs. asynchronized CS-US input on fear acquisition in a CS-generalization paradigm. In a 2-day lab-based fear conditioning paradigm, we modulated the luminance of five visual CSs and the amplitude of the aversive auditory US sinusoidally at 4 Hz. During acquisition, we then presented the overlapping CS+US in two independent groups of participants either with a phase shift of 0˚ (i.e., synchronized) or with a phase lag of 90˚, 180˚, and 270˚ (i.e., asynchronously). Intriguingly, the effects of theta-phase synchronization varied with different fear measures. Synchronized (as compared to asynchronized) presentation augmented contingency knowledge (US-expectancy) and affective evaluation, both assessed via ratings. However, it did not amplify conditioned responding in physiological arousal and visuocortical engagement. This suggests that the applied stimulation technique is better suited for declarative-like measures of a human (fear) conditioning task.

Although the previous studies [7, 8, 20] deliver initial evidence for phase synchronization as a shared mechanism across declarative and fear conditioning tasks, it remains to be examined

91

if the phase-synchronization effect in fear conditioning is specific to the theta band. The current study was designed to address this question. In accordance with Clouter et al. [7], here, we examined frequency specificity by contrasting the effects of synchronization vs. asynchronization not only in the theta but also in the delta band (1.7 Hz). Although the slow delta-frequency band is also associated with memory processing, it predominantly occurs during slow-wave-sleep, where it is regarded as an important factor for memory consolidation [2, 21] which is not tested within the current study (i.e., we did not assess delayed recall).

An important feature of the present study is its online character: The Covid-19 pandemic forced researchers to adapt to new standards of contact restrictions and hygiene concepts. For that reason, our study is, as far as we know, one of the first to test a web-based fear conditioning paradigm [for other examples: 22, 23]. The choice of an online-format was especially suitable because our laboratory study revealed effects in the rating-based measures only, which are easily assessable online. Thus, we used repetitive presentation of the visual and auditory stimuli in 4 Hz (theta, identical to the laboratory study) and at 1.7 Hz (delta). To confirm our previous findings, our procedure was adopted with maximal similarity to the laboratory study [20].

Nevertheless, as a consequence of the previous findings as well as the web-based approach, we implemented a few adjustments: Since the effects of synchronization were restricted to the ratings on day 1 in the lab-based study, here we only used a 1-day web-based conditioning task (with habituation, fear acquisition, and extinction). Removing day 2 should not interfere with confirming our previous results. A second adjustment concerns the volume of the auditory US that should be aversive enough to elicit conditioned fear. In a web-based study we have no direct access to a participant's hardware at home and cannot measure the actual sound pressure level. Thus, we decided to use an individually adjusted titration procedure to establish a sound volume that is unpleasant but individually tolerated. As classical fear conditioning is a passive task, we added a simple control task (between learning phases) to ensure that (a) participants have not reduced the audio volume, and (b) that participants are still in position in front of the computer screen.

Based on our previous findings [20] and the assumption that phase synchronization is frequency-specific to the theta frequency, we hypothesize that theta-phase synchronization (vs. asynchronization) improves the ability to discriminate between the CS+ and CS- gratings in valence, arousal, as well as US-expectancy ratings, i.e., it determines the width of the generalization across the CS orientations. Thus, for the theta frequency, we expect a narrower generalization (i.e., better discrimination between CS+ and neighboring orientations) after phase synchronization as compared to a broader generalization (i.e., attenuated discrimination between CS+ and most similar CS- gratings) after asynchronous CS-US presentation (orientation x synchronization interaction for customized contrast fits). In contrast, for the delta frequency, we expect a broad generalization for both, in-phase and out-of-phase groups.

In sum, the present study aims at extending the initial knowledge of synchronization in Pavlovian conditioning by examining whether the memory-improving effect is specific for theta-band stimulation and does not occur in the delta band. Due to the Covid-19 pandemic, we transferred our complex fear conditioning paradigm into a web-based procedure. Thus, the study also aims at providing knowledge of how to implement, control and validate a complex conditioning task in a web-environment. Our results prove a successful implementation of a complex generalization fear conditioning protocol in a web-based approach that is sensitive to fear acquisition and extinction. However, synchronization affected CS-US contingency knowledge in both theta and delta frequency, suggesting that low frequency (theta and delta) rather than theta-specific entrainment supports the (predominantly declarative) memory of CS-US contingency.

92

Materials and methods

Preregistration

The study was submitted to OSF as "Plog, E., Antov, M. I., Bierwirth, P., & Stockhorst, U. (2021, September 12). Effects of phase synchronization and frequency specificity in the encoding of fear—an online study. The preregistration is publicly available at osf.io/bgq9z". For the dataset including raw and z-transformed rating values see **S1 Dataset**.

Participants

Based on our laboratory experiment, the sample size was determined, using *Superpower* in the online shiny app (https://arcstats.io/shiny/anova-exact/ and https://arcstats.io/shiny/anova-power/) [24]. The algorithm uses Monte Carlo simulations to estimate power for an ANOVA. It allows power estimation for the specific form of an expected interaction, not merely for any kind of a significant interaction. Predicted effects are given by entering the means and standard deviations (SDs) [24]. To obtain a power of at least 80% with an alpha error of 0.05 for the hypothesized 5 x 2 x 2 interaction, we entered the means (*M*) and a common *SD* of the 5 (CS orientation) x 2 (theta-synchronization) interaction from our previous laboratory study [20] (see **S1 Table** for entered *M* and common *SD*s). For delta, we expected a broad generalization in both, in-phase and out-of-phase groups, similar to the theta out-of-phase group. For the delta-condition we therefore entered the *M* and *SD* from the theta out-of-phase group from our previous study [20] as an estimation for both, in-phase and out-of-phase effects (see **S1 Table**). The power analysis revealed a sample size of 160 participants, i.e., 40 participants in each of the four independent groups (see also section *Experimental design and stimuli*).

All participants were university students between 18 and 35 years. They were recruited via mailing lists of different universities and flyers on the campus of the University of Osnabrück. Female participants were only included if using monophasic oral contraceptives (pill) and were specifically instructed to attend our study between the 6th and 21st day of pill-intake. The screening for inclusion and exclusion criteria was conducted with an online questionnaire via SoSci-Survey (https://www.soscisurvey.de). Only participants that were identified as eligible by the screening received a link to continue to the main experiment hosted on Pavlovia (https://pavlovia.org/). Participants were excluded when suffering from acute or chronic physical and/or psychiatric disorders (e.g., migraine and epilepsy and neurological disorders). Further exclusion criteria encompassed impaired hearing, uncorrected vision deficits, tinnitus, acute medication (e.g., antibiotics, sedatives, antidepressants), drug abuse and an average alcohol consumption exceeding 20 g or 40 g ethanol per day (for women and men, respectively). Additionally, participants were screened for posttraumatic stress disorder (PTSD), using a translated version of the Posttraumatic Stress Diagnostic Scale [25, 26] and excluded if they met the DSM-IV criteria for PTSD. Moreover, technical inclusion criteria were demanded, comprising a laptop or desktop PC with an updated version of Windows 10 or macOS (10.12 or higher), participating via smartphone or tablet led to exclusion. Subjects had to use wired headphones connected to the laptop/PC to avoid possible time lags caused by wireless transmission. We also asked participants to use either Google Chrome, Edge (Windows 10 users), or Safari browsers (Apple users), as those delivered the best timing in our pretests.

Overall, 346 participants started the online screening. Of those, 10 discontinued before finishing the screening, and 54 were excluded due to ineligibility (e.g. migraine, epilepsy, substance abuse) and never started the main experiment. After passing the screening, participants were accepted in consecutive order to start the main experiment. Of those, 38 participants

93

discontinued the study before finishing the main experiment and were excluded from analysis. Additionally, seven participants were excluded due to a technical error.

We balanced the four experimental groups in terms of an equal number of men/women per group, and the trial order (equal number of participants with list A and list B per group). To achieve this, the online data collection assigned each participant that passed the screening to one of 16 subgroups (4 experimental groups x 2 sexes x 2 trial order lists). We needed complete datasets (finished experiment) from 160 participants, that also passed the cut-off criterion of the compliance control task. The check of the compliance criterion, however, was done offline by our team. Moreover, in an online experiment, multiple participants can participate simultaneously. Therefore, we unwillingly collected data from more than 160 participants. Of the 237 participants that finished the full experiment, 55 missed the 50% compliance criterion, and were excluded, leaving a sample of $N = 182$. The software delivers precise time stamps for each participant. As the exact time of participation can be assumed to be independent of any study-related variables, we used these time stamps to exclude those participants that were collected beyond the planned $N = 160$. Chronologically, the last participants in each group exceeding the planned sample size were excluded ($N = 20$ in total; 12 women). Importantly, these final exclusions were based solely on the time stamps provided by the software (i.e., blind to any behavioral data). Thus, the final sample consisted of 80 men, 80 women and 2 non-binary participants (age: $M = 23.49$, $SD = 3.16$). As the number of non-binary participants was insufficient to attend each of the 4 independent groups, the reported data analyses will only include male and female ($N = 160$) participants.

The study was approved by the ethics committee of the University of Osnabrück and conducted in accordance with the Declaration of Helsinki guidelines. Written informed consent was obtained from all participants after their confirmation of full understanding of the procedure. Participants that finished screening and the conditioning procedure received a voucher over 15 EUR. Students of the university of Osnabrück were free to choose between the voucher or 1.5 course credits.

Experimental design and stimuli

The study followed a 5 x 2 x 2 mixed factorial design (per learning phase, see *Conditioning procedure*), with 5 CS as the within-subject factor *orientation*, and the between-subjects factors *synchronization* (in-phase vs. out-of-phase), and *frequency* (theta [4 Hz] vs. delta [1.7 Hz]). Thus, the design had four independent groups *theta (in-phase)*, *theta (out-of-phase)*, *delta (in-phase)*, and *delta (out-of-phase)*.

As visual CS we used five high-contrast, black-and-white Gabor gratings (i.e., sine-wave gratings with a Gaussian envelope, **Fig 1A**) with a low spatial frequency. The five visual CS differed only in orientation (25˚, 35˚, 45˚, 55˚, 65˚) [20]. Each grating was presented in the middle of the screen on a dark grey background for 5 s (habituation and extinction) or 7 s (acquisition). The auditory US was the same 2 s, broadband white noise (20 Hz– 22 kHz, 44100 Bit/s, 16 Bits/sample) used in our previous laboratory study [20]. While US intensity was constant (max. 96.5 dB[A]) in the laboratory study, we now included an individual titration procedure at the beginning of the online study allowing each participant to set up a highly aversive yet tolerable volume of the US (see *Overall Procedure*).

The visual CS and the auditory US were modulated at either 4 Hz (theta group) or 1.7 Hz (delta group). The visual CS were luminance modulated from 0–100% luminance, the auditory US was amplitude modulated (0–100%) by multiplying the signal vector with a 4 Hz or 1.7 Hz sine wave, respectively.
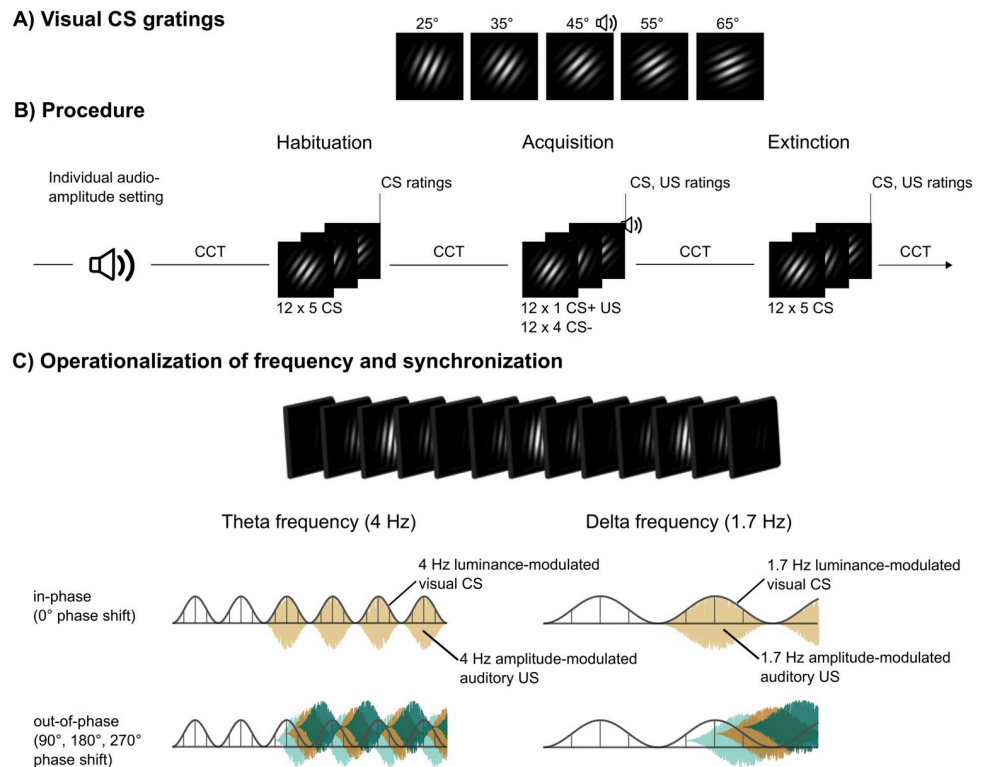
Fig 1. Experimental design. Gabor gratings, conditioning procedure, and the operationalization of in-phase versus the out-of-phase in a theta- (4 Hz) or delta- (1.7 Hz) frequency band. **(A)** For CS, we used Gabor gratings that only differed in orientation by 10˚. The 45˚ orientation served as CS+ and was therefore paired with the US during acquisition. The other four orientations (25˚, 35˚, 55˚, and 65˚) were used as CS- gratings, hence never paired with the US. **(B)** The fear conditioning paradigm comprised the learning phases habituation, acquisition, and extinction. Prior to habituation, participants conducted the individual audio-volume setting (titration) to select an US intensity that is extremely unpleasant but not painful. Within a learning phase, each CS orientation was presented 12 times. Only during acquisition, the US with the individually set intensity was presented together with the CS+ (45˚) orientation. After each learning phase, valence and arousal ratings were conducted for the CS and–after acquisition–the aversive US. US-expectancies were rated after acquisition and extinction. At four time points (before and after habituation, after acquisition, and after extinction) participants conducted the unheralded compliance control task (CCT). **(C)** Operationalization of the in-phase (0˚ phase shift) versus out-of-phase (90˚, 180˚, 270˚ phase shift) synchronization in a theta- (4 Hz) or delta- (1.7 Hz) frequency band. Each visual CS and auditory US was sinusoidally luminance or amplitude modulated, respectively, at either 4 Hz (theta) or 1.7 Hz (delta). The left column shows phase shifts for the theta band: in-phase, i.e., 0˚ (beige) shift at the top and out-of-phase, i.e., 90˚ (light green), 180˚ (brown), 270˚ (dark green) shift at the bottom. The right column depicts the same phase-shifts for delta.

The auditory white noise was downloaded from random.org (https://www.random.org/audio-noise/) and subsequently amplitude modulated (4 and 1.7 Hz) using a custom Matlab script (version R2021a). In the previous laboratory study [20], the luminance of the gratings was modulated on a frame-by-frame basis. However, the feature to generate grating stimuli in PsychoPy online, was not supported by the time we programmed the experiment. Thus, we wrote an offline python script that created the desired Gabor-Gratings, modulated their luminance with a 1.7 or 4 Hz sine-wave, and created (5–7 s long) video clips to upload and use as CS online. The timing of the auditory US (theta- or delta-modulated audio file) was defined in relation to the start of the video clip at the beginning of a trial. The experimental procedure was created in PsychoPy [27] (version v2021.2.3), uploaded as PsychoJS (java-script code) and hosted by the online platform Pavlovia (http://pavlovia.org).

95

Conditioning procedure

The study comprised the learning phases habituation, fear acquisition, and extinction (**Fig 1B**). Within each learning phase, the 5 CS orientations were presented 12 times each, resulting in a total of 60 CS presentations per learning phase [20]. The auditory US was presented during fear acquisition only. During inter-trial-intervals (ITIs), a white fixation cross, was presented in the center of the screen with intervals varying randomly between 4.5 s and 6.5 s. The duration of each CS differed between learning phases: During habituation and extinction, each CS was presented for 5 s. Within acquisition, the 7-s long, 45° CS grating (CS+) co-terminated with the aversive auditory US in the last 2 s of CS presentation. To ensure perceptual comparability between the gratings, the duration of all 5 CS gratings (CS+ and CS-) in acquisition were extended by 2 s, leading to a 7-s duration. As in the previous laboratory study, we selected the 45° orientation as CS+ for all subjects to provide the intended generalization design with symmetrically distributed CS- gratings around the CS+. Previous studies did not reveal systematic differences between CS orientations prior to acquisition and also showed successful conditioning across orientations [28, 29].

In all four experimental groups, the 2-s US overlapped with the last 2 s of the 7 s visual CS+ during acquisition. Participants in the theta and delta *in-phase groups* received 12 trials of CS+ US pairing where the oscillating visual CS+ and auditory US had a 0° phase shift. Participants in the theta and delta *out-of-phase groups* also received 12 trials of CS+ US pairings. However, for these 12 trials, each participant in the out-of-phase group received 4 CS+ US pairings with a phase-shift of 90°, four trials with a phase shift of 180°, and 4 trials with a phase-shift of 270° (pseudorandom order). In all 4 groups, we also accounted for the fact, that the transduction of auditory signals is faster compared to visual signals. Therefore, we added a fixed lag of 40 ms to the onset of the auditory US (for details, see [7, 8, 20]).

The sequence of the five CS gratings in each learning phase followed one of two trial orders that were counterbalanced within groups. These orders (trial lists) were created in a pseudorandomized way, with the only restriction of allowing no more than two consecutive gratings of the same orientation. Within acquisition, both trial lists started with a so-called booster session, i.e., a CS+US pairing occurred in five of the first seven trials [cf. 20, 28, 30].

Dependent variables

Due to the online restrictions and to replicate the main findings of the laboratory study [20], we assessed US-expectancy, valence, and arousal ratings, but not physiological arousal (measured via skin conductance responses) and visuocortical engagement (measured via steady-state visually evoked potentials). We adapted the 9-point Self-Assessment Manikin [SAM, 31] to an online version within PsychoPy to assess the valence and arousal ratings.

After habituation, acquisition, and extinction, participants were asked to evaluate each of the differently oriented gratings for its valence (from unpleasant 1 to pleasant 9) and arousal (from calm 1 to arousing 9). In addition, US-expectancy was assessed after acquisition and after extinction: Participants were asked to rate the likelihood that a US will follow each of the 5 CS gratings on a scale from -5 (certainly no US) over 0 (uncertain) to 5 (certainly US).

Overall procedure

The study consisted of two consecutive parts: 1) a screening and 2) the conditioning session. As described in the section *Conditioning procedure*, conditioning comprised the learning phases habituation, acquisition, and extinction that were separated by the valence, arousal, and US-expectancy ratings, resting periods, as well as the compliance control tasks (**Fig 1B**). Each

learning phase took 10 to 13 minutes, depending on the ITI (between 4.5 and 6.5 s) and the duration of CS stimuli that was extended for acquisition.

Screening

The screening (presented via https://www.soscisurvey.de/) included a description of the general procedure (participant information), checked the relevant inclusion and exclusion criteria (e.g., physical and psychological health, technical requirements, via self-report questionnaires), and obtained informed consent. At the end of the screening, eligible participants underwent the individual titration of US intensity (described below). Participants were instructed to set their laptop/desktop PC audio to the maximum volume (100%) and were automatically redirected to the conditioning procedure. The average duration for completing the screening and conditioning part was 1 hour and 5 minutes (SD = 32 minutes).

US-intensity titration

Prior to the habituation phase, participants were instructed to individually adjust the volume of a test stimulus (a low-amplitude, frequency-modulated white noise US, same frequency composition as the final US) to a level that is aversive but not painful, using a clickable controller. In a second step, the previously adjusted level was rated on a 10-point Likert scale from 0 (not unpleasant at all) to 10 (extremely unpleasant). A rating of 7 or higher finished the evaluation and saved the volume setting for the US. If the tone unpleasantness was rated less than 7, the volume was increased in small steps until it reached an unpleasantness rating of 7 or higher (M = 8.52).

Instructions

In the beginning of each learning phase, participants were instructed to sit comfortably and avoid any movement (except blinking) for the duration of the stimulus presentation. We also kindly instructed them to dim the room, if possible, to provide the best vision of the dark gratings. Participants were informed that a fixation cross will be presented in the center of the screen, followed by a frequency-modulated black and white grating that differed in orientation. In the resting periods between the learning phases, participants were encouraged to relax their eyes, without leaving the position in front of their laptop/PC. Before acquisition, we instructed the participants that during the next phase, a loud, pulsating noise will follow one of the gratings, without specifying which of the five gratings. Prior to extinction, we did not specifically inform them that the US will never follow the CS+ anymore.

Compliance control task

Compliance control was conducted to evaluate the participants' visual and auditory perception and thus their attention towards the experiment. At four time points throughout the experiment, a random number (between 1 and 4) of low volume auditory beeps were presented monoaurally either to the left or the right ear. After the presentation, participants were asked to identify (instructions on the screen) 1) how many beeps they had just heard and 2) on which ear they had received the tone (left or right ear). The compliance control task had several aims: 1) Playing the beep sounds at a low-volume (1/4 of the previously chosen "aversive" setting) provided a control for an adequate US-intensity titration of each participant. If participants muted their audio, chose a low volume at the individual setting in the beginning, or lowered their device volume during the task, they would be unable to hear the beep at all, and miss our criteria for successful participation. 2) Playing the beeps sounds without prior notice and

97

Table 1. Distribution of errors in the compliance control task[1].

Errors in *Number of beeps*	Participants	Errors in *Monoaural presentation side*	Participants
0	132	0	2
1	30	1	156
2	35	2	22
3	18	3	36
4	2	4	1

[1]Of note, error distributions were conducted including the two non-binary participants.

presenting the questions (concerning number of right or left direction) written on the screen ensured that participants kept sitting in front of the screen during the experiment. 3) The use of monoaural beeps ensured that participants wear headphones, as instructed, and additionally, wear them correctly on/in both ears. Our a priori-defined compliance criterion allowed a maximum of 2 out of 4 errors in both, the question about the number of presented beeps as well as the question about the side of beep occurrence (i.e., a minimum of 50% in each of the two questions). The distribution of errors is listed in **Table 1**.

Realizing the online set up

As described earlier, for the screening session we used the online platform SoSciSurvey. The main part of the study was programmed in Psychopy [27] and hosted by Pavlovia (http://pavlovia.org). We received payed support from the consultancy team of PsychoPy (https://psychopy.org/consultancy.html) on some specific programming issues. In order to anonymously identify each participant between both platforms, a pseudonymized ID was generated during the initial screening part in SoSciSurvey. In case of eligibility, participants were redirected to the main study with a URL that included the pseudonymized ID. To randomly assign each participant to one of the groups, we used the VESPR (Vertical Enhancement of Statistics and Psychological Research) study portal [32]. Due to a minor error that prevented the correct counterbalancing across the groups defined by synchronization, frequency, and trial lists, we switched to an assignment within PsychoPy for the last 69 participants of our sample. However, VESPR was used for all participants to guarantee the equal distribution of men and women. At the end of the experiment, the ID was displayed on the screen. Participants were instructed to send us an email, that included the ID and the selected compensation (voucher or course credits). After confirming the correctness of the ID, we compensated them with the voucher or course credits.

Statistical analysis

For each outcome measure (US-expectancy ratings, valence and arousal ratings) and learning phase (habituation, acquisition, extinction) we performed a repeated-measures mixed ANOVA including the within-subject factor *orientation* (25˚, 35˚, 45˚, 55˚, 65˚) and the between-subject-factors *synchronization* (in-phase vs. out-of-phase) and *frequency* (theta vs. delta). Of note, we will report Greenhouse-Geisser corrected values. The significance level was set to $p < .05$.

Before looking for effects of phase synchronization in the theta- or delta- frequency band, one major prerequisite concerns the ability to induce fear conditioning in a web-based study. To validate successful fear acquisition and extinction, we analyzed rating patterns across the CS orientation, independent of synchronization and frequency conditions. To account for the

fear generalization paradigm with CS- gratings symmetrically distributed around the CS+ grat-
ing, we utilized customized contrast weights. Over all groups (i.e., independent of factors fre-
quency and synchronization), we used generalization weights (-0.529, 0.247, 0.564, 0.247,
-0.529) to validate the successful conditioning with the greatest increase towards the CS+ orien-
tation. Additionally, we included the factor *learning phase (LP)* to examine a possible decrease
in fear responses from acquisition to extinction, validating successful extinction.

To analyze the hypothesized effects within each measure, we first examined the orientation
x synchronization x frequency interaction within the ANOVA described above. Due to unex-
pected pre-conditioning differences in ratings of valence and arousal with a linear decrease or
increase (25˚ to 65˚) with grating orientation, we additionally conducted habituation-correc-
tions within each participant. For this, individual valence and arousal ratings given after acqui-
sition and extinction were divided by the participant's corresponding rating after habituation.
The result was multiplied by 100, leading to a percentage score. The habituation-corrected
valence and arousal ratings are additionally shown in result figures or supporting information
for a better visualization of fear generalization patterns only. The statistics in the result section
are nonetheless based on raw data.

Since the expected effect of phase-synchronized stimulation in the theta but not delta group
could manifest in an altered generalization curve without changing the rating pattern dramati-
cally, ANOVA interactions might not be able to detect pattern differences across CS gratings.
Based on our previous study [20], for the theta-frequency band we expected a narrow generali-
zation (i.e., higher ratings to the CS+ compared with the neighboring CS-) within the in-phase
group and a broad generalization (i.e., high ratings to the CS+ and the neighboring CS-) in the
out-of-phase group. The interaction between synchronization and orientation should there-
fore resemble a "W" or "Mexican hat pattern" (by subtracting a broad generalization from a
narrow generalization; weights: 0.142, -0.489, 0.694, -0.489, and 0.142; [20]) when phase syn-
chronization causes better discrimination between the CS+ and similar CS- gratings (**Fig 2**).
Since we hypothesized the discrimination ability depends on the frequency, we aimed at
directly comparing the theta and delta group. In general, we expected a better discrimination in
the theta compared with the delta group (orientation x frequency x synchronization interaction
for contrast fits). Since we expected that the differences between in-phase and out-of-phase syn-
chronization in the delta-frequency band to be smaller compared with the theta group, we pre-
registered a planned test for another "Mexican hat" contrast fit of the orientation x synchroniza-
tion x frequency interaction. The latter contrast results from subtracting a hypothetical "flat"
contrast (no difference between in-phase and out-of-phase) in the delta group from the "Mexi-
can hat" of the theta group. However, it was not possible to implement custom contrast weights
for the comparison of two individual generalization patterns within the theta and delta group in
SPSS. Therefore, in contrast to our pre-registered analysis, we decided to use the subsequently
described discrimination indices (i.e., CS+ minus averaged CS-), as a similar measure of the dis-
crimination ability, to calculate a 2 x 2 ANOVA, including the factors frequency (theta vs. delta)
and synchronization (in-phase vs. out-of-phase). Differences between in-phase and out-of-
phase in theta but not delta should manifest in a significant frequency x synchronization inter-
action. For a better comparability with our laboratory study, however, we nevertheless calcu-
lated the "Mexican hat" contrast fits for each frequency band separately.

Discrimination indices were calculated by subtracting the mean of all CS- gratings (i.e., 25˚,
35˚, 55˚, 65˚) from the reinforced CS+ (45˚) orientation. Discrimination indices indicate a
simple measure for the preference of CS+ against CS- gratings. For better comparability to our
previous lab study [20], and as pre-registered, we z-transformed the discrimination indices,
using the mean and standard deviation (*SD*) of discrimination indices across learning phases
per participant.

99

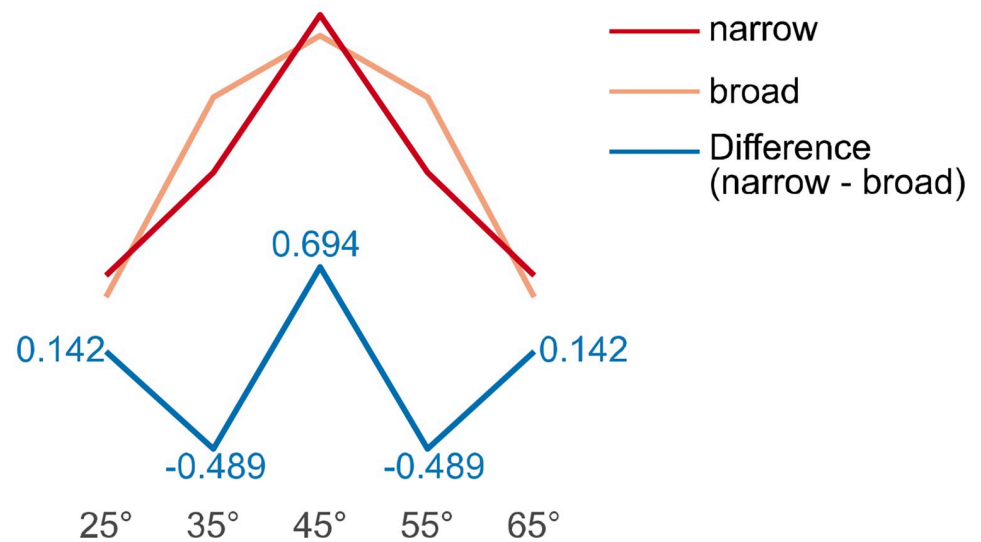## Interaction weights: Discrimination

Fig 2. Contrast weights of Mexican hat for the orientation x synchronization interaction. Contrast weights for the expected discrimination to test the synchronization × orientation interaction in the theta-band. The weights shown for a narrow (red) and broad (orange) generalization pattern are examples that if subtracted (narrow–broad) produce the exact discrimination weights we used for the group × orientation interaction contrast (numbers in black font, 0.142, −0.498, 0.694, −0.498, 0.142; [20]), resembling a *Mexican Hat* (blue line).

https://doi.org/10.1371/journal.pone.0281644.g002

Due to the fact that fear conditioning is subject to well-known sex differences, we conducted post hoc analyses including the factor *sex*. Hence, the 5 x 2 x 2 ANOVA was extended by a third between-subject factor *sex* (men vs. women), resulting in a 5 x 2 x 2 x 2 ANOVA. In case of significant differences including the additional factor, we subsequently conducted the 5 x 2 x 2 ANOVA within each sex. Further, "Mexican hat" contrast fits and discrimination indices were calculated separately for men and women, within the theta and delta frequency groups.

Results

We first describe the fulfilment of the prerequisite (compliance control task) and report the success of fear acquisition and extinction. We then address the main (pre-registered) questions, i.e., rating differences depending on synchronization (in-phase vs. out-of-phase) and frequency band (theta vs. delta). Finally, explorative analyses are reported, including the factor sex. For an overview of all statistics, each statistical value reported in the following is additionally listed in **S2 Table**.

Prerequisites: Compliance control and validation of web-based fear conditioning

Statistical analyses were conducted with data of those participants that passed the compliance control criteria, i.e., at least 50% correct identification of the number of beeps and the side of beep presentation. To check if this criterion helps separating participants that show learning from those that do not, we used the discrimination indices of the participants' ratings (CS + minus averaged CS- ratings) as dependent measures. We compared participants included ($N = 162$ [including 2 non-binary]; final sample comprised 80 men and 80 women, only) to

100

participants excluded due to the compliance control task ($N = 55$). Arousal and valence ratings reflect the affective evaluation of the CS-US association. Thus, we used both measures collected after acquisition in a 2 x 2 ANOVA, with *rating measure* (valence vs. arousal) as a within-subject factor and *compliance* (passed compliance control: yes vs. no) as the between-subject factor (valence data were multiplied by -1 to reverse polarity). Analysis showed that participants who passed the compliance task had higher discrimination indices (valence, passed: $M = 0.58$ [$SD = 0.80$]; valence, failed: $M = 0.06$ [$SD = 0.87$]; arousal, passed: $M = 0.60$ [$SD = 0.79$]; arousal, failed: $M = 0.16$ [$SD = 0.73$], compliance main effect $F(1,215) = 16.89$, $p < .001$, $\eta_p^2 = .145$).

Similarly, the z-standardized CS-US contingency knowledge (= US-expectancy), showed a trend-level main effect of compliance ($F(1,215) = 2.78$, $p = .097$, $\eta_p^2 = .013$). However, when analyzing the discrimination index of raw US-expectancy ratings, the effect is even clearer ($F(2,215) = 9.27$, $p = .003$, $\eta_p^2 = .041$). Comparable with the affective ratings, discrimination indices were higher for participants that were included in our final sample (passed: $M = 0.82$ [$SD = 0.95$]; failed: $M = 0.56$ [$SD = 1.04$] for z-values).

Finally, on average, the discrimination indices were positive in the final sample (i.e., larger for the CS+ compared to the average of all CS-) for valence, arousal, and for US-expectancy ratings). This suggests successful acquisition in the web-based fear conditioning task. Further supporting successful acquisition, we found main effects of CS orientation in analysis including all CS orientations for valence ($F(2.7, 414.0) = 111.19$, $p < .001$, $\eta_p^2 = .416$ **Fig 3A** left panel), arousal ($F(2.8, 431.1) = 107.17$, $p < .001$, $\eta_p^2 = .407$, **Fig 3A** right panel) and US-expectancy ($F(2.9, 452.3) = 140.24$, $p < .001$, $\eta_p^2 = .473$, **Fig 3B**). A specific preference for the CS+ orientation, was confirmed by fitting generalization contrasts within all of the three measures (valence: $F(1,156) = 88.80$ $p < .001$, $\eta_p^2 = .363$; arousal: $F(1,156) = 82.13$, $p < .001$, $\eta_p^2 = .345$; US-expectancy: $F(1,156) = 147.78$, $p < .001$; $\eta_p^2 = .486$).

Extinction learning should manifest in decreasing rating intensity after extinction when comparing ratings after acquisition and after extinction. As expected, we found that the general levels of arousal, valence, and the expectation that an US occurs with one of the CS orientations, was significantly reduced after extinction (main effects of *LP* in valence($F(1,156) = 18.65$, $p < .001$, $\eta_p^2 = .107$, arousal ($F(1,156) = 19.80$, $p < .001$, $\eta_p^2 = .113$, **Fig 3A** right panel, and US-expectancy ($F(1,156) = 35.50$, $p < .001$, $\eta_p^2 = .185$, **Fig 3B**).

In sum, our data strongly support that our online setting is suitable to successfully induce fear acquisition and extinction in a complex differential fear conditioning protocol with an auditory US.

OSF-registered hypothesis

US-expectancy ratings. Similar to our previous laboratory study [20], the current data revealed that synchronized input (in-phase groups) causes a narrower generalization of the US-expectancy ratings compared with asynchronized input (out-of-phase groups, main effect synchronization $F(1,156) = 10.17$, $p = .002$, $\eta_p^2 = .061$, **Fig 4**). However, it did not interact with the stimulation frequency (no synchronization x frequency interaction: $F(1,156) = 0.34$, $p = .560$, $\eta_p^2 = .002$, and no orientation x synchronization x frequency interaction: $F(2.9,452.3) = 0.27$, $p = .838$, $\eta_p^2 = .002$). Thus, contrary to our predictions, we did not find the expected theta-specific effect of synchronous CS+US presentation, also evident when comparing the discrimination indices (CS+ minus the mean of the CS- gratings) in dependence of synchronization and frequency (synchronization x frequency interaction for discrimination indices: $F(1,156) = 0.42$, $p = .518$, $\eta_p^2 = .003$). Accordingly, we did not find the Mexican hat contrast fit for the
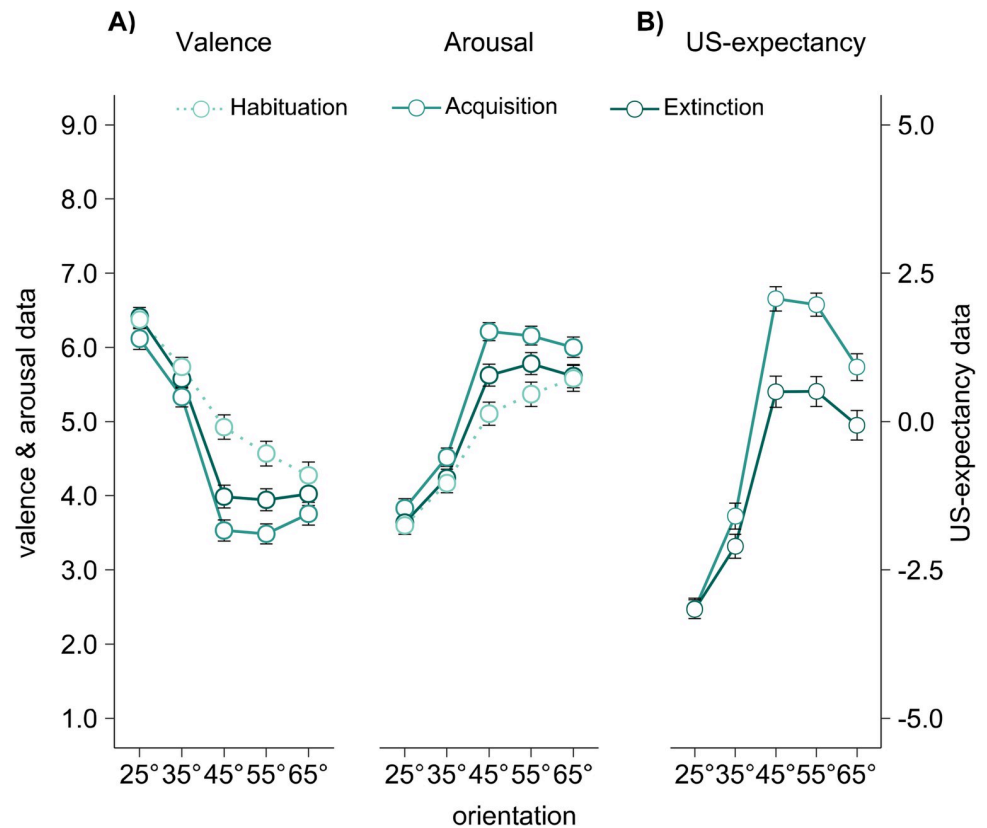
Fig 3. Validation of fear acquisition and extinction. Validation of fear acquisition and extinction for valence and arousal ratings **(A)** and US-expectancy ratings **(B)**. Valence of each CS grating was rated via Self-Assessment Manikins (SAM) on a 9-point scale from 1 (unpleasant) to 9 (pleasant). Similarly, arousal ratings were conducted via SAMs, here ranging from 1 (calm) to 9 (arousing) (see also *Materials and Methods section [Dependent variables]*). US expectancies after acquisition and extinction were rated on a scale from -5 (very certain, no US after this CS) over 0 (uncertain) to 5 (very certain, a US will follow this CS). Each data point represents averaged valence, arousal, or US-expectancy ratings, separately for acquisition and extinction but not differentiated for synchronization and frequency. Error bars show ±1 SEM.

synchronization x orientation interaction when separately analyzing within the theta frequency group ($F(1,78) = 0.40$, $p = .528$, $\eta_p^2 = .005$) and delta frequency group ($F(1,78) = 1.35$, $p = .249$, $\eta_p^2 = .005$), respectively.

Valence and arousal ratings

Valence ratings confirm a successful learning of CS-US pairings, with the most negative valence ratings towards the 45˚ (CS+) orientation (see *Prerequisites*). However, we did not find the expected difference between in-phase and out-of-phase presentation, when accounting for the theta and delta frequency (orientation x synchronization x frequency interaction: $F(2.6,414.0) = 0.39$, $p = .738$, $\eta_p^2 = .002$, **Fig 5A**). Accordingly, discrimination indices did not differ between synchronization and frequency conditions (synchronization x frequency interaction: $F(1,156) = 0.07$, $p = .798$, $\eta_p^2 = .000$) and there was no fit of Mexican hat contrast weights analyzed for theta ($F(1,78) = 1.36$, $p = .247$, $\eta_p^2 = .017$) or delta frequency ($F(1,78) = 0.05$, $p = .827$, $\eta_p^2 = .001$, **Fig 5A**), separately.

As already shown, arousal data after acquisition show successful conditioning, with highest arousal ratings towards the CS+ (see results of *validation*). However, we did not find the
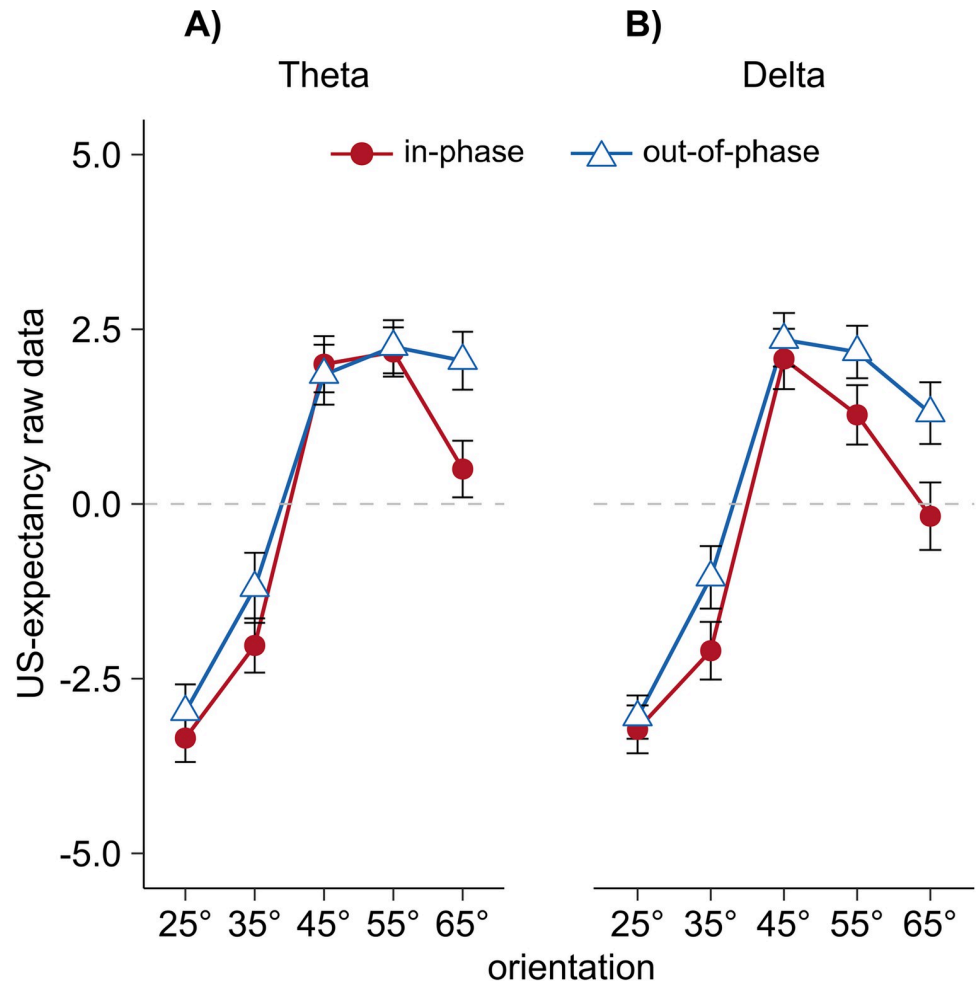
Fig 4. Raw US-expectancy data. Raw US-expectancy ratings separated for frequency (theta vs. delta) and synchronization condition (in-phase vs. out-of-phase). US-expectancies were collected as described in caption of **Fig 3** and the *Materials and Methods section (Dependent variables)*. Each data point represents mean US-expectancy ratings for each CS orientation over participants, separately for frequency and synchronization condition. Error bars show ±1 SEM. **S1 and S2 Figs** shows discrimination indices (CS+ minus the average of all CS-) and estimation statistics for z-transformed US-expectancy ratings. Discrimination indices were calculated for the comparison of in-phase vs. out-of-phase across frequency as well as separately for theta and delta frequency. The estimation plots in **S1 and S2 Figs** depict the estimation statistics including the individual values as well as effect sizes (Hedge's g) as a bootstrap confidence interval (5000 samples [33]). **S1 Fig** shows the comparison of both synchronization conditions across the mean of theta and delta frequency, **S2 Fig** presents the comparison between in-phase and out-of-phase synchronization within each frequency (theta vs. delta).

https://doi.org/10.1371/journal.pone.0281644.g004

expected orientation x synchronization x frequency interaction ($F(2.8,431.1) = 0.14$, $p = .924$, $\eta_p^2 = .001$, **Fig 5B**) and additionally no significant synchronization x frequency interaction in the discrimination indices ($F(1,156) = 0.14$, $p = .710$, $\eta_p^2 = .001$. This also became evident in a non-significant contrast fit of Mexican hat when comparing synchronization effects in theta ($F(1,78) = 0.77$, $p = .384$, $\eta_p^2 = .010$) or delta frequency ($F(1,78) = 0.55$, $p = .463$, $\eta_p^2 = .007$; **Fig 5B**).

In accordance with the ANOVA, estimation statistics of the comparison between in-phase and out-of-phase groups (calculated by subtracting the mean CS- from the CS+ orientation) did not reveal significant differences for valence (**S3 Fig**) and arousal ratings (**S4 Fig**).

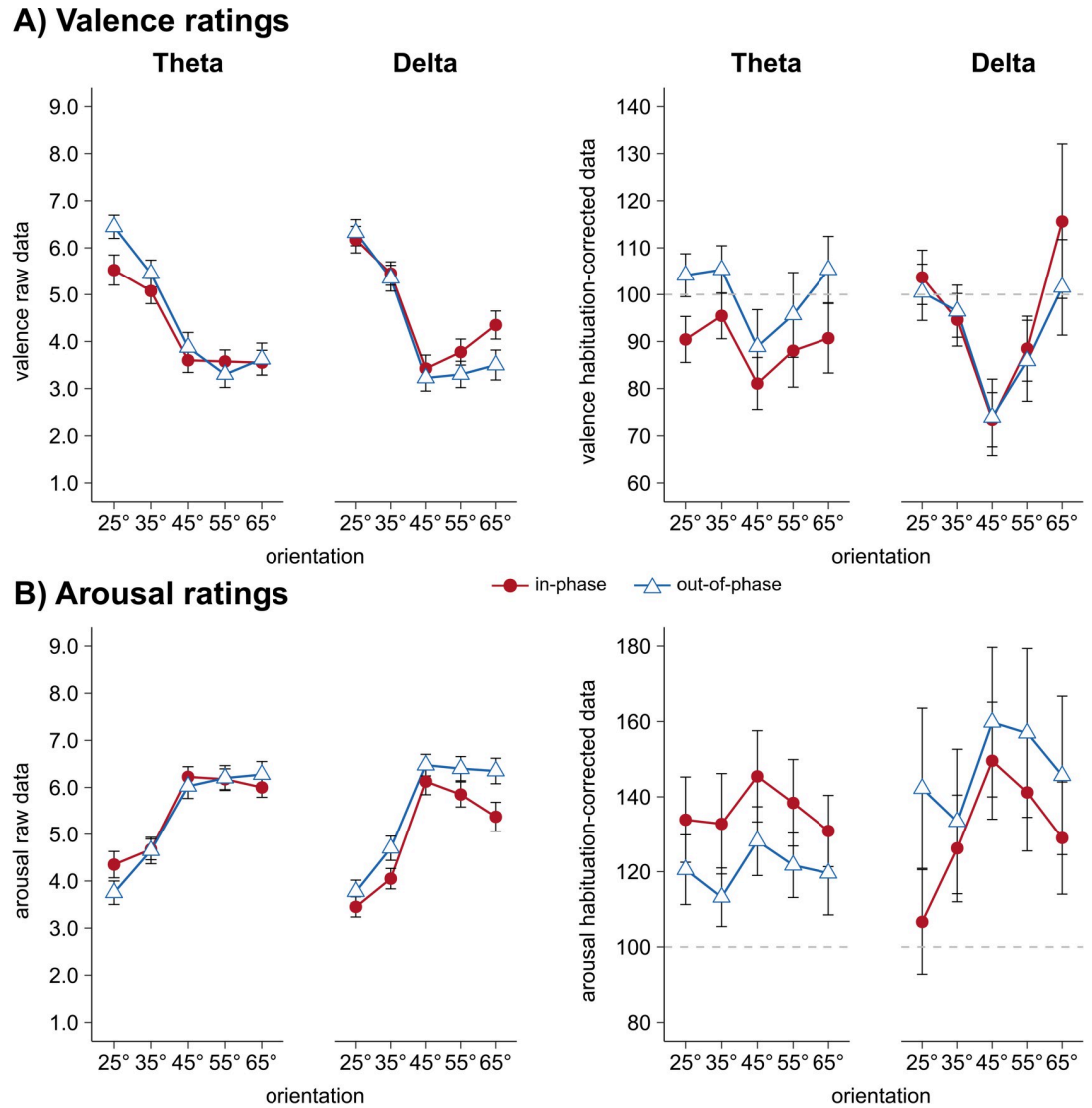## A) Valence ratings

B) Arousal ratings

Fig 5. Raw and habituation-corrected valence and arousal ratings. Raw (left panel) as well as habituation-corrected (right panel) valence **(A)** and arousal **(B)** ratings separately for frequency (theta vs. delta) and synchronization condition (in-phase vs. out-of-phase). Valence ratings were collected as described in captions of **Fig 3** and the *Materials and Methods section (Dependent variables)*. Each data point represents mean valence ratings for each CS orientation over participants per frequency and synchronization condition. Error bars show ±1 SEM. Note that habituation-corrected values are depicted for better visualization of the fear generalization pattern. However, the statistics in the result section are based on the raw data. **S3 and S4 Figs** show discrimination indices (CS+ minus the average of all CS-) and estimation statistics for z-transformed valence and arousal ratings, respectively. For each frequency band (theta vs. delta) the discrimination index of in-phase and out-of-phase was compared.

Explorative analysis

Our planned sample size comprised the same number of male and female participants. For explorative purpose only, we therefore repeated our analysis by adding the factor sex (men vs. women). For US-expectancies after acquisition, we found a significant main effect of sex ($F(1,152) = 6.06$, $p = .015$, $\eta_{p}^2 = .038$) as well as a synchronization x sex interaction ($F(1,152) = 4.47$, $p = .036$, $\eta_{p}^2 = .029$) that was based on greater differences between in-phase and out-phase
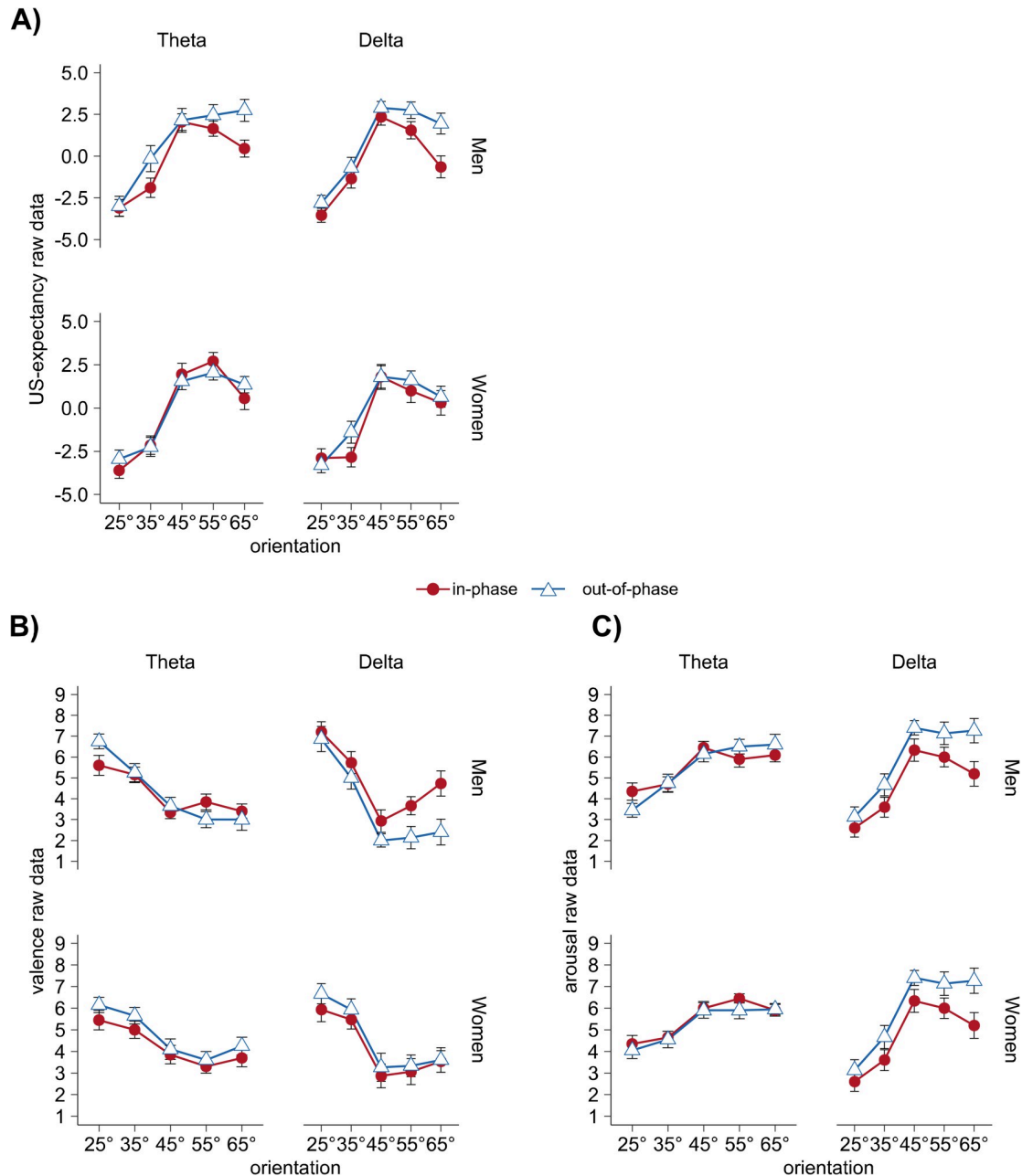
Fig 6. Valence, arousal, and US-expectancy data separately for men and women. US-expectancy ratings (**A**), valence ratings (**B**), and arousal ratings (**C**) after acquisition for each frequency (theta vs. delta) and synchronization (in-phase vs. out-of-phase), separated by sex: within each subplot, top row shows men (n = 80), bottom row shows women (n = 80). Each data point represents mean values for each CS orientation, separately for frequency, synchronization, and sex. Error bars show ±1 SEM. In order to improve the visualization of the fear generalization pattern, we corrected for the linear trend during habituation, acquisition, and extinction: **S5 Fig** shows these habituation-corrected valence and arousal rating.

presentation in men (**Fig 6A**). In addition, we found a significant interaction of synchronization x sex in valence ratings ($F(1,152) = 4.16$, $p = .043$, $\eta_{p}^{2} = .027$, **Fig 6B**) but not arousal ratings (synchronization x sex interaction: $F(1,152) = 1.44$, $p = .232$, $\eta_{p}^{2} = .009$, **Fig 6C**).

Repeating the 5 x 2 x 2 ANOVA for men and women separately, supported the above pattern for valence rating with a trend-level interaction of frequency x synchronization ($F(1,76)$ = 3.03, p = .086, η_p^2 = .038 in men (**Fig 6B** top panel), but not women (frequency x synchronization interaction: $F(1,76)$ = 0.12, p = .726, η_p^2 = .002) **Fig 6B** bottom panel). With **Fig 6C** showing a similar difference between men and women for the arousal data, we found a comparable frequency x synchronization (trend-level) interaction in men ($F(1,76)$ = 2.94 p = .090, η_p^2 = .037) as well as an additional trend-level main effect of synchronization ($F(1,76)$ = 2.81 p = .098, η_p^2 = .036) in men only. Interestingly, men in the theta group showed the expected Mexican hat contrast fit with narrow generalization after in-phase presentation and broader generalization in the out-of-phase group (trend-level Mexican hat fit for orientation x synchronization interaction: $F(1,38)$ = 3.49, p = .070, η_p^2 = .084). For the US-expectancy ratings, the separate analysis for men and women revealed a trend-level interaction of orientation x synchronization ($F(2.9,222.5)$ = 2.61, p = .054, η_p^2 = .033) as well as a significant main effect of synchronization ($F(1,76)$ = 11.57, p = .001, η_p^2 = .132) in men, but again, as seen in **Fig 6A**, women did not show comparable differences. For consistency across our measures, we also calculated the 2 x 2 ANOVA for the discrimination indices for men and women separately. However, due to the explorative character, they are only listed in the Supporting Information **S3 Table**.

In sum, in all three rating measures, the explorative analyses including the factor *sex* revealed more pronounced effects in men compared to women that depend on frequency and synchronization and partly (at least trendwise) interact with orientation and reveal the expected Mexican hat contrast fit in the theta-synchronization condition exclusively in men.

Discussion

The current study aimed at 1) transferring previous findings of augmented affective ratings and CS-US contingency knowledge by theta-phase synchronized (vs. asynchronized) sensory input from a laboratory fear conditioning study to a web-based paradigm, and 2) expanding on our previous findings of this synchrony-induced augmentation by testing theta-specificity via a comparison with synchronization in the delta band. Based on our laboratory findings and the work of Clouter et al. [7], we hypothesized a theta-specific effect of phase synchronization that becomes apparent in improved learning of the aversive CS-US association. It should manifest in a better discrimination between the CS+ and most similar CS- orientations when CS and US gratings were presented phase-synchronized (vs. asynchronized) in theta while presentation in 1.7-Hz delta should not lead to differences between phase-synchronous and asynchronous stimulation.

In line with recent work of Stegmann et al. [23] and Björkstrand et al. [22], our findings support the ability to induce associative fear learning as well as extinction in a web-based fear conditioning paradigm. We further have to acknowledge that we used a complex generalization protocol. We found that the CS+ US association was successfully formed in terms of the increased arousal and unpleasantness ratings towards the CS+, that decreased gradually with decreasing similarity of the CS- gratings. Additionally, the knowledge about the CS-US contingency manifested in a similar learned generalization, with the highest US expectancy ratings for the CS+ and a gradual decrease towards the neighboring CS- orientations. Thus, in all three measures the web-based conditioning results were highly comparable to those of the published lab-based version [20]. Importantly, this was achieved with only minimal changes compared to the previously published task.

106

In a web-based study, task engagement and compliance are a major concern especially in a long-lasting, passive and aversive fear conditioning task using loud noise as US. In the web-based setting, participants have many distractions that are outside of experimental control, and many opportunities to disengage from the task or even avoid the aversive noise altogether. In order to keep the core task unchanged in the web-version, but assessing compliance effectively without violating the subjects' privacy, we only introduced a very simple control task in the breaks between learning phases. Interestingly, this was sufficient to control for task engagement and unchanged auditory volume, as the results of our prerequisite analysis have shown. Moreover, our minimal compliance control task was a predictor of learning success.

Our results of enabling a rather complex fear generalization paradigm in a web-based approach, also emphasize the usability of discriminatory stimuli and open great opportunities for future (fear) research: Compared with laboratory studies, web-based designs have the advantage of being time-efficient and cost-effective. The time-efficiency also makes it a great tool for piloting data with new task designs. Additionally, a web-based design can potentially reach participants all over the world allowing the assessment of inter-cultural aspects that are difficult to include in one lab, and reducing bias from *testing western*, *educated*, *industrialized*, *rich*, *and democratic* (WEIRD) samples in psychology and neuroscience [34]. From the view of emotion research, web-based studies could also be a useful alternative when it comes to clinically relevant samples. While the typical study sample consists of healthy university students [35], participants that are confronted with symptoms of anxiety or phobias might avoid being part in a study that is conducted in a potentially stressful laboratory environment. The possibility of participating from home might help to collect data of so far underrepresented groups. On the other hand, it needs high responsibility in case of any decompensation.

While our data confirm fear acquisition and extinction, the expected effects of theta-phase specificity were ambiguous. Affective ratings of valence and arousal did not show any differences in generalization across the CS gratings that depended on phase synchronization or frequency. In contrast and as hypothesized, US-expectancy ratings that indicate the knowledge about the CS-US contingency revealed higher overall ratings in the out-of-phase group, suggesting that this group broadly generalizes across the CS orientations. Contrary to our expectations, however, this effect was independent of the frequency and hence, not specific for the theta-band. One possible reason for the discrepancy between the affective (valence and arousal) and cognitive (US expectancy) ratings concerns the perceived intensity of the aversive US. In both, our recent laboratory as well as the current web-based study, we instructed the participants to not only rate the affective quality of CS gratings but also asked for an evaluation of the valence and arousal of the auditory US after acquisition. Although both studies confirmed the US aversiveness by high arousal and low valence (i.e., unpleasant) ratings (laboratory study: arousal, $M = 8.13$, $SD = 0.822$; valence, $M = 1.9$, $SD = 1.1$; web-based study: arousal, $M = 6.26$, $SD = 1.6$; valence, $M = 2.58$, $SD = 1.6$), the comparison of both settings revealed lower arousal and unpleasantness (valence) ratings in the web-based study. This is probably based on the individual US-intensity adjustment in the current study. While the more declarative knowledge of CS-US contingency should be unaffected by lower US intensities, it might have an effect on emotional evaluation of CS valence and arousal, and may thus be less receptive for subtle differences in fear generalization. Future studies could try and avoid such problems by devising an even better procedure for the titration of US intensity and applying more rigorous control tasks (e.g., individualized near-threshold audio stimuli) to prevent participants from making even small changes in audio volume during the task.

The hypothesized theta-band specificity was based on overwhelming evidence in animal and human studies, revealing an involvement of theta synchronization in the communication between distinct brain regions and the coordination of neural activity [2, 3, 5, 6, 36, 37]. In the

processing of fear and extinction memories, for example, theta oscillations synchronize within and between the main structures of the fear circuitry (i.e., amygdala, hippocampus, and parts of the medial prefrontal cortex [mPFC]), enabling precisely timed neural activity that is crucial for synaptic plasticity [16, for reviews see 38–42]. However, a new line of evidence suggests that low frequency (theta and delta) entrainment in general rather than theta-band specific entrainment might induce memory enhancing effects [43, 44]. Earlier studies already showed that slow delta frequency entrainment provides optimized windows for information processing in perceptual discrimination tasks in macaque monkeys [45] and improves reaction times in those primates and also humans [45, 46]. Interestingly, more recent findings revealed that the effects of slow-frequency entrainment might not be restricted to perception, but also play a role in higher-order cognition like memory formation [47]. Slow-frequency entrainment might provide an optimized neural rhythm to, for instance, coordinate higher frequencies (so-called cross-frequency phase-amplitude coupling), a mechanism that was repeatedly associated with memory processing [for a review see 47–50]. In a memory encoding and recognition task, Jones et al. [51] found a better recognition for those items that were presented rhythmically (fixed ITI) vs. arrhythmically (variable ITI) in a slow 1.67 Hz delta frequency. In accordance, visual target stimuli that were presented "on-beat" (synchronous) with an auditory 1.25 Hz background rhythm compared with "off-beat" (asynchronous) improved memory in a subsequent recognition task, suggesting that delta entrainment is effective in cross-modal memory processing [52]. Using a comparable paradigm, Hickey et al. [43] linked the improvement of memory to neural entrainment (measured as phase coherence and increased power at 1.25 Hz), showing that a greater entrainment during the encoding phase predicted a better subsequent memory. Taken together, there is growing evidence that low-frequency entrainment (delta-theta range) orchestrates neural activity to a degree that is supportive for memory encoding.

Another mechanism for better discrimination after in-phase vs. out-of-phase audio-visual sensory input may rely on an increase in salience of the synchronous stimuli via attentional mechanisms, irrespective of the specific stimulation frequency and oscillatory brain mechanisms, i.e., via synchronization per se. The temporal co-occurrence of auditory and visual features per se (e.g., onset/offset in our synchronous groups) may be a strong signal, indicating that the sound and visual signal are the same event, which in turn may trigger multisensory integration. Indeed, when presented (at least mainly) synchronously, even task unrelated, uninformative, transient auditory stimuli can amplify spatial [53–55] and feature-specific visual attention [56] and amplify visual processing. Such attentional gain may also explain our current finding of a narrower generalization of US-expectancy ratings in both the theta and delta synchronous groups. Stimuli that were viewed with higher attention could be easier to discriminate even in a temporally delayed rating. Our task design does not allow us to disentangle these two alternatives (i.e. low-frequency entrainment supporting memory encoding vs. audiovisual synchrony amplifying attention). Previous work from Clouter et al. [7] with 4 Hz stimulation showed that participants were unable to correctly identify the audio-visual condition as synchronous or asynchronous. This may speak against the argument that audiovisual synchrony amplified attention. However, earlier studies on the discriminability of multimodal synchrony vs. asynchrony suggest that most participants are easily able to discriminate audio-visual synchrony (vs. asynchrony), as long as the stimuli are not modulated with a frequency of more than 4 Hz [57, 58]. Our study lacks a rating of stimulus synchrony-asynchrony. Future studies could include this to help disentangle the underlying mechanisms. Of note, attentional amplification does not need to be reflected in a clear subjective distinction of the stimulus streams as synchronous or asynchronous. Finally, although there is an ongoing debate [56], one of the proposed mechanisms of multisensory effects on attention, action, and memory is

synchronization of neural oscillations (but also phase resetting, see [59]). Thus, amplified attention for audio-visual synchrony and improved memory encoding via synchronization of low-frequency oscillations may in part share the same fundamental neurocomputational mechanism. Future neurostimulation and neurophysiological studies will hopefully improve our understanding of such mechanisms.

Given that fear conditioning is subject to well-known sex differences [e.g., 60–63], and in line with the higher prevalence of anxiety- and stress-related disorders in women [57–60], we conducted exploratory post-hoc analyses including the factor *sex*. Interestingly, in US-expectancy ratings only men responded differently to phase-synchronized vs. phase-asynchronized stimulation, independent of frequency. In contrast, women's US-expectancy ratings generalized across the CS orientations, without showing any effects of synchronization or frequency. Valence and arousal ratings showed descriptively (but not significantly) similar sex difference. Future studies might further examine this preliminary evidence for a sex difference by studying a wider range of women, including free-cycling women (we only examined women taking oral contraceptives, with suppressed levels of endogenously produced 17β estradiol and progesterone).

With the current study we were able to create a "pandemic-friendly" alternative of a laboratory fear conditioning paradigm. However, conducting a web-based conditioning contains some important limitations, discussed below.

First, web-based studies are mainly restricted to ratings or response times. Although our previous findings were restricted to valence, arousal, and US-expectancy, utilizing well-established fear measures like skin conductance responses are generally useful to operationalize a successful fear acquisition and extinction response. Regarding the specific question of entraining theta or delta frequency either in-phase or out-of-phase, EEG steady-state stimulus evoked signals would also have been a validation of the induction of CS and US at a given frequency. This is specifically interesting for frequencies as low as delta (1.7 Hz) since studies using steady-state visually evoked potentials (ssVEPs) typically work with frequencies of 4 Hz or higher so far–most studies even use frequencies between 8–10 Hz [64, 65]. Nevertheless, recent evidence of memory-enhancing effects after stimulus presentation in a delta rhythm support the entrainment at these very low frequencies [43, 51, 52]. As a future perspective, our findings should also be compared to a higher frequency band like alpha, to specify the idea of a special role for low-frequency phase synchronization for the encoding of memory [47]. Of importance, the length of a single rhythmic cycle decreases with increasing frequency (e.g., one full cycle at 2 Hz lasts 500 ms, one cycle at 10 Hz lasts only 100 ms). Thus, with increasing frequency, the time window of high excitability, e.g., defined as one quarter of the full cycle, decreases [2]. We therefore suggest testing higher frequencies in a standardized laboratory setting, since small variances in timing, caused by different browsers or internet connection result in greater phase-lags variabilities with increasing frequencies.

Second, since participants conducted our study at home, we did not have the same control of the environment that usually comes with studies in a laboratory setting only. With this, the most important limitation for this study concerns the optimized timing of CS-US input. As reported by Bridges et al. [66], the precision of timing varies in dependence of the operating systems and the browser. Although we tried to minimize the effect by uploading the complete stimulus material on the participants' PC at the beginning of the experiment and by instructing the participants to use one of the browsers that revealed the least deficits in timing, we were unable to control intra- or interindividual variance in the exact synchronization between the CS+ and US. However, even though the timing might not have been as exact as we planned, Fell & Axmacher [2] emphasizes that a lag of precisely 0 ms is not necessary for the induction of successful LTP. Instead, 10–20 ms delay of post-synaptic firing after activation of the

109

presynaptic neuron should be sufficient. Nevertheless, future studies should consider to systematically validate the stimulus timings by assessing intra- and interindividual variability of timings in the coded experiment for different operating systems, browsers, and internet connections to further strengthen the results.

Third, although the conducted compliance control task enabled us to proof the presence and general compliance towards the experiment, we cannot rule out that the participants distracted themselves during the aversive conditioning procedure. Importantly, this did obviously not influence the formation of the CS-US association per se.

Fourth, cross-trial temporal consistency of the phase shift between the CS+ and the US varied due to the 90˚, 180˚, 270˚ lags in the out-of-phase group, while it persisted at 0˚ in the in-phase groups. We cannot rule out that the subtle temporal variations within the out-of-phase condition (compared to the in-phase condition) might have led to perceptual differences between both groups that resulted in broader vs. narrower generalization patterns across the CS+. Nevertheless, previous studies examining episodic memory did not find learning differences between the 90˚, 180˚, 270˚ variation [7] or restricted the out-of-phase presentation to a 180˚ shift only [8]. In accordance with [8], future fear conditioning studies that specifically focus on generalization across perceptually similar CSs should better use a single phase shift in the out of phase group (i.e., 180˚ only) to avoid variability of CS-US shifting within the asynchronous condition.

Finally, an interesting—although from our perspective unfortunate—aspect is the strong linear relation across CS orientations prior to any experimental manipulation (i.e., in the habituation phase) as well as after acquisition and extinction. While we found evidence for affective evaluations that differed in dependence of the orientation of contour features in the literature [67], it is contrary to our findings: long horizontal contours were reported to be related to judgements of openness and depth, hence associated with safety and pleasantness. In contrast, vertical lines were related to an environment including long grass and trees that might hide potential danger [67]. Although we did not use perfectly horizontal or vertical orientations, the extremely robust orientation effect we found during habituation in all our ratings might be an interesting starting point for further studies.

In sum, the current study provides an example of how to use a complex generalization fear conditioning design in a web-based study. While we found robust fear acquisition and extinction, the ambiguous findings of synchronization or frequency effects suggest that low frequency rather than theta-specific entrainment supports the (predominantly declarative) memory of CS-US contingency. However, the limitations that come with the web-based approach underlines that time-critical questions might have greater success in a controllable laboratory environment. Nevertheless, from a methodological perspective, our study emphasizes some aspects that should be considered: when it comes to the US, using individually adjustable US-intensity is a great way to ensure a sufficient US aversiveness. In addition, we recommend the use of a compliance control task to check the presence and active participation. Besides, the choice of a low-volume beep sounds gave us a further guarantee that participants followed the instructions during the US-intensity adjustment. Hence, without prior notice, we added a control task that simultaneously tested for visual and auditory compliance. Importantly, despite these discussed limitations, the current study emphasizes augmented discriminations in the declarative knowledge of CS-US contingency when frequency-modulated stimuli are presented phase-synchronized (compared with phase-asynchronized) at a low frequency, i.e., our findings were not specific for the theta-frequency band. Interestingly, however, exploratory analyses showed theta-specific augmented discrimination became evident in US-expectancies in men, not women. Hence, future studies should include male and female participants.

Supporting information

S1 Dataset. Anonymized dataset, including raw and z-transformed ratings of US-expectancy, valence, and arousal. Dataset includes raw valence (val), arousal (aro), and US-expectancy (exp) ratings, as well as z-standardized ratings and discrimination indices (disidx). *Subject ID* is the anonymized subject identification number, *date* shows the date of participation, *val*:US and *aro_US* represents the valence and arousal rating of the auditory US that was assessed after acquisition. The learning phases are abbreviated by *hab* for habituation, *acq* for acquisition, and *ext* for extinction. Each grating orientation is shown by the value between *25* and *65*.
(XLSX)

S1 Table. Means and common SDs used to calculate power analysis for US-expectancy, valence, and arousal ratings.
(DOCX)

S2 Table. Summary of statistical analyses. Table shows statistical analyses including *p* value and effect size for each rating (US-expectancy, valence, arousal).
(DOCX)

S3 Table. Discrimination indices for explorative analysis, including the factor sex. For ratings after acquisition, discrimination indices (CS+ minus averaged CS-) are calculated to assess differences in the ability to discriminate the CS+ and adjacent CS- gratings between synchronization conditions (in-phase vs. out-of-phase) and frequency (theta vs. delta). Indices were used in a 2 x 2 ANOVA, including the between-subject factors *synchronization* and *frequency* for men and women separately. Within each ratings measure, the table lists the main effect of frequency, the main effect of synchronization, and the interaction between synchronization and frequency. For valence and arousal, as well as US-expectancies, discrimination indices are presented as z-values.
(DOCX)

S1 Fig. Discrimination indices for US-expectancy ratings, independent of frequency. The discrimination index was computed as the difference between the reinforced 45˚ orientation (CS+) grating and the average of the four CS–orientations. Data and effect sizes are shown as a Cumming estimation plot (http://www.estimationstats.com). Left column, Swarm plots show the z-standardized discrimination indices independent of frequency (each dot is the discrimination index of one participant). Group statistics are indicated to the right of each swarm as gapped lines (gap = mean, line length = 1 SD). Right column, Effect size estimates (Hedges' *g*, black dots) for the comparison between in-phase vs out-of-phase, across theta and delta frequency and their 95% confidence interval (CI; vertical error bars). The unpaired Hedge's *g* of out-of-phase (n = 80) minus in-phase (n = 80): -0.29 [95% CI, -0.594, 0.0298]. The 5000 bootstrap samples were taken for CI estimation; the CI is bias corrected and accelerated.
(TIF)

S2 Fig. Discrimination indices for US-expectancy ratings within the theta and delta frequency. The discrimination index was computed as the difference between the reinforced 45˚ orientation (CS+) grating and the average of the four CS–orientations. Data and effect sizes are shown as a Cumming estimation plot (http://www.estimationstats.com). Top row, Swarm plots show the z-standardized discrimination indices per frequency (each dot is the discrimination index of one participant). Group statistics are indicated to the right of each swarm as gapped lines (gap = mean, line length = 1 SD). Bottom row, Effect size estimates (Hedges' *g*, black dots) for the relevant comparisons (in-phase vs out-of-phase within theta and delta

111

frequency) and their 95% confidence interval (CI; vertical error bars). The unpaired Hedge's *g*: for the theta frequency our-of-phase (n = 40) minus Theta in-phase (n = 40): –0.403 [95% CI, -0.855, 0.0389]; for the delta frequency out-of-phase (n = 40) minus in-phase (n = 40): -0.18 [95% CI, –0.619, 0.273]. The 5000 bootstrap samples were taken for CI estimation; the CI is bias corrected and accelerated.
(TIF)

S3 Fig. Discrimination indices for valence ratings. The discrimination index was computed as the difference between the reinforced 45˚ orientation (CS+) grating and the average of the four CS–orientations. Data and effect sizes are shown as a Cumming estimation plot (http://www.estimationstats.com). Top row, Swarm plots show the z-standardized discrimination indices per frequency (each dot is the discrimination index of one participant). Group statistics are indicated to the right of each swarm as gapped lines (gap = mean, line length = 1 SD). Bottom row, Effect size estimates (Hedges' *g*, black dots) for the relevant comparisons (in-phase vs out-of-phase within theta and delta frequency) and their 95% confidence interval (CI; vertical error bars). The unpaired Hedge's *g*: for the theta frequency out-of-phase (n = 40) minus theta in-phase (n = 40): 0.11 [95% CI, -0.327, 0.538]; for the delta frequency out-of-phase (n = 40) minus in-phase (n = 40): 0.259 [95% CI, -0.207, 0.665]. The 5000 bootstrap samples were taken for CI estimation; the CI is bias corrected and accelerated.
(TIF)

S4 Fig. Discrimination indices for arousal ratings. The discrimination index was computed as the difference between the reinforced 45˚ orientation (CS+) grating and the average of the four CS–orientations. Data and effect sizes are shown as a Cumming estimation plot (http://www.estimationstats.com). Top row, Swarm plots show the z-standardized discrimination indices per frequency (each dot is the discrimination index of one participant). Group statistics are indicated to the right of each swarm as gapped lines (gap = mean, line length = 1 SD). Bottom row, Effect size estimates (Hedges' *g*, black dots) for the relevant comparisons (in-phase vs out-of-phase within theta and delta frequency) and their 95% confidence interval (CI; vertical error bars). The unpaired Hedge's *g*: for the theta frequency our-of-phase (n = 40) minus theta in-phase (n = 40): -0.204 [95% CI, -0.643, 0.24]; for the delta frequency out-of-phase (n = 40) minus in-phase (n = 40): -0.212 [95% CI, -0.639, 0.239]. The 5000 bootstrap samples were taken for CI estimation; the CI is bias corrected and accelerated.
(TIF)

S5 Fig. Habituation-corrected valence and arousal data separately for men and women. To improve the visualization of the fear generalization pattern for men and women separately, we corrected for the linear trend during habituation, acquisition, and extinction, conducting a habituation correction for valence **(A)** and arousal **(B)** data. Both valence and arousal data show ratings after acquisition for each frequency (theta vs. delta) and synchronization (in-phase vs. out-of-phase), separated by sex: within each subplot, top row shows men (n = 80), bottom row shows women (n = 80). Each data point represents mean, habituation-corrected values for each CS orientation, separately for frequency, synchronization, and sex. Error bars show ±1 SEM.
(TIF)

Acknowledgments

112

Author Contributions

Conceptualization: Elena Plog, Martin I. Antov, Philipp Bierwirth, Ursula Stockhorst.

Data curation: Elena Plog.

Formal analysis: Elena Plog.

Funding acquisition: Ursula Stockhorst.

Investigation: Elena Plog.

Methodology: Elena Plog, Martin I. Antov, Ursula Stockhorst.

Project administration: Elena Plog.

Software: Elena Plog, Martin I. Antov.

Supervision: Ursula Stockhorst.

Validation: Elena Plog.

Visualization: Elena Plog, Philipp Bierwirth.

Writing – original draft: Elena Plog.

Writing – review & editing: Elena Plog, Martin I. Antov, Philipp Bierwirth, Ursula Stockhorst.

References

1. Hanslmayr S, Axmacher N, Inman CS. Modulating human memory via entrainment of brain oscillations. Trends Neurosci 2019; 42(7): 485–99 https://doi.org/10.1016/j.tins.2019.04.004 PMID: 31178076

2. Fell J, Axmacher N. The role of phase synchronization in memory processes. Nat Rev Neurosci 2011; 12(2): 105–18 https://doi.org/10.1038/nrn2979 PMID: 21248789

3. Benchenane K, Peyrache A, Khamassi M, et al. Coherent theta oscillations and reorganization of spike timing in the hippocampal- prefrontal network upon learning. Neuron 2010; 66(6): 921–36 https://doi.org/10.1016/j.neuron.2010.05.013 PMID: 20620877

4. Place R, Farovik A, Brockmann M, Eichenbaum H. Bidirectional prefrontal-hippocampal interactions support context-guided memory. Nat Neurosci 2016; 19(8): 992–4 https://doi.org/10.1038/nn.4327 PMID: 27322417

5. Summerfield C, Mangels JA. Coherent theta-band EEG activity predicts item-context binding during encoding. Neuroimage 2005; 24(3): 692–703 https://doi.org/10.1016/j.neuroimage.2004.09.012 PMID: 15652304

6. Weiss S, Rappelsberger P. Long-range EEG synchronization during word encoding correlates with successful memory performance. Cognitive Brain Research 2000; 9(3): 299–312 https://doi.org/10.1016/s0926-6410(00)00011-2 PMID: 10808141

7. Clouter A, Shapiro KL, Hanslmayr S. Theta phase synchronization is the glue that binds human associative memory. Curr Biol 2017; 27(20): 3143–3148.e6 https://doi.org/10.1016/j.cub.2017.09.001 PMID: 28988860

8. Wang D, Clouter A, Chen Q, Shapiro KL, Hanslmayr S. Single-trial phase entrainment of theta oscillations in sensory regions predicts human associative memory performance. J Neurosci 2018; 38(28): 6299–309 https://doi.org/10.1523/JNEUROSCI.0349-18.2018 PMID: 29899027

9. LeDoux JE. Emotion circuits in the brain. Annu Rev Neurosci 2000; 23: 155–84 https://doi.org/10.1146/annurev.neuro.23.1.155 PMID: 10845062

10. Maren S. Neurobiology of Pavlovian fear conditioning. Annu Rev Neurosci 2001; 24: 897–931 https://doi.org/10.1146/annurev.neuro.24.1.897 PMID: 11520922

11. Fanselow MS. Neural organization of the defensive behavior system responsible for fear. Psychon Bull Rev 1994; 1(4): 429–38 https://doi.org/10.3758/BF03210947 PMID: 24203551

12. Orsini CA, Maren S. Neural and cellular mechanisms of fear and extinction memory formation. Neurosci Biobehav Rev 2012; 36(7): 1773–802 https://doi.org/10.1016/j.neubiorev.2011.12.014 PMID: 22230704

13. Herry C, Johansen JP. Encoding of fear learning and memory in distributed neuronal circuits. Nat Neurosci 2014; 17(12): 1644–54 https://doi.org/10.1038/nn.3869 PMID: 25413091

14. Johansen JP, Hamanaka H, Monfils MH, et al. Optical activation of lateral amygdala pyramidal cells instructs associative fear learning. Proc Natl Acad Sci U S A 2010; 107(28): 12692–7 https://doi.org/10.1073/pnas.1002418107 PMID: 20615999

15. Headley DB, Paré D. Common oscillatory mechanisms across multiple memory systems. NPJ Sci Learn 2017; 2 https://doi.org/10.1038/s41539-016-0001-2 PMID: 30294452

16. Taub AH, Perets R, Kahana E, Paz R. Oscillations synchronize amygdala-to-prefrontal primate circuits during aversive learning. Neuron 2018; 97(2): 291–298.e3 https://doi.org/10.1016/j.neuron.2017.11.042 PMID: 29290553

17. Lesting J, Daldrup T, Narayanan V, Himpe C, Seidenbecher T, Pape H-C. Directional theta coherence in prefrontal cortical to amygdalo-hippocampal pathways signals fear extinction. PLoS One 2013; 8 (10): e77707 https://doi.org/10.1371/journal.pone.0077707 PMID: 24204927

18. Lesting J, Narayanan RT, Kluge C, Sangha S, Seidenbecher T, Pape H-C. Patterns of coupled theta activity in amygdala-hippocampal-prefrontal cortical circuits during fear extinction. PLoS One 2011; 6 (6) https://doi.org/10.1371/journal.pone.0021714 PMID: 21738775

19. Chen S, Tan Z, Xia W, et al. Theta oscillations synchronize human medial prefrontal cortex and amygdala during fear learning. Sci Adv 2021; 7(34) https://doi.org/10.1126/sciadv.abf4198 PMID: 34407939

20. Plog E, Antov MI, Bierwirth P, Keil A, Stockhorst U. Phase-synchronized stimulus presentation augments contingency knowledge and affective evaluation in a fear-conditioning task. eNeuro 2022; 9(1) https://doi.org/10.1523/ENEURO.0538-20.2021 PMID: 34857589

21. Neske GT. The slow oscillation in cortical and thalamic networks: mechanisms and functions. Front Neural Circuits 2015; 9: 88 https://doi.org/10.3389/fncir.2015.00088 PMID: 26834569

22. Björkstrand J, Pine DS, Frick A. Evaluating an internet-delivered fear conditioning and extinction protocol using response times and affective ratings. Sci Rep 2022; 12(1): 4014 https://doi.org/10.1038/s41598-022-07999-3 PMID: 35256733

23. Stegmann Y, Andreatta M, Pauli P, Wieser MJ. Associative learning shapes visual discrimination in a web-based classical conditioning task. Sci Rep 2021; 11(1): 15762 https://doi.org/10.1038/s41598-021-95200-6 PMID: 34344923

24. Lakens D, Caldwell AR. Simulation-Based Power Analysis for Factorial Analysis of Variance Designs. Advances in Methods and Practices in Psychological Science 2021; 4(1): 251524592095150 [https://doi.org/10.1177/2515245920951503]

25. Foa EB. Posttraumatic diagnostic scale manual. Minneapolis, MN: National Computer Systems 1995.

26. Steil R, Ehlers A. Posttraumatische Diagnoseskala (PDS). Jena, Germany: Psychologisches Institut, Universität Jena 2000.

27. Peirce J, Gray JR, Simpson S, et al. PsychoPy2: Experiments in behavior made easy. Behav Res Methods 2019; 51(1): 195–203 https://doi.org/10.3758/s13428-018-01193-y PMID: 30734206

28. McTeague LM, Gruss LF, Keil A. Aversive learning shapes neuronal orientation tuning in human visual cortex. Nat Commun 2015; 6: 7823 https://doi.org/10.1038/ncomms8823 PMID: 26215466

29. Moratti S, Keil A. Cortical activation during Pavlovian fear conditioning depends on heart rate response patterns: an MEG study. Cognitive Brain Research 2005; 25(2): 459–71 https://doi.org/10.1016/j.cogbrainres.2005.07.006 PMID: 16140512

30. Antov MI, Plog E, Bierwirth P, Keil A, Stockhorst U. Visuocortical tuning to a threat-related feature persists after extinction and consolidation of conditioned fear. Sci Rep 2020; 10(1): 3926 https://doi.org/10.1038/s41598-020-60597-z PMID: 32127551

31. Bradley MM, Lang PJ. Measuring emotion: The self-assessment manikin and the semantic differential. Journal of Behavior Therapy and Experimental Psychiatry 1994; 25(1): 49–59 https://doi.org/10.1016/0005-7916(94)90063-9 PMID: 7962581

32. Morys-Carter WL, Paltpglou AE, Davies EL. Vertical enhancement of second-year psychology research. Psychology Teaching Review 2015; (21): 68–72.

33. Ho J, Tumkaya T, Aryal S, Choi H, Claridge-Chang A. Moving beyond P values: data analysis with estimation graphics. Nat Methods 2019; 16(7): 565–6 https://doi.org/10.1038/s41592-019-0470-3 PMID: 31217592

34. Rad MS, Martingano AJ, Ginges J. Toward a psychology of Homo sapiens: Making psychological science more representative of the human population. Proc Natl Acad Sci U S A 2018; 115(45): 11401–5 https://doi.org/10.1073/pnas.1721165115 PMID: 30397114

35. Hanel PHP, Vione KC. Do student samples provide an accurate estimate of the general public? PLoS One 2016; 11(12): e0168354 https://doi.org/10.1371/journal.pone.0168354 PMID: 28002494

36. Kota S, Rugg MD, Lega BC. Hippocampal theta oscillations support successful associative memory formation. J Neurosci 2020; 40(49): 9507–18 https://doi.org/10.1523/JNEUROSCI.0767-20.2020 PMID: 33158958

37. Klimesch W, Freunberger R, Sauseng P. Oscillatory mechanisms of process binding in memory. Neurosci Biobehav Rev 2010; 34(7): 1002–14 https://doi.org/10.1016/j.neubiorev.2009.10.004 PMID: 19837109

38. Bocchio M, Nabavi S, Capogna M. Synaptic plasticity, engrams, and network oscillations in amygdala circuits for storage and retrieval of emotional memories. Neuron 2017; 94(4): 731–43 https://doi.org/10.1016/j.neuron.2017.03.022 PMID: 28521127

39. Çalışkan G, Stork O. Hippocampal network oscillations as mediators of behavioural metaplasticity: Insights from emotional learning. Neurobiol Learn Mem 2018; 154: 37–53 https://doi.org/10.1016/j.nlm.2018.02.022 PMID: 29476822

40. Karalis N, Dejean C, Chaudun F, et al. 4-Hz oscillations synchronize prefrontal-amygdala circuits during fear behavior. Nat Neurosci 2016; 19(4): 605–12 https://doi.org/10.1038/nn.4251 PMID: 26878674

41. Zheng J, Stevenson RF, Mander BA, et al. Multiplexing of theta and alpha rhythms in the amygdala-hippocampal circuit supports pattern separation of emotional information. Neuron 2019; 102(4): 887–898.e5 https://doi.org/10.1016/j.neuron.2019.03.025 PMID: 30979537

42. Seidenbecher T, Laxmi TR, Stork O, Pape H-C. Amygdalar and hippocampal theta rhythm synchronization during fear memory retrieval. Science 2003; 301(5634): 846–50 https://doi.org/10.1126/science.1085818 PMID: 12907806

43. Hickey P, Merseal H, Patel AD, Race E. Memory in time: Neural tracking of low-frequency rhythm dynamically modulates memory formation. Neuroimage 2020; 213: 116693 https://doi.org/10.1016/j.neuroimage.2020.116693 PMID: 32135262

44. Hickey P, Barnett-Young A, Patel AD, Race E. Environmental rhythms orchestrate neural activity at multiple stages of processing during memory encoding: Evidence from event-related potentials. PLoS One 2020; 15(11): e0234668 https://doi.org/10.1371/journal.pone.0234668 PMID: 33206657

45. Lakatos P, Karmos G, Mehta AD, Ulbert I, Schroeder CE. Entrainment of neuronal oscillations as a mechanism of attentional selection. Science 2008; 320(5872): 110–3 https://doi.org/10.1126/science.1154735 PMID: 18388295

46. Stefanics G, Hangya B, Hernádi I, Winkler I, Lakatos P, Ulbert I. Phase entrainment of human delta oscillations can mediate the effects of expectation on reaction speed. J Neurosci 2010; 30(41): 13578–85 https://doi.org/10.1523/JNEUROSCI.0703-10.2010 PMID: 20943899

47. Hickey P, Race E. Riding the slow wave: Exploring the role of entrained low-frequency oscillations in memory formation. Neuropsychologia 2021; 160: 107962 https://doi.org/10.1016/j.neuropsychologia.2021.107962 PMID: 34284040

48. Köster M, Finger H, Graetz S, Kater M, Gruber T. Theta-gamma coupling binds visual perceptual features in an associative memory task. Sci Rep 2018; 8(1): 17688 https://doi.org/10.1038/s41598-018-35812-7 PMID: 30523336

49. Köster M, Martens U, Gruber T. Memory entrainment by visually evoked theta-gamma coupling. Neuroimage 2019; 188: 181–7 https://doi.org/10.1016/j.neuroimage.2018.12.002 PMID: 30529173

50. Friese U, Köster M, Hassler U, Martens U, Trujillo-Barreto N, Gruber T. Successful memory encoding is associated with increased cross-frequency coupling between frontal theta and posterior gamma oscillations in human scalp-recorded EEG. Neuroimage 2013; 66: 642–7 https://doi.org/10.1016/j.neuroimage.2012.11.002 PMID: 23142278

51. Jones A, Ward EV. Rhythmic temporal structure at encoding enhances recognition memory. J Cogn Neurosci 2019; 31(10): 1549–62 https://doi.org/10.1162/jocn_a_01431 PMID: 31172861

52. Johndro H, Jacobs L, Patel AD, Race E. Temporal predictions provided by musical rhythm influence visual memory encoding. Acta Psychol (Amst) 2019; 200: 102923 https://doi.org/10.1016/j.actpsy.2019.102923 PMID: 31759191

53. van der Burg E, Olivers CNL, Bronkhorst AW, Theeuwes J. Pip and pop: nonspatial auditory signals improve spatial visual search. J Exp Psychol Hum Percept Perform 2008; 34(5): 1053–65 https://doi.org/10.1037/0096-1523.34.5.1053 PMID: 18823194

54. van der Burg E, Cass J, Olivers CNL, Theeuwes J, Alais D. Efficient visual search from synchronized auditory signals requires transient audiovisual events. PLoS One 2010; 5(5): e10664 https://doi.org/10.1371/journal.pone.0010664 PMID: 20498844

55. Covic A, Keitel C, Porcu E, Schröger E, Müller MM. Audio-visual synchrony and spatial attention enhance processing of dynamic visual stimulation independently and in parallel: A frequency-tagging

115

study. Neuroimage 2017; 161: 32–42 https://doi.org/10.1016/j.neuroimage.2017.08.022 PMID: 28802870

56. Keitel C, Müller MM. Audio-visual synchrony and feature-selective attention co-amplify early visual processing. Exp Brain Res 2016; 234(5): 1221–31 https://doi.org/10.1007/s00221-015-4392-8 PMID: 26226930

57. Fujisaki W, Nishida S. Temporal frequency characteristics of synchrony-asynchrony discrimination of audio-visual signals. Exp Brain Res 2005; 166(3–4): 455–64 https://doi.org/10.1007/s00221-005-2385-8 PMID: 16032402

58. Fujisaki W, Nishida S. Feature-based processing of audio-visual synchrony perception revealed by random pulse trains. Vision Res 2007; 47(8): 1075–93 https://doi.org/10.1016/j.visres.2007.01.021 PMID: 17350068

59. Bauer A-KR, Debener S, Nobre AC. Synchronisation of Neural Oscillations and Cross-modal Influences. Trends Cogn Sci 2020; 24(6): 481–95 https://doi.org/10.1016/j.tics.2020.03.003 PMID: 32317142

60. Bierwirth P, Sperl MFJ, Antov MI, Stockhorst U. Prefrontal theta oscillations are modulated by estradiol status during fear recall and extinction recall. Biol Psychiatry Cogn Neurosci Neuroimaging 2021; 6 (11): 1071–80 https://doi.org/10.1016/j.bpsc.2021.02.011 PMID: 33711549

61. Velasco ER, Florido A, Milad MR, Andero R. Sex differences in fear extinction. Neurosci Biobehav Rev 2019; 103: 81–108 https://doi.org/10.1016/j.neubiorev.2019.05.020 PMID: 31129235

62. Merz CJ, Wolf OT. Sex differences in stress effects on emotional learning. J Neurosci Res 2017; 95(1–2): 93–105 https://doi.org/10.1002/jnr.23811 PMID: 27870431

63. Stockhorst U, Antov MI. Modulation of fear extinction by stress, stress hormones and estradiol: a review. Front Behav Neurosci 2016; 9: 359 https://doi.org/10.3389/fnbeh.2015.00359 PMID: 26858616

64. Norcia AM, Appelbaum LG, Ales JM, Cottereau BR, Rossion B. The steady-state visual evoked potential in vision research: A review. J Vis 2015; 15(6): 4 https://doi.org/10.1167/15.6.4 PMID: 26024451

65. Skrandies W. The effect of stimulation frequency and retinal stimulus location on visual evoked potential topography. Brain Topogr 2007; 20(1): 15–20 https://doi.org/10.1007/s10548-007-0026-1 PMID: 17587164

66. Bridges D, Pitiot A, MacAskill MR, Peirce JW. The timing mega-study: comparing a range of experiment generators, both lab-based and online. PeerJ 2020; 8: e9414 https://doi.org/10.7717/peerj.9414 PMID: 33005482

67. Damiano C, Walther DB, Cunningham WA. Contour features predict valence and threat judgements in scenes. Sci Rep 2021; 11(1): 19405 https://doi.org/10.1038/s41598-021-99044-y PMID: 34593933

Supporting information

Title: Effects of phase synchronization and frequency specificity in the encoding of conditioned fear–a web-based fear conditioning study.

Authors: Elena Plog, Martin I. Antov, Philipp Bierwirth, and Ursula Stockhorst

S1 Dataset. **Anonymized dataset, including raw and z-transformed ratings of US-expectancy, valence, and arousal.** https://doi.org/10.1371/journal.pone.0281644.s001

Dataset includes raw valence (val), arousal (aro), and US-expectancy (exp) ratings, as well as z-standardized ratings and discrimination indices (disidx). *Subject ID* is the anonymized subject identification number, *date* shows the date of participation, *val*:*US* and *aro_US* represents the valence and arousal rating of the auditory US that was assessed after acquisition. The learning phases are abbreviated by *hab* for habituation, *acq* for acquisition, and *ext* for extinction. Each grating orientation is shown by the value between *25* and *65*.

S1 Table. Means and common standard deviations for power analysis based on [20].

	US-expectancy ratings	Arousal ratings	Valence ratings
Means for each cell in the design			
In-sync, theta, 25°	-2.2	4.45	5.55
In-sync, theta, 35°	-0.85	5.05	4.9
In-sync, theta, 45°	2.5	6.95	3.55
In-sync, theta, 55°	-0.55	5.25	5.15
In-sync, theta, 65°	-2	4.15	5.7
In-sync, delta, 25°	-0.45	5.35	4.65
In-sync, delta, 35°	1.6	5.85	4.05
In-sync, delta, 45°	2.4	6.3	4.05
In-sync, delta, 55°	0.7	5.85	4.45
In-sync, delta, 65°	-1.4	4.8	5.4
A-sync, theta, 25°	-0.45	5.35	4.65
A-sync, theta, 35°	1.6	5.85	4.05
A-sync, theta, 45°	2.4	6.3	4.05
A-sync, theta, 55°	0.7	5.85	4.45
A-sync, theta, 65°	-1.4	4.8	5.4
A-sync, delta, 25°	-0.45	5.35	5.65
A-sync, delta, 35°	1.6	5.85	4.05
A-sync, delta, 45°	2.4	6.3	4.05
A-sync, delta, 55°	0.7	5.85	4.45
A-sync, delta, 65°	-1.4	6.3	5.4
Common SDs			
	1.3	1.3	1.3

S1 Table. Means and common SDs used to calculate power analysis for US-expectancy, valence, and arousal ratings.

S2 Table. Summary of statistical analyses.

Table shows statistical analyses including *p* value and effect size for each rating (US-expectancy, valence, arousal).

DV & Learning-phase	Test	Effects	Statistics	*p*-value	Effect size (η^2p)
Prerequisite: Compliance Control Task					
Valence & Arousal					
	ANOVA	ME C	$F_{(1,215)} = 16.89$	<.001	.145
	ANOVA	ME AR	$F_{(1,215)} = 1.97$	.162	.009
	ANOVA	INT C x AR	$F_{(1,215)} = 0.78$	.379	.004
US expectancy					
	ANOVA$_{z\text{-values}}$	ME C	$F_{(1,215)} = 2.78$	.097	.013
	ANOVA$_{raws}$	ME C	$F_{(1,215)} = 9.27$	.003	.041
Validation: Acquisition and extinction					
Acquisition					
	ANOVA$_{Val}$	ME O	$F_{(2.7,414.0)} = 111.19$	<.001	.416
	ANOVA$_{Aro}$	ME O	$F_{(2.8,431.1)} = 107.17$	<.001	.407
	ANOVA$_{US\text{-exp}}$	ME O	$F_{(2.9,452.3)} = 140.24$	<.001	.473
	ANOVA$_{Val}$	Gen	$F_{(1,156)} = 88.80$	<.001	.363
	ANOVA$_{Aro}$	Gen	$F_{(1,156)} = 82.13$	<.001	.345
	ANOVA$_{US\text{-exp}}$	Gen	$F_{(1,156)} = 147.78$	<.001	.486
Acq vs. Ext	ANOVA$_{Val}$	ME LP	$F_{(1,156)} = 18.65$	<.001	.107
	ANOVA$_{Aro}$	ME LP	$F_{(1,156)} = 19.80$	<.001	.113
	ANOVA$_{US\text{-exp}}$	ME LP	$F_{(1,156)} = 35.50$	<.001	.185
OSF-registered analyses					
US-expectancy (after acquisition)					
	ANOVA	ME S*	$F_{(1,156)} = 10.17$	.002	.061
	ANOVA	INT F x S	$F_{(1,156)} = 0.34$	.560	.002
	ANOVA	ME O x F x S	$F_{(2.9,452.3)} = 0.27$	.838	.002
	ANOVA$_{Index}$	INT S x F	$F_{(1,156)} = 0.42$	.518	.003
	ANOVA	„Mex" (Theta) INT O x S	$F_{(1,78)} = 0.40$	.528	.005
	ANOVA	„Mex" (Delta) INT O x S	$F_{(1,78)} = 1.35$	.249	.017
Valence (after acquisition)					
	ANOVA	ME O x F x S	$F_{(2.6,414.0)} = 0.39$	.738	.002
	ANOVA$_{Index}$	INT S x F	$F_{(1,156)} = 0.07$	.798	.000
	ANOVA	„Mex" (Theta) INT O x S	$F_{(1,78)} = 1.36$	.247	.017

ANOVA	„Mex" (Delta) INT O x S	$F_{(1,78)} = 0.05$	.827	.001
Arousal (after acquisition)				
ANOVA	ME O x F x S	$F_{(2.8,431.1)} = 0.14$	.924	.001
ANOVA$_{Index}$	INT S x F	$F_{(1,156)} = 0.14$	.710	.001
ANOVA	„Mex" (Theta) INT O x S	$F_{(1,78)} = 0.77$	.384	.010
ANOVA	„Mex" (Delta) INT O x S	$F_{(1,78)} = 0.55$	.463	.007
Explorative Analyses (including the factor *sex*)				
5 x 2 x 2 x 2 ANOVA				
ANOVA$_{US-exp}$	ME Sex	$F_{(1,152)} = 6.06$	.015	.038
ANOVA$_{US-exp}$	S x Sex	$F_{(1,152)} = 4.47$	.036	.029
ANOVA$_{val}$	S x Sex	$F_{(1,152)} = 4.16$	.043	.027
ANOVA$_{Aro}$	S x Sex	$F_{(1,152)} = 1.44$	.232	.009
5 x 2 x 2 ANOVA				
Men ANOVA$_{val}$	INT F x S	$F_{(1,76)} = 3.03$	.086	.038
Women ANOVA$_{val}$	INT F x S	$F_{(1,76)} = 0.12$	.726	.002
Men ANOVA$_{Aro}$	INT F x S	$F_{(1,76)} = 2.94$	.090	.037
ANOVA$_{Aro}$	ME S	$F_{(1,76)} = 2.81$	.098	.036
ANOVA$_{Aro}$	„Mex" (Theta) INT O x S	$F_{(1,38)} = 3.49$	.070	.084
Men ANOVA$_{US-exp}$	INT O x S	$F_{(2.9,222.5)} = 2.61$	.054	.033
ANOVA$_{US-exp}$	ME S	$F_{(1,76)} = 11.57$	.001	.132
Women ANOVA$_{US-exp}$	INT O x S	$F_{(2.7,208.3)} = 0.43$	.714	.006
ANOVA$_{US-exp}$	ME S	$F_{(1,76)} = 0.87$	.011	.011

Notes: AR = affective ratings; Aro = Arousal ratings; ANOVA = repeated-measures ANOVA; C = compliance; DV = dependent variable; F = frequency; Gen = generalization contrast fit; Index = Discrimination Index (CS+ minus averaged CS-); INT = interaction; LP = learning phase; ME = main effect; Mex = Mexican hat contrast fit; η^2_p = partial η^2; O = orientation; raw = raw values; S = synchronization; US-exp = US-Expectancy ratings; Val = Valence ratings; z-values = z-standardized values

*within the OSF pre-registration, we did not expect the synchronization effect to be independent of the factor frequency.
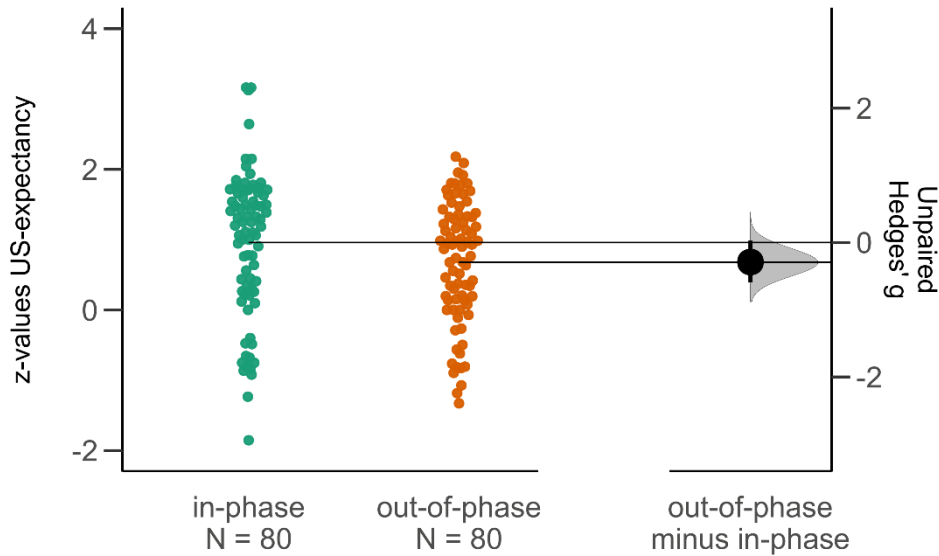
S2 Table. Summary of statistical analyses.

Table shows statistical analyses including *p* value and effect size for each rating (US-expectancy, valence, arousal).

S3 Table. Discrimination indices (z-transformed) for explorative analysis, including the factor sex.

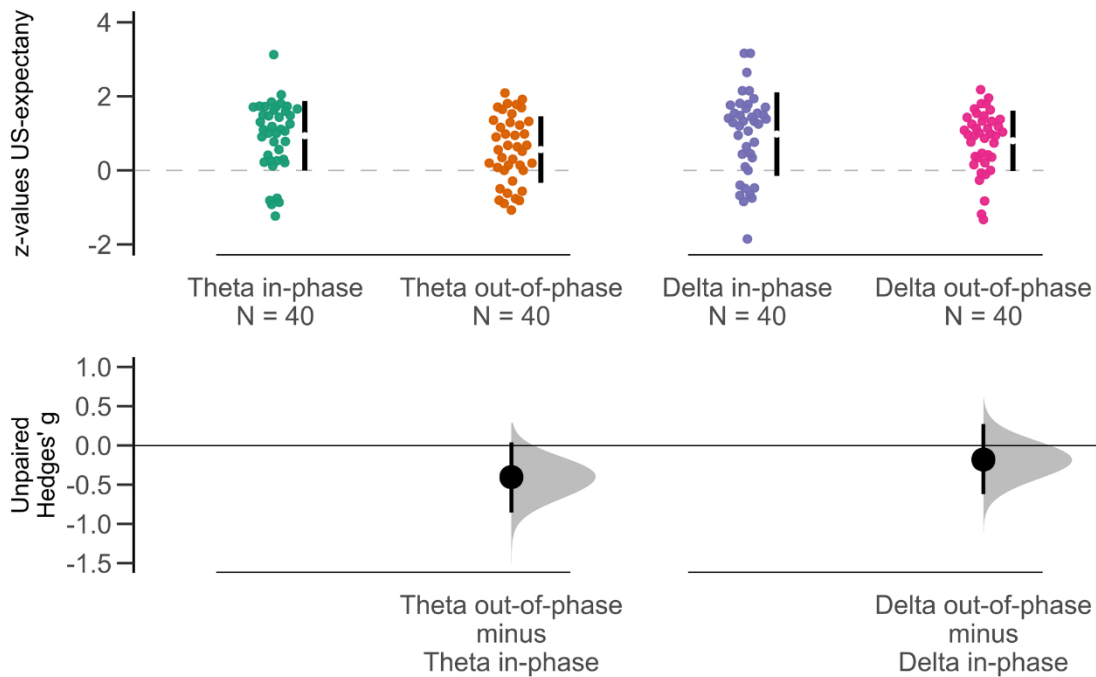| Effects	Statistics
Valence ratings	
Men	
Main effect frequency	$F_{(1,76)}$ = 4.34, p = .041, η^2p = 054
Main effect synchronization	$F_{(1,76)}$ = 1.64, p = .204, η^2p = .021
Synchronization x frequency interaction	$F_{(1,76)}$ = 0.07, p = .790, η^2p = .001
Women	
Main effect frequency	$F_{(1,76)}$ = 2.06, p = .155, η^2p = .026
Main effect synchronization	$F_{(1,76)}$ = 0.28, p = .597, η^2p = .004
Synchronization x frequency interaction	$F_{(1,76)}$ = .0.38, p = .541, η^2p = .005
Arousal ratings	
Men	
Main effect frequency	$F_{(1,76)}$ = 1.06, p = .306, η^2p = .014
Main effect synchronization	$F_{(1,76)}$ = 0.76, p = .388, η^2p = .010
Synchronization x frequency interaction	$F_{(1,76)}$ = 0.02, p = .896, η^2p = .000
Women	
Main effect frequency	$F_{(1,76)}$ = 0.61, p = .437, η^2p = .008
Main effect synchronization	$F_{(1,76)}$ = 1.04, p = .311, η^2p = .014
Synchronization x frequency interaction	$F_{(1,76)}$ = 0.31, p = .578, η^2p = .004
US-expectancy ratings	
Men	
Main effect frequency	$F_{(1,76)}$ = 1.227, p = .272, η^2p = .016
Main effect synchronization	$F_{(1,76)}$ = 4:615, p = .035, η^2p = .057
Synchronization x frequency interaction	$F_{(1,76)}$ = 0:555, p = .459, η^2p = .007
Women	
Main effect frequency	$F_{(1,76)}$ = 0:094, p = .760, η^2p = .001
Main effect synchronization	$F_{(1,76)}$ = 0:423, p = .542, η^2p = .005
Synchronization x frequency interaction	$F_{(1,76)}$ = 0:051, p = .821, η^2p = .001

S3 Table. Discrimination indices for explorative analysis, including the factor sex.

For ratings after acquisition, discrimination indices (CS+ minus averaged CS-) are calculated to assess differences in the ability to discriminate the CS+ and adjacent CS- gratings between synchronization conditions (in-phase vs. out-of-phase) and frequency (theta vs. delta). Indices were used in a 2 x 2 ANOVA, including the between-subject factors *synchronization* and *frequency* for men and women separately. Within each ratings measure, the table lists the main effect of frequency, the main effect of synchronization, and the interaction between synchronization and frequency. For valence and arousal, as well as US-expectancies, discrimination indices are presented as z-values.
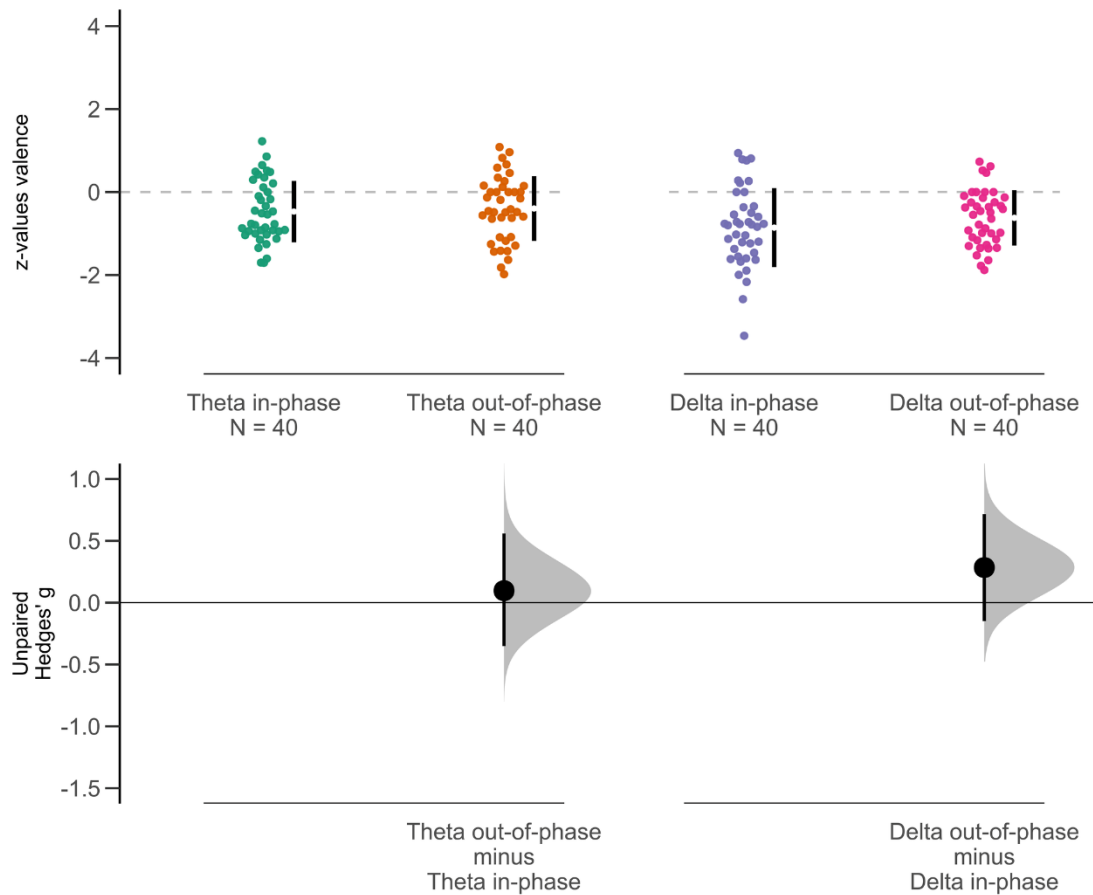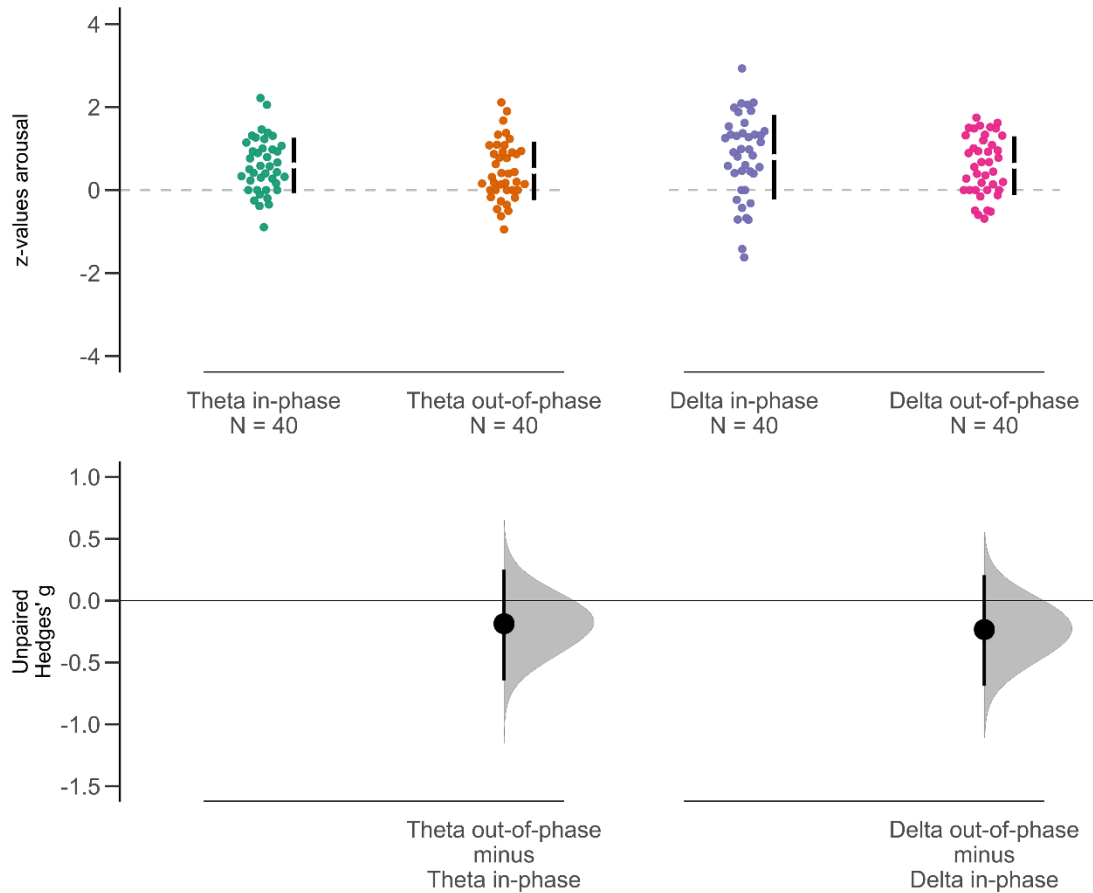
S1 Fig. **Discrimination indices for US-expectancy ratings, independent of frequency.**

The discrimination index was computed as the difference between the reinforced 45° orientation (CS+) grating and the average of the four CS–orientations. Data and effect sizes are shown as a Cumming estimation plot (http://www.estimationstats.com). Left column, Swarm plots show the z-standardized discrimination indices independent of frequency (each dot is the discrimination index of one participant). Group statistics are indicated to the right of each swarm as gapped lines (gap = mean, line length = 1 SD). Right column, Effect size estimates (Hedges' *g*, black dots) for the comparison between in-phase vs out-of-phase, across theta and delta frequency and their 95% confidence interval (CI; vertical error bars). The unpaired Hedge's *g* of out-of-phase (n = 80) minus in-phase (n = 80): -0.29 [95% CI, -0.594, 0.0298]. The 5000 bootstrap samples were taken for CI estimation; the CI is bias corrected and accelerated.

S2 Fig. Discrimination indices for US-expectancy ratings within the theta and delta frequency.

The discrimination index was computed as the difference between the reinforced 45° orientation (CS+) grating and the average of the four CS–orientations. Data and effect sizes are shown as a Cumming estimation plot (http://www.estimationstats.com). Top row, Swarm plots show the z-standardized discrimination indices per frequency (each dot is the discrimination index of one participant). Group statistics are indicated to the right of each swarm as gapped lines (gap = mean, line length = 1 SD). Bottom row, Effect size estimates (Hedges' *g*, black dots) for the relevant comparisons (in-phase vs out-of-phase within theta and delta frequency) and their 95% confidence interval (CI; vertical error bars). The unpaired Hedge's *g*: for the theta frequency our-of-phase (n = 40) minus Theta in-phase (n = 40): –0.403 [95% CI, -0.855, 0.0389]; for the delta frequency out-of-phase (n = 40) minus in-phase (n = 40): -0.18 [95% CI, –0.619, 0.273]. The 5000 bootstrap samples were taken for CI estimation; the CI is bias corrected and accelerated.
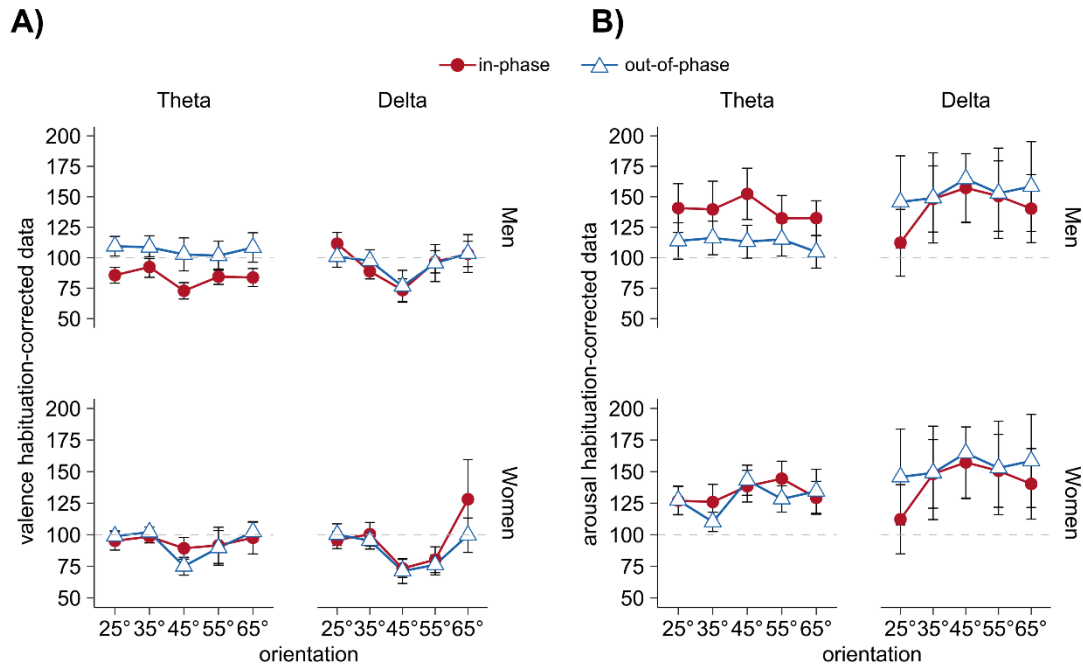
S3 Fig. Discrimination indices for valence ratings.

The discrimination index was computed as the difference between the reinforced 45° orientation (CS+) grating and the average of the four CS–orientations. Data and effect sizes are shown as a Cumming estimation plot (http://www.estimationstats.com). Top row, Swarm plots show the z-standardized discrimination indices per frequency (each dot is the discrimination index of one participant). Group statistics are indicated to the right of each swarm as gapped lines (gap = mean, line length = 1 SD). Bottom row, Effect size estimates (Hedges' *g*, black dots) for the relevant comparisons (in-phase vs out-of-phase within theta and delta frequency) and their 95% confidence interval (CI; vertical error bars). The unpaired Hedge's *g*: for the theta frequency out-of-phase (n = 40) minus theta in-phase (n = 40): 0.11 [95% CI, -0.327, 0.538]; for the delta frequency out-of-phase (n = 40) minus in-phase (n = 40): 0.259 [95% CI, -0.207, 0.665]. The 5000 bootstrap samples were taken for CI estimation; the CI is bias corrected and accelerated.

S4 Fig. Discrimination indices for arousal ratings.

The discrimination index was computed as the difference between the reinforced 45° orientation (CS+) grating and the average of the four CS–orientations. Data and effect sizes are shown as a Cumming estimation plot (http://www.estimationstats.com). Top row, Swarm plots show the z-standardized discrimination indices per frequency (each dot is the discrimination index of one participant). Group statistics are indicated to the right of each swarm as gapped lines (gap = mean, line length = 1 SD). Bottom row, Effect size estimates (Hedges' *g*, black dots) for the relevant comparisons (in-phase vs out-of-phase within theta and delta frequency) and their 95% confidence interval (CI; vertical error bars). The unpaired Hedge's *g*: for the theta frequency our-of-phase (n = 40) minus theta in-phase (n = 40): -0.204 [95% CI, -0.643, 0.24]; for the delta frequency out-of-phase (n = 40) minus in-phase (n = 40): -0.212 [95% CI, -0.639, 0.239]. The 5000 bootstrap samples were taken for CI estimation; the CI is bias corrected and accelerated.

A)

B)

— in-phase   —△— out-of-phase

S5 Fig. **Habituation-corrected valence and arousal data separately for men and women.**

To improve the visualization of the fear generalization pattern for men and women separately, we corrected for the linear trend during habituation, acquisition, and extinction, conducting a habituation correction for valence **(A)** and arousal **(B)** data. Both valence and arousal data show ratings after acquisition for each frequency (theta vs. delta) and synchronization (in-phase vs. out-of-phase), separated by sex: within each subplot, top row shows men (n = 80), bottom row shows women (n = 80). Each data point represents mean, habituation-corrected values for each CS orientation, separately for frequency, synchronization, and sex. Error bars show ±1 SEM.

5　General Discussion

The present thesis aimed at investigating the neurobiological mechanisms underlying aversive learning by measuring and manipulating brain activity using sensory repetitive rhythmic stimulation. In detail, we assessed visuocortical engagement via ssVEPs towards a threat-predictive stimulus and its persistence across the acquisition, extinction, and a 24-hours delayed recall of a fear memory. Further, we used sensory rhythmic stimulation to manipulate the exact timing between the oscillatory phase of the CS and US to examine the causal role of frequency-specificity of phase synchronization (in the theta- and delta band) for the acquisition of a multisensory CS-US association.

In the subsequent sections, I will first summarize and discuss the main findings of visuocortical engagement (via sensory entrained ssVEPs; 5.1.1). Next, our results of directly manipulating the phase synchronization and frequency of the repetitive sensory stimulation are addressed in terms of advantages for the formation of the CS-US association (5.1.2). Lastly, I will discuss some of the main limitations (5.1.3) of our studies and derive outstanding questions that are of interest for future studies (5.1.4).

5.1　Summary and discussion of the main findings

5.1.1　Visuocortical engagement in fear conditioning and its persistence over time

The visual cortex is affected by plastic changes when the organism encounters stimuli that are associated with threats. In a previous study, visuocortical tuning was found to rapidly develop during fear acquisition and to decline during extinction (McTeague et al., 2015), revealing a sensitivity of early-processing visual cortex areas to emotional learning While this study did not account for potential consolidation effects that might result in a return-of-fear in delayed recall, there is first evidence of one human fMRI study, suggesting persistent conditioned-related cortical activity after auditory fear conditioning (Apergis-Schoute et al., 2014). Study 1 of the current thesis thus wanted to close the gap for visual processing, probing the persistence of early sensory activity in the visual system. To guarantee the involvement of early activity, we utilized an EEG-measure with its high temporal resolution to assess ssVEPs in a fear conditioning procedure including fear acquisition, extinction, and a 24-hour delayed recall.

The excellent signal-to-noise ratio of ssVEPs allowed the investigation of dynamic changes of visuocortical activity on a trial-by-trial basis. In accordance with McTeague et al. (2015), we revealed a *rapid development* of *visuocortical tuning* towards the threat-predictive CS+ at the occipital pole that extinguished almost instantly during extinction learning on day 1. During recall on day 2, however, occipital activity briefly re-emerged with a tuning towards the CS+ grating and suppressed activity towards the neighboring CS-. Intriguingly, explorative analysis of overall cortical activity during the 24-hour delayed revealed even more pronounced and longer lasting re-tuning across the lateral temporo-occipital cortex- again - despite diminished responses throughout extinction on day 1. Resembling a pattern of lateral inhibition, visuocortical activity was strongest for the CS+ and decreased towards most similar CS-.

In accordance with findings for the auditory cortex in rats which revealed that older memories recruit other sets of neurons than newly acquired memories (Cambiaghi, Grosso, Likhtik, et al., 2016; Cambiaghi, Grosso, Renna, & Sacchetti, 2016), the 24-hour consolidation period might result in a redistribution of the engaged cortical areas (i.e., occipital vs. temporo-occipital). In contrast to the activation in occipital and specifically the temporo-occipital cortex, after the 24-hour consolidation interval skin conductance responses, as a valid measure of physiological arousal (Lonsdorf et al., 2017), showed marginally and diffuse increases at the very beginning of the delayed recall on day 2 only. Interestingly, the physiological arousal declined before the re-tuning was evident in the cortical areas.

Our findings of visuocortical engagement during acquisition and extinction replicated the previous findings of McTeague et al. (2015). However, for the first time we found evidence for sustained threat processing in electrophysiological EEG measures in early visual cortices without inevitably prompting peripheral physiological threat responses. This suggests that visuocortical activity might prepare the organism for fast re-learning in case the respective stimulus changes its affective value in the future.

While we specifically focused on the very early visual processing by assessing ssVEPs which are known to reflect activity within the first 500 ms (Miskovic & Keil, 2012), a recent study supported our findings of persistent activity in the later stage of visual processing (Panitz et al., 2019). The authors examined the suppression of oscillatory alpha power as an indicator for increased excitability in the visual cortex in a differential fear conditioning paradigm that also included a delayed recall 24 hours after acquisition. They found alpha suppression during recall on day 2,

probably reflecting sustained prioritization of the threat-predictive CS+ and indicating an increased attentional demand. Interestingly, the suppression occurred independent if the CS+ was subject to extinction on day 1 or not (i.e., non-extinguished CS+). Therefore, the data rather show a return-of-fear phenomenon than sustained activity throughout extinction, which is in line with our findings. Thus, visuocortical tuning to threat-predictive features seems to be particularly resistant to fear extinction.

Given that the organism has limited capacities to process information, mechanisms that help us to selectively attend to threat-related stimuli seem to be beneficial. Persistent prioritized processing in the visual cortex was previously related to increase the efficiency and speed to successfully detect threat-related stimuli (Anderson, 2005; Öhman et al., 2001). However, the *return-of-fear in sensory cortices* of Study 1 that was also suggested by others (Apergis-Schoute et al., 2014; Panitz et al., 2019), is a re-emergence of conditioned fear that might also be maladaptive and related to a number of phenomena observed in clinical samples.

Our results thus include several important clinical implications. Concretely, one of the hallmark symptoms of PTSD encompasses intrusive memories that can be triggered by external or internal cues and lead to *flashbacks* that, interestingly, are often *visually-driven* (Iyadurai et al., 2019; Sündermann et al., 2013). In addition, PTSD patients were repeatedly shown to experience attentional biases towards threat stimuli and additionally exhibit increased detection of threat-related cues. This was linked to increased responding of the visual cortex (for reviews see Bomyea et al., 2017; Kleim et al., 2012; Shvil et al., 2013; Todd et al., 2015). Activation of early visual cortices was also assumed to be involved in the development of such vivid mental images (Pearson et al., 2015) probably due to a *lack* of contextualization of single cues to their given environment (Brewin & Burgess, 2014; Meyer et al., 2017). Interestingly, a recent study specifically focused on inhibiting the lower-tier visual cortex using repetitive TMS in healthy individuals (Herz et al., 2022). Participants were confronted with trauma-related visual scenes to examine the effect of inhibition on intrusive memories on days that followed memory reactivation. The authors revealed decreased emotional intensity of visual intrusions after inhibition of the lower-tier visual cortex (compared to control stimulation), suggesting that long-term activation of visual processing might contribute to the development of intrusive memories (Herz et al., 2022).

In sum, the findings of Study 1 support *dynamic changes in activation of lower-tier visual cortex towards fear conditioned stimuli*, induced by *rhythmic visual stimulations* that elicit ssVEPs.

Importantly, persisting increases of activity in early visual processing after extinction and a 24-hour consolidation supports the involvement of distributed networks like the sensory systems in the formation of *long-term fear memories*. Given that psychiatric disorders related to trauma and stress (like PTSD) typically suffer from intrusive memories that can be triggered by (visual) cues, often lacking contextualization, and exhibit attentional biases towards threat-cues, there should be a greater focus on potentially sustained differences in sensory processing that might contribute to these main symptoms and can be assessed by ssVEPs.

5.1.2 The causal role of phase synchronization in frequency-modulated CS and US for fear acquisition

In Study 1, we used rhythmically modulated visual CS presentations to induce ssVEPs as a measure for early visuocortical activity. Under the premise that ssVEPs represent an entrained neuronal oscillation that continue after the external stimulation ended (Halbleib et al., 2012), the use of ssVEPs opens the opportunity to directly affect cognitive processes that are related to a specific frequency (Herrmann et al., 2016). Based on previous findings that indicate an important role of theta oscillations, and specifically, theta phase synchronization within the fear network, Study 2 and Study 3 extended the single-modality visual (CS) rhythmic stimulation *to stimulation of both visual (CS) and auditory (US) cortex* in a theta band. Importantly, we additionally modulated the phase relation between CS and US to directly assess the *causal role of theta phase synchronization* (vs. asynchronization) for fear conditioning during acquisition, extinction, and a delayed recall 24 hours later. To additionally test for the theta-frequency specificity of phase synchronization, Study 3 included synchronization (vs. asynchronization) in a theta as well as delta (1.7 Hz). In contrast to the laboratory Study 2 covering two consecutive days, Study 3 was (1) a web-based fear conditioning paradigm and (2) restricted to habituation, fear acquisition, and extinction phase, thus covered only day 1.

To get an extensive insight in the various facets of fear conditioning responses, we assessed physiological arousal (skin conductance), affective ratings of valence and arousal, US-expectancy ratings, i.e., CS-US contingency, and visuocortical engagement via ssVEPs in Study 2[4].

---

[4] Note that the web-based approach of Study 3 only allowed the collection of rating data, hence only included subjective valence and arousal ratings as well as US-expectancy ratings.

Remarkably, synchronized (vs. asynchronized) CS-US presentation augmented the discrimination of the CS+ and most similar CS- gratings in subjective valence and arousal ratings as well as in the US-expectancy ratings right after acquisition. In contrast, skin conductance responses as well as visuocortical engagement (ssVEPs) were unaffected by the specific phase modulation between CS and US during acquisition. Although ssVEPs did not differ between in-phase and out-of-phase, we were able to confirm the visuocortical tuning towards the CS+. On day 2, however, we did not replicate the re-occurrence in the tuning pattern that was found in Study 1. Nonetheless, the phase-synchronization resulted in generally higher ssVEP-power compared with phase-asynchronization, suggesting that synchronized CS-US presentation led to stronger engagement of the early visual processing. In concern of the missing re-tuning on day 2, it is important to note, that the re-emergence in Study 1 became evident on a trial-by-trial basis only. However, due to the shifted focus towards differences between rhythmic in-phase vs. out-of-phase CS-US presentation in Study 2, we only addressed activity for the whole learning phases.

A possible explanation for the discrepancy between the fear measures in Study 2 (valence, arousal and US-expectancy on the one hand vs. peripheral-physiological measures and visuocortical engagement on the other hand) might lie on the activation of different types of memories. Although fear conditioning is typically assigned to implicit memory, it often includes both implicit and explicit aspects (Bechara et al., 1995; Boddez et al., 2013; Knight et al., 2003). Skin conductance responses – as a measure for physiological arousal – are thought to reflect implicit aspects of the fear memory (Christopoulos et al., 2019; Knight et al., 2003, 2006; but see also Lovibond & Shanks, 2002; Sevenster et al., 2014) while the knowledge of the CS-US contingency is specifically assigned to declarative memory (Boddez et al., 2013). Importantly, the allocations to the different memory systems are accompanied by the supposed involvement of different brain structures: skin conductance responses were related to amygdala activity, the processing of the declarative nature of US-expectancy ratings is predominantly assigned to the hippocampus (Bechara et al., 1995). Following the assumption that the sensory entrainment is not restricted to early sensory processing but also affects deeper brain structures involved in higher-order processes like memory (e.g., the hippocampus or the amygdala), we cautiously speculate that our entrainment acted differently in the two systems: theta-phase synchronization may have helped binding the visual CS and auditory US within the hippocampus (Clouter et al., 2017), without influencing the affective conditioning comprising the amygdala.

Consequently, precise phase-synchronization between CS and US inputs might either play a minor role for fear encoding, or the propagation of CS and US information to the amygdala requires a different timing than implemented in our study. The latter assumption is specifically based on two separate routes (subcortical or "low road" versus cortical or "high road") the sensory information follows to reach the amygdala (Silverstein & Ingvar, 2015). Considering that we used a global theta-synchronized input without the ability to specify the exact way of propagation, the timing might have been insufficient to initiate synchronization within the amygdala. Further, because of the relatively long CS–US overlap of 2 s, we additionally cannot rule out that our synchronized stimulation reached the amygdala via the thalamic route first, but then also via cortical routes, leading to cancellation of the first CS–US phase synchronization, hence minimizing the suggested effects. Since the EEG measure that was used in our study is not suitable to assess potential mechanisms in deeper brain structures, the underlying mechanism needs to be investigated in the future.

In sum, Study 2 provided the first *causal* evidence for the involvement of theta-phase synchronization in the acquisition of fear. Importantly, the effects of synchronization depended on the concrete measure of fear: While phase-synchronization augmented the discrimination of the CS+ and most similar CS- gratings in the US-expectancy ratings and subjective ratings of valence and arousal, it did not change the tunings towards the CS+ in the ssVEP-power or the generalization in the skin conductance responses.

One of the main limitations of Study 2 concerns the missing evidence of a specificity of the theta frequency to "bind" the CS-US association memory, since we did not include a control frequency like a slow delta or faster alpha, beta, or gamma frequency. In the study of Clouter et al. (2017), the effect of improved declarative video-tone association memory was only supported in the theta frequency, but not in delta (1.7 Hz) or alpha (10.5 Hz) frequency, suggesting that the improved association is specific for the memory-relevant theta band. To extend this finding for aversive fear conditioning, we tested the effects of phase-synchronization in an additional slow delta frequency (1.7 Hz) in Study 3.

Due to the COVID-19 pandemic and the accompanying contact restriction, we decided to use a novel web-based fear conditioning paradigm (see Björkstrand et al., 2022; Stegmann et al., 2021 for further examples). Due to the restrictions of an online setting – and importantly – due to the findings of Study 2, we focused on the assessment of the subjective ratings of valence and arousal

as well as the US-expectancies. Additionally, we tested for theta frequency-specificity of the previous effects, including a second delta stimulation. To enable the induction of fear via an aversive US in a web-based approach, we applied an audio titration task in the beginning of the fear conditioning.

Comparing theta and delta did not support our prediction that the improvement of fear acquisition after phase synchronization is specific to the theta range. Instead, participants *of both frequency groups* showed overall higher US-expectancy ratings after asynchronous presentation (compared with synchronous CS-US). However, as expected, it also occurred towards the CS- gratings and therefore resembled the hypothesized broader generalization already seen in Study 2. The affective ratings of valence and arousal, in contrast, were not affected by the modulation of phase synchronization (and also not to frequency). Thus, they might have been less sensitive for subtle differences in phase-synchronization due to a reduced aversiveness of the US in the online study where loudness was obtained via individual titration. In contrast, in the laboratory Study 2, a constant white noise of 96.5 dB(A) without any titration procedure was used for each participant. Therefore, the US most likely more aversive in Study 2. Accordingly, exploratory comparison of US ratings between both studies revealed slightly lower arousal and unpleasantness in the web-based study after acquisition. For the declarative US-expectancies, however, the different aversiveness ratings seemed to have no effect as observable in the improved discrimination of the CS+ and most similar CS- gratings.

In explorative analysis, we additionally tested for potential differences between men and women of our sample. Interestingly, it revealed discrimination improvements after synchronized input in theta, but not delta only in men. Women, in contrast, showed broad generalization independently of the phase-synchronization condition. Hence, differences between sex or sex hormones like estradiol might affect the receptivity to modulations in phase synchronization that manifest in different generalization patterns.

Contrary to our hypothesis of a synchronization effect that is specific for the theta-frequency and in some contrast to the overwhelming evidence suggesting a special role for theta phase synchronization as an epiphenomenon of memory, our findings in the web-based study lead to the (cautious) assumption that phase synchronization in low frequencies in general rather than only theta are beneficial for discrimination a CS+ from CS- in fear conditioning. However, replicating

the effect of delta in a highly controllable laboratory setting is needed to increase its internal validity.

Importantly, this assumption is in line with recent findings from a laboratory study, suggesting that low frequency entrainment (i.e., in the delta and theta range) provides optimized windows for memory-enhancing effects (Hickey & Race, 2021). For example, greater entrainment in a delta frequency (1.25 Hz) during memory encoding predicted the recall in a subsequent memory task (Hickey, Merseal, et al., 2020). In addition, addressing memory-improving effects of phase synchronization (vs. out-of-phase presentation) in delta, provides interesting evidence: Improved memory recognition was found for items that were presented rhythmically (fixed inter-trial-intervals) compared with arrhythmically (variable inter-trial-intervals) (Jones & Ward, 2019) and for visual targets that occurred "on-beat" (compared with "off-beat") with an auditory stimulus. This also suggests the important role of synchronization in cross-modal memories (Johndro et al., 2019). In line with our findings, these studies suggest that the brain might use external rhythms at slow frequencies to coordinate its neural activity that helps improving memory encoding.

In Study 2, our results emphasized memory-enhancing effects after phase-synchronized (vs. asynchronized) CS-US input in the theta frequency. In correspondence with Clouter et al. (2017), we assumed that these findings are supportive to the idea that the formation of multimodal associations is specifically improved by entrainment in the theta-frequency – an important indicator within the (fear) memory circuitry (Çalışkan & Stork, 2018; Lesting et al., 2013; Likhtik et al., 2014; Seidenbecher et al., 2003; Taub et al., 2018). However, considering our findings of Study 3 and other results for episodic memory (e.g., Hickey, Barnett-Young, et al., 2020; Hickey, Merseal, et al., 2020; Hickey & Race, 2021; Johndro et al., 2019; Jones & Ward, 2019), the effects might not be restricted to theta-frequency. Instead, augmented discriminations in our fear conditioning paradigm might rather rely on coordinated neural activity via slow-rhythmic (i.e., delta-theta range) than theta-specific entrainment. One possible mechanism by which the slow oscillations might improve higher-order cognition (e.g., memory) is the well-established cross-frequency phase-amplitude coupling that describes the coordination of fast oscillatory activity (e.g. gamma) by the oscillatory phase of slow (delta or theta) rhythms and was repeatedly related to memory processing (Daume et al., 2017; Fell & Axmacher, 2011; e.g., Friese et al., 2013; Hickey & Race, 2021; Köster et al., 2018; Köster et al., 2019; Lega et al., 2016).

In sum, our results include first evidence for the notion that low-frequency rather than theta-specific phase synchronization (vs. asynchronization) between a visual CS and auditory US augments the encoding of the declarative knowledge of the CS-US contingency in a laboratory as well as web-based fear conditioning paradigm. Additionally, phase synchronization-dependent differences in the subjective ratings of valence and arousal were only observed in the laboratory approach, using entrainment in a theta band. Therefore, clarification is needed for the discrepancy in subjective valence and arousal ratings between the laboratory and the web-based study.

5.2 Limitations

In the above section, I already described the strengths of our studies and their contribution to the field of aversive learning. However, in the following, I will present a number of limitations of the studies that might encourage new investigations in the future.

In each of the three human studies, we used *simple Gabor gratings as CS* that only differed in orientation. The simple stimuli allowed us to take advantage of the orientation selectivity within the primary visual cortex, measuring early visuocortical tuning via ssVEPs in Study 1 and Study 2. On the other hand, however, the use of simple gratings lacks ecological validity which limits the transfer of our findings to the complexity of the 'real world'. Evidence for the capability of inducing rhythmicity for (declarative) memory improvements with more complex stimuli comes from Clouter et al. (2017) and Wang et al. (2018), who used short frequency-modulated video-clips. Similarly, Köster et al. (2019) presented object pictures for the induction of ssVEPs. These findings should be considered to investigate more complex stimulus material in the area of fear conditioning.

One limitation that generally comes with the induction of ssVEPs, is that rhythmically presented stimuli evoke brain responses in the externally given frequency. While this method has obvious advantages in directly modulating cortical activity, it impedes the distinction between the *exogenously induced rhythmic responses and endogenous brain oscillations* that might have important implications themselves. In addition to putative confounds in the evoked frequency itself (e.g., for theta: 4 Hz), neural entrainment is often observable in the frequency harmonics (i.e., 8 Hz, 12 Hz, 16 Hz, etc.), therefore affecting various frequency bands at the same time (Zhou et al., 2016). Additionally, there is an ongoing debate if rhythmic sensory stimulation is capable of

entraining neural oscillations or reflects repetitive evoked potentials (Capilla et al., 2011; Ding & Simon, 2014; Zhou et al., 2016). Despite this debate, the vast majority of SSR-studies assumes that rhythmicity functions as generator for oscillatory activity without discussing the consequences if this would not be the case (Zoefel et al., 2018). In an extensive review, Zoefel et al. (2018) discussed the opposing evidence for both theories with the majority pointing towards the induction of neural oscillations instead of simply evoking repetitive responses. For example, oscillatory activation aligned to the frequency of external stimulation was even observed after the stimulus offset which clearly speaks for the *induction of entrained oscillations* rather than a stimulus-evoked response (Halbleib et al., 2012; Lakatos et al., 2013). Distinguishing both mechanisms might improve the understanding of entrained rhythmic activity and open further options for the use of rhythmic sensory stimulation.

An additional limitation specifically concerns the fear conditioning protocol of Study 1 and Study 2, where we included a 24-hour delayed recall to assess different fear measures over time. As described in the introduction of the current thesis, fear conditioning includes two distinct memories that coexist: The first memory trace is defined by the CS-US association, formed during fear acquisition (i.e., *fear memory* trace). The second trace is formed after the CS is repeatedly presented without the aversive US. This *extinction memory* consists of a CS-noUS association and is assumed to act in concurrence to the CS-US fear association (Maren & Quirk, 2004; Milad & Quirk, 2012). Both coexisting memories are subject to separate consolidation processes that can be assessed by including a delayed fear and/or extinction recall (Bierwirth et al., 2021; Mueller et al., 2014; Orsini & Maren, 2012; Quirk & Mueller, 2008; Sperl et al., 2019). Since our studies included only one CS+ that was subjected to extinction on day 1, the delayed recall on day 2 included mixed information of both, the fear and extinction memory trace. Therefore, our data do not allow a clear distinction of both memories which might provide interesting insights into the mere fear or extinction memory trace. Especially in Study 2, where the modulation of theta-phase synchronization took place during fear acquisition only, the consolidation and recall of the fear memory without confounds of extinction might have interesting implications for the persistence of phase synchronization. As a consequence, future studies might use so called *multi cue protocols,* including more than one CS+ that are either extinguished or not extinguished (Lonsdorf et al., 2017). This protocol has the advantage of a clear distinction of fear and extinction recall, allowing to draw conclusions for each memory trace separately.

One important limitation of Study 2 and Study 3 is the missing evidence concerning the brain structures that are affected by the frequency-modulated phase synchronization. In Study 2 phase-synchronization effects differed in dependence of the observed fear measure. In detail, skin conductance responses that are typically described as amygdala dependent (e.g., Christopoulos et al., 2019; Lovibond & Shanks, 2002), did not respond differently to theta-phase synchronous vs. asynchronous the CS-US presentation. In contrast, the declarative knowledge of CS-US contingency which is assumed to involve hippocampus activity (Bechara et al., 1995; Boddez et al., 2013), revealed augmented discrimination of the CS+ and the most similar CS- gratings. Therefore, one might speculate that the hippocampus might specifically benefit from entrained low-frequency phase synchronization, while the precise timing plays a less important role for the CS-US convergence within the amygdala. Future studies using invasive techniques in humans (e.g., intracranial EEG measures) or animal models should address the role of low-frequency phase synchronization has within and between specific brain structures to resolve how entrainment dynamically affects neuronal activity and brain structures.

5.3 Future perspectives

The current thesis provides new perspectives regarding the advantages of rhythmic sensory stimulation for the investigation of fear memory processing.

Study 1 revealed re-emerged visuocortical activity towards recently fear-associated stimuli when measured after 24-hours. Regarding the clinical importance, sustained visuocortical engagement with the potential to biases perception or attention were found in patients suffering from anxiety or trauma-related disorders. The used consolidation interval of 24-hours in Study 1 is rather insufficient and might not capture all of the processes that are subject to consolidation over time (Roesler & McGaugh, 2010). Therefore, futures studies should consider longer intervals when assessing delayed fear- and/or extinction recall phases. Additionally, persistent changes in neural activity after encountering a threat were previously associated with differences in behavior like attentional biases (e.g., Kleim et al., 2012). However, we did not account for the behavioral impact the examined tunings might have. Specific attention-related tasks like the *attentional blink* (Keil et al., 2006; McHugo et al., 2013; Smith et al., 2006) would clarify the potential behavioral

importance of early visuocortical tunings within fear conditioning that interestingly, returned in the absence of other fear measures like the skin conductance response.

In our human studies (Study 1-3), we used a generalization paradigm including one CS+ that was paired with US and other (6 [Study 1] or 4 [Study 2 and 3]), very similar CS- that had to be distinguished from the CS+. Since our results were reflected in augmented discriminations of the CS+ and most similar CS- gratings, future studies might want to untangle the effects of phase synchronization on either the ability to discriminate between similar stimuli or forming the actual CS-US association. A recent study highlighted the role of theta phase synchronization between the amygdala and hippocampus for the discrimination of emotional stimuli as measured with intracranial EEG in a cohort of epileptic patients (Zheng et al., 2019). Interestingly, they found that the successful discrimination was accompanied by theta synchronization between both structures, while increased alpha activity was related to discrimination errors. Therefore, testing if phase-synchronization in an alpha frequency impairs the discrimination of the CS+ and most similar CS-gratings might help in collecting further evidence of the actual role of phase synchronization.

After conducting Study 2 and Study 3, we declared that the differences we found for phase-synchronized vs. asynchronized CS-US presentation seem to rely on low-frequency (≤ 4 Hz) rather than on theta-frequency specific stimulation. To enhance the internal validity of these findings, we, first of all, recommend replicating the memory-improving effects of delta *and* theta-dependent phase-synchronization in a strictly controllable laboratory setting. Additionally, so far, we did not include entrainment in fast frequencies like in a beta or gamma range, due to challenges regarding the requirement of precisely timed CS and US in the web-based fear conditioning study. Especially gamma frequencies might be of interest, since these fast oscillations are not only related to memory processing per se but were additionally found to be involved in binding processes of object features (e.g., Elliott & Müller, 1998; Fell & Axmacher, 2011; Gray et al., 1989). Testing phase synchronized entrainment in fast gamma frequencies compared with the low frequencies might lead to two conclusion: 1) in case fast gamma oscillations fail to improve memory, it supports the suggested notion that low frequency entrainment is specifically suited to coordinate neural activity, 2) if fast gamma synchronization also facilitates memory, it would provide new insights in *frequency-dependent* mechanisms of entrainment in (fear) memory processing that would promote the understanding of the involved oscillatory processes (e.g., due to binding processes). Based on the experiences in our laboratory (Study 1 and Study 2) vs. the web-based fear conditioning

approach (Study 3), we highly recommend investigating fast frequencies in the lab, since it allows a much better control of the stimulus timings. This is specifically important when examining phase synchronization between stimuli, since the cycle length of an oscillatory frequency decreases the faster the tested frequency is. For example, a ¼ cycle that reflects the peak of oscillatory activity at a slow delta (2 Hz) frequency lasts for 500 ms, while in a fast gamma frequency of 30 Hz it only lasts for 8.3 ms. Thus, in the fast frequencies even small shifts in timing (e.g., due to differences in the internet connection or lags of technical devices) have a great impact on the individual phase. Therefore, time-critical approaches like this should be conducted in a controlled laboratory environment.

In Study 3, we found interesting sex differences, with men responding to the modulation of phase synchronization while women did not show any differences between in-phase and out-of-phase stimulation. Importantly, in men we found the expected discrimination improvement after phase-synchronized (compared with phase-asynchronized) CS-US presentation, while women, on the other hand, showed broad generalization patterns in both synchronization conditions. Considering that we accounted for hormonal fluctuations in women by only including those women that took oral contraceptives (with suppressed endogenous estradiol production) and were in their pill-on phase, it would be interesting to additionally account for potential sex differences that, for example, might rely on the fluctuating levels of the *sex hormone estradiol*. Estradiol (more precisely 17β-estradiol) was repeatedly shown as an important modulator of fear- and extinction recall (Antov & Stockhorst, 2014; Bierwirth et al., 2021; Stockhorst & Antov, 2015). Interestingly, in both animals and humans, females with high levels of estradiol and men (able to convert testosterone into estradiol) were found to show better extinction recall compared females with low endogenous estradiol levels (Milad et al., 2009; Milad et al., 2010). Therefore, future studies should address the role of estradiol as a potential factor for the differences we revealed between men and women.

A general restriction that comes with EEG-measures in human is the lack of evidence for subcortical areas. We speculated that our phase-synchronization modulation not only affects cortical areas but propagates to further structure like the hippocampus or the amygdala. Therefore, measures of activity in such regions would provide progress in understanding the non-invasive entrainment of phase-synchronized (vs. asynchronized) rhythms for memory and fear conditioning. Therefore, a combination of external sensory entrainment with invasive measures of amygdala activity (e.g., via intracranial EEG in epileptic patients, see Chen et al., 2021 as an example) would

help with understanding if the "poor men's optogentic" (Hanslmayr et al., 2019) can modulate fear memory engrams (Bocchio et al., 2017) by differently activating structures like the amygdala. Alternatively, simultaneously entraining two sensory modalities (i.e., the CS modality and the US modality), could be conducted within animals, where effects of phase-synchronized rhythmic sensory stimulation onto structures like the hippocampus or the amygdala were, to the best of my knowledge, not assessed so far.

In an interesting approach, Johansen et al. (2010) paired auditory CSs with optogenetically activated pyramidal neurons in the lateral amygdala as a substitute for an aversive US. Similarly, rhythmically presented CS and US in different frequencies and measuring the synaptic changes within the given neurons in the lateral amygdala should reveal if the external rhythms propagate to the amygdala. In addition, using various frequency-stimulations of sensory neurons within amygdala slices *in vitro* would allow to measure the effects on LTP or LTD (Nabavi et al., 2014). Synaptic plasticity in the form of LTP or LTD is most extensively examined in rodent hippocampus slices. For example, in a pilot study that was also developed and conducted as part of the profile line P3: "Human – Brain – Computer – Interactions" at the University of Osnabrück, we examined theta-burst induced LTP under pharmacological influence of insulin (vs. placebo) in hippocampal slices of mice that differed in their glucocorticoid-mediated reactivity to stress[5]. First evidence revealed that the administration of insulin has memory improving effects in rodents (Park et al., 2000; Zhao et al., 1999) and humans (Benedict et al., 2004; Hallschmid, 2021). Interestingly, a recent study revealed that intranasal insulin in humans conducting a 3-day fear conditioning paradigm, improved extinction (Ferreira de Sá et al., 2020). Therefore, in a next step, examining the effects of pharmacological modulations on the formation of fear memory engrams - besides those that are typically related to fear learning (e.g., glutamate) - should be considered. Insulin with its suggested memory-restoring effects might provide a good starting point.

In sum, investigating the effects of entrainment in behavioral and cognitive components in the living organism in combination with electrophysiological and pharmacological measures in vitro, would provide an important impact on our understanding of the development, maintenance and retrieval of aversive memories.

---

[5]Since the implementation of this pilot project would leave the scope of this thesis, preliminary analyses are not included here.

5.4 Conclusion

Causally modulating brain activity was for a long time restricted to animal work and a few clinical samples with intracranial electrodes (e.g., epileptic patients). Rhythmic sensory stimulation is a promising approach to directly manipulate oscillatory brain activity in humans and measure its outcome in behavior and cognition. In the current thesis, rhythmic visual stimulation (via flickering Gabor gratings) enabled the assessment of dynamical responding of visuocortical engagement in fear learning and provided evidence for persistent visuocortical tuning towards threat predictive stimuli. Sustained sensory activation might have important clinical implications, considering biases in perception and attention that are related to anxiety- and trauma-related disorders. Further, using rhythmic visual *and* auditory stimulation to manipulate the precise phase shift between the to-be-associated CS and US in low frequencies (rather than theta only) augmented the ability to discriminate similar stimuli in a generalization procedure. Both, discriminating threat from safety as well as prioritizing cues that were recently associated with danger, are important mechanisms of adaptive behavior as a result of certain experiences. Therefore, the current thesis advances the neurobiological understanding of adaptive threat responding, using direct modulations of rhythmic brain activity in humans.

References

Alford, S., Frenguelli, B. G., Schofield, J. G., & Collingridge, G. L. (1993). Characterization of Ca2+ signals induced in hippocampal CA1 neurones by the synaptic activation of NMDA receptors. *The Journal of Physiology*, *469*, 693–716. https://doi.org/10.1113/jphysiol.1993.sp019838

Anagnostaras, S. G., Wood, S. C., Shuman, T., Cai, D. J., Leduc, A. D., Zurn, K. R., Zurn, J. B., Sage, J. R., & Herrera, G. M. (2010). Automated assessment of pavlovian conditioned freezing and shock reactivity in mice using the video freeze system. *Frontiers in Behavioral Neuroscience*, *4*. https://doi.org/10.3389/fnbeh.2010.00158

Anderson, A. K. (2005). Affective influences on the attentional dynamics supporting awareness. *Journal of Experimental Psychology: General*, *134*(2), 258–281. https://doi.org/10.1037/0096-3445.134.2.258

Antov, M. I., Plog, E., Bierwirth, P., Keil, A., & Stockhorst, U. (2020). Visuocortical tuning to a threat-related feature persists after extinction and consolidation of conditioned fear. *Scientific Reports*, *10*(1), 3926. https://doi.org/10.1038/s41598-020-60597-z.

Antov, M. I., & Stockhorst, U. (2014). Stress exposure prior to fear acquisition interacts with estradiol status to alter recall of fear extinction in humans. *Psychoneuroendocrinology*, *49*, 106–118. https://doi.org/10.1016/j.psyneuen.2014.06.022

Apergis-Schoute, A. M., Schiller, D., LeDoux, J. E., & Phelps, E. A. (2014). Extinction resistant changes in the human auditory association cortex following threat learning. *Neurobiology of Learning and Memory*, *113*, 109–114. https://doi.org/10.1016/j.nlm.2014.01.016

Arnulfo, G., Wang, S. H., Myrov, V., Toselli, B., Hirvonen, J., Fato, M. M., Nobili, L., Cardinale, F., Rubino, A., Zhigalov, A., Palva, S., & Palva, J. M. (2020). Long-range phase synchronization of high-frequency oscillations in human cortex. *Nature Communications*, *11*(1), 5363. https://doi.org/10.1038/s41467-020-18975-8

Bakin, J. S., & Weinberger, N. M. (1990). Classical conditioning induces CS-specific receptive field plasticity in the auditory cortex of the guinea pig. *Brain Research*, *536*(1-2), 271–286. https://doi.org/10.1016/0006-8993(90)90035-A

Barot, S. K., Kyono, Y., Clark, E. W., & Bernstein, I. L. (2008). Visualizing stimulus convergence in amygdala neurons during associative learning. *Proceedings of the National Academy of*

Sciences of the United States of America, *105*(52), 20959–20963. https://doi.org/10.1073/pnas.0808996106

Bauer, E. P., Schafe, G. E., & LeDoux, J. E. (2002). NMDA receptors and l-type voltage-gated calcium channels contribute to long-term potentiation and different components of fear memory formation in the lateral amygdala. *The Journal of Neuroscience*, *22*(12), 5239–5249. https://doi.org/10.1523/JNEUROSCI.22-12-05239.2002

Bechara, A., Tranel, D., Damasio, H., Adolphs, R., Rockland, C., & Damasio, A. R. (1995). Double dissociation of conditioning and declarative knowledge relative to the amygdala and hippocampus in humans. *Science*, *269*(5227), 1115–1118. https://doi.org/10.1126/science.7652558

Becher, A.-K., Höhne, M., Axmacher, N., Chaieb, L., Elger, C. E., & Fell, J. (2015). Intracranial electroencephalography power and phase synchronization changes during monaural and binaural beat stimulation. *The European Journal of Neuroscience*, *41*(2), 254–263. https://doi.org/10.1111/ejn.12760

Benchenane, K., Peyrache, A., Khamassi, M., Tierney, P. L., Gioanni, Y., Battaglia, F. P., & Wiener, S. I. (2010). Coherent theta oscillations and reorganization of spike timing in the hippocampal- prefrontal network upon learning. *Neuron*, *66*(6), 921–936. https://doi.org/10.1016/j.neuron.2010.05.013

Benedict, C., Hallschmid, M., Hatke, A., Schultes, B., Fehm, H. L., Born, J., & Kern, W. (2004). Intranasal insulin improves memory in humans. *Psychoneuroendocrinology*, *29*(10), 1326–1334. https://doi.org/10.1016/j.psyneuen.2004.04.003

Bhattarai, J. P., Schreck, M., Moberly, A. H., Luo, W., & Ma, M. (2020). Aversive learning increases release probability of olfactory sensory neurons. *Current Biology: CB*, *30*(1), 31-41.e3. https://doi.org/10.1016/j.cub.2019.11.006

Bierwirth, P., Sperl, M. F. J., Antov, M. I., & Stockhorst, U. (2021). Prefrontal theta oscillations are modulated by estradiol status during fear recall and extinction recall. *Biological Psychiatry. Cognitive Neuroscience and Neuroimaging*, *6*(11), 1071–1080. https://doi.org/10.1016/j.bpsc.2021.02.011

Björkstrand, J., Pine, D. S., & Frick, A. (2022). Evaluating an internet-delivered fear conditioning and extinction protocol using response times and affective ratings. *Scientific Reports*, *12*(1), 4014. https://doi.org/10.1038/s41598-022-07999-3

Blair, H. T., Schafe, G. E., Bauer, E. P., Rodrigues, S. M., & LeDoux, J. E. (2001). Synaptic plasticity in the lateral amygdala: A cellular hypothesis of fear conditioning. *Learning & Memory (Cold Spring Harbor, N.Y.)*, *8*(5), 229–242. https://doi.org/10.1101/lm.30901

Bliss, T. V., Collingridge, G. L., Morris, R. G., & Reymann, K. G. (2018). Long-term potentiation in the hippocampus: discovery, mechanisms and function. *Neuroforum*, *24*(3), A103-A120. https://doi.org/10.1515/nf-2017-A059

Bliss, T. V., & Lomo, T. (1973). Long-lasting potentiation of synaptic transmission in the dentate area of the anaesthetized rabbit following stimulation of the perforant path. *The Journal of Physiology*, *232*(2), 331–356. https://doi.org/10.1113/jphysiol.1973.sp010273

Bocchio, M., Nabavi, S., & Capogna, M. (2017). Synaptic plasticity, engrams, and network oscillations in amygdala circuits for storage and retrieval of emotional memories. *Neuron*, *94*(4), 731–743. https://doi.org/10.1016/j.neuron.2017.03.022

Boddez, Y., Baeyens, F., Luyten, L., Vansteenwegen, D., Hermans, D., & Beckers, T. (2013). Rating data are underrated: Validity of US expectancy in human fear conditioning. *Journal of Behavior Therapy and Experimental Psychiatry*, *44*(2), 201–206. https://doi.org/10.1016/j.jbtep.2012.08.003

Bolles, R. C. (1970). Species-specific defense reactions and avoidance learning. *Psychological Review*, *77*(1), 32–48. https://doi.org/10.1037/h0028589

Bomyea, J., Johnson, A., & Lang, A. J. (2017). Information processing in PTSD: evidence for biased attentional, interpretation, and memory processes. *Psychopathology Review*, *a4*(3), 218–243. https://doi.org/10.5127/pr.037214

Boucsein, W., Fowles, D. C., Grimnes, S., Ben-Shakhar, G., roth, W. T., Dawson, M. E., & Filion, D. L. (2012). Publication recommendations for electrodermal measurements. *Psychophysiology*, *49*(8), 1017–1034. https://doi.org/10.1111/j.1469-8986.2012.01384.x

Bouton, M. E., Maren, S., & McNally, G. P. (2021). Behavioral and neurobiological mechanisms of pavlovian and instrumental extinction learning. *Physiological Reviews*, *101*(2), 611–681. https://doi.org/10.1152/physrev.00016.2020

Bouton, M. E., & Moody, E. W. (2004). Memory processes in classical conditioning. *Neuroscience & Biobehavioral Reviews*, *28*(7), 663–674. https://doi.org/10.1016/j.neubiorev.2004.09.001

Bradley, M. M., & Lang, P. J. (1994). Measuring emotion: The self-assessment manikin and the semantic differential. *Journal of Behavior Therapy and Experimental Psychiatry*, *25*(1), 49–59. https://doi.org/10.1016/0005-7916(94)90063-9

Brewin, C. R., & Burgess, N. (2014). Contextualisation in the revised dual representation theory of PTSD: A response to Pearson and colleagues. *Journal of Behavior Therapy and Experimental Psychiatry*, *45*(1), 217–219. https://doi.org/10.1016/j.jbtep.2013.07.011

Çalışkan, G., & Stork, O. (2018). Hippocampal network oscillations as mediators of behavioural metaplasticity: Insights from emotional learning. *Neurobiology of Learning and Memory*, *154*, 37–53. https://doi.org/10.1016/j.nlm.2018.02.022

Cambiaghi, M., Grosso, A., Likhtik, E., Mazziotti, R., Concina, G., Renna, A., Sacco, T., Gordon, J. A., & Sacchetti, B. (2016). Higher-order sensory cortex drives basolateral amygdala activity during the recall of remote, but not recently learned fearful memories. *The Journal of Neuroscience*, *36*(5), 1647–1659. https://doi.org/10.1523/JNEUROSCI.2351-15.2016

Cambiaghi, M., Grosso, A., Renna, A., & Sacchetti, B. (2016). Differential recruitment of auditory cortices in the consolidation of recent auditory fearful memories. *The Journal of Neuroscience*, *36*(33), 8586–8597. https://doi.org/10.1523/JNEUROSCI.0561-16.2016

Capilla, A., Pazo-Alvarez, P., Darriba, A., Campo, P., & Gross, J. (2011). Steady-state visual evoked potentials can be explained by temporal superposition of transient event-related responses. *PloS One*, *6*(1), e14543. https://doi.org/10.1371/journal.pone.0014543

Chen, S., Tan, Z., Xia, W., Gomes, C. A., Zhang, X., Zhou, W., Liang, S., Axmacher, N., & Wang, L. (2021). Theta oscillations synchronize human medial prefrontal cortex and amygdala during fear learning. *Science Advances*, *7*(34). https://doi.org/10.1126/sciadv.abf4198

Christopoulos, G. I., Uy, M. A., & Yap, W. J. (2019). The body and the brain: Measuring skin conductance responses to understand the emotional experience. *Organizational Research Methods*, *22*(1), 394–420. https://doi.org/10.1177/1094428116681073

Clouter, A., Shapiro, K. L., & Hanslmayr, S. (2017). Theta phase synchronization is the glue that binds human associative memory. *Current Biology : CB*, *27*(20), 3143-3148.e6. https://doi.org/10.1016/j.cub.2017.09.001

Daume, J., Gruber, T., Engel, A. K., & Friese, U. (2017). Phase-amplitude coupling and long-range phase synchronization reveal frontotemporal interactions during visual working

memory. *The Journal of Neuroscience*, *37*(2), 313–322. https://doi.org/10.1523/JNEUROSCI.2130-16.2016

Di Russo, F., Pitzalis, S., Aprile, T., Spitoni, G., Patria, F., Stella, A., Spinelli, D., & Hillyard, S. A. (2007). Spatiotemporal analysis of the cortical sources of the steady-state visual evoked potential. *Human Brain Mapping*, *28*(4), 323–334. https://doi.org/10.1002/hbm.20276

Ding, N., & Simon, J. Z. (2014). Cortical entrainment to continuous speech: Functional roles and interpretations. *Frontiers in Human Neuroscience*, *8*, 311. https://doi.org/10.3389/fnhum.2014.00311

Dolan, R. J., Heinze, H. J., Hurlemann, R., & Hinrichs, H. (2006). Magnetoencephalography (MEG) determined temporal modulation of visual and auditory sensory processing in the context of classical conditioning to faces. *NeuroImage*, *32*(2), 778–789. https://doi.org/10.1016/j.neuroimage.2006.04.206

Duvarci, S., & Pare, D. (2014). Amygdala microcircuits controlling learned fear. *Neuron*, *82*(5), 966–980. https://doi.org/10.1016/j.neuron.2014.04.042.

Edeline, J. M., Pham, P., & Weinberger, N. M. (1993). Rapid development of learning-induced receptive field plasticity in the auditory cortex. *Behavioral Neuroscience*, *107*(4), 539–551. https://doi.org/10.1037//0735-7044.107.4.539

Edeline, J. M., & Weinberger, N. M. (1991). Thalamic short-term plasticity in the auditory system: Associative retuning of receptive fields in the ventral medial geniculate body. *Behavioral Neuroscience*, *105*(5), 618–639. https://doi.org/10.1037/0735-7044.105.5.618

Edeline, J. M., & Weinberger, N. M. (1993). Receptive field plasticity in the auditory cortex during frequency discrimination training: Selective retuning independent of task difficulty. *Behavioral Neuroscience*, *107*(1), 82–103. https://doi.org/10.1037//0735-7044.107.1.82

Elliott, M. A., & Müller, H. J. (1998). Synchronous information presented in 40-Hz flicker enhances visual feature binding. *Psychological Science*, *9*(4), 277–283. https://doi.org/10.1111/1467-9280.00055

Fell, J., & Axmacher, N. (2011). The role of phase synchronization in memory processes. *Nature Reviews. Neuroscience*, *12*(2), 105–118. https://doi.org/10.1038/nrn2979

Fell, J., Klaver, P., Lehnertz, K., Grunwald, T., Schaller, C., Elger, C. E., & Fernández, G. (2001). Human memory formation is accompanied by rhinal-hippocampal coupling and decoupling. *Nature Neuroscience*, *4*(12), 1259–1264. https://doi.org/10.1038/nn759

Ferreira de Sá, D. S., Römer, S., Brückner, A. H., Issler, T., Hauck, A., & Michael, T. (2020). Effects of intranasal insulin as an enhancer of fear extinction: A randomized, double-blind, placebo-controlled experimental study. *Neuropsychopharmacology : Official Publication of the American College of Neuropsychopharmacology*, *45*(5), 753–760. https://doi.org/10.1038/s41386-019-0593-3

Fries, P. (2005). A mechanism for cognitive dynamics: Neuronal communication through neuronal coherence. *Trends in Cognitive Sciences*, *9*(10), 474–480. https://doi.org/10.1016/j.tics.2005.08.011

Friese, U., Köster, M., Hassler, U., Martens, U., Trujillo-Barreto, N., & Gruber, T. (2013). Successful memory encoding is associated with increased cross-frequency coupling between frontal theta and posterior gamma oscillations in human scalp-recorded EEG. *NeuroImage*, *66*, 642–647. https://doi.org/10.1016/j.neuroimage.2012.11.002

Fullana, M. A., Dunsmoor, J. E., Schruers, K. R. J., Savage, H. S., Bach, D. R., & Harrison, B. J. (2020). Human fear conditioning: From neuroscience to the clinic. *Behaviour Research and Therapy*, *124*, 103528. https://doi.org/10.1016/j.brat.2019.103528

Galván, V. V., & Weinberger, N. M. (2002). Long-term consolidation and retention of learning-induced tuning plasticity in the auditory cortex of the guinea pig. *Neurobiology of Learning and Memory*, *77*(1), 78–108. https://doi.org/10.1006/nlme.2001.4044

Gray, C. M., König, P., Engel, A. K., & Singer, W. (1989). Oscillatory responses in cat visual cortex exhibit inter-columnar synchronization which reflects global stimulus properties. *Nature*, *338*(6213), 334–337. https://doi.org/10.1038/338334a0.

Gruber, M. J., Hsieh, L.-T., Staresina, B. P., Elger, C. E., Fell, J., Axmacher, N., & Ranganath, C. (2018). Theta phase synchronization between the human hippocampus and prefrontal cortex increases during encoding of unexpected information: A case study. *Journal of Cognitive Neuroscience*, *30*(11), 1646–1656. https://doi.org/10.1162/jocn_a_01302

Halbleib, A., Gratkowski, M., Schwab, K., Ligges, C., Witte, H., & Haueisen, J. (2012). Topographic analysis of engagement and disengagement of neural oscillators in photic driving: A combined electroencephalogram/magnetoencephalogram study. *Journal of Clinical Neurophysiology*, *29*(1), 33–41. https://doi.org/10.1097/WNP.0b013e318246ad6e

Hallschmid, M. (2021). Intranasal insulin. *Journal of Neuroendocrinology*, *33*(4), e12934. https://doi.org/10.1111/jne.12934

Hanslmayr, S., Axmacher, N., & Inman, C. S. (2019). Modulating human memory via entrainment of brain oscillations. *Trends in Neurosciences*, *42*(7), 485–499. https://doi.org/10.1016/j.tins.2019.04.004

Headley, D. B., & Paré, D. (2017). Common oscillatory mechanisms across multiple memory systems. *NPJ Science of Learning*, *2.* https://doi.org/10.1038/s41539-016-0001-2

Herrmann, C. S., Strüber, D., Helfrich, R. F., & Engel, A. K. (2016). Eeg oscillations: From correlation to causality. *International Journal of Psychophysiology*, *103*, 12–21. https://doi.org/10.1016/j.ijpsycho.2015.02.003

Herron, C. E., Lester, R. A., Coan, E. J., & Collingridge, G. L. (1986). Frequency-dependent involvement of NMDA receptors in the hippocampus: A novel synaptic mechanism. *Nature*, *322*(6076), 265–268. https://doi.org/10.1038/322265a0

Herry, C., & Johansen, J. P. (2014). Encoding of fear learning and memory in distributed neuronal circuits. *Nature Neuroscience*, *17*(12), 1644–1654. https://doi.org/10.1038/nn.3869

Herz, N., Bar-Haim, Y., Tavor, I., Tik, N., Sharon, H., Holmes, E. A., & Censor, N. (2022). Neuromodulation of visual cortex reduces the intensity of intrusive memories. *Cerebral Cortex (New York, N.Y. : 1991)*, *32*(2), 408–417. https://doi.org/10.1093/cercor/bhab217

Hickey, P., Barnett-Young, A., Patel, A. D., & Race, E. (2020). Environmental rhythms orchestrate neural activity at multiple stages of processing during memory encoding: Evidence from event-related potentials. *PloS One*, *15*(11), e0234668. https://doi.org/10.1371/journal.pone.0234668

Hickey, P., Merseal, H., Patel, A. D., & Race, E. (2020). Memory in time: Neural tracking of low-frequency rhythm dynamically modulates memory formation. *NeuroImage*, *213*, 116693. https://doi.org/10.1016/j.neuroimage.2020.116693

Hickey, P., & Race, E. (2021). Riding the slow wave: Exploring the role of entrained low-frequency oscillations in memory formation. *Neuropsychologia*, *160*, 107962. https://doi.org/10.1016/j.neuropsychologia.2021.107962

Hitchcock, J. M., & Davis, M. (1991). Efferent pathway of the amygdala involved in conditioned fear as measured with the fear-potentiated startle paradigm. *Behavioral Neuroscience*, *105*(6), 826–842. https://doi.org/10.1037//0735-7044.105.6.826.

Hubel, D. H., & Wiesel, T. N. (1974). Sequence regularity and geometry of orientation columns in the monkey striate cortex. *The Journal of Comparative Neurology*, *158*(3), 267–293. https://doi.org/10.1002/cne.901580304

Huerta, P. T., & Lisman, J. E. (1995). Bidirectional synaptic plasticity induced by a single burst during cholinergic theta oscillation in CA1 in vitro. *Neuron*, *15*(5), 1053–1063. https://doi.org/10.1016/0896-6273(95)90094-2

Humeau, Y., Herry, C., Kemp, N., Shaban, H., Fourcaudot, E., Bissière, S., & Lüthi, A. (2005). Dendritic spine heterogeneity determines afferent-specific Hebbian plasticity in the amygdala. *Neuron*, *45*(1), 119–131. https://doi.org/10.1016/j.neuron.2004.12.019

Iyadurai, L., Visser, R. M., Lau-Zhu, A., Porcheret, K., Horsch, A., Holmes, E. A., & James, E. L. (2019). Intrusive memories of trauma: A target for research bridging cognitive science and its clinical application. *Clinical Psychology Review*, *69*, 67–82. https://doi.org/10.1016/j.cpr.2018.08.005

Jensen, O., Spaak, E., & Zumer, J. M. (2019). Human brain oscillations: from physiological mechanisms to analysis and cognition. In S. Supek & C. J. Aine (Eds.), *Magnetoencephalography* (pp. 471–517). Springer International Publishing. https://doi.org/10.1007/978-3-030-00087-5_17

Johansen, J. P., Hamanaka, H., Monfils, M. H., Behnia, R., Deisseroth, K., Blair, H. T., & LeDoux, J. E. (2010). Optical activation of lateral amygdala pyramidal cells instructs associative fear learning. *Proceedings of the National Academy of Sciences of the United States of America*, *107*(28), 12692–12697. https://doi.org/10.1073/pnas.1002418107

Johndro, H., Jacobs, L., Patel, A. D., & Race, E. (2019). Temporal predictions provided by musical rhythm influence visual memory encoding. *Acta Psychologica*, *200*, 102923. https://doi.org/10.1016/j.actpsy.2019.102923

Jones, A., & Ward, E. V. (2019). Rhythmic temporal structure at encoding enhances recognition memory. *Journal of Cognitive Neuroscience*, *31*(10), 1549–1562. https://doi.org/10.1162/jocn_a_01431

Jutras, M. J., & Buffalo, E. A. (2010). Synchronous neural activity and memory formation. *Current Opinion in Neurobiology*, *20*(2), 150–155. https://doi.org/10.1016/j.conb.2010.02.006

Kalin, N. H., Shelton, S. E., & Davidson, R. J. (2004). The role of the central nucleus of the amygdala in mediating fear and anxiety in the primate. *The Journal of Neuroscience*, *24*(24), 5506–5515. https://doi.org/10.1523/JNEUROSCI.0292-04.2004

Karalis, N., Dejean, C., Chaudun, F., Khoder, S., Rozeske, R. R., Wurtz, H., Bagur, S., Benchenane, K., Sirota, A., Courtin, J., & Herry, C. (2016). 4-Hz oscillations synchronize

prefrontal-amygdala circuits during fear behavior. *Nature Neuroscience*, *19*(4), 605–612. https://doi.org/10.1038/nn.4251

Keil, A., Gruber, T., Müller, M. M., Moratti, S., Stolarova, M., Bradley, M. M., & Lang, P. J. (2003). Early modulation of visual perception by emotional arousal: Evidence from steady-state visual evoked brain potentials. *Cognitive, Affective & Behavioral Neuroscience*, *3*(3), 195–206. https://doi.org/10.3758/CABN.3.3.195

Keil, A., Ihssen, N., & Heim, S. (2006). Early cortical facilitation for emotionally arousing targets during the attentional blink. *BMC Biology*, *4*, 23. https://doi.org/10.1186/1741-7007-4-23

Kleim, B., Ehring, T., & Ehlers, A. (2012). Perceptual processing advantages for trauma-related visual cues in post-traumatic stress disorder. *Psychological Medicine*, *42*(1), 173–181. https://doi.org/10.1017/S0033291711001048

Knight, D. C., Nguyen, H. T., & Bandettini, P. A. (2003). Expression of conditional fear with and without awareness. *Proceedings of the National Academy of Sciences of the United States of America*, *100*(25), 15280–15283. https://doi.org/10.1073/pnas.2535780100

Knight, D. C., Nguyen, H. T., & Bandettini, P. A. (2006). The role of awareness in delay and trace fear conditioning in humans. *Cognitive, Affective & Behavioral Neuroscience*, *6*(2), 157–162. https://doi.org/10.3758/cabn.6.2.157

Knight, D. C., Smith, C. N., Stein, E. A., & Helmstetter, F. J. (1999). Functional MRI of human Pavlovian fear conditioning: Patterns of activation as a function of learning. *Neuroreport*, *10*(17), 3665–3670. https://doi.org/10.1097/00001756-199911260-00037

Köster, M., Finger, H., Graetz, S., Kater, M., & Gruber, T. (2018). Theta-gamma coupling binds visual perceptual features in an associative memory task. *Scientific Reports*, *8*(1), 17688. https://doi.org/10.1038/s41598-018-35812-7

Köster, M., Martens, U., & Gruber, T. (2019). Memory entrainment by visually evoked theta-gamma coupling. *NeuroImage*, *188*, 181–187. https://doi.org/10.1016/j.neuroimage.2018.12.002

Lakatos, P., Musacchia, G., O'Connel, M. N., Falchier, A. Y., Javitt, D. C., & Schroeder, C. E. (2013). The spectrotemporal filter mechanism of auditory selective attention. *Neuron*, *77*(4), 750–761. https://doi.org/10.1016/j.neuron.2012.11.034

LeDoux, J. E. (2000). Emotion circuits in the brain. *Annual Review of Neuroscience*, *23*, 155–184. https://doi.org/10.1146/annurev.neuro.23.1.155

LeDoux, J. E., & Pine, D. S. (2016). Using neuroscience to help understand fear and anxiety: A two-system framework. *The American Journal of Psychiatry*, *173*(11), 1083–1093. https://doi.org/10.1176/appi.ajp.2016.16030353

Lega, B., Burke, J., Jacobs, J., & Kahana, M. J. (2016). Slow-theta-to-gamma phase-amplitude coupling in human hippocampus supports the formation of new episodic memories. *Cerebral Cortex (New York, N.Y. : 1991)*, *26*(1), 268–278. https://doi.org/10.1093/cercor/bhu232

Leon, M. I., Miasnikov, A. A., Wright, E. J., & Weinberger, N. M. (2017). Cs-specific modifications of auditory evoked potentials in the behaviorally conditioned rat. *Brain Research*, *1670*, 235–247. https://doi.org/10.1016/j.brainres.2017.06.030

Lesting, J., Daldrup, T., Narayanan, V., Himpe, C., Seidenbecher, T., & Pape, H.-C. (2013). Directional theta coherence in prefrontal cortical to amygdalo-hippocampal pathways signals fear extinction. *PloS One*, *8*(10), e77707. https://doi.org/10.1371/journal.pone.0077707

Lesting, J., Narayanan, R. T., Kluge, C., Sangha, S., Seidenbecher, T., & Pape, H.-C. (2011). Patterns of coupled theta activity in amygdala-hippocampal-prefrontal cortical circuits during fear extinction. *PloS One*, *6*(6), e21714. https://doi.org/10.1371/journal.pone.0021714

Likhtik, E., Stujenske, J. M., Topiwala, M. A., Harris, A. Z., & Gordon, J. A. (2014). Prefrontal entrainment of amygdala activity signals safety in learned fear and innate anxiety. *Nature Neuroscience*, *17*(1), 106–113. https://doi.org/10.1038/nn.3582

Lonsdorf, T. B., Menz, M. M., Andreatta, M., Fullana, M. A., Golkar, A., Haaker, J., Heitland, I., Hermann, A., Kuhn, M., Kruse, O., Meir Drexler, S., Meulders, A., Nees, F., Pittig, A., Richter, J., Römer, S., Shiban, Y., Schmitz, A., Straube, B., . . . Merz, C. J. (2017). Don't fear 'fear conditioning': Methodological considerations for the design and analysis of studies on human fear acquisition, extinction, and return of fear. *Neuroscience and Biobehavioral Reviews*, *77*, 247–285. https://doi.org/10.1016/j.neubiorev.2017.02.026

Lovibond, P. F., & Shanks, D. R. (2002). The role of awareness in Pavlovian conditioning: Empirical evidence and theoretical implications. *Journal of Experimental Psychology. Animal Behavior Processes*, *28*(1), 3–26. https://doi.org/10.1037//0097-7403.28.1.3

Lynch, M. A. (2004). Long-term potentiation and memory. *Physiological Reviews*, *84*(1), 87–136. https://doi.org/10.1152/physrev.00014.2003

Maren, S. (2001). Neurobiology of Pavlovian fear conditioning. *Annual Review of Neuroscience*, *24*, 897–931. https://doi.org/10.1146/annurev.neuro.24.1.897

Maren, S., Phan, K. L., & Liberzon, I. (2013). The contextual brain: Implications for fear conditioning, extinction and psychopathology. *Nature Reviews. Neuroscience*, *14*(6), 417–428. https://doi.org/10.1038/nrn3492

Maren, S., & Quirk, G. J. (2004). Neuronal signalling of fear memory. *Nature Reviews. Neuroscience*, *5*(11), 844–852. https://doi.org/10.1038/nrn1535

McGann, J. P. (2015). Associative learning and sensory neuroplasticity: How does it happen and what is it good for? *Learning & Memory (Cold Spring Harbor, N.Y.)*, *22*(11), 567–576. https://doi.org/10.1101/lm.039636.115

McHugo, M., Olatunji, B. O., & Zald, D. H. (2013). The emotional attentional blink: What we know so far. *Frontiers in Human Neuroscience*, *7*, 151. https://doi.org/10.3389/fnhum.2013.00151

McTeague, L. M., Gruss, L. F., & Keil, A. (2015). Aversive learning shapes neuronal orientation tuning in human visual cortex. *Nature Communications*, *6*, 7823. https://doi.org/10.1038/ncomms8823

Meyer, T., Krans, J., van Ast, V., & Smeets, T. (2017). Visuospatial context learning and configuration learning is associated with analogue traumatic intrusions. *Journal of Behavior Therapy and Experimental Psychiatry*, *54*, 120–127. https://doi.org/10.1016/j.jbtep.2016.07.010

Milad, M. R., Igoe, S. A., Lebron-Milad, K., & Novales, J. E. (2009). Estrous cycle phase and gonadal hormones influence conditioned fear extinction. *Neuroscience*, *164*(3), 887–895. https://doi.org/10.1016/j.neuroscience.2009.09.011

Milad, M. R., & Quirk, G. J. (2012). Fear extinction as a model for translational neuroscience: Ten years of progress. *Annual Review of Psychology*, *63*, 129–151. https://doi.org/10.1146/annurev.psych.121208.131631

Milad, M. R., Zeidan, M. A., Contero, A., Pitman, R. K., Klibanski, A., Rauch, S. L., & Goldstein, J. M. (2010). The influence of gonadal hormones on conditioned fear extinction in healthy humans. *Neuroscience*, *168*(3), 652–658. https://doi.org/10.1016/j.neuroscience.2010.04.030

Miskovic, V., & Keil, A. (2012). Acquired fears reflected in cortical sensory processing: A review of electrophysiological studies of human classical conditioning. *Psychophysiology*, *49*(9), 1230–1241. https://doi.org/10.1111/j.1469-8986.2012.01398.x

Molchan, S. E., Sunderland, T., McIntosh, A. R., Herscovitch, P., & Schreurs, B. G. (1994). A functional anatomical study of associative learning in humans. *Proceedings of the National Academy of Sciences of the United States of America*, *91*(17), 8122–8126. https://doi.org/10.1073/pnas.91.17.8122

Montoya, P., Larbig, W., Pulvermüller, F., Flor, H., & Birbaumer, N. (1996). Cortical correlates of semantic classical conditioning. *Psychophysiology*, *33*(6), 644–649. https://doi.org/10.1111/j.1469-8986.1996.tb02359.x

Morris, J. S., Friston, K. J., & Dolan, R. J. (1998). Experience-dependent modulation of tonotopic neural responses in human auditory cortex. *Proceedings. Biological Sciences*, *265*(1397), 649–657. https://doi.org/10.1098/rspb.1998.0343

Morris, R. (1999). D.O. Hebb: The Organization of Behavior, Wiley: New York; 1949. *Brain Research Bulletin*, *50*(5-6), 437. https://doi.org/10.1016/s0361-9230(99)00182-3

Mueller, E. M., Panitz, C., Hermann, C., & Pizzagalli, D. A. (2014). Prefrontal oscillations during recall of conditioned and extinguished fear in humans. *The Journal of Neuroscience*, *34*(21), 7059–7066. https://doi.org/10.1523/JNEUROSCI.3427-13.2014

Myers, K. M., & Davis, M. (2007). Mechanisms of fear extinction. *Molecular Psychiatry*, *12*(2), 120–150. https://doi.org/10.1038/sj.mp.4001939

Nabavi, S., Fox, R., Proulx, C. D., Lin, J. Y., Tsien, R. Y., & Malinow, R. (2014). Engineering a memory with LTD and LTP. *Nature*, *511*(7509), 348–352. https://doi.org/10.1038/nature13294

Norcia, A. M., Appelbaum, L. G., Ales, J. M., Cottereau, B. R., & Rossion, B. (2015). The steady-state visual evoked potential in vision research: A review. *Journal of Vision*, *15*(6), 4. https://doi.org/10.1167/15.6.4

Öhman, A., Flykt, A., & Esteves, F. (2001). Emotion drives attention: Detecting the snake in the grass. *Journal of Experimental Psychology: General*, *130*(3), 466–478. https://doi.org/10.1037/0096-3445.130.3.466

Orsini, C. A., & Maren, S. (2012). Neural and cellular mechanisms of fear and extinction memory formation. *Neuroscience and Biobehavioral Reviews*, *36*(7), 1773–1802. https://doi.org/10.1016/j.neubiorev.2011.12.014

Padmala, S., & Pessoa, L. (2008). Affective learning enhances visual detection and responses in primary visual cortex. *The Journal of Neuroscience*, *28*(24), 6202–6210. https://doi.org/10.1523/JNEUROSCI.1233-08.2008

Panitz, C., Keil, A., & Mueller, E. M. (2019). Extinction-resistant attention to long-term conditioned threat is indexed by selective visuocortical alpha suppression in humans. *Scientific Reports*, *9*(1), 15809. https://doi.org/10.1038/s41598-019-52315-1

Park, C. R., Seeley, R. J., Craft, S., & Woods, S. C. (2000). Intracerebroventricular insulin enhances memory in a passive-avoidance task. *Physiology & Behavior*, *68*(4), 509–514. https://doi.org/10.1016/s0031-9384(99)00220-6

Pearson, J., Naselaris, T., Holmes, E. A., & Kosslyn, S. M. (2015). Mental Imagery: Functional Mechanisms and Clinical Applications. *Trends in Cognitive Sciences*, *19*(10), 590–602. https://doi.org/10.1016/j.tics.2015.08.003

Place, R., Farovik, A., Brockmann, M., & Eichenbaum, H. (2016). Bidirectional prefrontal-hippocampal interactions support context-guided memory. *Nature Neuroscience*, *19*(8), 992–994. https://doi.org/10.1038/nn.4327

Plog, E., Antov, M. I., Bierwirth, P., Keil, A., & Stockhorst, U. (2022). Phase-synchronized stimulus presentation augments contingency knowledge and affective evaluation in a fear-conditioning task. *ENeuro*, *9*(1). https://doi.org/10.1523/ENEURO.0538-20.2021

Polanía, R., Nitsche, M. A., Korman, C., Batsikadze, G., & Paulus, W. (2012). The importance of timing in segregated theta phase-coupling for cognitive performance. *Current Biology : CB*, *22*(14), 1314–1318. https://doi.org/10.1016/j.cub.2012.05.021

Popa, D., Duvarci, S., Popescu, A. T., Léna, C., & Paré, D. (2010). Coherent amygdalocortical theta promotes fear memory consolidation during paradoxical sleep. *Proceedings of the National Academy of Sciences of the United States of America*, *107*(14), 6516–6519. https://doi.org/10.1073/pnas.0913016107

Quirk, G. J., & Mueller, D. (2008). Neural mechanisms of extinction learning and retrieval. *Neuropsychopharmacology : Official Publication of the American College of Neuropsychopharmacology*, *33*(1), 56–72. https://doi.org/10.1038/sj.npp.1301555

Quirk, G. J., Repa, J. C., & LeDoux, J. E. (1995). Fear conditioning enhances short-latency auditory responses of lateral amygdala neurons: Parallel recordings in the freely behaving rat. *Neuron*, *15*(5), 1029–1039. https://doi.org/10.1016/0896-6273(95)90092-6

Rhodes, L. J., Ruiz, A., Ríos, M., Nguyen, T., & Miskovic, V. (2018). Differential aversive learning enhances orientation discrimination. *Cognition & Emotion*, *32*(4), 885–891. https://doi.org/10.1080/02699931.2017.1347084

Roesler, R., & McGaugh, J. L. (2010). Memory Consolidation. In *Encyclopedia of Behavioral Neuroscience* (pp. 206–214). Elsevier. https://doi.org/10.1016/B978-0-08-045396-5.00147-0

Romanski, L. M., Clugnet, M.-C., Bordi, F., & LeDoux, J. E. (1993). Somatosensory and auditory convergence in the lateral nucleus of the amygdala. *Behavioral Neuroscience*, *107*(3), 444–450. https://doi.org/10.1037/0735-7044.107.3.444

Rudy, J. W. (2014). Learning about danger: the neurobiology of fear memories. In J. W. Rudy (Ed.), *The neurobiology of learning and memory.* Sinauer Associates.

Seidenbecher, T., Laxmi, T. R., Stork, O., & Pape, H.-C. (2003). Amygdalar and hippocampal theta rhythm synchronization during fear memory retrieval. *Science*, *301*(5634), 846–850. https://doi.org/10.1126/science.1085818

Sevenster, D., Beckers, T., & Kindt, M. (2014). Fear conditioning of SCR but not the startle reflex requires conscious discrimination of threat and safety. *Frontiers in Behavioral Neuroscience*, *8*, 32. https://doi.org/10.3389/fnbeh.2014.00032

Sherry, D. F., & Schacter, D. L. (1987). The evolution of multiple memory systems. *Psychological Review*, *94*(4), 439–454. https://doi.org/10.1037/0033-295X.94.4.439

Shvil, E., Rusch, H. L., Sullivan, G. M., & Neria, Y. (2013). Neural, psychophysiological, and behavioral markers of fear processing in PTSD: A review of the literature. *Current Psychiatry Reports*, *15*(5), 358. https://doi.org/10.1007/s11920-013-0358-3

Silverstein, D. N., & Ingvar, M. (2015). A multi-pathway hypothesis for human visual fear signaling. *Frontiers in Systems Neuroscience*, *9*, 101. https://doi.org/10.3389/fnsys.2015.00101

Smith, S. D., Most, S. B., Newsome, L. A., & Zald, D. H. (2006). An emotion-induced attentional blink elicited by aversively conditioned stimuli. *Emotion (Washington, D.C.)*, *6*(3), 523–527. https://doi.org/10.1037/1528-3542.6.3.523

Sperl, M. F. J., Panitz, C., Rosso, I. M., Dillon, D. G., Kumar, P., Hermann, A., Whitton, A. E., Hermann, C., Pizzagalli, D. A., & Mueller, E. M. (2019). Fear extinction recall modulates human frontomedial theta and amygdala activity. *Cerebral Cortex (New York, N.Y. : 1991)*, *29*(2), 701–715. https://doi.org/10.1093/cercor/bhx353

Squire, L. R. (1998). Memory systems. *Comptes Rendus De L'académie Des Sciences - Series III - Sciences De La Vie*, *321*(2-3), 153–156. https://doi.org/10.1016/S0764-4469(97)89814-9

Squire, L. R. (2004). Memory systems of the brain: A brief history and current perspective. *Neurobiology of Learning and Memory*, *82*(3), 171–177. https://doi.org/10.1016/j.nlm.2004.06.005

Squire, L. R., & Dede, A. J. O. (2015). Conscious and unconscious memory systems. *Cold Spring Harbor Perspectives in Biology*, *7*(3), a021667. https://doi.org/10.1101/cshperspect.a021667

Stegmann, Y., Andreatta, M., Pauli, P., & Wieser, M. J. (2021). Associative learning shapes visual discrimination in a web-based classical conditioning task. *Scientific Reports*, *11*(1), 15762. https://doi.org/10.1038/s41598-021-95200-6

Steinberg, C., Bröckelmann, A.-K., Rehbein, M., Dobel, C., & Junghöfer, M. (2013). Rapid and highly resolving associative affective learning: Convergent electro- and magnetoencephalographic evidence from vision and audition. *Biological Psychology*, *92*(3), 526–540. https://doi.org/10.1016/j.biopsycho.2012.02.009

Stockhorst, U., & Antov, M. I. (2015). Modulation of fear extinction by stress, stress hormones and estradiol: A review. *Frontiers in Behavioral Neuroscience*, *9*, 359. https://doi.org/10.3389/fnbeh.2015.00359

Stolarova, M., Keil, A., & Moratti, S. (2006). Modulation of the C1 visual event-related component by conditioned stimuli: Evidence for sensory plasticity in early affective perception. *Cerebral Cortex (New York, N.Y. : 1991)*, *16*(6), 876–887. https://doi.org/10.1093/cercor/bhj031

Stujenske, J. M., Likhtik, E., Topiwala, M. A., & Gordon, J. A. (2014). Fear and safety engage competing patterns of theta-gamma coupling in the basolateral amygdala. *Neuron*, *83*(4), 919–933. https://doi.org/10.1016/j.neuron.2014.07.026

Summerfield, C., & Mangels, J. A. (2005). Coherent theta-band EEG activity predicts item-context binding during encoding. *NeuroImage*, *24*(3), 692–703. https://doi.org/10.1016/j.neuroimage.2004.09.012

Sun, Y., Gooch, H., & Sah, P. (2020). Fear conditioning and the basolateral amygdala. *F1000Research*, *9*. https://doi.org/10.12688/f1000research.21201.1

Sündermann, O., Hauschildt, M., & Ehlers, A. (2013). Perceptual processing during trauma, priming and the development of intrusive memories. *Journal of Behavior Therapy and Experimental Psychiatry*, *44*(2), 213–220. https://doi.org/10.1016/j.jbtep.2012.10.001

Taub, A. H., Perets, R., Kahana, E., & Paz, R. (2018). Oscillations synchronize amygdala-to-prefrontal primate circuits during aversive learning. *Neuron*, *97*(2), 291-298.e3. https://doi.org/10.1016/j.neuron.2017.11.042

Thomas, M. E., Lane, C. P., Chaudron, Y. M. J., Cisneros-Franco, J. M., & Villers-Sidani, É. de (2020). Modifying the adult rat tonotopic map with sound exposure produces frequency discrimination deficits that are recovered with training. *The Journal of Neuroscience*, *40*(11), 2259–2268. https://doi.org/10.1523/JNEUROSCI.1445-19.2019

Todd, R. M., MacDonald, M. J., Sedge, P., Robertson, A., Jetly, R., Taylor, M. J., & Pang, E. W. (2015). Soldiers with posttraumatic stress disorder see a world full of threat: Magnetoencephalography reveals enhanced tuning to combat-related cues. *Biological Psychiatry*, *78*(12), 821–829. https://doi.org/10.1016/j.biopsych.2015.05.011

Wang, D., Clouter, A., Chen, Q., Shapiro, K. L., & Hanslmayr, S. (2018). Single-trial phase entrainment of theta oscillations in sensory regions predicts human associative memory performance. *The Journal of Neuroscience*, *38*(28), 6299–6309. https://doi.org/10.1523/JNEUROSCI.0349-18.2018

Weinberger, N. M. (2015). New perspectives on the auditory cortex: Learning and memory. *Handbook of Clinical Neurology*, *129*, 117–147. https://doi.org/10.1016/B978-0-444-62630-1.00007-X

Weinberger, N. M., & Bakin, J. S. (1998). Learning-induced physiological memory in adult primary auditory cortex: Receptive fields plasticity, model, and mechanisms. *Audiology & Neuro-Otology*, *3*(2-3), 145–167. https://doi.org/10.1159/000013787

Weinberger, N. M., Javid, R., & Lepan, B. (1993). Long-term retention of learning-induced receptive-field plasticity in the auditory cortex. *Proceedings of the National Academy of Sciences of the United States of America*, *90*(6), 2394–2398. https://doi.org/10.1073/pnas.90.6.2394

Weiss, S., & Rappelsberger, P. (2000). Long-range EEG synchronization during word encoding correlates with successful memory performance. *Cognitive Brain Research*, *9*(3), 299–312. https://doi.org/10.1016/S0926-6410(00)00011-2

Wong, P. S., Bernat, E., Bunce, S., & Shevrin, H. (1997). Brain indices of nonconscious associative learning. *Consciousness and Cognition*, *6*(4), 519–544. https://doi.org/10.1006/ccog.1997.0322

Zhao, W., Chen, H., Xu, H., Moore, E., Meiri, N., Quon, M. J., & Alkon, D. L. (1999). Brain insulin receptors and spatial memory. Correlated changes in gene expression, tyrosine phosphorylation, and signaling molecules in the hippocampus of water maze trained rats. *The Journal of Biological Chemistry*, *274*(49), 34893–34902. https://doi.org/10.1074/jbc.274.49.34893

Zheng, J., Stevenson, R. F., Mander, B. A., Mnatsakanyan, L., Hsu, F. P. K., Vadera, S., Knight, R. T., Yassa, M. A., & Lin, J. J. (2019). Multiplexing of theta and alpha rhythms in the amygdala-hippocampal circuit supports pattern separation of emotional information. *Neuron*, *102*(4), 887-898.e5. https://doi.org/10.1016/j.neuron.2019.03.025

Zhou, H., Melloni, L., Poeppel, D., & Ding, N. (2016). Interpretations of frequency domain analyses of neural entrainment: Periodicity, fundamental frequency, and harmonics. *Frontiers in Human Neuroscience*, *10*, 274. https://doi.org/10.3389/fnhum.2016.00274

Zoefel, B., Oever, S. ten, & Sack, A. T. (2018). The involvement of endogenous neural oscillations in the processing of rhythmic input: More than a regular repetition of evoked neural responses. *Frontiers in Neuroscience*, *12*, 95. https://doi.org/10.3389/fnins.2018.00095